Engineering Zwitterionic Biomaterials for Immune Modulation and Drug Delivery

Bowen Li

A dissertation

submitted in partial fulfillment of the

requirements for the degree of

Doctor of Philosophy

University of Washington

2019

Reading Committee:

Shaoyi Jiang, Ph.D., Chair

Suzie H. Pun, Ph.D.

Bruce Hinds, Ph.D.

Program Authorized to Offer Degree:

Department of Bioengineering

University of Washington

Abstract

Engineering Zwitterionic Biomaterials for Immune Modulation and Drug Delivery

Bowen Li

Chair of the Supervisory Committee:

Professor Shaoyi Jiang

Chemical Engineering

The development of biotherapeutics, which hold promising potential to treat diverse disease, is limited by their inadequate circulation half-lives and inherent immunogenicity. Conjugation of non-ionic poly (ethylene glycol) (PEG), known as PEGylation, has been widely employed as the gold standard to ameliorate the pharmacokinetic (PK) and immunological profiles of proteins. Unfortunately, PEG grafted onto immunogenic proteins has been shown to induce anti-PEG antibodies (Abs) that could cause loss of efficacy and even lethal adverse reactions. To confront the "PEG dilemma", zwitterionic materials with superhydrophilicity are emerging as promising alternatives for PEG. This dissertation summarizes recent studies from the design, synthesis and characterization of zwitterionic polymers to the *in vitro* and *in vivo* studies of poly(zwitterion)-protein nanomedicine. The influence of PEG and zwitterionic poly(carboxy betaine) (PCB) on immune systems is firstly discussed, revealing the low immunogenic risk of zwitterionic materials. Based on this design principle, new protein-delivery tactics are proposed to avoid the generation of undesirable immune responses, either by completely shielding proteins from immune recognition or by actively inducing antigen-specific immune tolerance. Furthermore, new classes of naturally-inspired inert or immunomodulatory zwitterionic materials are developed to further improve the efficacy and safety of protein therapeutics, enriching the arsenal of biomaterial tools for drug delivery.

Acknowledgements

Foremost, I hope to express my most sincere thanks to my doctoral advisor, Dr. Shaoyi Jiang for his invaluable mentorship and support. Dr. Jiang is a great scientist as well as a great mentor, who offered me a fantastic opportunity to work in his lab and continuously inspires me to strive for success. His office door is always open to me whenever I need help or discussion. Dr. Jiang's extensive guidance and unique vision deeply influences my perspective in both work and life. It is my goal to follow in his footsteps pursuing excellence in the academic career.

I also would like to thank other members of my supervisory committee: Drs. Suzie Pun, Buddy Ratner and Bruce Hinds for their generous help and insightful critiques. To me, they are all my role models in academia.

I am grateful for my brilliant colleagues in Jiang group and my friends in Seattle who give me selfless assistance and precious inputs. I will not be able to accomplish my research goals without their backup and encouragement.

Special thanks to my parents who provide me with unconditional support and understanding along this long journey.

Table of content

CHAPTER 1 Introduction **8**

CHAPTER 2 Revealing the Immunogenic Risk of Polymers

2.1 Abstract **18**
2.2 Introduction **19**
2.3 Experimental Section **22**
2.3.1 Materials 22
2.3.2 Synthesis of 3-acrylamido-N-(2-(tert-butoxy)-2-oxoethyl)-N,N-dimethylpropan-1-aminium (t-Butyl CBAAm) (Scheme 1-1) 22
2.3.3 Synthesis of chain transfer agent (CTA) for PCB synthesis (Scheme 1-2) 23
2.3.4 Synthesis of PCB-SH (Scheme 1-3) and mPEG-SH 24
2.3.5 Conjugation of polymers to proteins (Scheme 1-4) 25
2.3.6 Animal studies 25
2.3.7 Immunogenicity study of proteins 25
2.3.8 Animal immunization with protein-polymer conjugates 26
2.3.9 ELISA test 26
2.3.10 SPR detection of anti-polymer antibodies 27
2.3.11 Statistics 28
2.4 Results and Discussion **29**
2.4.1 Immunogenicity index of bare proteins 29
2.4.2 Preparation of polymer-protein conjugates 30
2.4.3 Detection of anti-polymer Ab responses 31
2.5 Conclusions **33**
2.6 Schemes, Figures and Tables **34**
2.7 References **53**

CHAPTER 3 Modulation of Inflammatory Immune Responses with Hydrophilic Nanoparticles

3.1 Abstract **59**
3.2 Introduction **60**
3.3 Experimental Section **61**
3.3.1 Materials 61
3.3.2 Preparation of PEG, PSB and PCB nanogels 61
3.3.3 *In vitro* immune activation study 62
3.3.4 ROS detection 62
3.4 Results and Discussion **63**
3.4.1 Effect of hydrophilic nanogels on the secretion of proinflmmatory cytokines 63
3.4.2 Effect of hydrophilic nanogels on ROS production 65
3.4.3 Effect of hydrophilic nanogels on inflammatory animals 66
3.5 Conclusions **69**
3.6 Schemes, Figures, and Tables **71**
3.7 References **77**

CHAPTER 4 Zwitterionic Nanocages Improve the Efficacy and Safety of Biologic Drugs

4.1 Abstract **82**
4.2 Introduction **83**
4.3 Experimental Section **86**
4.3.1 Materials 86
4.3.2 Preparation of nanocage for uricase encapsulation 86
4.3.3 Nanocage characterization 87
4.3.4 Animal studies 87

4.3.5 Immunogenicity study 88
4.3.6 PK and bio-distribution study 88
4.4 Results and Discussion 91
4.4.1 Zwitterionic nanocages physically encapsulate uricase 91
4.4.2 Immunogenicity study 93
4.4.3 PK and biodistribution study 95
4.4.4 Efficacy study in gouty animal model 96
4.5 Conclusions 98
4.6 Schemes, Figures, and Tables 99
4.7 References 108

CHAPTER 5 A Chromatin-Mimetic Nanomedicine for Therapeutic Tolerance Induction
5.1 Abstract 114
5.2 Introduction 115
5.3 Experimental section 117
5.3.1 Materials 117
5.3.2 Synthesis and characterization of DCN 118
5.3.3 Cell uptake study 119
5.3.4 Lysotracker colocalization assay 120
5.3.5 Cell viability study 120
5.3.6 Animals 121
5.3.7 KLH tolerance study 121
5.3.8 OVA specificity study 123
5.3.9 PEGylated uricase study 123
5.3.10 OVA-induced allergic asthma study 124
5.4 Results and Discussion 126
5.4.1 Preparation and characterization of DCN 126
5.4.2 DCN induces immune tolerance to protein antigens 1288
5.4.3 DCN improves therapeutic properties of PEG-uricase 130
5.4.4 DCN alleviates the allergic asthma 132
5.5 Conclusions 133
5.6 Scheme, Figures and Tables 135
5.7 References 152

CHAPTER 6 Trimethylamine N-oxide Derived Zwitterionic Polymers: A New Class of Ultra-low Fouling Bioinspired Materials
6.1 Abstract 159
6.2 Introduction 160
6.3 Experimental Section 162
6.3.1 Materials 162
6.3.2 Synthesis of TMAO monomer 163
6.3.3 Preparation of TMAO hydrogel 163
6.3.4 Fibrinogen adsorption test 164
6.3.5 Cell adhesion test 164
6.3.6 Complement activation test 165
6.3.7 Preparation of TMAO-coated surface by SI-ATRP 165
6.3.8 SPR test in human serum 166
6.3.9 Preparation of PTMAO-KLH conjugate 166
6.3.10 Preparation of PEGylated KLH 167
6.3.11 Preparation of PTMAO-uricase conjugate 168

6.3.12 Preparation of PEGylated uricase 168
6.3.13 Stability test 169
6.3.14 Animal studies 169
6.3.15 Immunogenicity study of PTMAO 169
6.3.16 *In vivo* non-fouling performance of PTMAO 171
6.3.17 MD simulations 171
6.4 Results and Discussion 173
6.4.1 Synthesis of TMAO-analogue monomer 173
6.4.2 *In vitro* fouling tests of TMAO polymers 173
6.4.3 Minimal immunogenic potential of TMAO polymers 175
6.4.4 Improved circulation and efficacy of PTMAO-conjugated proteins 177
6.4.5 Non-fouling mechanism of TMAO at molecular level 179
6.5 Conclusions 180
6.6 Scheme, Figures and Tables 181
6.7 References 195

CHAPTER 7 Immunosuppressive Zwitterionic Polymers Inspired by Apoptotic Cell Death for Protein Conjugation
7.1 Abstract 200
7.2 Introduction 201
7.3 Experimental Section 203
7.3.1 Materials 203
7.3.2 Synthesis of Compound 3 203
7.3.3 Synthesis of ZPS monomer (Compound 4) 204
7.3.4 Synthesis of Compound 5 204
7.3.5 Synthesis of NZPS monomer (Compound 6) 205
7.3.6 Non-specific protein adsorption test 205
7.3.7 Preparation of NZPS and ZPS nanogels 206
7.3.8 Anti-inflammation test 208
7.3.9 Annexin V blocking test 208
7.3.10 Cell uptake study 209
7.3.11 Preparation of polymer-uricase conjugates 210
7.3.12 *In vitro* immunogenicity study 210
7.3.13 Animal study 210
7.4 Results and Discussion 212
7.4.1 Design and Synthesis of PS-analogue monomers 212
7.4.2 Non-specific protein adsorption test 213
7.4.3 Anti-inflammation effect on macrophages 214
7.4.4 Effect of ZPS and NZPS on uricase immunogenicity and PK 216
7.5 Conclusions 220
7.6 Scheme, Figures and Tables 221
7.7 References 229

CHAPTER 8 Conclusions 234

CHAPTER 1 Introduction

Naturally derived biologic agents comprise a broad reservoir of drug candidates with exceptional medicinal potency and specificity[1]. However, many of these protein-based therapeutics are highly immunogenic, eliciting undesirable immune reactions characterized by antibody (Ab) generation[2-4]. Binding of antigen-specific Abs to protein drugs may result in poor clinical outcomes, either through directly neutralizing the pharmacological activity of proteins or by causing accelerated blood clearance (ABC) [5, 6]. PEGylation, the covalent binding of polyethylene glycol (PEG) molecules to biologics, is a widely used strategy to improve the clinical outcomes of protein therapies[7-9]. It is well established that large PEG groups conjugated to protein surfaces can shield the underlying epitopes from immune recognition and delay mononuclear phagocyte system (MPS) and kidney clearance, thus elongating protein circulation time[9]. To date, over a dozen PEGylated biologics have been approved by the US Food and Drug Administration (FDA) and many more are in clinical pipelines[8]. However, in parallel to the rise of PEGylation, an increasing number of reports have highlighted the immunogenicity of PEG itself as an additional cause of antibody generation[10-14]. The proliferation of anti-PEG Abs could deprive patients of their life-sustaining therapies, and in some cases, cause adverse effects such as hypersensitivity reactions that prevent further treatment. For example, anti-PEG Abs were detected in the sera of 89% of refractory chronic gout (RCG) patients after receiving pegloticase (Krystexxa®), a PEGylated uricase product approved by the FDA in 2010[15]. Of particular concerns, the clinical problems with pegloticase have been predominantly associated with anti-PEG Abs, instead of anti-uricase Abs[16-19]. Among patients who developed high-level anti-PEG Ab responses, 93% consequently became non-responders to pegloticase therapy, and many suffered life-threatening infusion reactions[17]. High titers of anti-PEG Abs have also been reported to impair the safety and efficacy of other

PEGylated proteins on the market, including PEG-asparaginase (Oncaspar®)[20, 21] and PEG-interferon alfa (Pegasys®)[22]. Along with the issues surrounding these treatment-induced anti-PEG Abs, the negative impact of pre-existing anti-PEG Abs—found in patients even before their first exposure to a PEGylated therapy[23]—has recently seen greater emphasis. In one case study of pegloticase, pre-existing anti-PEG Abs rapidly neutralized therapeutic efficacy in all five treatment-naïve patients[16]. Alarmingly, the prevalence of these pre-existing Abs in healthy individuals has been rising since their first detection three decades ago, likely resulting from high exposure to PEG-containing foods, cosmetics, and household products[12, 24]. As anti-PEG Abs from any source can cross-react with PEGylated products and render them ineffective, the future of PEGylation in biopharmaceuticals is uncertain and several alternative strategies have been proposed. One example is bioinformatics-driven protein engineering, which aims to directly remove potentially immunogenic epitopes from the sequence of a non-human protein[25]. However, such modifications may unexpectedly alter the secondary or tertiary structure of a therapeutic protein and thus adversely affect its pharmacological activity. Moreover, the implementation of this approach must be redesigned from the ground up for each new protein, which is complex and time-consuming. Alternatively, the most popular strategies as alternatives to PEGylation are to shield proteins with hydrophilic polymers, including synthetic polymers (e.g., poly(N-vinylpyrrolidone)[26], polyoxazoline[27] and poly(N-acryloyl morpholine)[28]) and naturally derived polymers (e.g., polysaccharide[29] and polypeptide[30]). Similar to PEGylation, these polymers are often attached to reactive groups (e.g., thiol, amine and carboxy) on a protein surface via so-called "graft-to" methods. So-called 'graft-from' conjugation methods have been employed to achieve a somewhat higher grafted polymer density, but these involve polymerizations such as atom transfer radical polymerization (ATRP) in the presence of metal ions, making clinical translation arduous.

It should be pointed out that the critical issue of anti-polymer Ab responses to these alternative materials is rarely studied.

Zwitterionic materials, which bear a pair of oppositely charged ions (or zwitterions) in the same moiety while maintain overall neutral charge, are renowned for their strong hydration effect mediated by electrostatic interactions between zwitterions and surrounding water molecules. Recently, proteins conjugated to PCB[31,32], a biomimetic zwitterionic polymer derived from glycine betaine, or protected by PCB hydrogels,[33] have demonstrated greater stability, superior pharmacokinetics (PK) and reduced immunogenicity in comparison with native and PEGylated proteins. Results showed that no anti-PCB Abs could be detected after three intravenous (IV) administrations of a PCB-modified protein, while a conspicuously high level of anti-PEG Abs developed in groups injected with its PEGylated counterpart[32,33]. These results suggest that PCB is a promising non-immunogenic alternative to PEG. Moving forward from these studies, this dissertation systemically explores new properties and applications of zwitterionic materials and beyond in the field of drug delivery and immune tolerance.

Chapters 2 and 3 cover fundamental studies on the immunological properties of zwitterionic materials. In Chapter 2, the immunogenic risk of non-ionic neutral PEG and zwitterionic PCB is discussed. A strong quantitative correlation between the level of PEG-specific Abs and the immunogenicity of proteins carrying PEG is established, revealing the propensity of PEG to become immunogenic. In contrast, PCB is manifested to contain low immunogenic risk, as the generation of PCB-specific Abs is negligible regardless of carrier proteins. In Chapter 3, the ability of hydrophilic materials including PEG and zwitterionic materials to regulate immune responses

during an immunological challenge (i.e., inflammation) is investigated. The treatment of peripheral blood mononuclear cells with hydrophilic nanogels resulted in attenuated immune responses to stimulation by lipopolysacchride both *in vitro* and *in vivo*. It is further shown that the immunomodulatory effect of hydrophilic materials is closely related to their hydration characteristics and their ability to resist non-specific binding in complex media.

Chapters 4 and 5 report new strategies that improve the safety and efficacy of protein drugs by eradicating the immune responses in a passive or proactive way. In Chapter 4, a zwitterionic PCB nanocage is developed to physically encase proteins while keeping their structure intact. PCB nanocage encapsulation of uricase, a highly immunogenic enzyme drug, is demonstrated to passively shield uricase from immune recognition and thus eliminate all the possible immune responses. PCB-nanocage-shrouded uricase displays a high therapeutic performance in a gouty rat model without evoking efficacy loss even after five repetitive administrations, greatly outperforming the industry standard PEGylated counterpart. In Chapter 5, a DNA-protein polymeric nanocomplex that can mimic the tolerogenic function of chromatin and induce an immune tolerance to its protein cargos is developed. This chromatin-mimetic nanomedicine containing GpG oligonucleotides and protein antigens provides a useful tool to specifically suppress unwanted immunogenicity of protein drugs for therapeutic purposes. It is the first reported attempt that exploits the immunosuppressive potential of nucleotide to actively improve the therapeutic performance of protein drugs in an antigen-specific manner.

Chapters 6 and 7 introduce two new classes of naturally-inspired zwitterionic materials. In Chapter 6, a zwitterionic polymer (PTMAO) is developed as a new class of ultra-low fouling biomaterials.

The structure of PTMAO derives from trimethylamine N-oxide (TMAO), a zwitterionic osmolyte and the most effective protein stabilizer. PTMAO displays exceptional non-fouling property and minimal immunogenicity under harsh *in vitro* and *in vivo* conditions, and the mechanism accounting for the extraordinary hydration of PTMAO is elucidated by molecular dynamic simulations. PTMAO represents the fourth class of non-fouling zwitterionic material after PCB, poly(phosphorylcholine) (PPC), poly(sulfobetaine) (PSB), and is expected to find wide applications in biomedical fields. In Chapter 7, a zwitterionic phosphatidylserine (PS)-mimic polymer (ZPS) is developed, which has the phosphoryl serine group as an immunosuppressive functional moiety to proactively inhibit immune reactions. In contrast to the inert zwitterionic polymers, which alleviate the immunogenicity of proteins by passively hiding their immunogenic epitopes from immune surveillance, ZPS polymers have been shown to actively suppress the immune system, resulting in immune tolerance towards their associated proteins. Such an immunomodulatory property of ZPS is particularly meaningful to the protein drugs with limited reactive groups on surfaces. On the other hand, ZPS retains the typical super-hydrophilic property of zwitterionic materials. Conjugation of ZPS polymers to uricase shows to completely eradicate the protein immunogenicity while prolonging the circulation time.

References

1. Aggarwal, R. S., What's fueling the biotech engine-2012 to 2013. *Nat Biotechnol* 2014, *32* (1), 32-9.

2. Moussa, E. M.; Panchal, J. P.; Moorthy, B. S.; Blum, J. S.; Joubert, M. K.; Narhi, L. O.; Topp, E. M., Immunogenicity of Therapeutic Protein Aggregates. *J Pharm Sci* 2016, *105* (2), 417-30.

3. Rosenberg, A. S., Immunogenicity of biological therapeutics: a hierarchy of concerns. *Dev Biol (Basel)* 2003, *112*, 15-21.

4. Yin, L.; Chen, X.; Vicini, P.; Rup, B.; Hickling, T. P., Therapeutic outcomes, assessments, risk factors and mitigation efforts of immunogenicity of therapeutic protein products. *Cell Immunol* 2015, *295* (2), 118-26.

5. Nechansky, A.; Kircheis, R., Immunogenicity of therapeutics: a matter of efficacy and safety. *Expert Opin Drug Discov* 2010, *5* (11), 1067-79.

6. Baker, M. P.; Reynolds, H. M.; Lumicisi, B.; Bryson, C. J., Immunogenicity of protein therapeutics: The key causes, consequences and challenges. *Self Nonself* 2010, *1* (4), 314-322.

7. Zhang, P.; Sun, F.; Liu, S.; Jiang, S., Anti-PEG antibodies in the clinic: Current issues and beyond PEGylation. *J Control Release* 2016, *244* (Pt B), 184-193.

8. Alconcel, S. N. S.; Baas, A. S.; Maynard, H. D., FDA-approved poly(ethylene glycol)-protein conjugate drugs. *Polym Chem-Uk* 2011, *2* (7), 1442-1448.

9. Suk, J. S.; Xu, Q. G.; Kim, N.; Hanes, J.; Ensign, L. M., PEGylation as a strategy for improving nanoparticle-based drug and gene delivery. *Adv Drug Deliver Rev* 2016, *99*, 28-51.

10. Ishida, T.; Kiwada, H., Anti-polyethyleneglycol Antibody Response to PEGylated Substances. *Biol Pharm Bull* 2013, *36* (6), 889-891.

11. Schellekens, H.; Hennink, W. E.; Brinks, V., The Immunogenicity of Polyethylene Glycol: Facts and Fiction. *Pharm Res-Dordr* 2013, *30* (7), 1729-1734.

12. Yang, Q.; Lai, S. K., Anti-PEG immunity: emergence, characteristics, and unaddressed questions. *Wires Nanomed Nanobi* 2015, *7* (5), 655-677.

13. Richter, A. W.; Akerblom, E., Antibodies against Polyethylene-Glycol Produced in Animals by Immunization with Monomethoxy Polyethylene-Glycol Modified Proteins. *Int Arch Aller a Imm* 1983, *70* (2), 124-131.

14. Garay, R. P.; El-Gewely, R.; Armstrong, J. K.; Garratty, G.; Richette, P., Antibodies against polyethylene glycol in healthy subjects and in patients treated with PEG-conjugated agents. *Expert Opin Drug Del* 2012, *9* (11), 1319-1323.

15. Lipsky, P. E.; Calabrese, L. H.; Kavanaugh, A.; Sundy, J. S.; Wright, D.; Wolfson, M.; Becker, M. A., Pegloticase immunogenicity: the relationship between efficacy and antibody development in patients treated for refractory chronic gout. *Arthritis Res Ther* 2014, *16* (2).

16. Hershfield, M. S.; Ganson, N. J.; Kelly, S. J.; Scarlett, E. L.; Jaggers, D. A.; Sundy, J. S., Induced and pre-existing anti-polyethylene glycol antibody in a trial of every 3-week dosing of pegloticase for refractory gout, including in organ transplant recipients. *Arthritis Res Ther* 2014, *16* (2).

17. Sundy, J. S.; Baraf, H. S. B.; Yood, R. A.; Edwards, N. L.; Gutierrez-Urena, S. R.; Treadwell, E. L.; Vazquez-Mellado, J.; White, W. B.; Lipsky, P. E.; Horowitz, Z.; Huang, W.; Maroli, A. N.; Waltrip, R. W.; Hamburger, S. A.; Becker, M. A., Efficacy and Tolerability of Pegloticase for the Treatment of Chronic Gout in Patients Refractory to Conventional Treatment Two Randomized Controlled Trials. *Jama-J Am Med Assoc* 2011, *306* (7), 711-720.

18. Hershfield, M. S.; Ganson, N. J.; Kelly, S. J.; Scarlett, E. L.; Jaggers, D. A.; Sundy, J. S., Pharmacokinetics and Immunogenicity of Pegloticase (Pl) Infused Every 3 Weeks to Treat Refractory Gout (Rg), Including in Organ Transplant Recipients (Tr). *Ann Rheum Dis* 2012, *71*, 440-440.

19. Ganson, N. J.; Kelly, S. J.; Scarlett, E.; Sundy, J. S.; Hershfield, M. S., Control of hyperuricemia in subjects with refractory gout, and induction of antibody against poly(ethylene glycol) (PEG), in a phase I trial of subcutaneous PEGylated urate oxidase. *Arthritis Res Ther* 2006, *8* (1).

20. Armstrong, J.; Hempel, G.; Koling, S.; Chan, L. S.; Meiselman, H. J.; Fisher, T. C.; Garratty, G., Rapid clearance of PEG-asparaginase in ALL patients by an antibody against poly (ethylene glycol). *Blood* 2006, *108* (11), 526a-526a.

21. Armstrong, J. K.; Hempel, G.; Koling, S.; Chan, L. S.; Fisher, T.; Meiselman, H. J.; Garratty, G., Antibody against poly(ethylene glycol) adversely affects PEG-asparaginase therapy in acute lymphoblastic leukemia patients. *Cancer-Am Cancer Soc* 2007, *110* (1), 103-111.

22. Yang, Q., Jacob, T. M., McCallen, J. D., Moore, D. T., Huckaby, J. T., Edelstein, J. N., Lai, S. K., Analysis of Pre-existing IgG and IgM Antibodies against Polyethylene Glycol (PEG) in the General Population. *Anal Chem* 2016, *88* (23), 11804-11812.

23. Povsic, T. J.; Lawrence, M. G.; Lincoff, A. M.; Mehran, R.; Rusconi, C. P.; Zelenkofske, S. L.; Huang, Z.; Sailstad, J.; Armstrong, P. W.; Steg, P. G.; Bode, C.; Becker, R. C.; Alexander, J. H.; Adkinson, N. F.; Levinson, A. I.; Investigators, R.-P., Pre-existing anti-PEG antibodies are associated with severe immediate allergic reactions to pegnivacogin, a PEGylated aptamer. *J Allergy Clin Immun* 2016, *138* (6), 1712-1715.

24. Chen, B. M.; Su, Y. C.; Chang, C. J.; Burnouf, P. A.; Chuang, K. H.; Chen, C. H.; Cheng, T. L.; Chen, Y. T.; Wu, J. Y.; Roffler, S. R., Measurement of Pre-Existing IgG and IgM Antibodies against Polyethylene Glycol in Healthy Individuals. *Anal Chem* 2016, *88* (21), 10661-10666.

25. King, C.; Garza, E. N.; Mazor, R.; Linehan, J. L.; Pastan, I.; Pepper, M.; Baker, D., Removing T-cell epitopes with computational protein design. *P Natl Acad Sci USA* 2014, *111* (23), 8577-8582.

26. Qi, Y. Z.; Chilkoti, A., Protein-polymer conjugation - moving beyond PEGylation. *Curr Opin Chem Biol* 2015, *28*, 181-193.

27. Mero, A.; Fang, Z. H.; Pasut, G.; Veronese, F. M.; Viegas, T. X., Selective conjugation of poly(2-ethyl 2-oxazoline) to granulocyte colony stimulating factor. *Journal of Controlled Release* 2012, *159* (3), 353-361.

28. Veronese, F. M.; Visco, C.; Massarotto, S.; Benassi, C. A.; Ferruti, P., New Acrylic Polymers for Surface Modification of Enzymes of Therapeutic Interest and for Enzyme Immobilization. *Ann Ny Acad Sci* 1987, *501*, 444-448.

29. Hardwicke, J.; Ferguson, E. L.; Moseley, R.; Stephens, P.; Thomas, D. W.; Duncan, R., Dextrin-rhEGF conjugates as bioresponsive nanomedicines for wound repair. *Journal of Controlled Release* 2008, *130* (3), 275-283.

30. Schellenberger, V.; Wang, C. W.; Geething, N. C.; Spink, B. J.; Campbell, A.; To, W.; Scholle, M. D.; Yin, Y.; Yao, Y.; Bogin, O.; Cleland, J. L.; Silverman, J.; Stemmer, W. P. C., A recombinant polypeptide extends the *in vivo* half-life of peptides and proteins in a tunable manner. *Nature Biotechnology* 2009, *27* (12), 1186-U155.

31. Chirmule, N.; Jawa, V.; Meibohm, B., Immunogenicity to Therapeutic Proteins: Impact on PK/PD and Efficacy. *Aaps J* 2012, *14* (2), 296-302.

32. Shiraishi, K.; Hamano, M.; Ma, H. L.; Kawano, K.; Maitani, Y.; Aoshi, T.; Ishii, K. J.; Yokoyama, M., Hydrophobic blocks of PEG-conjugates play a significant role in the accelerated blood clearance (ABC) phenomenon. *Journal of Controlled Release* 2013, *165* (3), 183-190.

33. Sherman, M. R.; Williams, L. D.; Sobczyk, M. A.; Michaels, S. J.; Saifer, M. G. P., Role of the Methoxy Group in Immune Responses to mPEG-Protein Conjugates. *Bioconjugate Chem* 2012, *23* (3), 485-499.

CHAPTER 2

Revealing the Immunogenic Risk of Polymers

2.1 Abstract

Conjugation of poly (ethylene glycol) (PEG), known as PEGylation, has been the "gold standard" to ameliorate the pharmacokinetic (PK) and immunological profiles of proteins. Though free PEG polymer exhibits little or no immunogenicity, it tends to become immunogenic once attached to proteins, evoking PEG-specific antibody (Ab) responses much like a hapten. Clinical reports indicate that anti-PEG Abs could cause PEGylated biologic treatments to fail and even result in lethal adverse reactions. This immunogenic issue faced by PEG has motivated the introduction of zwitterionic poly(carboxybetaine) (PCB) as a PEG substitute for protein modification. However, while the importance of polymers' immunological safety has been increasingly recognized, there is not a comprehensive approach to scrutinize their immunogenic risks. Herein, we address this question for the first time by conjugating PEG and PCB polymers to a series of carrier proteins with escalating immunogenicity, and systemically assessing the tendency of anti-polymer Ab induction. Results indicate that titers of PEG-specific Abs were quantitatively correlated to the immunogenicity of carrier proteins at a high slope, revealing the propensity of PEG to become immunogenic. In comparison, the generation of PCB-specific Abs was minimal and insensitive to increased protein immunogenicity. Given the expanding pervasiveness of anti-PEG Abs and their detrimental impact in the clinic, this work casts insight into the immunological properties of PEG and PCB and has far-reaching implications for the development of polymer-protein conjugates.

2.2 Introduction

In the past decades, biotherapeutics have obtained huge success in the pharmaceutical market. While the remarkable specificity and potency of biologics enable them to provide great health benefits [1], their exploitation is subject to unique challenges including short *in vivo* half-life [2] and inherent immunogenicity [3, 4]. To hurdle these barriers and render proteins more suitable for therapeutic use, the attachment of PEG, a water-soluble synthetic polymer has been widely adopted as the "gold standard" [5-9]. PEG brushes densely grafted on protein surfaces can physically shield their epitopes from the immune surveillance and thus mitigate the immune responses specific to proteins. Moreover, the hydration layer formed by PEG through hydrogen bonding [10] increases the hydrodynamic size of underlying proteins and helps them to resist opsonization [11], thereby retarding the clearance of proteins and extending their circulation time [7, 9]. Since the first launch of commercial PEGylated protein, pegademase bovine in 1990 [12], over a dozen PEGylated biologics have been approved by the US Food and Drug Administration (FDA) and many more are in clinical pipelines [13, 14].

Notably, though the free form of PEG is believed to lack immunogenicity, PEG has been revealed to be immunogenic when attached onto immunogenic carriers, functioning like a hapten[15-17]. Up to now, a growing body of literature has highlighted the PEG immunogenicity as confirmed by the presence of PEG-specific Abs in both animals and humans [16-21]. Of particular concern, anti-PEG Abs have seen paramount negative impacts in clinical treatments as they could deprive patients of their life-sustaining therapies and result in life-threatening side effects. For example, pegloticase (Krystexxa®), a PEGylated uricase product approved by the US FDA in 2010, induced anti-PEG Abs in 89% of refractory chronic gout (RCG) patients[22-24]. Most of the patients who developed

high-level anti-PEG Abs consequently became non-responders to pegloticase and suffered severe adverse reactions such as infusion reactions[25]. Likewise, several other PEGylated protein drugs such as PEG-asparaginase (Oncaspar®) have also been plagued by the generation of anti-PEG Abs, which significantly hampered their safety and efficacy [26]. Exacerbating the matter, a markedly high occurrence (~72%) of pre-existing anti-PEG Abs was reported in a population of 377 healthy blood donors probably because of their long-term exposure to PEG-containing products in cosmetics, processed foods, and pharmaceuticals[19, 27-29]. These pre-existing anti-PEG Abs could cause severe allergic reactions when the patient received PEGylated therapeutics for the first time [23]. As a result, the titer of anti-PEG Abs in patients need to be pre-screened and monitored prior to and throughout a course of treatment with PEGylated proteins[17]. Altogether, the immunogenic nature of PEG raises serious concerns about its safety and applications in the pharmaceutical industry.

Recently, it was shown that the capacity of hydrophilic materials in mitigating immune responses closely correlated with the degree of their hydrophilicity [30]. Therefore, zwitterionic materials, a class of super-hydrophilic biomaterials that possess exceptional ion-induced hydration, are expected to own improved immunological properties [31, 32]. Among zwitterionic materials, poly(carboxybetaine) (PCB) deriving from glycine betaine, a naturally occurring osmolyte in the human body and a protein stabilizer, has attracted particular attention due to its unique biomimetic property [33-35]. The merits of PCB including good biocompatibility and superior hydrophilicity have motivated the exploitation of PCB as a PEG surrogate for protein modifications [36]. In the most recent demonstrations of this effort, PCB in the form of nanogel or conjugation was shown to improve the *in vivo* performance of uricase, an immunogenic enzyme [37-39]. While PEGylated

uricase led to a high level of anti-PEG Abs, no anti-PCB Abs were elicited by PCB-modified uricase, indicating that PCB retained non-immunogenic after being attached to uricase. However, clarifying the immunogenicity of PEG and PCB anchoring on certain proteins such as uricase could only partially unveil the immunological safety of these two polymers. It is still difficult to predict their immunological safety when they are attached to different proteins. In order to fully apprehend the immunogenic attributes of PEG and PCB, a detailed and comprehensive elucidation is necessitated.

The hapten-like character of PEG implies that attaching a polymer to carrier proteins could facilitate the exhibition of this polymer's immunogenicity. Therefore, systemically exploring the potential immune responses induced by a polymer under the immune-stimulating effect of diverse carrier proteins will shed light on the immunogenic risk of the polymer from a holistic point of view. Herein, PEG and PCB were conjugated to a series of proteins with the immunogenicity escalating from low to high (Fig. 2-1) and these conjugates were subcutaneously (SC.) injected to C57BL/6J mice at one dose per week for four-week immunization. The subsequent evaluation of polymer-specific Abs in mice sera has revealed a quantitative correlation between the titers of anti-PEG Abs and the immunogenicity of PEG's carrier proteins, validating the haptenic character of PEG while disclosing its strong potential to be immunogenic. The establishment of this relationship also allows the estimation of potential PEG-induced immune responses in protein conjugation based on the protein immunogenicity. In comparison, negligible levels of anti-PCB Abs were observed in the whole study. Such minimal immunogenicity of zwitterionic PCB was insensitive to the increased protein immunogenicity, suggesting the extremely low immunogenic risk of PCB.

2.3 Experimental Section

2.3.1 Materials

All chemicals and proteins, MSA, BSA, OVA, β-glucosidase, KLH were purchased from Sigma-Aldrich (St. Louis, MO) unless otherwise noted and were used as received. Methoxy-PEG- amine (mPEG-NH_2, 5kDa, 10kDa, and 20 kDa, 95%) were purchased from Nanocs Corporation. Goat anti-mouse IgM antibody and goat anti-mouse IgG antibody was purchased from Bethyl labs. The PCB polymers terminated with thiol group (PCB-SH, 5kDa, 10kDa, and 20 kDa) were synthesized as described below and freshly used. DTNB (Ellman's reagent) (5,5-dithio-bis-(2-nitrobenzoic acid) was purchased from Thermo Fisher Scientific (Waltham, MA). Pierce Protein Concentrators (150k MWCO) were purchased from Thermo Fisher Scientific (Waltham, MA). 3,3′,5,5′-Tetramethylbenzidine (TMB) substrate solution was purchased from eBioscience (San Diego, CA).

2.3.2 Synthesis of 3-acrylamido-N-(2-(tert-butoxy)-2-oxoethyl)-N,N-dimethylpropan-1-aminium (t-Butyl CBAAm) (Scheme 1-1)

The synthesis of t-Butyl CBAAm monomer was according to our previous published protocol. Typically, in a 1-L round-bottom flask fitted with a stir bar, N,N-dimethylaminopropyl acrylamide (1, 60.01 g, 0.384 mol, 1 eq), tert-butyl bromoacetate (85.1 mL, 0.576 mol, 1.5 eq), and hydroquinone (500 mg as a polymerization inhibitor) were dissolved in acetonitrile (350 mL). The reaction mixture was stirred in an oil bath (60 °C) for 12 h and then cooled to room temperature (RT). The product was then precipitated in diethyl ether for 8 h, filtered via a fritted funnel, and dried under vacuum overnight to yield a white powder. Yield: 98%. Proton ^{1}H NMR (300 MHz,

CDCl3) δ (ppm): 8.13 (t, 1H, J = 5.6 Hz), 6.35 (dd, 1H, J = 17.1, 10.2 Hz), 6.13 (dd, 1H, J = 17.1, 1.8 Hz), 5.48 (dd, 1H, J = 10.2, 1.8 Hz), 4.34 (s, 2H), 3.92 (m, 2H), 3.40 (s, 6H), 3.32 (m, 2 H), 2.02 (m, 2H), 1.37 (s, 9H).

2.3.3 Synthesis of chain transfer agent (CTA) for PCB synthesis (Scheme 1-2)

In a rubber-stoppered 250-mL RB flask with stir bar, 2-(dodecylthiocarbonothioylthio)-2-methylpropionic acid N-hydroxysuccinimide ester (2, 1.13g, 2.45 mmol, 1.1 eq) was dissolved in 20 mL anhydrous dichloromethane. The flask was placed in a low-form 500-mL vacuum flask containing ethanol and dry ice was added until the ethanol bath dropped to below -20 °C. In a separate rubber-stoppered 100-mL RB flask, N-Boc-ethylenediamine (1, 0.36 g, 2.25 mmol, 1 eq) and triethylamine (0.25 g, 2.47 mmol, 1.1 eq) were dissolved in 10 mL anhydrous dichloromethane and delivered via syringe into solution 2. The reaction was stirred for 12 h while the ethanol bath was manually kept to ≤20 °C with dry ice, then transferred to a 250-mL separatory funnel for 3x deionized water wash and 1x brine wash to remove unreacted water-soluble agents. The organic phase was dried with sodium sulfate for 1 h at RT, filtered to remove the insoluble salt, and fractionated on a silica gel column (Isco Chromatography system, Teledyne Technologies, Thousand Oaks, CA) using a mixture of ethyl acetate and hexane (ramping over 45 min from 0% to 15% EtoAc). The fractions containing the product 3 were combined, rotavapored, and further dried under vacuum for 48 h. Yield: 94%. Proton ^{1}H NMR (300 MHz, CDCl3) δ (ppm): 6.91 (s, 1H), 4.85 (s, 1H), 3.28 (dt, J = 14.8, 6.7 Hz, 6H), 1.68 (s, 6H), 1.46-1.34 (m, 11H), 1.31-1.18 (m, 18H), 0.85 (t, J = 6 Hz, 3H).

2.3.4 Synthesis of PCB-SH (Scheme 1-3) and mPEG-SH

PCB-SH was prepared by a combination of reversible addition fragmentation chain-transfer (RAFT) polymerization, aminolysis, acid deprotection and amine-to-thiol conversion steps. In a typical procedure of PCB-SH (20KDa, MW) preparation, CTA (0.27 mmol, 1 eq), t-Butyl CBAAm (1, 6.745 g, 19.2 mmol, 70 eq), V-501 (initiator, 8.9 mg, 0.054 mmol, 0.2 eq) were firstly dissolved in anhydrous dimethylformamide (DMF, 35 mL) in a 100-mL round-bottom flask fitted with a stir bar. The flask was sealed with a rubber septum and bubbled with N_2 for 30 min, then transfer to an oil bath (70 °C) for 4 h of stirring. The resultant polymer, P(tBu-CBAAm) (2), was precipitated in ice-cold ethyl acetate three times and dried under vacuum. Triethylamine (280 μL, 2.009 mmol, 10 eq), hexylamine (264 μL, 1.998 mmol, 10 eq) and tris(2-carboxyethyl) phosphine hydrochloride (TCEP, 86.2 mg, 0.301 mmol, 1.5 eq) were dissolved in anhydrous DMF (3 mL) to remove the trithiocarbonate group from 995.0 mg of P(tBu-CBAAm). After stirring at RT for 5 h, the reaction solution turned into colorless. Then the product (3) was precipitated in ice-cold ethyl acetate and dried under vacuum. Then, PCB-NH_2 (4) was obtained after 4h of acid deprotection (TFA, ~2 mL per 1 g polymer, ~10 eq), followed with three times of precipitation and a dialysis-lyophilization step. For protein conjugation, PCB-NH_2 was converted to PCB-SH (5). PCB-NH_2 (10mg for 5kDa, 20mg for 10kDa, 40mg for 20kDa) was reacted with Traut's reagent (molar ratio 1/1) in 0.5mL PBS for 2h and freeze-drying for 48h. Similarly, mPEG-NH_2 polymers (5kDa, 10kDa, 20kDa) purchased directly from Nanocs were also converted to thiol-terminated (PEG-SH) by reaction with Traut's reagent at a molar ratio of 1:1 in PBS (pH7.4) for 2h and freeze-drying for 48h.

2.3.5 Conjugation of polymers to proteins (Scheme 1-4)

Protein powder (1mg) was dissolved in 0.5mL pH7.4 PBS buffer (50mM) and BMPS crosslinker (0.175mg, 40mg/mL in DMSO) were added into the above solution (crosslinker/accessible lysines=2-2.5/1) for 1-h reaction. After washing the proteins for 3 times using 30kDa ultrafiltration, thiol-terminated methoxy PEG (mPEG-SH) or thiol-terminated PCB (PCB-SH) was dissolved in PBS buffer (10mg for 5k PEG, 20mg for 10kDa PEG, 40mg for 20k PEG, 0.5ml) and then added into the protein residue for conjugation. After 2-h reaction at room temperature, the product was purified again with 100kDa ultrafiltration. The number of PEG and PCB polymers grafted on each protein was estimated by Ellman's reagent, which reacts quantitatively with free thiol groups (-SH). Briefly, after the protein-polymer conjugation step, the rest of unreacted polymers (mPEG-SH, PCB-SH) was quantified by the Ellman's reagent following the manufacturer's protocol. Then, the number of polymers grafted on each protein could be calculated by (mole of total polymers – mole of unreacted polymers) / mole of proteins.

2.3.6 Animal studies

The University of Washington Institutional Animal Care and Use Committee (IACUC) approved all animal experiments under protocol #4203-01. Male C57BL/6J mice of ~20 g were randomly divided.

2.3.7 Immunogenicity study of proteins

To clarify the protein immunogenicity, male C57BL/6J mice in groups of five were immunized with bare proteins. Each group of mice was subjected for four SC. injections of proteins (MSA/BSA/OVA/beta-glucosidase/KLH) at one dose (2mg/kg weight) per week. The mice sera

were collected on the 28th day (one week after the last injection) and prepared for the ELISA test of protein-specific IgM and IgG respectively.

2.3.8 Animal immunization with protein-polymer conjugates

To examine the immunogenicity of PEG and PCB after being attached to proteins, male C57BL/6J mice in groups of five were immunized with the protein-polymer conjugates. Thirty groups of animals were subjected to four SC. injections of proteins (MSA/BSA/OVA/beta-glucosidase/KLH) conjugated with PEG (5kDa/10kDa/20kDa) or PCB (5kDa/10kDa/20kDa) respectively at one dose (2mg protein/kg weight) per week. Sera were collected from mice in each group on the 28th day (one week after the last injection) and prepared for the next ELISA and SPR test.

2.3.9 ELISA test

For the detection of anti-protein antibodies, antigens used in direct ELISAs for plate coating consisted of MSA, BSA, OVA, beta-glucosidase, and KLH. For the detection of anti-polymer antibodies, antigens used in direct ELISAs for plate coating consisted of PEG-BSA conjugates (for the mice sera immunized with PEG-conjugated MSA, OVA, beta-glucosidase, and KLH), PEG-OVA conjugates (for the mice sera immunized with PEG-conjugated BSA), PCB-BSA conjugates (for mice sera immunized with PCB-conjugated MSA, OVA, beta-glucosidase, or KLH) and PCB-OVA conjugates (for mice sera immunized with PCB-conjugated BSA).

For ELISA experiments, 100 μL antigen solution (10 μg/mL of protein concentration) prepared in 0.1 M sodium carbonate buffer (pH 10.5), was used to coat each well of the 96-well plates. During

coating procedure, plates were incubated at 4 °C overnight. After removing antigen solutions, the plates were washed five times using PBS (pH 7.4) and then filled with blocking buffer (1% nonfat milk solution in 0.1 M Tris buffer, pH 8.0). It is important to avoid using any buffer that contains PEG-like detergents, e.g., Tween 20 and Tween 80. After incubation at room temperature for 1 h, blocking buffer was removed, and all wells were washed by PBS for another five times. Serial dilutions of monoclonal anti-PEG abs in PBS containing 1% nonfat milk were added to the plates (100 μL/well), which were incubated for 1 h at 37 °C. The plates were then washed five times with PBS, followed by adding secondary antibody HRP conjugates (100 μL/well, dilution 1:50000, Bethyl Labs). After adding the secondary antibody, plates were incubated at room temperature for 1 h and then washed five times using PBS before the addition of 100 μL/well HRP substrate 3,3′,5,5′-tetramethylbenzidine. The plates were shaken for 15 min, and 100 μL stop solution (0.2 M H_2SO_4) was added to each well. Absorbance at 450 (signal) and 570 nm (background) was recorded by a microplate reader.

2.3.10 SPR detection of anti-polymer antibodies

For coating of PCB on gold chips, UV-cleaned SPR sensor chips were firstly coated with ATRP initiator self-assembled monolayers were prepared by soaking in 0.2 mM mercaptoundecyl bromoisobutyrate in pure ethanol for 24 h. The chips were then removed, rinsed with ethanol, THF, and ethanol, and then blown dry using filtered air and placed into a custom glass tube reactor. In a separate glass tube, 8.86 mg CuBr, 57.87 mg 2,2′-bipyridine, and 600 mg of CBAAm were added. Both tubes were then placed under nitrogen protection. Appropriate volumes of nitrogen-purged methanol and water were then added (total volume was 4 mL) to the solids according to the necessary solvent ratio. For example, an ATRP water content of 10% was obtained by adding

3.6 mL of methanol and 0.4 mL of water. The water content was varied from 0 to 90% (v/v). After dissolving the solids (~15 min), the mixture was then transferred to the reactor tube under nitrogen protection and allowed to react for 3 h at 25 °C in a shaker set to 120 rpm. Following the reaction, the chips were rinsed with water and then submerged overnight in PBS. For the coating of PEG on gold chips, the gold SPR chip was modified with mPEG-SH by immersing the UV-ozone cleaned chips in the corresponding mPEG-SH ethanol solution (0.1 mg/mL). The thickness of PCB and mPEG brushes coated on the chip was measured by a spectroscopic ellipsometry (Sentech SE-850). For the detection of anti-polymer antibodies in sera, SPR experiments were conducted following the SPR program designed as below:

The gold chips coated with PCB or mPEG were flowed step by step with PBS for 10 min, 1:20 diluted mice serum in PBS for 10 min and PBS for 20 min at flow rate of 30 μL/min. Polymer-specific antibodies if any existing in the serum will bind to the chip surface. After the potential adsorption of anti-polymer antibodies, goat anti-mouse IgM or IgG (10 μg/mL) was flowed continuously for 10 min, followed by PBS for 15 min. This step allows the differentiation of IgG and IgM isotypes among the adsorbed anti-polymer antibodies. A custom-built SPR sensor was used in this study and a 1-nm SPR wavelength shift represents a surface coverage of ~17 ng/cm^2 for proteins. Detection limit for the SPR sensor used in this work is 0.3 ng/cm^2.

2.3.11 Statistics

All measurements are represented as mean ± standard deviation. The two-tailed student t-test was used to assess statistical differences between a pair of groups. Significant difference was assumed at $P < 0.05$.

2.4 Results and Discussion

2.4.1 Immunogenicity index of bare proteins

To assess the immunogenic risk of polymers, five types of proteins from different sources: murine serum albumin (MSA), bovine serum albumin (BSA), ovalbumin (OVA), beta-glucosidase, Keyhole limpet hemocyanin (KLH) were chosen as the carrier proteins to promote the exhibition of polymer's immunogenicity. It is noteworthy that KLH with extremely high immunogenicity in mammalian hosts is the most commonly used to facilitate the induction of immune responses to haptens, due to its remarkable immune-stimulating properties, large size, numerous sites for conjugation.

The immunogenicity of these protein carriers was evaluated. Briefly, five groups of C57BL/6J mice (n=5) were subjected to four weekly SC. immunization with each protein sample, after which mice sera were collected on the 28th day to detect anti-protein Abs. Two main types of Ab elicited by proteins, IgM and IgG, were measured by ELISA tests (Fig. 2-2) and their titers were summarized in Fig. 2-3. It is noticeable that the protein immunogenicity depends on the genetic distance between the protein source and the injected host. In order to directly and quantitatively gauge the protein immunogenicity, we here defined a parameter of "protein immunogenicity index", calculated as the sum of anti-protein IgM titer (-log10) and anti-protein IgG titer (-log10) after four weekly SC. immunizations of a specific protein. Based on the protein immunogenicity index, we were able to quantitatively compare the immunogenicity of selected carrier proteins and rank it in the following order: MSA < BSA < OVA < beta-glucosidase < KLH.

2.4.2 Preparation of polymer-protein conjugates

Besides the attributes of polymers and their anchoring proteins [18], other factors including the linkage chemistry [19], molecular weight [20] and coating density [40] of polymers may also affect the generation of polymer-induced immune responses and thus complicate this investigation on the immunological property of polymers. Therefore, these factors should be considered and reasonably controlled to derive a convincing conclusion on the potential of a polymer to evoke immune responses. In order to exclude the impact of linkages that connect proteins and polymers, PEG and PCB were conjugated onto proteins through the same thiol-ene chemistry. Briefly, primary amine groups provided by free lysine residues on protein surfaces were firstly activated by a heterobifunctional cross-linker (BMPS) to introduce thiol-reactive maleimide groups. Then, thiol-terminated PEG and PCB were both grafted onto protein surfaces through an efficient maleimide-thiol reaction. For a fair comparison, the immunogenicity of protein-anchored PEG would be parallelly compared to that of PCB at the same molecular weight. Thus, three molecular weight (5kDa, 10kDa, and 20kDa) of PEG and PCB were selected to comprehensively examine the immunological properties of these two polymers. For a fair comparison, the immunogenicity of protein-anchored PEG was parallelly compared to that of PCB at the same molecular weight. Additionally, to maximize the induction of polymer-specific Abs and ensure a similar exposure of immunogenic epitopes on carrier proteins for a fair comparison, densities of PEG and PCB chains grafted on different proteins were adjusted to be at a moderate, but similar level as confirmed by the gel permeation chromatogram (GPC, Fig. 2-4 – 2-9, Table 2-1–2-5) and Ellman's test (Fig. 2-10).

2.4.3 Detection of anti-polymer Ab responses

Following the same injection schedule of bare proteins, the four weekly SC. immunizations of PEG-protein and PCB-protein conjugates were conducted on C57BL/6 mice at one dose per week and mice sera were collected on the 28th day (one week after the last immunization). The generation of polymer-induced Abs was measured by the ELISA test (Fig. 2-11) and titers of IgM and IgG specific to PEG or PCB are summarized in Fig. 2-12. Based on the data above, we were able to outline a linear trendline of polymer immunogenicity (anti-polymer IgM/IgG titer versus protein immunogenicity index) (Fig. 2-13), which reveals a quantitative correlation between the immunogenicity of proteins and protein-associated polymers. Notably, this trend is particularly phenomenal in the case of protein conjugates containing all three molecular weights of PEG (5kDa, 10kDa, and 20kDa), which is consistent with previous findings that the anchoring to carrier proteins would drive the exhibition of PEG immunogenicity. It also confirms the role of haptenic effect in the generation of anti-PEG antibodies. Moreover, the level of anti-PEG Abs sharply increases with the escalation in protein immunogenicity, reflecting the high propensity of PEG to become immunogenic. In stark contrast, the PCB-specific Ab elicited by PCB-protein conjugates was barely detected in the ELISA tests, even for the one containing the most immunogenic carrier protein, KLH. PCB with three molecular weights (5kDa, 10kDa, 20kDa) all exhibited minimal immunogenicity in the whole study and insensitivity to the change of their carrier proteins.

To confirm the presence or absence of anti-polymer Abs in the mice sera immunized with PEG-KLH or PCB-KLH conjugates, SPR tests were employed in addition to ELISA. Compared to ELISA, SPR is a non-label, fast and highly-sensitive detection technique. To detect anti-PEG or anti-PCB antibodies, we modified the surface of gold chips with PEG self-assembled monolayer

(SAM) or PCB polymer brush layers. Both PEG and PCB can effectively resist nonspecific protein adsorption from diluted serum to create a non-fouling background for highly sensitive and specific detections. When serum samples flow over a modified chip surface, polymer-specific antibodies if any will bind to the surface. The subsequent flow of secondary Ab (anti-IgM or anti-IgG) will be able to amplify the SPR signal and verify the existence of anti-IgM and anti-IgG antibodies against the surface coated polymer. Consistent with ELISA results, all the mice sera treated by PEG-KLH conjugates displayed a relatively high-level adsorption of anti-IgM Abs and anti-IgG Abs (Fig. 2-14), further demonstrating the immunogenic risk of PEG. Besides, higher adsorption of anti-IgM Abs than anti-IgG Abs on SPR chips also substantiates that anti-PEG Abs are mainly composed of IgM isotype. In comparison, none of the blood sera treated with PCB-KLH conjugates showed a detectable response on a PCB-coated chip surface, convincingly confirming the immune-stealth property of zwitterionic PCB as well as its immunological safety.

Though the exact biological mechanism of PEG immunogenicity is not completely clear, recent studies have pinpointed its chemical origin. The hydrophobicity of PEG was found to account for the generation of anti-PEG Abs [41]. PEG is known for its amphiphilic character, containing both hydrophilic and hydrophobic moieties and being soluble in both polar and nonpolar organic solvents [42]. The direct and competitive ELISA tests have manifested the hydrophobic blocks in PEG including its backbone ($-CH_2-CH_2-$) and methoxy terminal ($-OCH_3$) as the antigenic and immunogenic epitopes of PEG [20, 43, 44]. Replacing the methoxy group of PEG with a relatively more hydrophilic hydroxyl group was shown to alleviate anti-PEG Ab responses [44]. The low potential of PCB to induce immune responses can be ascribed to its super-hydrophilicity, which not only blocks the immune recognition but also makes it extremely difficult for the immune

system to develop Abs specifically binding to PCB. In contrast to PEG that contains hydrophobic moieties, the entirely-hydrophilic PCB possesses a minimal propensity for any hydrophobic interactions. A recent study with sum frequency generation (SFG) vibrational spectroscopy shows that the hydration layer of PEG surface was disrupted as protein molecules approach the surface, making it vulnerable to protein adsorption whereas the hydration layer of zwitterionic material was not disturbed in the presence of protein molecules, resulting in little or no association with proteins [45]. In the absence of interactions with proteins, strongly hydrated zwitterionic PCB is less likely to exhibit hapten-like character when covalently attached to proteins and thus contains very low immunogenic risk.

2.5 Conclusions

In summary, this work has comprehensively examined the immunogenic risk of PEG and PCB, shedding light on their immunological safety for biomedical applications. The quantitative relationship between the level of anti-PEG Ab responses and the immunogenicity of carrier proteins was clearly observed and established, revealing the high immunogenic risk of PEG. This correlation also allows one to estimate the potential of anti-PEG Ab response based on the protein immunogenicity. Moreover, we showed the low immunogenic risk of PCB as evidenced by the negligible titers of Abs reactive with PCB even when it is conjugated even to highly immunogenic KLH as confirmed by ELISA and SPR tests. This work not only proposes a holistic way to assess the immunogenic risk of polymers but also provides valuable information to guide the development of safe therapeutics involving polymers.

2.6 Schemes, Figures and Tables

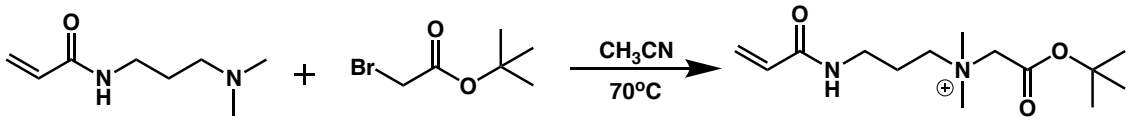

Scheme 1-1. Synthesis scheme of t-Butyl CBAAm monomer

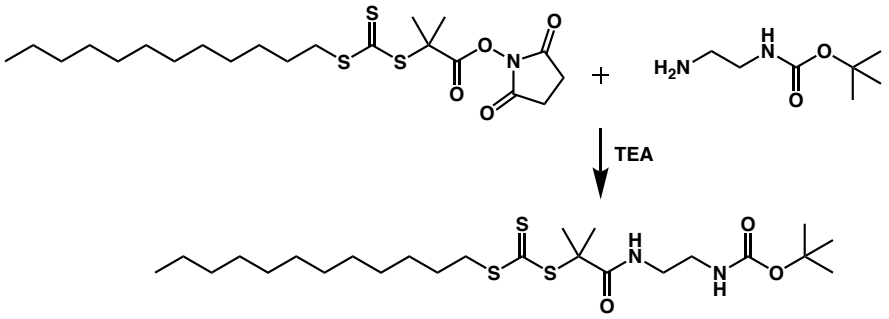

Scheme 1-2. Synthesis scheme of the CTA for PCB polymerization

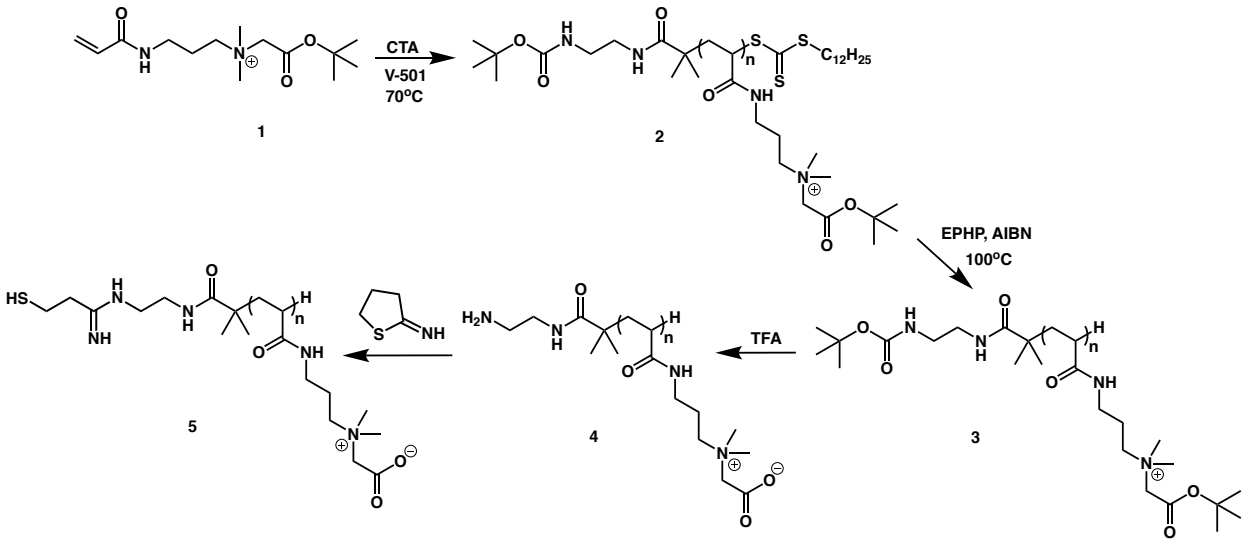

Scheme 1-3. Synthesis scheme of PCB-SH.

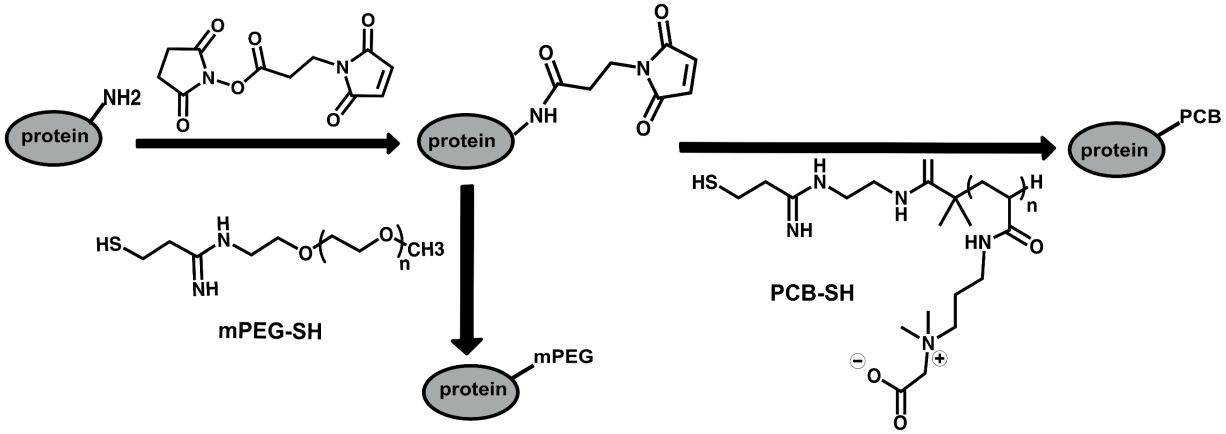

Scheme 1-4. Scheme of the conjugation chemistry.

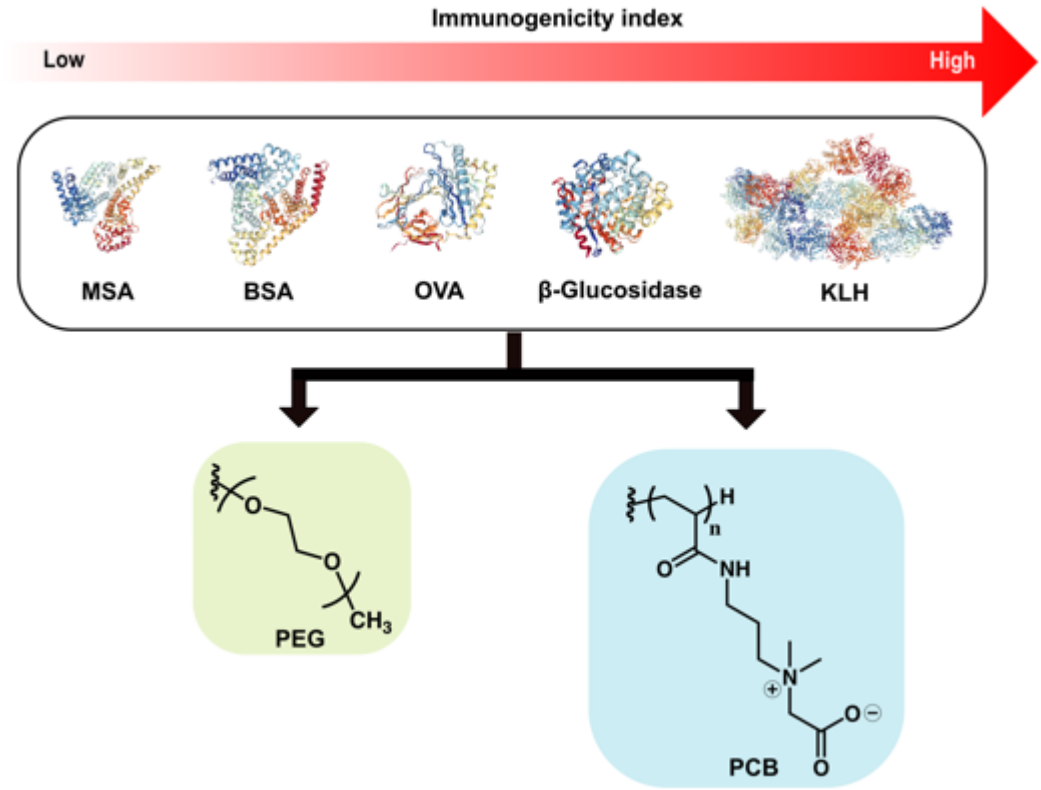

Figure 2-1. Illustration of the proteins and polymers used for conjugation.

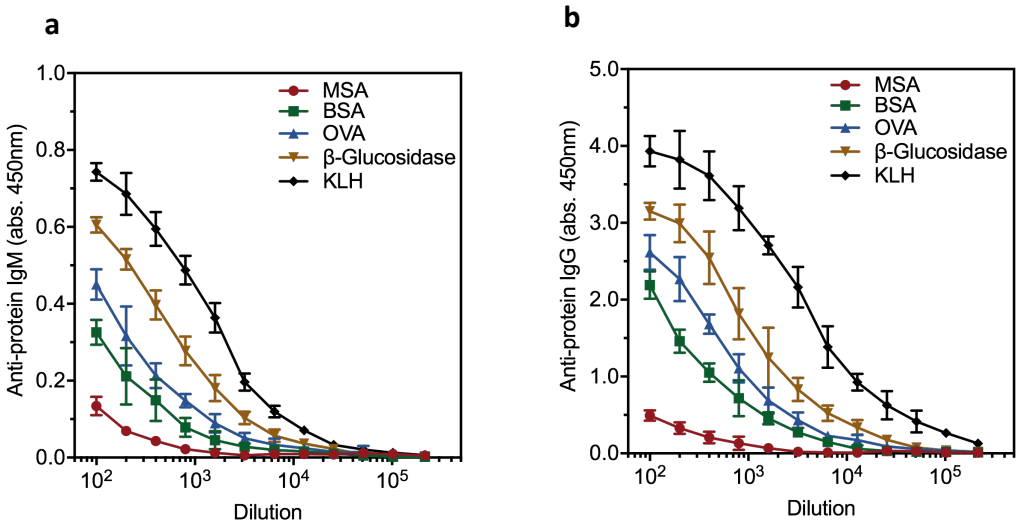

Figure 2-2. ELISA test of protein immunogenicity: Ab responses (a. IgM, b. IgG) towards bare proteins after four weekly SC. administrations of MSA, BSA, OVA, beta-gluocosidase, and KLH. Results are shown as OD 450nm vs. dilution fold.

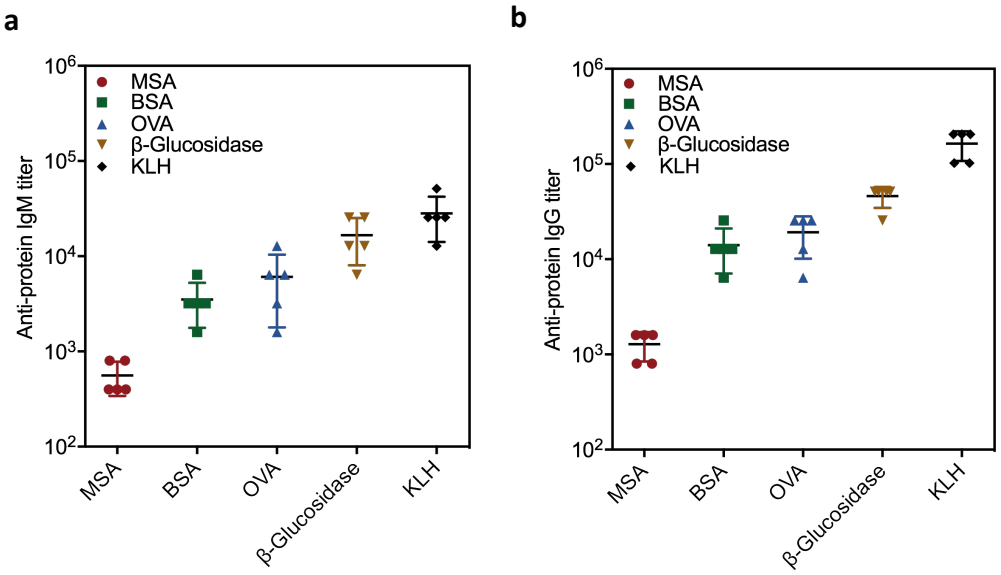

Figure 2-3. Study of protein immunogenicity. Titers of protein-specific IgM (a) and IgG (b) after four weekly SC. administrations of MSA, BSA, OVA, beta-gluocosidase, and KLH in C57BL/6J mice were measured by ELISA tests.

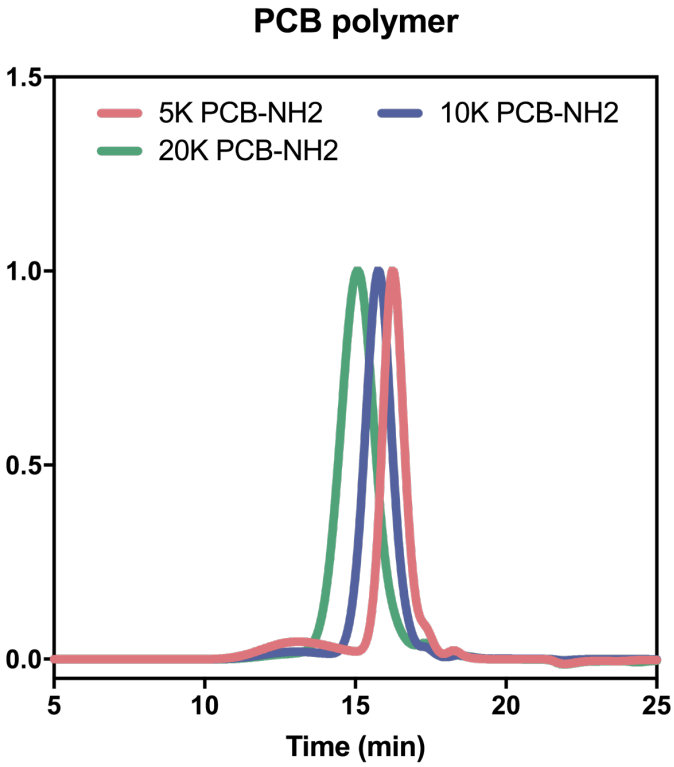

Figure 2-4. GPC traces of PCB polymers (5kDa, 10kDa, 20kDa) for protein conjugation.

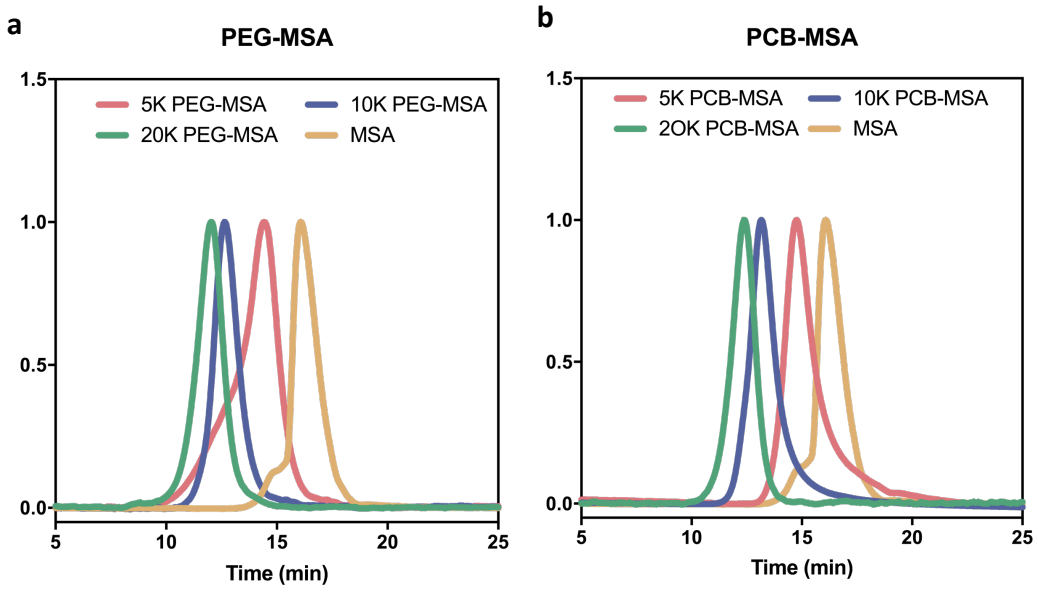

Figure 2-5. GPC traces of MSA conjugated with PEG (a) and PCB (b).

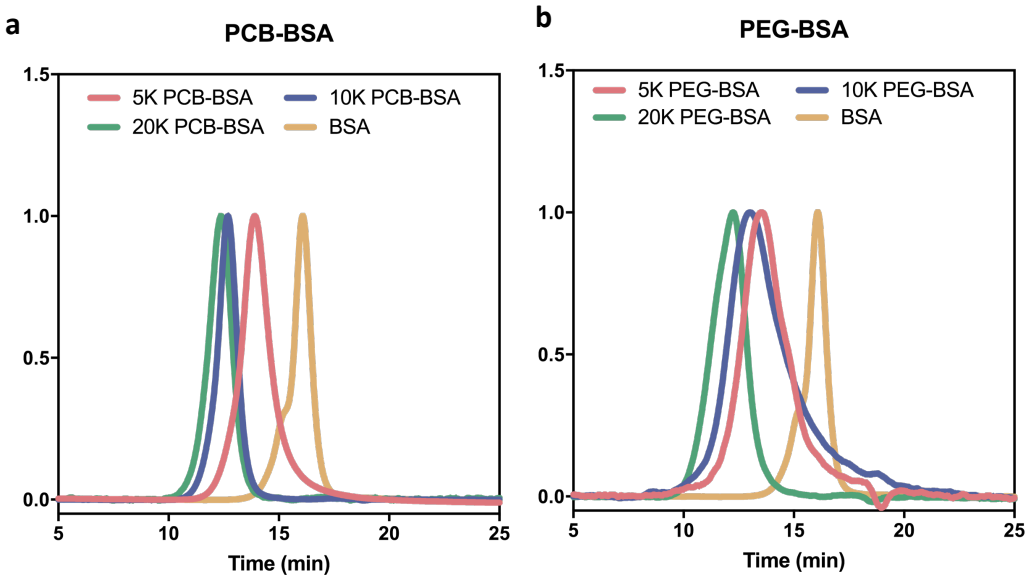

Figure 2-6. GPC traces of BSA conjugated with PEG (a) and PCB (b).

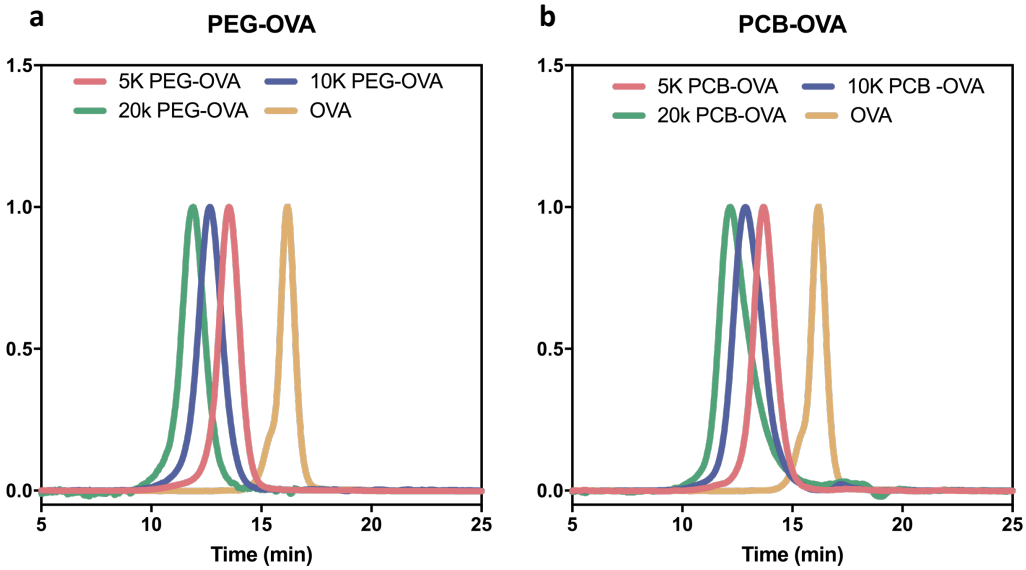

Figure 2-7. GPC traces of OVA conjugated with PEG (a) and PCB (b).

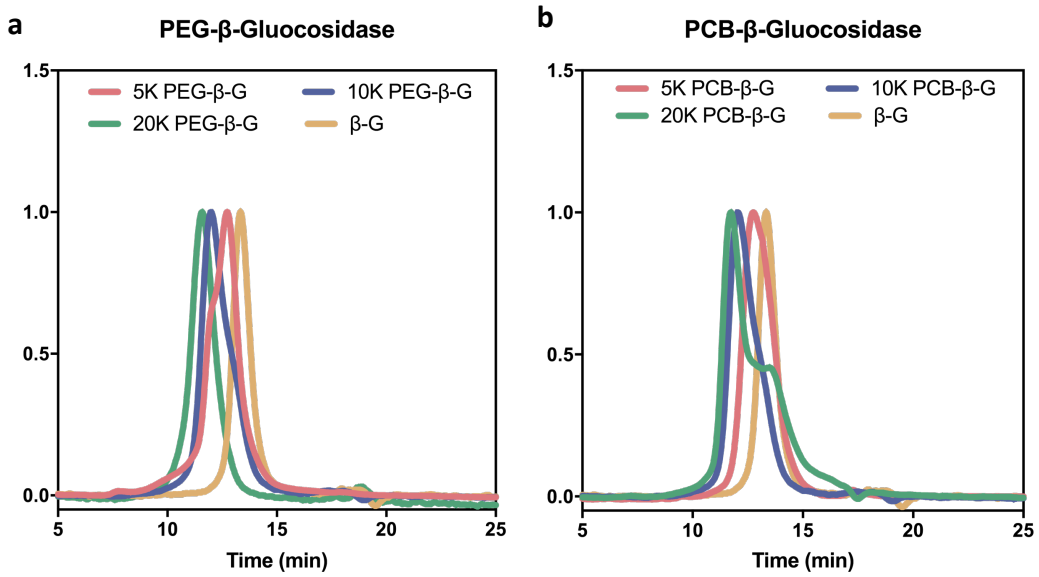

Figure 2-8. GPC traces of β-Glucosidase conjugated with PEG (a) and PCB (b).

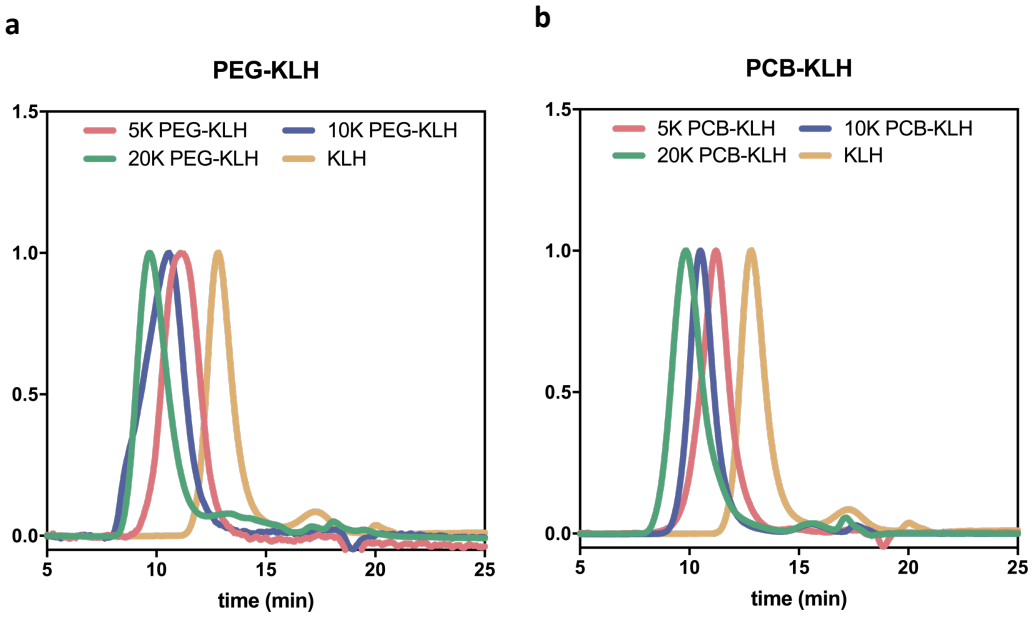

Figure 2-9. GPC traces of KLH conjugated with PEG (a) and PCB (b).

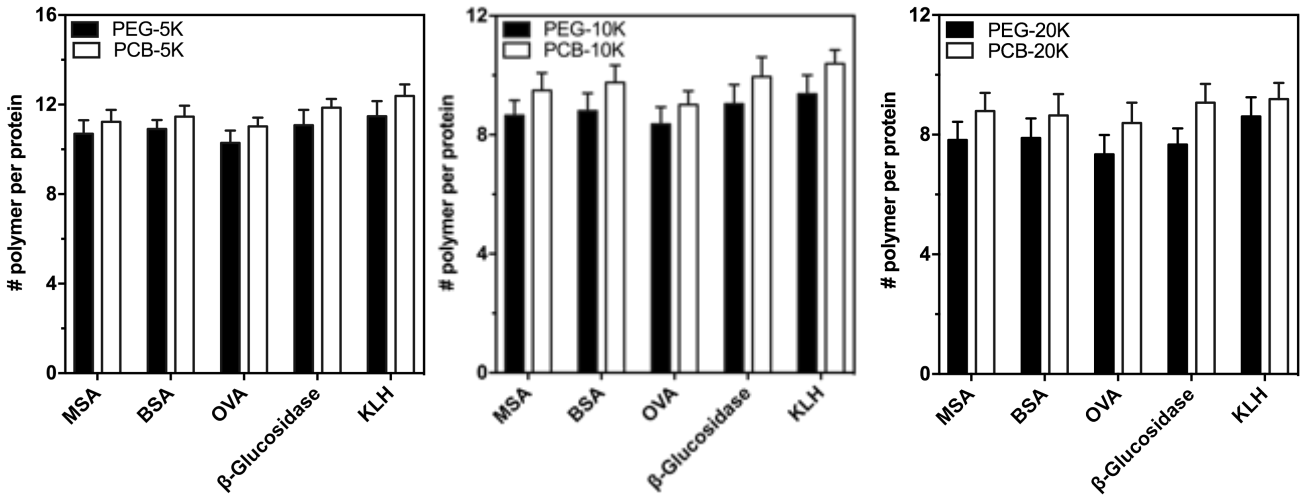

Figure 2-10. Number of PEG and PCB polymer chains grafted on proteins at the molecular weight of 5kDa (a), 10kDa (b) and 20kDa (c).

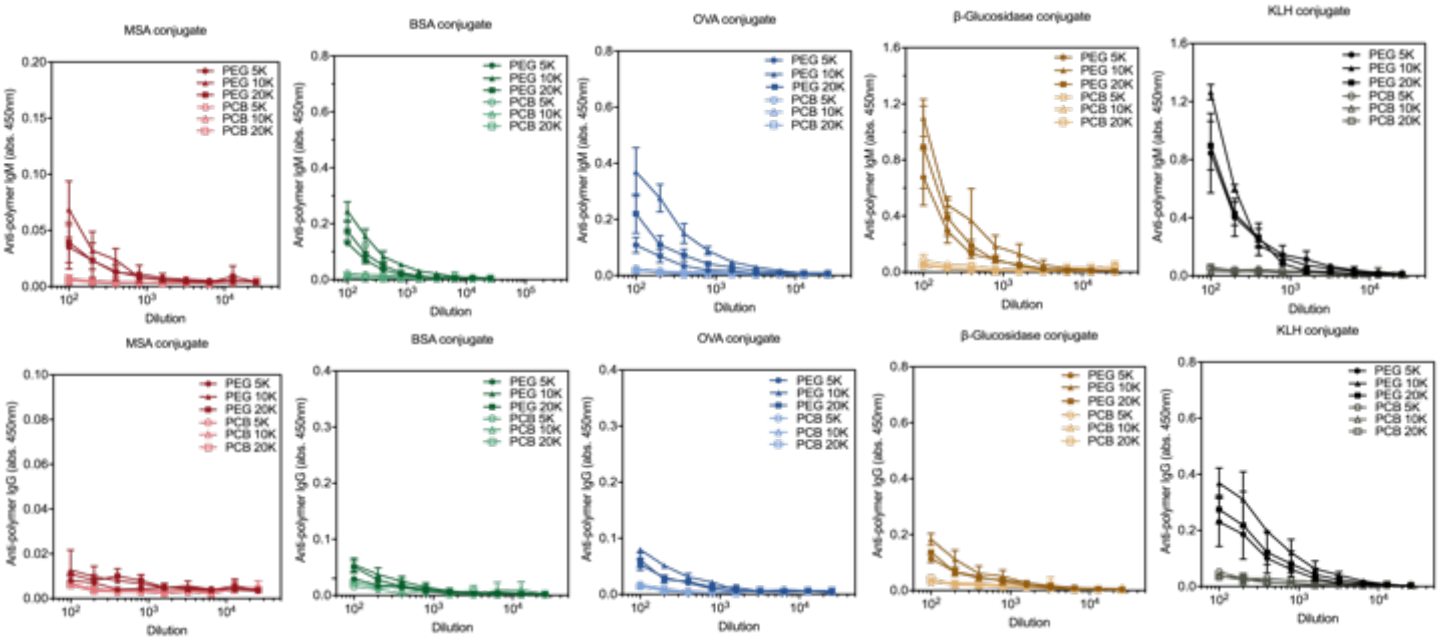

Figure 2-11. ELISA test of polymer immunogenicity: Ab responses towards protein-associated PEG (5/10/20 kDa) and PCB (5/10/20 kDa) after four weekly SC. administrations of polymer-protein (MSA/BSA/OVA/beta-gluocosidase/KLH) conjugates. Results are shown as OD 450nm vs. dilution fold.

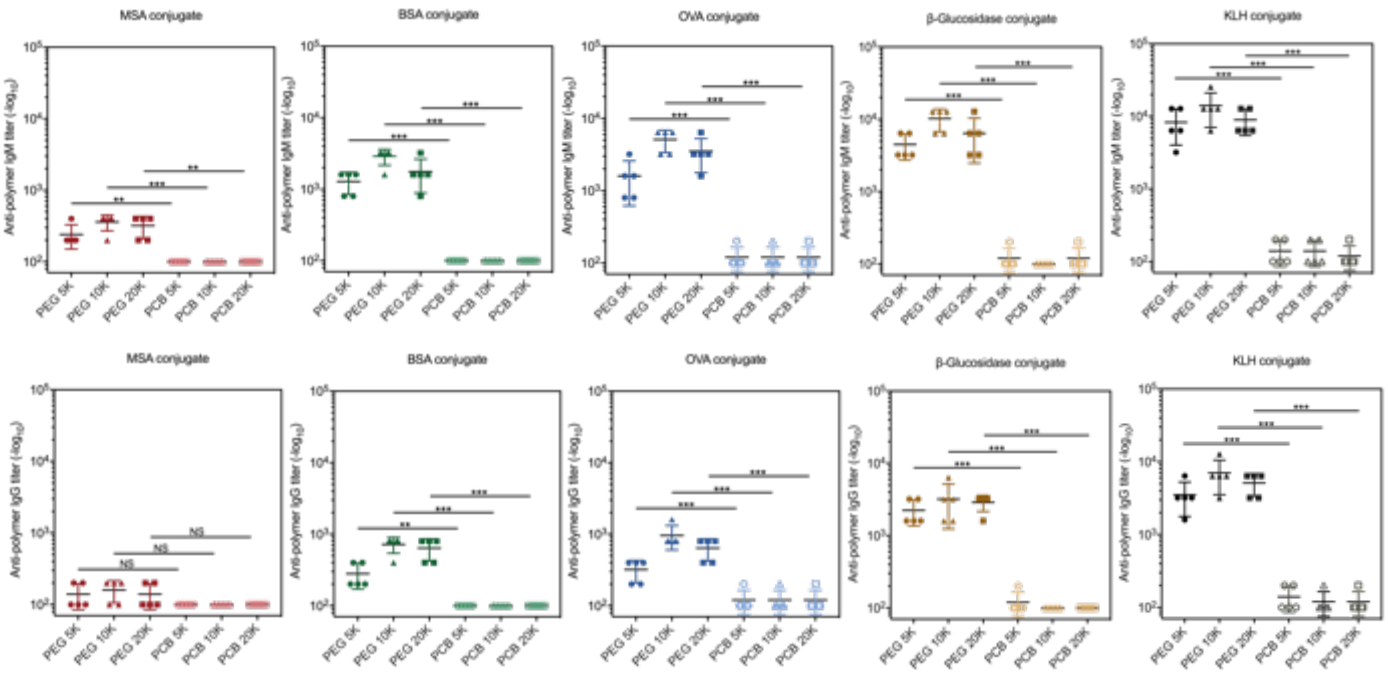

Figure 2-12. Study of polymer immunogenicity. Titers of PEG- or PCB-specific IgM (above) and IgG (bottom) were measured by ELISA tests after four weekly SC. administrations of polymer-protein (MSA/BSA/OVA/beta-gluocosidase/KLH) conjugates in C57BL/6J mice. The immunogenicity of PEG (5/10/20kDa) are compared to that of PCB at the same molecular weight using student test for statistical analyses. *P<0.05; **P<0.01; ***P<0.005.

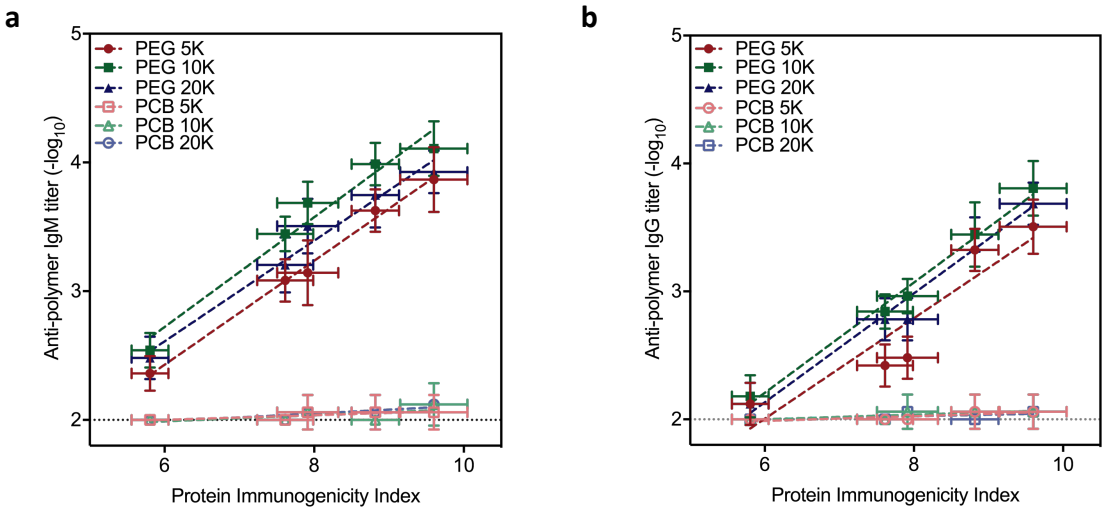

Figure 2-13. Correlation of the anti-polymer Ab response (a. IgM; b. IgG) and protein immunogenicity index. The protein immunogenicity index is defined as the sum of anti-protein IgM titer (-log10) and anti-protein IgG titer (-log10) after four weekly SC. immunizations with a specific protein in C57BL6 mice (n=5).

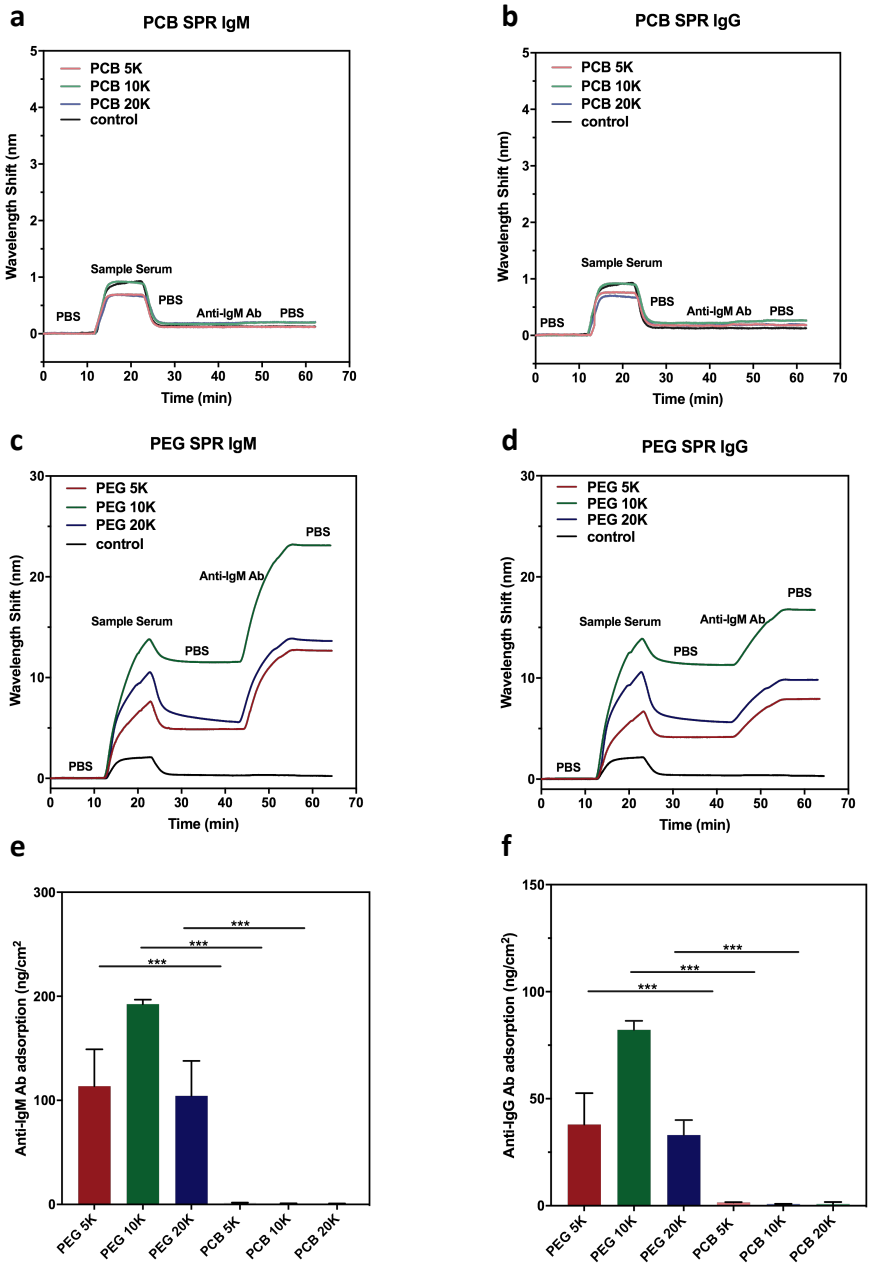

Figure 2-14 (a-d) Representative SPR sensorgrams for the detection of anti-PCB Ab IgM (a) and IgG (b), and anti-PEG IgM (c) and IgG (d) in the sera from mice immunized with the KLH conjugates conjugated with the specific polymer. The secondary adsorption of goat anti-mouse IgM (e) and goat anti-mouse IgG (f) detected by SPR was summarized for statistical analyses using student test. ***P<0.005

Table 2-1. The parameters of the final MSA conjugates.

Samples	Molecular Weight (KDa)	# polymer per monomer protein
MSA	67	-
5K PEG-MSA	112±10	7-11
10K PEG-MSA	140±5	7-8
20K PEG-MSA	215±11	7-8
5K PCB-MSA	116±9	8-12
10K PCB-MSA	155±8	8-10
20K PCB-MSA	229±14	7-9

Table 2-2. The parameters of the final BSA conjugates.

Samples	Molecular Weight (KDa)	# polymer per monomer protein
BSA	67	-
5K PEG-BSA	114±5	8-10
10K PEG-BSA	151±8	8-9
20K PEG-BSA	215±12	7-8
5K PCB-BSA	120±10	9-13
10K PCB-BSA	162±16	8-11
20K PCB-BSA	235±11	8-9

Table 2-3. The parameters of the final OVA conjugates.

Samples	Molecular Weight (KDa)	# polymer per monomer protein
OVA	43	-
5K PEG-OVA	86±4	8-9
10K PEG-OVA	122±5	7-8
20K PEG-OVA	183±10	7-8
5K PCB-OVA	95±5	9-11
10K PCB-OVA	141±6	9-10
20K PCB-OVA	200±11	7-8

Table 2-4. The parameters of the final β-Glucosidase conjugates.

Samples	Molecular Weight (KDa)	# polymer per monomer protein
β-Glucosidase	340	-
5K PEG-β-G	387±8	8-11
10K PEG- β-G	420±12	7-9
20K PEG- β-G	492±15	7-8
5K PCB- β-G	390±11	8-12
10K PCB- β-G	430±14	8-10
20K PCB- β-G	500±23	7-9

Table 2-5. The parameters of the final KLH conjugates.

Samples	Molecular Weight (KDa)	# polymer per monomer protein
KLH	390	-
5K PEG-KLH	443±8	9-12
10K PEG-KLH	479±16	7-11
20K PEG-KLH	557±20	7-9
5K PCB-KLH	445±6	10-12
10K PCB-KLH	491±12	9-11
20K PCB-KLH	572±22	8-10

2.7 References

1. Berkowitz, S. A.; Engen, J. R.; Mazzeo, J. R.; Jones, G. B., Analytical tools for characterizing biopharmaceuticals and the implications for biosimilars. *Nat Rev Drug Discov* 2012, *11* (7), 527-40.

2. Werle, M.; Bernkop-Schnurch, A., Strategies to improve plasma half life time of peptide and protein drugs. *Amino Acids* 2006, *30* (4), 351-67.

3. Tovey, M. G.; Lallemand, C., Immunogenicity and other problems associated with the use of biopharmaceuticals. *Ther Adv Drug Saf* 2011, *2* (3), 113-28.

4. Krishna, M.; Nadler, S. G., Immunogenicity to Biotherapeutics - The Role of Anti-drug Immune Complexes. *Front Immunol* 2016, *7*, 21.

5. Harris, J. M.; Chess, R. B., Effect of pegylation on pharmaceuticals. *Nat Rev Drug Discov* 2003, *2* (3), 214-21.

6. Veronese, F. M.; Pasut, G., PEGylation, successful approach to drug delivery. *Drug Discov Today* 2005, *10* (21), 1451-8.

7. Jevsevar, S.; Kunstelj, M.; Porekar, V. G., PEGylation of therapeutic proteins. *Biotechnol J* 2010, *5* (1), 113-28.

8. Mitragotri, S.; Burke, P. A.; Langer, R., Overcoming the challenges in administering biopharmaceuticals: formulation and delivery strategies. *Nat Rev Drug Discov* 2014, *13* (9), 655-672.

9. Kolate, A.; Baradia, D.; Patil, S.; Vhora, I.; Kore, G.; Misra, A., PEG - a versatile conjugating ligand for drugs and drug delivery systems. *J Control Release* 2014, *192*, 67-81.

10. Branca, C.; Magazu, S.; Maisano, G.; Migliardo, F.; Migliardo, P.; Romeo, G., Hydration study of PEG/water mixtures by quasi elastic light scattering, acoustic and rheological measurements. *J Phys Chem B* 2002, *106* (39), 10272-10276.

11. Zheng, J.; Li, L.; Chen, S.; Jiang, S., Molecular simulation study of water interactions with oligo (ethylene glycol)-terminated alkanethiol self-assembled monolayers. *Langmuir* 2004, *20* (20), 8931-8.

12. Booth, C.; Gaspar, H. B., Pegademase bovine (PEG-ADA) for the treatment of infants and children with severe combined immunodeficiency (SCID). *Biologics* 2009, *3*, 349-58.

13. Kang, J. S.; Deluca, P. P.; Lee, K. C., Emerging PEGylated drugs. *Expert Opin Emerg Drugs* 2009, *14* (2), 363-80.

14. Alconcel, S. N. S.; Baas, A. S.; Maynard, H. D., FDA-approved poly(ethylene glycol)-protein conjugate drugs. *Polym Chem-Uk* 2011, *2* (7), 1442-1448.

15. Verhoef, J. J.; Carpenter, J. F.; Anchordoquy, T. J.; Schellekens, H., Potential induction of anti-PEG antibodies and complement activation toward PEGylated therapeutics. *Drug Discov Today* 2014, *19* (12), 1945-52.

16. Garay, R. P.; El-Gewely, R.; Armstrong, J. K.; Garratty, G.; Richette, P., Antibodies against polyethylene glycol in healthy subjects and in patients treated with PEG-conjugated agents. *Expert Opin Drug Deliv* 2012, *9* (11), 1319-23.

17. Ishida, T.; Kiwada, H., Anti-polyethyleneglycol antibody response to PEGylated substances. *Biol Pharm Bull* 2013, *36* (6), 889-91.

18. Zhang, P.; Sun, F.; Liu, S.; Jiang, S., Anti-PEG antibodies in the clinic: Current issues and beyond PEGylation. *J Control Release* 2016.

19. Yang, Q.; Lai, S. K., Anti-PEG immunity: emergence, characteristics, and unaddressed questions. *Wiley Interdiscip Rev Nanomed Nanobiotechnol* 2015, *7* (5), 655-77.

20. Richter, A. W.; Akerblom, E., Antibodies against polyethylene glycol produced in animals by immunization with monomethoxy polyethylene glycol modified proteins. *Int Arch Allergy Appl Immunol* 1983, *70* (2), 124-31.

21. Schellekens, H.; Hennink, W. E.; Brinks, V., The immunogenicity of polyethylene glycol: facts and fiction. *Pharm Res* 2013, *30* (7), 1729-34.

22. Sundy, J. S.; Baraf, H. S.; Yood, R. A.; Edwards, N. L.; Gutierrez-Urena, S. R.; Treadwell, E. L.; Vazquez-Mellado, J.; White, W. B.; Lipsky, P. E.; Horowitz, Z.; Huang, W.; Maroli, A. N.; Waltrip, R. W., 2nd; Hamburger, S. A.; Becker, M. A., Efficacy and tolerability of pegloticase for the treatment of chronic gout in patients refractory to conventional treatment: two randomized controlled trials. *JAMA* 2011, *306* (7), 711-20.

23. Hershfield, M. S.; Ganson, N. J.; Kelly, S. J.; Scarlett, E. L.; Jaggers, D. A.; Sundy, J. S., Induced and pre-existing anti-polyethylene glycol antibody in a trial of every 3-week dosing of pegloticase for refractory gout, including in organ transplant recipients. *Arthritis Res Ther* 2014, *16* (2), R63.

24. Sherman, M. R.; Saifer, M. G. P.; Perez-Ruiz, F., PEG-uricase in the management Of treatment-resistant gout and hyperuricemia. *Adv Drug Deliver Rev* 2008, *60* (1), 59-68.

25. Lipsky, P. E.; Calabrese, L. H.; Kavanaugh, A.; Sundy, J. S.; Wright, D.; Wolfson, M.; Becker, M. A., Pegloticase immunogenicity: the relationship between efficacy and antibody development in patients treated for refractory chronic gout. *Arthritis Res Ther* 2014, *16* (2), R60.

26. Armstrong, J. K.; Hempel, G.; Koling, S.; Chan, L. S.; Fisher, T.; Meiselman, H. J.; Garratty, G., Antibody against poly(ethylene glycol) adversely affects PEG-asparaginase therapy in acute lymphoblastic leukemia patients. *Cancer* 2007, *110* (1), 103-11.

27. Yang, Q.; Jacobs, T. M.; McCallen, J. D.; Moore, D. T.; Huckaby, J. T.; Edelstein, J. N.; Lai, S. K., Analysis of Pre-existing IgG and IgM Antibodies against Polyethylene Glycol (PEG) in the General Population. *Anal Chem* 2016, *88* (23), 11804-11812.

28. Chen, B. M.; Su, Y. C.; Chang, C. J.; Burnouf, P. A.; Chuang, K. H.; Chen, C. H.; Cheng, T. L.; Chen, Y. T.; Wu, J. Y.; Roffler, S. R., Measurement of Pre-Existing IgG and IgM Antibodies against Polyethylene Glycol in Healthy Individuals. *Anal Chem* 2016, *88* (21), 10661-10666.

29. Armstrong, J. K.; Leger, R.; Wenby, R. B.; Meiselman, H. J.; Garratty, G.; Fisher, T. C., Occurrence of an antibody to poly(ethylene glycol) in normal donors. *Blood* 2003, *102* (11), 556a-556a.

30. Li, B.; Xie, J.; Yuan, Z.; Jain, P.; Lin, X.; Wu, K.; Jiang, S., Mitigation of Inflammatory Immune Responses with Hydrophilic Nanoparticles. *Angew Chem Int Ed Engl* 2018.

31. Jiang, S. Y.; Cao, Z. Q., Ultralow-Fouling, Functionalizable, and Hydrolyzable Zwitterionic Materials and Their Derivatives for Biological Applications. *Adv Mater* 2010, *22* (9), 920-932.

32. Ladd, J.; Zhang, Z.; Chen, S.; Hower, J. C.; Jiang, S., Zwitterionic polymers exhibiting high resistance to nonspecific protein adsorption from human serum and plasma. *Biomacromolecules* 2008, *9* (5), 1357-1361.

33. Ueland, P. M.; Holm, P. I.; Hustad, S., Betaine: a key modulator of one-carbon metabolism and homocysteine status. *Clin Chem Lab Med* 2005, *43* (10), 1069-1075.

34. Ashraf, M.; Foolad, M. R., Roles of glycine betaine and proline in improving plant abiotic stress resistance. *Environ Exp Bot* 2007, *59* (2), 206-216.

35. Zhang, L.; Cao, Z.; Bai, T.; Carr, L.; Ella-Menye, J. R.; Irvin, C.; Ratner, B. D.; Jiang, S., Zwitterionic hydrogels implanted in mice resist the foreign-body reaction. *Nat Biotechnol* 2013, *31* (6), 553-6.

36. Keefe, A. J.; Jiang, S. Y., Poly(zwitterionic)protein conjugates offer increased stability without sacrificing binding affinity or bioactivity. *Nat Chem* 2012, *4* (1), 60-64.

37. Liu, S. J.; Jiang, S. Y., Chemical conjugation of zwitterionic polymers protects immunogenic enzyme and preserves bioactivity without polymer-specific antibody response. *Nano Today* 2016, *11* (3), 285-291.

38. Zhang, P.; Sun, F.; Tsao, C.; Liu, S.; Jain, P.; Sinclair, A.; Hung, H. C.; Bai, T.; Wu, K.; Jiang, S., Zwitterionic gel encapsulation promotes protein stability, enhances pharmacokinetics, and reduces immunogenicity. *Proc Natl Acad Sci U S A* 2015, *112* (39), 12046-51.

39. Li, B.; Yuan, Z.; Zhang, P.; Sinclair, A.; Jain, P.; Wu, K.; Tsao, C.; Xie, J.; Hung, H. C.; Lin, X.; Bai, T.; Jiang, S., Zwitterionic Nanocages Overcome the Efficacy Loss of Biologic Drugs. *Adv Mater* 2018, *30* (14), e1705728.

40. Li, C.; Cao, J.; Wang, Y.; Zhao, X.; Deng, C.; Wei, N.; Yang, J.; Cui, J., Accelerated blood clearance of pegylated liposomal topotecan: influence of polyethylene glycol grafting density and animal species. *J Pharm Sci* 2012, *101* (10), 3864-76.

41. Shiraishi, K.; Hamano, M.; Ma, H.; Kawano, K.; Maitani, Y.; Aoshi, T.; Ishii, K. J.; Yokoyama, M., Hydrophobic blocks of PEG-conjugates play a significant role in the accelerated blood clearance (ABC) phenomenon. *J Control Release* 2013, *165* (3), 183-90.

42. Shao, Q.; Jiang, S., Molecular understanding and design of zwitterionic materials. *Adv Mater* 2015, *27* (1), 15-26.

43. Saifer, M. G.; Williams, L. D.; Sobczyk, M. A.; Michaels, S. J.; Sherman, M. R., Selectivity of binding of PEGs and PEG-like oligomers to anti-PEG antibodies induced by methoxyPEG-proteins. *Mol Immunol* 2014, *57* (2), 236-46.

44. Sherman, M. R.; Williams, L. D.; Sobczyk, M. A.; Michaels, S. J.; Saifer, M. G., Role of the methoxy group in immune responses to mPEG-protein conjugates. *Bioconjug Chem* 2012, *23* (3), 485-99.

45. Leng, C.; Hung, H. C.; Sun, S.; Wang, D.; Li, Y.; Jiang, S.; Chen, Z., Probing the Surface Hydration of Nonfouling Zwitterionic and PEG Materials in Contact with Proteins. *ACS Appl Mater Interfaces* 2015, *7* (30), 16881-8.

CHAPTER 3

Modulation of Inflammatory Immune Responses with Hydrophilic Nanoparticles

3.1 Abstract

While hydrophobic nanoparticles (NPs) have been long recognized to boost the immune activation, whether hydrophilic NPs modulate an immune system challenged by immune stimulators and how their hydrophilic properties may affect the immune response is still unclear. To answer this question, three polymers, poly(ethylene glycol) (PEG), poly(sulfobetaine) (PSB) and poly(carboxybetaine) (PCB), which are commonly considered as "hydrophilic", are studied in this work. For fair comparison, nanogels with uniform size and pure surface functionalities were made from these polymers. Peripheral blood mononuclear cells (PBMCs) stimulated by lipopolysaccharide (LPS), and LPS-induced lung inflammation murine model were used to investigate the influence of nanogels on the immune system, respectively. Results show that the treatment of hydrophilic nanogels attenuated the immune responses elicited by LPS both *in vitro* and *in vivo*. Moreover, we found that PCB nanogels with the strongest hydration and the lowest non-specific protein binding manifested the best performance in alleviating the immune activation, followed by PSB and PEG nanogels. This reveals that the immunomodulatory effect of hydrophilic materials is closely related to their hydration characteristics and their ability to resist non-specific binding in complex media.

3.2 Introduction

The initiation, maintenance, and suppression of immune responses mostly depend upon the communication occurring at the natural interfaces[1-3]. The cell-cell or cell-particulate interface plays an essential role in directing the behavior of immune systems, and inspire the design of nanoparticles (NPs) with immune activity[3-5]. The function of NPs in tuning the immune response is determined by the physicochemical properties of NP surfaces[6-8]. It is now well known that NPs with large hydrophobic surfaces are able to trigger the initiation of innate immune response. Increase in the hydrophobicity of NPs could even promote inflammatory outcomes including the expression of pro-inflammatory cytokines and activation of antigen presenting cells. This phenomenon corresponds to the classical "Hyppo" in which hydrophobic portions are ascribed to be integral parts of both exogenous and endogenous immune-stimulators[9]. By contrast, hydrophilic nanomaterials are known to generate minimal immune reactions and cause less inflammation than their hydrophobic counterparts[4]. Recent studies showed that PCB-uricase nanogels did not generate anti-polymer antibodies while anti-PEG antibodies were observed after multiple injections of PEG-uricase conjugates. These results indicate that not all "hydrophilic" materials behave the same towards the immune system. Since hydrophilic materials are extensively used in nanomedicine, it is of paramount importance to understand if hydrophilic NPs can modulate an immune system challenged by immune stimulators and how hydrophilic properties may affect the immune responses.

To probe the effect of surface chemistry on biological systems, inorganic NPs such as AuNPs decorated with different functions groups have been employed[6, 7]. However, heterogeneous polymer coatings on these NPs could not guarantee that only the pure functional group will be

presented and studied [6]. Due to limited surface packing densities, the core of inorganic NPs may even expose and affect cell behaviors, leading to inconclusive results on the effect of surface chemistry. In contrast, nanogels that provide uniform size and the surface with pure functionality are ideal for our studies. Nonionic and neutral polymer, PEG and zwitterionic polymers, PCB and PSB are commonly used as "hydrophilic" materials to protect implants or foreign macromolecules to evade the undesirable activation of host immune system[10-13]. In this work, using nanogels made from these three types of polymers (Scheme 3-1), we investigated and compared the impact of hydrophilic NPs on navigating immune responses.

3.3 Experimental Section

3.3.1 Materials

Mouse cytokine (IL-1β, IL-6, TNF-α) quantikine ELISA kits were purchased form R&D systems. All the chemicals were purchased from Sigma-Aldrich unless otherwise noted and were used as received. CBAA monomer was synthesized following our previously published method[17].

3.3.2 Preparation of PEG, PSB and PCB nanogels

AOT (sodium bis(2-ethylhexyl) sulfosuccinate, 237mg) and Brij 30 (poly(ethylene glycol) dodecyl ether, 459mg) were added to a 20mL glass vial to which a stir bar was added(43). The vial was sealed with a Teflon-lined septum cap and purged with dry nitrogen for 10min. Nitrogen-deoxygenated hexane (10mL) was then added to the vial under vigorous stirring. For the aqueous phase, monomers (PEGMA, SBMA, CBAA) and crosslinker (MBA) was dissolved in PBS buffer (pH 7.4, 250 μL) at a mole ratio of 95%:5%. Dry nitrogen was bubbled through the monomer solution for 2min, after which the aqueous phase was slowly added to the organic continuous phase

dropwise. The vial was sonicated to form a stable nanoemulsion. A 20% (w/v) solution of ammonium persulfate in deionized water (10 μL) was then added to the emulsion. After 5 min, polymerization was initiated by the addition of tetramethylethylenediamine (TEMED, 6 μL) and maintained at 4°C under rapid magnetic stirring. After the 2-hour reaction, the organic solvent was removed by rotary evaporator and the nanogel was precipitated and washed with THF for three times. The nanogel was re-suspended in PBS buffer and purified with 100-KDa molecular weight cutoff centrifugal filters to remove the unreacted monomer and crosslinker.

3.3.3 In vitro immune activation study

PBMCs were seeded into a 24-well plate (10^6 cells/well) and cultured in a complete medium consisting of RPMI 1640 medium (Invitrogen) supplemented with 10% fetal bovine serum (FBS) and penicillin/streptomycin. PBS and different nanogel solutions (final concentration: 50mM) were added into each well, and LPS solution were also added with a final concentration of 100ng/ml. After 24-h incubation, supernatants of cell culture medium were taken for cytokine detection (IL-1β, IL-6, and TNF-α) with ELISA kit (eBioscience). In a separate experiment, PBMCs (10^6/well) seeded in 24-well plate were treated with LPS/OVA mixture (100ng/ml) and PBS or nanogels (50mM) for 72h. Then, the cells were washed with PBS for three time and stained with anti-CD86-PE and anti-MHCII-FITC Abs for flow cytometry analysis.

3.3.4 ROS detection

PBMCs were seeded into a 96-well plate (10^5 cells/well) and cultured in a complete medium consisting of RPMI 1640 medium (Invitrogen) supplemented with 10% fetal bovine serum (FBS) and penicillin/streptomycin. PBS and different nanogel solutions (final concentration: 50mM)

were added into each well, and LPS solution were also added into each well with a final concentration of 0, 0.1, 1, 10, 100 and 500ng/ml. Then, cells were wash with PBS buffer for three times and then mixed with the 2',7'-dichlorodihydrofluorescein diacetate (DCFDA,150 μL/well, 10μM). After incubating for 30min, the cells were washed with PBS for three times and added with trypsin (200μL) for 5min incubation. The cells were subsequently transferred to EP tube for 5min centrifugation at 1500rpm. Then, each EP tube was added with 300ul lysis buffer and kept in dark for 30min, after which the EP tubes were centrifuged at 1500rpm for 5min. The supernatant in each tube was then transferred to a black 96-well plate and the fluorescence intensity, resulting from the oxidation of dye, was recorded (excitation/emission: 488 nm/520 nm).

3.4 Results and Discussion

3.4.1 Effect of hydrophilic nanogels on the secretion of proinflmmatory cytokines

Herein, monomers of poly(ethylene glycol) methacrylate (PEGMA), sulfobetaine methacrylate (SBMA) and carboxybetaine acrylate (CBAA) were polymerized respectively with the cross-linker N,N'-methylene-bisacrylamide (MBA) for the nanogel fabrication via the inverse nano-emulsion method[14]. As shown in Fig. 3-1 and Table 3-1, all the three nanogels display similar structural parameters including size and zeta potential. Cytokines, the glycoproteins produced by immune cells are the essential regulators in modulating immune response[15, 16]. However, abnormal production of cytokines could result in immune-mediated disorders, including infectious disease, cancer, autoimmunity and allergy. Thus, it is meaningful to examine how these nanogels may impact the cytokine level in an immune system challenged by immune-stimulators. As an *in vitro* model, peripheral blood mononuclear cells (PBMCs), mainly consisting of immune cells such as lymphocytes, monocytes, and dendritic cells were harvested from mice. After being seeded into

24-well plate, PBMCs in each well (10^6/well,1ml) were mixed with lipopolysaccharide (LPS, 100ng/ml), an amphiphilic immune-stimulatory endotoxin found in the outer membrane of gram-negative bacteria. In the presence of LPS, PBMCs were exposed to PBS vehicle and three nanogel solutions (50mM) respectively. After 24-h incubation, three cytokines including IL-1β, IL-6, TNF-α as crucial biomarkers of the inflammatory immune response were detected in the supernatants of PBMC culture medium with ELISA kits. By measuring the production and release of pro-inflammatory cytokines, we were able to evaluate the immune-competence and activation status of the immune cells. Interestingly, the three nanogel-treated groups displayed different extents of reduced immune responses as reflected by a relatively decreased level of TNF-α, lower than that detected in the positive group treated with LPS and PBS vehicle (Fig. 3-2a). In addition to TNF-α, PBMCs treated with PSB and PCB nanogels, which are believed to have stronger hydrophilicity than PEG nanogels, even displayed reduced secretion of another two pro-inflammatory cytokines (IL-1β, IL-6). Moreover, LPS as a type of adjuvant is known to boost the effect of allergens such as ovalbumin (OVA) in promoting the maturation of antigen presenting cells (APCs)[17]. To further confirm the impact of hydrophilic NPs on immune cells, we also exposed PBMCs to the LPS/OVA mixture, and meanwhile added PBS or nanogels into each well respectively. After 72-h incubation, the ratio of activated antigen presenting cells (APC, MHCII+CD86+) was analyzed by the flow cytometry. As shown in Fig. 3-2b-c, compared to the cells stimulated with LPS-rich OVA, PBMC cultured with hydrophilic nanogels displayed a relatively lower activated ratio of APC, further verifying the modulation of hydrophilic NPs on immune responses. Notably, PCB nanogel manifested the greatest capacity in reducing the APC activation and the cytokine secretion elicited by LPS.

3.4.2 Effect of hydrophilic nanogels on ROS production

The production of Reactive Oxygen Species (ROS) including superoxide, hydrogen peroxide, and hydroxyl radical is not only a key indicator of inflammatory immune responses but also a direct impetus for monocyte activation as well as the secretion of pro-inflammatory cytokines[18, 19]. PEG-coated NPs were shown to rapidly scavenge superoxide, and thus mitigate the deleterious effects of superoxide on traumatized tissue[20]. Thus, to further elucidate the mechanism behind the immune-regulatory effect of these hydrophilic nanogels, we monitored the generation of ROS by PBMCs in the presence of nanogel (50mM) and LPS ranging from 0.1 to 500ng/ml. After 24-h exposure, the PBMCs were washed, lysed and mixed with 2',7'-dichlorodihydrofluorescein diacetate (DCFDA), a pro-fluorophore that can be activated by ROS. As shown in Fig. 3-3, the addition of LPS leads to an obvious escalation in DCFDA fluorescence, evincing that the production of ROS by PBMCs rises with the increase of LPS concentration. When the concentration of LPS is low (0, 0.1ng/ml, 1ng/ml), the production of ROS in PBMC is limited and thus the cells treated with PBS and nanogels all displayed relatively high viability with no significant statistic difference. However, as high-level ROS stress could be cytotoxic, when the concentration of LPS increases to be above 10ng/ml, the impairment of ROS on the viability of PBMC became more and more significant along with the augment in its production. Notably, the addition of hydrophilic nanogels nanogel strikingly attenuated tendency of ROS rise in PBMC, indicating that the hydrophilic nanogels may curb the immune activation by alleviating the secretion of ROS or via ROS scavenging. Furthermore, the mitigation of ROS by hydrophilic NPs particularly PCB thus affords a relatively higher cell viability when the concentration LPS is above 10ng/ml.

3.4.3 Effect of hydrophilic nanogels on inflammatory animals

Given the *in vitro* results that hydrophilic NPs favor the constraint of the immune activation, we next extended our exploration to *in vivo* studies. Due to physiological barriers including dilution effect, biodistribution and serum protein binding, *in vivo* investigations post to systemic administration (e.g., intravenous injection) are significantly complicated. In comparison, it is more straightforward to study the immune-regulating effect of hydrophilic NPs by locally administering nanogels. To do this, we selected an acute lung inflammation model induced by LPS[21]. The innate immune system of the lung includes itinerant leukocytes such as neutrophils, monocytes/macrophages, mast cells, dendritic cells. Inflammation at lung site will cause the infiltration of more leukocytes from the bloodstream to alveoli, accumulating in lung airspace and secreting various soluble factors that may exacerbate or modulate the inflammatory response[22]. In our work, LPS solution (2mg/ml, 50ul) as the stimulator of lung inflammation was intratracheally administered to four groups of mice (4 mice in each group), subsequent to which PBS and the three types of nanogel solutions (100mM, 50ul) were intratracheally administered into each mice cohort respectively. In parallel, healthy mice in a fifth group were administered with PBS vehicle as the negative control. After 12h, the mice were sacrificed for the harvesting of bronchoalveolar lavage fluids (BALF). Previous studies on healthy mice have shown that single administration of hydrophilic nanomaterials elicited little or no inflammation whereas equivalent surface area doses of the hydrophobic nanoparticles induced neutrophil infiltration, and elevation of proinflammatory cytokines[23]. Herein, intratracheal administration of hydrophilic nanogels with LPS remarkably alleviate the LPS-induced inflammation as demonstrated by the decreased pro-inflammatory cytokines (TNF-α, IL-6) and reduced number of infiltrated cell number in BALF (Fig. 3-4a-c). Consistent with the *in vitro* studies, PBS nanogel also manifested the most significant capability

in mitigating the immune responses as lower TNF-α level and infiltrated cell number were detected in its treated group. Similar trend (Fig. 3-4d-e) was also observed in the luminol assay of cells in BALF. Luminol as a redox-sensitive compound can emit bioluminescence when exposed to myeloperoxidase (MPO)[24, 25], a biomarker of activated phagocytes and thus has been used for the imaging of MPO activity as well as inflammatory phagocytes[26-29]. To further assess the status of immune cells collected from lung BALF, we re-suspended the cells extracted from mice BALF in Modified Earle's Balanced Salt Solution (MEBSS) and loaded them into wells on a black 96-well plate ($1x10^5$ cells/well, 190ul)[29]. Then 10ul luminol stock solution (2mM) was added in each well for 15 min incubation, after which the luminescence was acquired by IVIS series 200 from PerkinElmer (acquisition time = 15 min; F/Stop = 1; binning = 16). As shown in the luminescent images (Fig. 3-4d-e), administration of hydrophilic nanogels, particularly PCB nanogels reduced the luminescent signals, further indicating that hydrophilic nanogels could exert restraint on the phagocyte activation. These results revealed that hydrophilic NPs could interfere with the immune activation promoted by hydrophobic immune-stimulators and are favorable to maintain the equilibrium of the immune system. In fact, such immunomodulatory property of PCB has also been found in our previous study on PCB hydrogels. After being implanted in mice, PCB hydrogels were shown to dramatically lessen the differentiation of inflammatory macrophage phenotype (M1) in their surrounding tissues and could resist capsule formation and inflammation for at least three months[10].

These results reveal that the performance of hydrophilic NPs in mitigating immune responses could be correlated to the degree of hydrophilicity as their immunomodulatory effect both *in vitro* and *in vivo* is further improved with increasing hydrophilicity as presented before. In fact, there is no clear definition of hydrophilicity yet and no single parameter is used to describe the degree of

hydrophilicity. While the degree of hydrophobicity can be described by the contact angle, contact angle does not work well for the hydrophilic end. For example, although hydroxyl surface has a much lower contact angle than hydroxyl-terminated PEG surface, it is not necessarily more hydrophilic than PEG surface.

Based on prior simulation and experimental studies, we herein define the "*degree of hydrophilicity"* based on two aspects: (a) the degree of hydration and (b). the existence of hydrophobicity. The latter is not as obvious as the former and here we will provide the reasoning. The containment of hydrophobic domains improves the solubility of hydrophilic materials such as PEG in organic solvents. However, due to such a hydrophobic characteristic, PEG will compromise the bioactivity of the enzyme when conjugated to an enzyme[30] and can be recognized by the immune system leading to the generation of anti-PEG antibodies[11]. The amphiphilic nature of PEG has been further revealed at the molecular level and clearly demonstrated using molecular simulations[31, 32]. For the degree of hydration, while PEG binds water molecules via hydrogen bonding, zwitterions bind water molecules via electrostatic-induced hydration, which is stronger than hydrogen-bonding hydration. The calculation of hydration free energies of carboxy betaine (CB), sulfobetaine (SB), and oligo ethylene glycol (OEG) moieties using the free energy perturbation method revealed that the hydration free energy of zwitterionic CB and SB moieties is much lower than that of nonionic OEG moieties, indicating that zwitterionic materials exhibit stronger hydration[33]. Hence, PEG bears the lower degree of hydrophilicity than that of zwitterionic PSB and PCB due to the existence of hydrophobicity and lower hydration.

Furthermore, although the hydration free energy is able to distinguish PEG from highly hydrated zwitterionic materials, it is insufficient to rank the degree of hydrophilicity among zwitterionic materials[34]. When assessing the hydration degree of polymers in complex media, one needs to consider not only the number and binding strength of water molecules around their molecular chains (the degree of hydration), but also the associations of their molecular chains with themselves (self-association) and with other molecules (e.g. proteins), which can reduce their hydration effects and result in nonspecific binding. For example, both CB and SB moieties are shown to have strong hydration, yet differ in their interaction with water molecules[33]. SB moieties attract more water molecules than CB moieties do whereas the latter attracts individual water molecules more tightly. Moreover, weak self-association in CB due to incompatible cationic and anionic sites maximizes its hydration while the hydration of SB is accordingly reduced by its strong self-association [35]. In addition, another further study shows that among all zwitterions, CB has the least association with proteins [36]. Because of all of these, PCB polymer manifests much better nonfouling behaviors than PSB polymer: PCB surfaces fully resisted protein adsorption in 100% blood serum and plasma which cannot be achieved by PSB[37-39]. Thus, the order of the degree of hydrophilicity is determined as PCB>PSB>PEG in this work.

3.5 Conclusions

Using three hydrophilic materials in the form of nanogel, we demonstrated that their modulation upon immune system is related to the degree of their hydrophilicity and thus their ability to resist non-specific binding. Results show that the degree of hydrophilicity is related to the regulation of the immune system irritated by immune stimulators as well as the maintenance of immune balance. This finding offers valuable guidance to the design of nanocarriers and implantable materials with minimum immune response and for control of immune dysregulations.

3.6 Schemes, Figures, and Tables

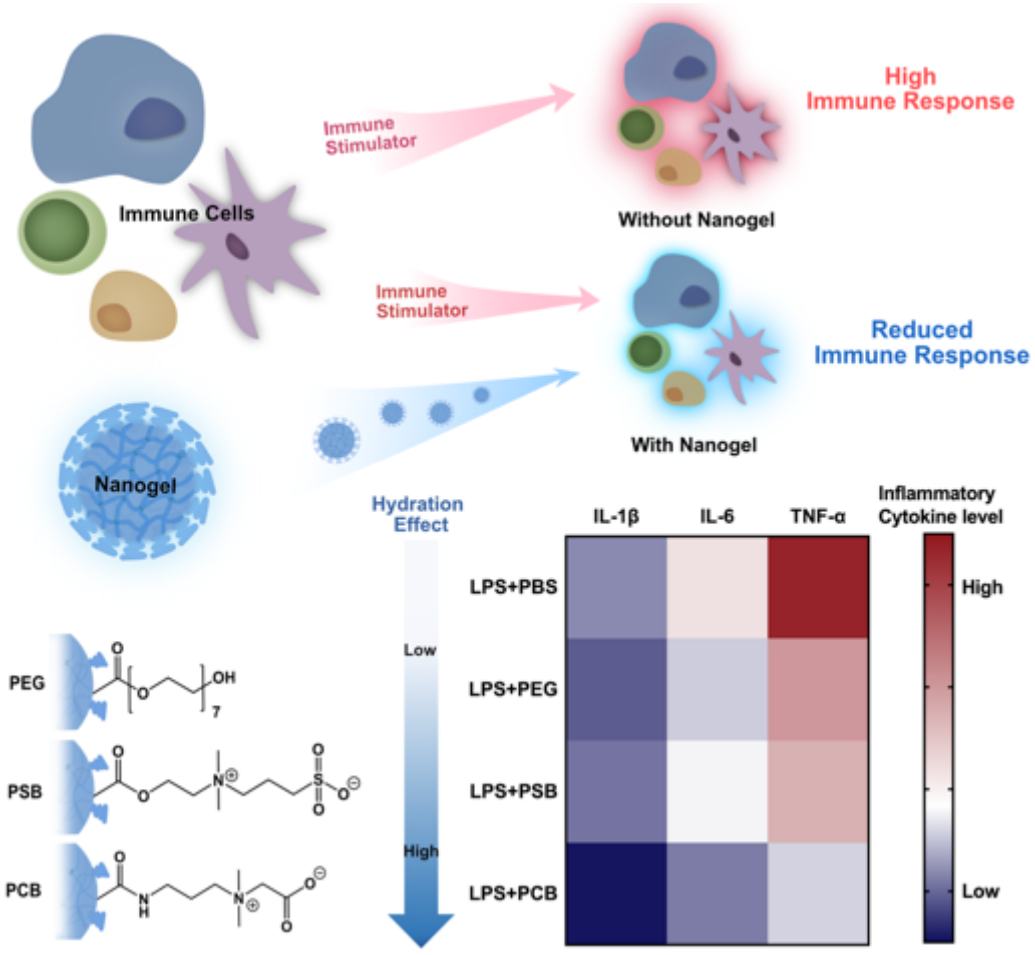

Scheme 3-1. The treatment of peripheral blood mononuclear cells with hydrophilic nanogels resulted in attenuated immune response to stimulation by lipopolysaccharide both *in vivo* and *in vitro*. This immunomodulatory effect of hydrophilic materials is closely related to their hydration characteristics and their ability to resist nonspecific binding in complex media.

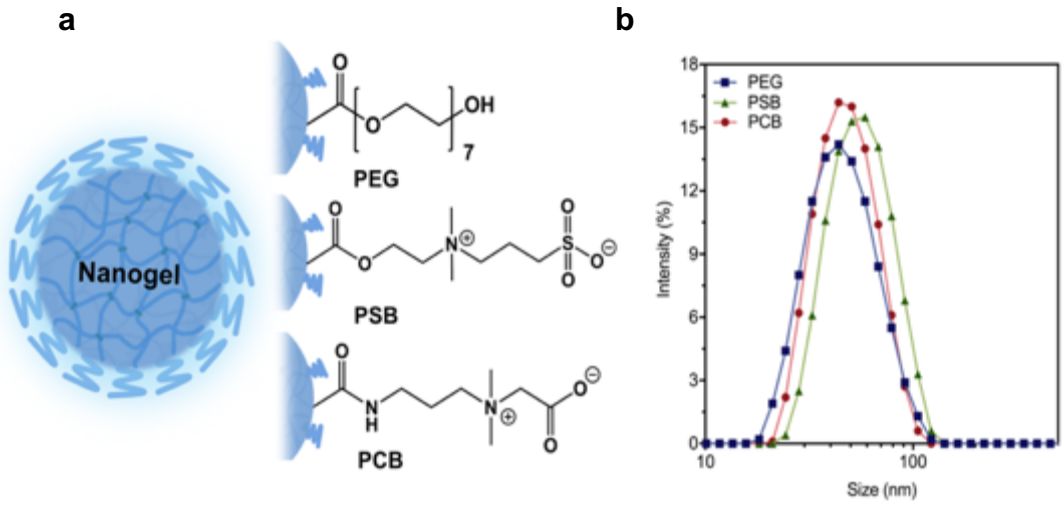

Figure 3-1. a, Scheme of three hydrophilic nanogels composed of PEG, PSB and PCB. b, Size distribution of these nanogels measured by dynamic light scattering.

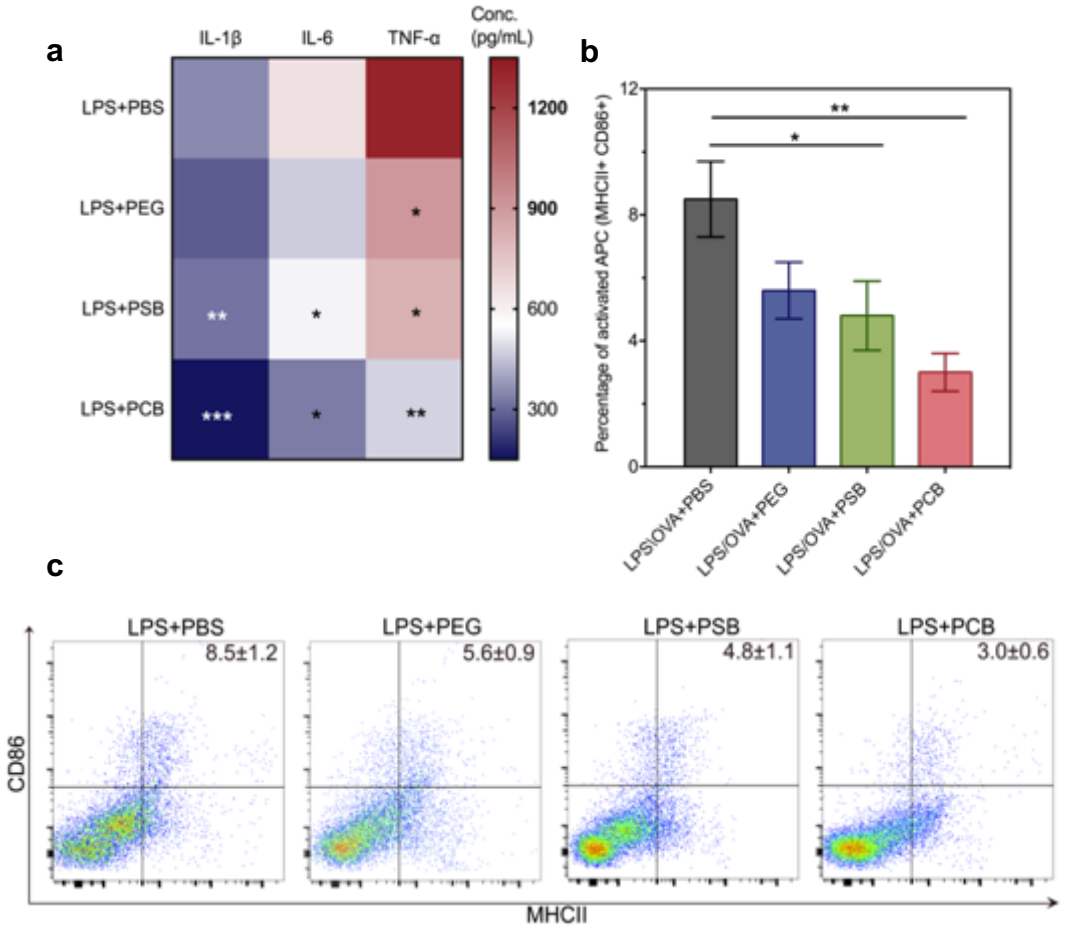

Figure 3-2. a, Cytokine secretion of IL-1b, IL-6, and TNF-α by mice PBMC after incubation with LPS (100ng/ml) and PBS or nanogels (50mM) for 24h. In a separate experiment, PBMCs were treated with LPS/OVA mixture (100ng/ml) and PBS or nanogels for 72h. b, The ratio of activated APC (MHCII+CD86+) measured as a percentage of the total mice PBMCs. c, Representative dot plots for PBMC. The groups treated with LPS/nanogel or LPS/OVA/nanogel were compared to the positive controls, the group treated with LPS/PBS or LPS/OVA/PBS and statistical analyses were performed using student test. Results are plotted as mean ± s.d. (n = 3). *P < 0.05; **P < 0.01; ***P < 0.005.

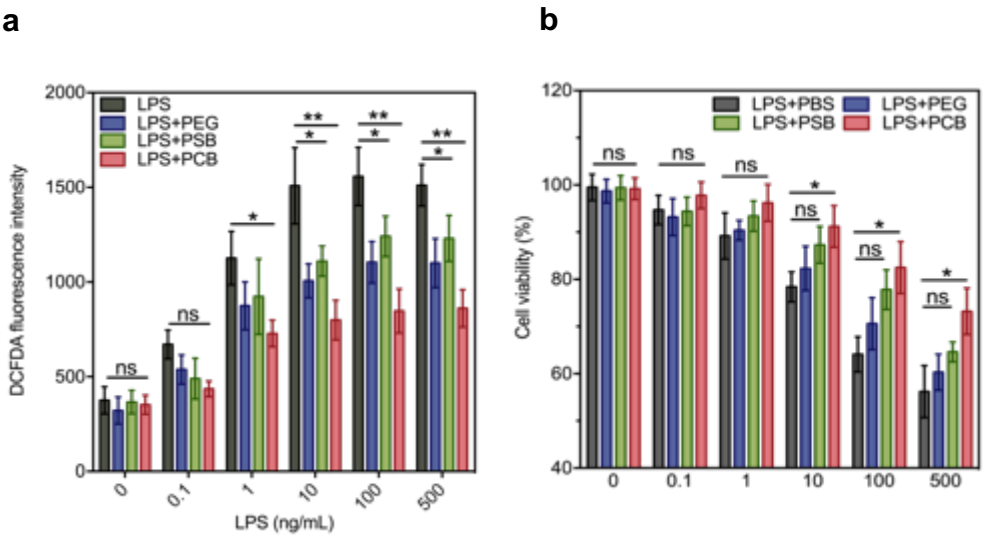

Figure 3-3. a, ROS detection in PBMC after incubation with LPS(0-500ng/ml) and nanogels (50mM) or PBS for 24h. b, Cell viability of PBMC after incubation with LPS(0-500ng/ml) and nanogels (50mM) or PBS for 24h. The groups treated with LPS/nanogel were compared to the positive control, the group treated with LPS/PBS and statistical analyses were performed using student test. Results are plotted as mean ± s.d. (n = 3). *P < 0.05.

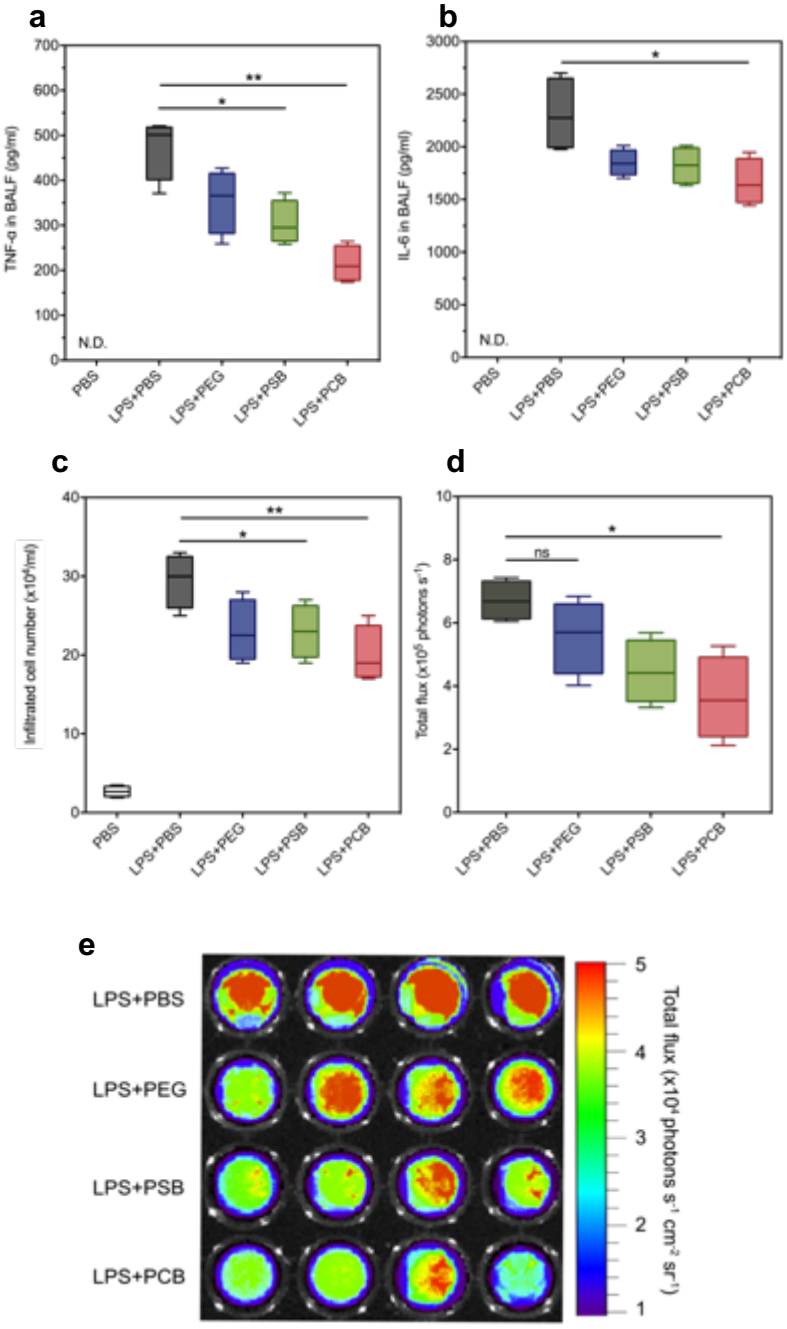

Figure 3-4. Detection of TNF-α (a), IL-6 (b) and infiltrated cell number (c) in mice BALF. d-e, Ex vivo luminol bioluminescence in cells from mice BALF. The groups treated with LPS/nanogel were compared to the positive control, the group treated with LPS/PBS and statistical analyses were performed using student test. Results are plotted as mean ± s.d. (n = 4). *P < 0.05; **P < 0.01.

Table 3-1. Characteristics of nanogels

Nanogel	Mole% of crosslinking	Hydrodynamic size (nm)	PDI	Zeta potential
PEG	5	50.8±4.2	0.18±0.2	-2.46±1.07
PSB	5	58.7±3.1	0.12±0.1	-2.01±0.78
PCB	5	52.6±2.3	0.09±0.1	-1.89±0.65

3.7 References

1. Thaiss, C. A.; Zmora, N.; Levy, M.; Elinav, E., The microbiome and innate immunity. *Nature* 2016, *535* (7610), 65-74.

2. Janeway, C. A., Jr.; Medzhitov, R., Innate immune recognition. *Annu Rev Immunol* 2002, *20*, 197-216.

3. Garapaty, A.; Champion, J. A., Biomimetic and synthetic interfaces to tune immune responses. *Biointerphases* 2015, *10* (3), 030801.

4. Boehler, R. M.; Graham, J. G.; Shea, L. D., Tissue engineering tools for modulation of the immune response. *Biotechniques* 2011, *51* (4), 239-40, 242, 244 passim.

5. Moon, J. J.; Huang, B.; Irvine, D. J., Engineering nano- and microparticles to tune immunity. *Adv Mater* 2012, *24* (28), 3724-46.

6. Moyano, D. F.; Liu, Y.; Ayaz, F.; Hou, S.; Puangploy, P.; Duncan, B.; Osborne, B. A.; Rotello, V. M., Immunomodulatory effects of coated gold nanoparticles in LPS-stimulated *in vitro* and *in vivo* murine model systems. *Chem* 2016, *1* (2), 320-327.

7. Moyano, D. F.; Goldsmith, M.; Solfiell, D. J.; Landesman-Milo, D.; Miranda, O. R.; Peer, D.; Rotello, V. M., Nanoparticle Hydrophobicity Dictates Immune Response. *J Am Chem Soc* 2012, *134* (9), 3965-3967.

8. Dobrovolskaia, M. A.; McNeil, S. E., Immunological properties of engineered nanomaterials. *Nat Nanotechnol* 2007, *2* (8), 469-78.

9. Seong, S. Y.; Matzinger, P., Hydrophobicity: an ancient damage-associated molecular pattern that initiates innate immune responses. *Nat Rev Immunol* 2004, *4* (6), 469-78.

10. Zhang, L.; Cao, Z.; Bai, T.; Carr, L.; Ella-Menye, J. R.; Irvin, C.; Ratner, B. D.; Jiang, S., Zwitterionic hydrogels implanted in mice resist the foreign-body reaction. *Nat Biotechnol* 2013, *31* (6), 553-6.

11. Zhang, P.; Sun, F.; Tsao, C.; Liu, S.; Jain, P.; Sinclair, A.; Hung, H. C.; Bai, T.; Wu, K.; Jiang, S., Zwitterionic gel encapsulation promotes protein stability, enhances pharmacokinetics, and reduces immunogenicity. *Proc Natl Acad Sci U S A* 2015, *112* (39), 12046-51.

12. Jiang, S.; Cao, Z., Ultralow-fouling, functionalizable, and hydrolyzable zwitterionic materials and their derivatives for biological applications. *Adv Mater* 2010, *22* (9), 920-32.

13. Morais, J. M.; Papadimitrakopoulos, F.; Burgess, D. J., Biomaterials/tissue interactions: possible solutions to overcome foreign body response. *AAPS J* 2010, *12* (2), 188-96.

14. Cohen, J. A.; Beaudette, T. T.; Tseng, W. W.; Bachelder, E. M.; Mende, I.; Engleman, E. G.; Frechet, J. M. J., T-Cell Activation by Antigen-Loaded pH-Sensitive Hydrogel Particles *in Vivo*: The Effect of Particle Size. *Bioconjugate Chem* 2009, *20* (1), 111-119.

15. Mogensen, T. H., Pathogen recognition and inflammatory signaling in innate immune defenses. *Clin Microbiol Rev* 2009, *22* (2), 240-73, Table of Contents.

16. Elsabahy, M.; Wooley, K. L., Cytokines as biomarkers of nanoparticle immunotoxicity. *Chem Soc Rev* 2013, *42* (12), 5552-5576.

17. Mac Sharry, J.; Shalaby, K. H.; Marchica, C.; Farahnak, S.; Chieh-Li, T.; Lapthorne, S.; Qureshi, S. T.; Shanahan, F.; Martin, J. G., Concomitant exposure to ovalbumin and endotoxin augments airway inflammation but not airway hyperresponsiveness in a murine model of asthma. *PLoS One* 2014, *9* (6), e98648.

18. Naik, E.; Dixit, V. M., Mitochondrial reactive oxygen species drive proinflammatory cytokine production. *J Exp Med* 2011, *208* (3), 417-20.

19. Mittal, M.; Siddiqui, M. R.; Tran, K.; Reddy, S. P.; Malik, A. B., Reactive oxygen species in inflammation and tissue injury. *Antioxid Redox Signal* 2014, *20* (7), 1126-67.

20. Samuel, E. L. G.; Marcano, D. C.; Berka, V.; Bitner, B. R.; Wu, G.; Potter, A.; Fabian, R. H.; Pautler, R. G.; Kent, T. A.; Tsai, A. L.; Tour, J. M., Highly efficient conversion of superoxide to oxygen using hydrophilic carbon clusters. *P Natl Acad Sci USA* 2015, *112* (8), 2343-2348.

21. Chu, D. F.; Gao, J.; Wang, Z. J., Neutrophil-Mediated Delivery of Therapeutic Nanoparticles across Blood Vessel Barrier for Treatment of Inflammation and Infection. *Acs Nano* 2015, *9* (12), 11800-11811.

22. Suzuki, T.; Chow, C. W.; Downey, G. P., Role of innate immune cells and their products in lung immunopathology. *Int J Biochem Cell B* 2008, *40* (6-7), 1348-1361.

23. Jones, M. C.; Jones, S. A.; Riffo-Vasquez, Y.; Spina, D.; Hoffman, E.; Morgan, A.; Patel, A.; Page, C.; Forbes, B.; Dailey, L. A., Quantitative assessment of nanoparticle surface hydrophobicity and its influence on pulmonary biocompatibility. *J Control Release* 2014, *183*, 94-104.

24. Allen, R. C.; Loose, L. D., Phagocytic Activation of a Luminol-Dependent Chemiluminescence in Rabbit Alveolar and Peritoneal Macrophages. *Biochem Bioph Res Co* 1976, *69* (1), 245-252.

25. Dechatelet, L. R.; Long, G. D.; Shirley, P. S.; Bass, D. A.; Thomas, M. J.; Henderson, F. W.; Cohen, M. S., Mechanism of the Luminol-Dependent Chemi-Luminescence of Human-Neutrophils. *J Immunol* 1982, *129* (4), 1589-1593.

26. Heinecke, J. W., Mechanisms of oxidative damage by myeloperoxidase in atherosclerosis and other inflammatory disorders. *J Lab Clin Med* 1999, *133* (4), 321-325.

27. Klebanoff, S. J., Myeloperoxidase: friend and foe. *J Leukocyte Biol* 2005, *77* (5), 598-625.

28. Tseng, J. C.; Kung, A. L., *In Vivo* Imaging of Inflammatory Phagocytes. *Chem Biol* 2012, *19* (9), 1199-1209.

29. Gross, S.; Gammon, S. T.; Moss, B. L.; Rauch, D.; Harding, J.; Heinecke, J. W.; Ratner, L.; Piwnica-Worms, D., Bioluminescence imaging of myeloperoxidase activity *in vivo*. *Nat Med* 2009, *15* (4), 455-461.

30. Keefe, A. J.; Jiang, S., Poly(zwitterionic)protein conjugates offer increased stability without sacrificing binding affinity or bioactivity. *Nat Chem* 2011, *4* (1), 59-63.

31. Shao, Q.; Jiang, S., Molecular understanding and design of zwitterionic materials. *Adv Mater* 2015, *27* (1), 15-26.

32. He, Y.; Hower, J.; Chen, S.; Bernards, M. T.; Chang, Y.; Jiang, S., Molecular simulation studies of protein interactions with zwitterionic phosphorylcholine self-assembled monolayers in the presence of water. *Langmuir* 2008, *24* (18), 10358-64.

33. Shao, Q.; He, Y.; White, A. D.; Jiang, S., Difference in hydration between carboxybetaine and sulfobetaine. *J Phys Chem B* 2010, *114* (49), 16625-31.

34. Shao, Q.; Jiang, S., Effect of carbon spacer length on zwitterionic carboxybetaines. *J Phys Chem B* 2013, *117* (5), 1357-66.

35. Shao, Q.; Mi, L.; Han, X.; Bai, T.; Liu, S.; Li, Y.; Jiang, S., Differences in cationic and anionic charge densities dictate zwitterionic associations and stimuli responses. *J Phys Chem B* 2014, *118* (24), 6956-62.

36. Shao, Q.; Jiang, S., Influence of Charged Groups on the Properties of Zwitterionic Moieties: A Molecular Simulation Study. *J Phys Chem B* 2014, *118* (27), 7630-7637.

37. Ladd, J.; Zhang, Z.; Chen, S.; Hower, J. C.; Jiang, S., Zwitterionic polymers exhibiting high resistance to nonspecific protein adsorption from human serum and plasma. *Biomacromolecules* 2008, *9* (5), 1357-61.

38. Yang, W.; Xue, H.; Li, W.; Zhang, J.; Jiang, S., Pursuing "zero" protein adsorption of poly(carboxybetaine) from undiluted blood serum and plasma. *Langmuir* 2009, *25* (19), 11911-6.

39. Yang, W.; Chen, S.; Cheng, G.; Vaisocherova, H.; Xue, H.; Li, W.; Zhang, J.; Jiang, S., Film thickness dependence of protein adsorption from blood serum and plasma onto poly(sulfobetaine)-grafted surfaces. *Langmuir* 2008, *24* (17), 9211-4.

CHAPTER 4

Zwitterionic Nanocages Improve the Efficacy and Safety of Biologic Drugs

4.1 Abstract

For bio-therapeutics that require multiple administrations to fully cure diseases, the induction of undesirable immune response is one common cause for the failure of their treatment. Covalent binding of hydrophilic polymers to proteins is commonly employed to mitigate potential immune responses. However, while this technique is proved to partially reduce the antibodies (Abs) reactive to proteins, it may induce Abs towards their associated polymers and thus result in the loss of efficacy. Zwitterionic poly(carboxybetaine) (PCB) has been recently shown to improve the immunologic properties of proteins without inducing any anti-polymer Abs against itself. However, it is unclear if the improved immunologic profiles can translate to better clinical outcomes since improved immunogenicity cannot directly reflect amelioration in efficacy. Here, we developed a PCB nanocage (PCB NC), which can physically encase proteins while keeping their structure intact. PCB NC encapsulation of uricase, a highly immunogenic enzyme, was demonstrated to eradicate all the immune responses. To bridge the gap between immunogenicity and efficacy studies, the therapeutic performance of PCB NC uricase was evaluated and compared with its PEGylated counterpart in a clinical-mimicking gouty rat model to determine any loss of efficacy evoked after five administrations.

4.2 Introduction

Naturally derived biologic agents comprise a broad reservoir of drug candidates with exceptional medicinal potency and specificity[1]. However, many of these protein-based therapeutics are highly immunogenic, eliciting adverse immune reactions characterized by antibody (Ab) generation[2-4]. When antigen-specific Abs bind to therapeutic proteins, poor clinical outcomes result—whether through directly neutralizing a drug's pharmacological activity or by causing accelerated blood clearance (ABC), therapeutic exposure is diminished[5, 6]. PEGylation, the covalent binding of polyethylene glycol (PEG) molecules to biologics, is a widely used strategy to improve the clinical outcomes of protein therapies[7-9]. It is well established that large PEG groups conjugated to protein surfaces can shield the underlying epitopes from immune recognition and delay mononuclear phagocyte system (MPS) and kidney clearance, thus elongating protein circulation time[9]. To date, over a dozen PEGylated biologics have been approved by the US Food and Drug Administration (FDA) and many more are in clinical pipelines[8]. However, an increasing number of reports have highlighted the immunogenic nature of PEG itself [10-14]. The proliferation of pre-existing or induced anti-PEG Abs could deprive patients of their life-sustaining therapies, and in some cases, cause adverse effects such as hypersensitivity reactions that prevent further treatment. For example, anti-PEG Abs were detected in the sera of 89% of refractory chronic gout (RCG) patients after receiving pegloticase (Krystexxa®), a PEGylated uricase product approved by the FDA in 2010[15]. Of particular concern, the clinical problems with pegloticase have been predominantly associated with anti-PEG Abs, instead of anti-uricase Abs[16-19]. Among patients who developed high-level anti-PEG Ab responses, 93% consequently became non-responders to pegloticase therapy, and many suffered life-threatening infusion reactions[17]. High titers of anti-PEG Abs have also been reported to impair the safety and efficacy of other PEGylated proteins on the market, including PEG-

asparaginase (Oncaspar®)[20, 21]. Along with the issues surrounding these treatment-induced anti-PEG Abs, the negative impact of pre-existing anti-PEG Abs—found in patients even before their first exposure to a PEGylated therapy[22]—has recently seen greater emphasis. In one case study of pegloticase, pre-existing anti-PEG Abs rapidly neutralized therapeutic efficacy in all five treatment-naïve patients[16]. Alarmingly, the prevalence of these pre-existing Abs in healthy individuals has been rising to ~72% since their first detection three decades ago, resulting from high exposure to PEG-containing foods, cosmetics, and household products[12, 23, 24]. As anti-PEG Abs from any source can cross-react with PEGylated products and render them ineffective, the future of PEGylation in biopharmaceuticals is uncertain and several alternative strategies have been proposed. One example is bioinformatics-driven protein engineering, which aims to directly remove potentially immunogenic epitopes from the sequence of a non-human protein[25]. However, such modifications may unexpectedly alter the pharmacological activity of therapeutic proteins. Moreover, this approach is not universal. Alternatively, the most popular strategies as substitutes to PEGylation are to shield proteins with hydrophilic polymers, including synthetic polymers (e.g., poly(N-vinylpyrrolidone)[26], polyoxazoline[27] and poly(N-acryloyl morpholine)[28]) and naturally derived polymers (e.g., polysaccharide[29]and polypeptide[30]). Similar to PEGylation, these polymers are often attached to reactive groups (e.g., thiol, amine or carboxy) on a protein surface. However, the immunological property of these alternative materials has been rarely studied and their potential in eliciting anti-polymer Ab responses is still unknown.

Recently, proteins conjugated to PCB[31,32], a biomimetic zwitterionic polymer derived from glycine betaine, or protected by PCB hydrogels[33] have demonstrated greater stability, superior pharmacokinetic (PK) properties and reduced immunogenicity in comparison with native and

PEGylated proteins. Results showed that no anti-PCB Abs could be detected after three intravenous (IV) administrations of a PCB-modified protein, while a conspicuously high level of anti-PEG Abs developed in groups injected with its PEGylated counterpart[32,33]. These results suggest that PCB is a promising non-immunogenic alternative to PEG. Nevertheless, the improved immunological and PK profiles demonstrated in previous studies may not necessarily translate to better clinical outcomes. They only depict the body's reaction to foreign drugs, and cannot directly reflect the biochemical or physiological effects of drugs on the body[31]. To better understand whether PCB can overcome the efficacy loss that plagues PEGylated therapies, we must bridge the gap between immunogenicity/PK and efficacy studies. As many treatment regimens such as enzyme replacement therapies require several repeated administrations to fully cure the disease, further investigation is needed into whether a PCB-protected protein retains its immunological stealth and efficacy after three or more injections. In addition, previously reported PCB modification strategies all require surface-accessible groups such as amines for polymer attachment. Therefore, a generalized method to protect any protein with PCB, while keeping its structure fully intact and independent of surface conjugation sites, would be particularly useful.

To address these needs, we have developed a zwitterionic PCB nanocage (NC) encapsulation technology—a generalized approach to physically encase proteins and advance their safety and efficacy (Fig. 4-1a). In addition to markedly improving the immunological and PK profiles of encapsulated uricase even after five consecutive administrations, PCB NC encapsulation strikingly enhanced the therapeutic efficacy of uricase in a rat model mimicking clinical gout presentation (Fig. 4-1b). Furthermore, we have investigated and revealed the mechanism enabling PCB NC encapsulation to inhibit a humoral immune response. To the best of our knowledge, this is the first

reported strategy to convincingly mitigate the efficacy loss encountered by current PEGylated biologics. This is particularly promising for clinical translation, given the expanding pervasiveness of pre-existing and induced anti-PEG Abs[12].

4.3 Experimental Section

4.3.1 Materials

Recombinant uricase from Candida sp. and all chemicals were purchased from Sigma-Aldrich unless otherwise noted and were used as received. Methoxy polyethylene glycol succinimidyl carbonate, molecular weight 10 kDa (mPEG-NHS, 95%), was obtained from Nanocs. 2-((3-acrylamidopropyl) dimethylammonio) acetate (CBAA) and 1-carboxy-N-methyl-N-di(2-methacryloyloxy-ethyl) methanaminium inner salt (CBMAX) were synthesized following our previously published method[32].

4.3.2 Preparation of nanocage for uricase encapsulation

AOT (sodium bis(2-ethylhexyl) sulfosuccinate, 237mg) and Brij 30(poly(ethylene glycol) dodecyl ether, 459mg) were added to a 20mL glass vial to which a stir bar was added[33]. The vial was sealed with a Teflon-lined septum cap and purged with dry nitrogen for 10min. Nitrogen-deoxygenated hexane (10mL) was then added to the vial under vigorous stirring. For the aqueous phase, uricase (2mg) was dissolved in HEPES buffer (pH 8.5, 250 ul), to which CBAA (40mg) and 1-carboxy-N-methyl-N-di(2-methacryloyloxy-ethyl) CBMAX (10mg) were added and dissolved. Dry nitrogen was bubbled through the monomer/protein solution for 2min, after which the aqueous phase was slowly added to the organic continuous phase dropwise. The vial was sonicated to form a stable microemulsion. A 20% (w/v) solution of ammonium persulfate in deionized water (10ul)

was then added to the emulsion. After 5 min, polymerization was initiated by the addition of tetramethylethylenediamine (TEMED, 6 ul) and maintained at 4℃ under rapid magnetic stirring. After the 2-hour reaction, the organic solvent was removed by rotary evaporator and the nanocage was precipitated and washed with THF for three times. The nanocage was re-suspended in PBS buffer and purified with 300-KDa molecular weight cutoff centrifugal filters to remove the free uricase.

4.3.3 Nanocage characterization

Size and zeta potential of PCB NCs was measured by Malvern Zetasizer. Residual activity of uricase after NC encapsulation was measured by Amplex™ Red uric acid/uricase assay kit following the manufacture's protocol. The circular dichroism (CD) spectra of native uricase, PEG-uricase and PCB-uricase were carried out in a buffer containing 50mM KH2PO4/K2HPO4, pH7.4 and collected in the range of 210-260 nm (JASCO J-720 Circular Dichroism Spectrometer). For thermal stability test, modified protein samples in PBS buffer (pH 7.4) were incubated at a various temperature ranging from 25°C to 60°C in water bath for 30 minutes, after which each sample was taken out and quenched in an ice bath for the assay of uricase activity.

4.3.4 Animal studies

All animal experiments adhered to federal guidelines and were approved by the University of Washington Institutional Animal Care and Use Committee (IACUC). Animals were randomized to treatment groups at the beginning of each study. A sample size of three animals per group was used. Spraque–Dawley rats (male, body weight 74–100 g) were obtained from Jackson Laboratories (Seattle, WA).

4.3.5 Immunogenicity study

Native uricase, PEG-uricase, and PCB-uricase at a dose of 5U were IV administered into the rats via the tail vein. The administrations of uricase samples were repeated five times with one week as the time interval between each immunization. At the end of the fifth week (35^{th} day), all the rats were euthanized. The rats were sacrificed and their blood collected through cardiac puncture were handled for ELISA test[34]. The spleens of rats were harvested and the splenocyte was isolated by 100μm cell strainer (Fisherbrand™). The rat splenocytes from each group were stained with anti-rat Abs to MHCII and CD86 (eBioscience) and then analyzed by flow cytometry. For the test of T cell activation, rat splenocytes from each group were cultured in 12-well plate (10^6/well) and re-stimulated with native uricase, PEG-uricase, and PCB-uricase (1mg/ml) respectively. The splenocytes from each rat were cultured in two wells as duplicates. After 72h, the cell culture medium from each well was collected for the quantification of IL-4 using IL-4 Rat ELISA kit (Life Technologies).

4.3.6 PK and bio-distribution study

Each uricase sample was administered to the rats via tail vein injection at the dose of 25 U/kg body weight. The IV injections and bleeding procedure were repeated five times with one week as the time interval between each injection. Blood was collected from the tail vein at 5 min, 4h, 8h, 24 h, 48 h, and 72 h during the first and fifth week. The uricase concentration in plasma was estimated based on the enzyme activity. To exclude the disturbance of inherent uricase contained in rats, uricase concentration from the rat sera naïve to the administration of uricase samples were subtracted as background. All PK parameters were calculated using PKSolver following the instructions[35]. For the biodistribution study, all rats were given FITC-labeled uricase sample as the

fifth dose after four-week administration of unlabeled uricase samples (one dose per week). At 72 h post-fifth-injection, the rats were sacrificed for the collection of blood and main organs including heart, liver, spleen, lung, kidney. After tissues homogenization, the fluorescence of uricase sample in each tissue was measured and normalized based on the tissue weight.

Gouty rat model. Native uricase, PEG-uricase, and PCB-uricase at a dose of 25U/kg body weight and PBS vehicle were IV administered into the rats via the tail vein. The IV injections and bleeding procedure were repeated five times with one week as the time interval between each injection. The acute gout was induced in these four groups of rats on the fifth week following the protocol previously reported[36, 37]. Briefly, MSU crystals were prepared using the Denko and Whitehouse method modified by Scanu et al.[38], sterilized and suspended in sterile PBS at a concentration of 50mg/ml. Then 50µl of MSU suspensions were injected intra-articularly (IA.) into the left knee on isoflurane-anesthetized rats at 6 hours before the fifth injection of uricase samples. To alleviate the pain of rats, Buprenorphine HCl extended-release injectable suspension(ZooPharm or Animalgesics®) was administered by subcutaneous (SC.) injection. During the first and fifth week, the urate concentration from the rat sera before the administration of uricase samples was measured ($C_{0,urate}$) by assaying the blood with Amplex™ Red uric acid/uricase assay kit and the plasma urate concentration at 5 min, 4h, 8h, 24 h, 48 h, and 72 h after the injection of uricase samples ($C_{t,urate}$) was also monitored. The PD effect of uricase samples was calculated as $\Delta C_{urate}\% = (C_{0,urate}-C_{t,urate})/C_{0,urate}*100\%$. $\Delta C_{urate}\%$ of 100% indicates a complete elimination of urate in the blood.

The transverse diameters of left and right knee joints in the rats after the injection of uricase samples (0, 24h, 48h, 72h) were measured using a digital calliper. The swelling score of each rat

was determined based on the size difference between gouty left and normal right knee joints: 0, 0 ~ 10%;1,10%~25%; 2, 25%~50%; 3, >50%. At the same time point, an observer who was blinded to the interventions gave a lameness score for each rat based on its gait and posture: 0, no observable abnormality; actively and freely move like normal rats; 1, slight abnormality; still be able to move freely but the gait is slightly different from normal rats; 2, obvious abnormality; still be able to move but obvious abnormal gait can be recognized; 3, severe abnormality; unable to move or move in an extremely abnormal way and have difficulty to reach food/water. The clinical scores of rats were calculated as the sum of swelling score plus lameness score. The rats were sacrificed at the 72h after the fifth injection of uricase samples. Synovial cavities of the left knee joint were then washed with 300ul (three times of 100ul each) of PBS by inserting a 25G needle into the rat knee joint. IL-1b and TNF-α in synovial washes was determined by ELISA kit (BD Biosciences), and the leukocyte number was counted under Leica inverted microscope. All knee joints were dissected and fixed in 4% paraformaldehyde for 24h; then decalcified in 5% nitric acid-ethanol for 48h, and embedded in paraffin. Periarticular tissue sections (4μm) were stained with H&E to assess inflammatory cell infiltrates; slices of knee joints were stained with safranin-O dye to assess cartilage proteoglycan content and osteoarthritis. The semi-quantitative scores of OA severity were determined based on the scoring system reported by S.S. Glasson et al[39].

4.4 Results and Discussion

4.4.1 Zwitterionic nanocages physically encapsulate uricase

Effective *in vivo* applications of therapeutic proteins are stymied by complex physiological obstacles, including opsonization, antigen-specific Abs response, and reticuloendothelial system (RES) clearance. PEGylation is widely employed to hurdle these barriers by reducing their susceptibility to opsonization and immune recognition. However, PEG attached to proteins has been shown to induce Abs reactive against its hydrophobic backbone (–CH2-CH2-O)[40] as well as the methoxy terminal (-OCH3)[41]. It is interesting to know that the replacement of the methoxy group in PEG with a more hydrophilic hydroxyl group can reduce anti-PEG Abs[36]. Additionally, PEGylation is oftentimes limited by the number of functional groups on a protein surface. Sparse PEG molecules grafted to proteins not only amplify the PEG immunogenicity via haptic effects, but also shield insufficiently the underlying protein from immune recognition[42].

Recognizing the shortcomings of PEGylation, we developed a zwitterionic PCB NC capable of physically and comprehensively wrapping proteins in an entirely hydrophilic PCB polymer network. Zwitterionic materials, which bear a pair of oppositely charged ions in the same moiety while maintaining an overall neutral charge, are known for their strong hydration effects mediated by the electrostatic interactions between zwitterions and surrounding water molecules[43]. Among these zwitterionic materials, PCB is emerging as a promising alternative for PEG. Its superhydrophility enables PCB polymer to be an excellent nonfouling material[44]. PCB-coated surfaces can reduce nonspecific protein adsorption from whole blood to an ultra-low level[45]. PCB is also known for its minimal immunogenicity and inertness to biological systems. Hydrogel

implants polymerized from zwitterionic carboxy betaine (CB) were able to resist the foreign-body reaction in mice for at least three months[46].

In the present work, CB-derived monomers[34] and bifunctional cross-linkers[32] are used to prepare protein-loaded PCB NCs in inverse nanoemulsions. As the direct polymerization process involves no reactions with functional groups on protein surfaces, this technology is promising to generalize protein encapsulation while maintaining the intact structure of protein drugs. The high bioactivity (Table 4-1) of uricase encased in PCB NC suggests its enzymatic function is unaltered and confirms our presumption that urate substrates are small enough to freely diffuse into the polymer mesh and reach the catalytic domain within the enzyme. After three formulations of PCB NC were compared, formulation #2 with a uniform size around 100nm (PDI 0.19) was chosen for the rest of studies, owing to its high yield and good maintenance of protein bioactivity (Fig. 4-2a). The relatively low encapsulation percentage (6.8%) of uricase in formulation #2 implies a thick polymer coverage on the core protein, which is favorable to circumvent the recognition and presentation by immune cells.

The intact structure of uricase was revealed by circular dichroism (CD) spectra, which indicates that no significant changes in the secondary structure of uricase occurred during PCB NC encapsulation (Fig. 4-2b). Considering that a stable protein formulation is essential to protect the protein from activity loss during long-term storage, the thermal stability of various uricase formulations was gauged over a temperature range from 25℃ to 60℃ (Fig. 4-2c). While the residual activity of naked uricase and PEGylated uricase (PEG-uricase) at the same temperature decreased to 20% and 60% respectively, uricase encapsulated by PCB-NC (PCB-uricase) retained

90% of enzyme activity at 60℃, evincing that PCB NC could dramatically increase the protein stability. This merit of PCB NC can be explained by the unique properties of PCB and the NC structure. First, the zwitterionic PCB polymer is a biomimetic derivative of CB, which is a naturally-occurring osmolyte and protein stabilizer and can provide a stabilizing environment for proteins. Second, coverage of PCB NCs to some extent limits the conformational change of the core protein, and thus restricts its tendency to denature under harsh conditions.

4.4.2 Immunogenicity study

Like many foreign proteins, uricase of non-human origins suffers a variety of immunogenicity-related issues, which heavily restrain its effectiveness in the clinic. PEGylation of uricase, while capable of reducing the generation of anti-uricase Abs, elicits additional anti-PEG Abs and cause non-responsiveness and adverse reactions in patients. To improve the safety and efficacy of protein drugs, it is crucial to eradicate all the potential immune response, regardless of whether they are reactive against the protein or its associated materials. In our recent study, no anti-PCB Abs in rat sera were detected by enzyme-linked immunosorbent assay (ELISA) and surface plasmon resonance (SPR) after three IV administrations of proteins modified with PCB polymer. In the present work, two more doses (five in total) of native uricase, PEG-uricase and PCB-uricase were IV injected to healthy Sprague-Dawley (SD) rats for five consecutive weeks (one dose per week), after which rat sera were collected on 35th day for Ab tests (Fig. 4-3 a-d).

As the non-responders to pegloticase produced IgG and IgM[15, 18], titers of both two Ab isotypes were measured and listed in Table 2-2. PEGylation failed to completely mitigate the generation of anti-protein Abs, even though the anti-uricase IgM and IgG titers decreased to 1:400 and 1:3200

respectively, much lower than that of the native uricase group (IgM titers 1:6400; IgG titers >1:25600). Consistent with clinical findings suggesting anti-PEG Abs rather than anti-uricase Abs to be the main culprit for the efficacy loss, a high level of anti-PEG Abs (IgM titers 1:6400; IgG titers 1:1600) was detected in the group treated with PEG-uricase. Notably, high-affinity anti-PEG IgG, which shows to increase the likelihood of efficacy loss in the clinic[15], was also clearly detected. This indicates that T-cell-dependent (Td) humoral immune responses characterized by Ig heavy chain isotype switching are involved in the production of anti-PEG Abs. By contrast, neither anti-uricase Abs nor anti-PCB Abs were detected in the rat group treated with PCB-uricase, which is consistent with the previous study and demonstrates that PCB NC made from the minimally immunogenic PCB material is able to completely eliminate the Ab response against its protected proteins while introducing no Ab response against itself[34, 47].

To elucidate the mechanism by which PCB NC inhibits an immune response, we harvested the rat spleens at the terminal time point and investigated the status of antigen presenting cells (APC) among splenocytes. As shown in (Fig. 4-3 g-f), the ratio of stimulated APC (CD86+MHCII+) in splenocytes was clearly elevated after the treatment of uricase (10.8±1.2) and PEG-uricase (6.4±0.6). In comparison, such percentage of activated APC (2.6±0.3) in the PCB-uricase group was as low as that in the unstimulated control group (2.5±0.1), indicating a quiescent status of APC. This demonstrates that PCB NC is able to restrict the antigen-presenting capability of APC likely by reducing protein endocytosis, interfering with protein proteolysis and physically blocking MHCII-epitope binding. Once APC are activated, they have increased capacity to capture and present antigens for T-cell stimulation, which in turn will lead to B cell maturation, clonal expansion, and the generation of higher affinity Abs[48, 49]. In this way, the constraining effect of

PCB NC on APC is also favorable to hinder T cell activity, which plays a pivotal role in amplifying the Td humoral immune response. As shown in Fig. 4-3e, the level of IL-4, a marker of T cell stimulation and proliferation, was strikingly low in the splenocytes harvested from the PCB-uricase group (Fig. 4-3 g-f). However, elevated secretion of IL-4 was detected in the cohorts treated with native uricase and PEG-uricase. Consistent with the results in Ab test, these data corroborate the hypothesis that PCB NC attenuates the humoral immune response by restraining the stimulation of APC and T cells, which otherwise will contribute to B cell maturation and large production of Abs.

4.4.3 PK and biodistribution study

Following the same dosing schedule as in the immunogenicity study, we next characterized the PK profiles of native uricase, PEG-uricase and PCB-uricase in SD rats after single and multiple IV injections. As shown in Fig. 4-4 a-c, the first-week and fifth-week concentration-time kinetics of each uricase sample are fitted to the one-compartment model, based on which key PK parameters were derived (Table 4-3). After the first injection, native uricase displayed a half-life ($t_{1/2}$) as short as 3.8h, which further decreased to 1.6h after five repeated administrations, resulting in 2.5-fold increased clearance (CL). PEGylation apparently extended circulation behavior ($t_{1/2}$=16.8h) of uricase after a single injection (Fig. 4-4a). However, an accelerated CL phenomenon was observed for PEG-uricase, in which the $t_{1/2}$ shrunk to 6.3h after five administrations (Fig. 4-4b). Corresponding to the decreased residence time in blood circulation and the escalated anti-PEG/anti-uricase Ab titers, both PEG-uricase and native uricase lost over 60% of their initial bioavailability (AUC) after five injections. In contrast, PCB-uricase manifested a persistently superb $t_{1/2}$ as long as 35.9h (1st dose) and 34.6h (5th dose). Due to the absence of any Ab response,

repeated administrations did not induce accelerated clearance or detectable bioavailability loss of PCB-uricase (Fig. 4-4c).

Moreover, the bio-distribution of uricase samples was examined by measuring the fluorescence of FITC-labeled uricase samples in main organs/serum harvested at 72h post-fifth-injection (Fig. 4-4d). In agreement with the PK result, the accumulation of PCB-uricase in serum is obviously higher than that of native uricase and PEG-uricase due to its slow elimination rate and elongated residence time in the blood (Table 4-3). The extended presence of PCB NC in systemic circulation revealed by both PK and bio-distribution studies promotes the sustained pharmacodynamic (PD) effect of PCB-uricase in catalyzing urate metabolism. PCB-uricase also exhibits increased distribution in other main organs, especially the liver and spleen (Fig. 4-4d). This can be partially explained by the non-fouling property of PCB NC, which allows PCB-uricase to evade engulfment by the RES system, the main route accounting for nanoparticle clearance. Though PCB-uricase may eventually be internalized, the coverage with PCB NC tends to retard degradation of the encased enzyme, thereby leading to high accumulation in liver and spleen.

4.4.4 Efficacy study in gouty animal model

To demonstrate the therapeutic benefit of PCB NC in a clinical-mimicking system, we compared the efficacy of three uricase samples in an acute gouty rat model. As illustrated in Fig. 4-5a, four groups of SD rats were IV injected with PBS, native uricase, PEG-uricase and PCB-uricase, respectively, with one dose per week for four consecutive weeks. Six hours before the fifth injection of PBS or uricase samples, monosodium urate (MSU) crystals (2.5mg) were intra-articularly (IA) injected into the left knee of rats to induce gouty arthritis. The PD effect of uricase

samples after single and multiple injections was gauged as the change percentage of serum urate concentration $\Delta C_{urate}\% = (C_{0,urate}-C_{t,\ urate})/C_{0,urate}*100\%$ (Fig. 4-5 b-d). A $\Delta C_{urate}\%$ of 100% indicates the complete elimination of urate in the blood. Rats injected with native uricase and PEG-uricase showed relatively low magnitudes of urate reduction and the AUC_{0-72h} of ΔC_{urate} suffered a slump after five repetitive administrations. In contrast, PCB-uricase demonstrates sustained and enhanced PD profiles, still maintaining a $\Delta C_{urate}\%$ above 80% for more than 72h post-injection. The results of PD study provide direct evidence that correlates the improved immunological/PK profiles of PCB NC with the capacity to boost therapeutic effects.

Furthermore, the clinical symptoms of gouty rats after the fifth injection of each uricase sample was monitored and scored. As shown in Fig. 4-5e, right after the fifth administrations of uricase samples (time 0), all rats in each of the four groups exhibited the same level of arthritis symptoms owing to the pre-6h IA injection of MSU. During a monitoring window of 72h, gouty rats treated with PBS sham, native uricase, and PEG-uricase showed a limited extent of disease improvement (Fig. 4-5e). By comparison, rehabilitation was greatly expedited in the PCB-uricase group: the clinical score rapidly declined from 3.67±0.57 (0h) to 1±0.57 (72h) under treatment with PCB-uricase. In addition, the assay of synovial fluids aspirated from the gouty rats' knee joints also supports the improved therapeutic effect of PCB-uricase (Fig. 4-5f, Table 4-4). The arthritis inflammation is maintained by a substantial influx of leukocytes including monocytes and neutrophils into the synovial area, and the proinflammatory cytokines released from these leukocytes may exacerbate the inflammation and trigger tissue destruction. Herein, the treatment of PCB-uricase significantly inhibited the leukocyte numbers and proinflammatory cytokines including TNF-α and IL-1β in synovial fluids (Fig. 4-5f), confirming that uricase encased in PCB

NC could efficiently catalyze the metabolism of urate and thus lessen the deposition of inflammation incentive MSU at knee joints. Moreover, histopathological analysis of the periarticular tissues further suggests the efficacy of PCB-uricase in soothing gouty arthritis. In the cohort treated with PCB-uricase, the proliferation of lining cells around the synovium is greatly reduced (Fig. 4-5h) and only small cartilage loss could be observed (Fig. 4-5i). In stark contrast, the cohorts treated with native uricase and PEG-uricase exhibited a relatively high histologic score (Fig. 4-5g) and more severe osteoarthritis (OA) characterized by the moderate multifocal destruction of the femoral cartilage.

4.5 Conclusions

Immunogenicity is a widely recognized risk factor in the safe and effective application of therapeutic proteins. Among the variety of approaches that aim to reduce undesirable immune responses and improve the efficacy of biologics, PEGylation remains the gold standard in both academia and industry. Though PEG was initially presumed to be immunologically inert, both pre-existing and induced anti-PEG Abs have been found in patients receiving PEGylated drugs as well as in the general population; these are causing adverse clinical events and a growing resistance to many biologics. A safe and efficient alternative to PEGylation is urgently needed. In this work, our results establish that PCB NC encapsulation is able to significantly boost the efficacy of therapeutic enzymes and completely prevent a humoral immune response derived from either protein or polymer. Apart from these properties, PCB-based materials strongly resist fouling, are immunologically inert and simple to synthesize, with numerous functional groups for targeting drug delivery and diagnostics. Thus, PCB NC encapsulation is a broadly applicable platform and an excellent alternative to PEGylation.

4.6 Schemes, Figures, and Tables

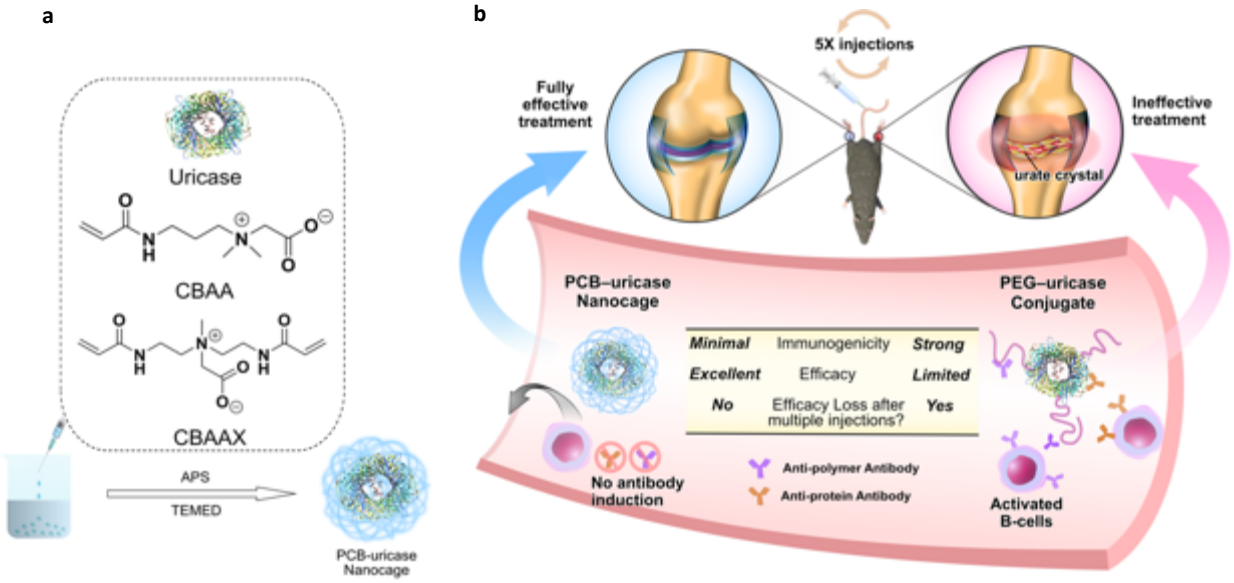

Figure 4-1. (a) encapsulation of uricase with zwitterionic PCB NC. (b) Schematic illustration of the sequence of events after native uricase, PEGylated uricase and uricase encapsulated by PCB NC enter the blood stream. Both anti-uricase and anti-PEG Abs are produced after multiple injections of PEG-uricase conjugate, leading to the loss of efficacy in gout treatment. PCB NC shields uricase from immune recognition and produces no anti-polymer or anti-uricase Abs, leading to enhanced pharmacokinetics and improved efficacy in gout treatment.

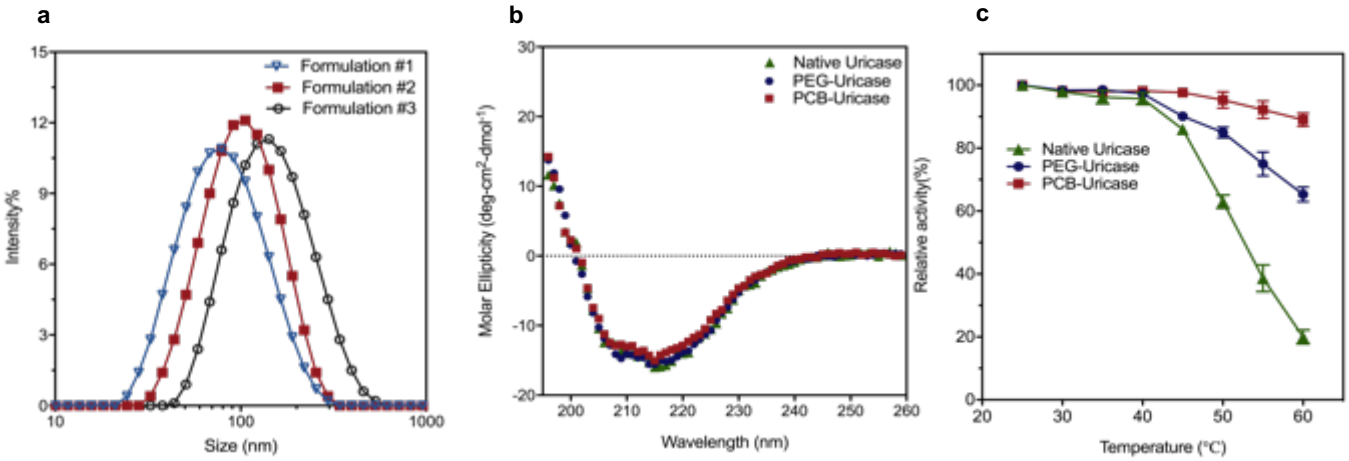

Figure 4-2. Encapsulation of uricase with zwitterionic PCB NC. (a) Size distributions of three PCB NC formulations measured by dynamic light scattering. (b) CD spectra of native and modified uricase; c, Thermal stabilities of native and modified uricase.

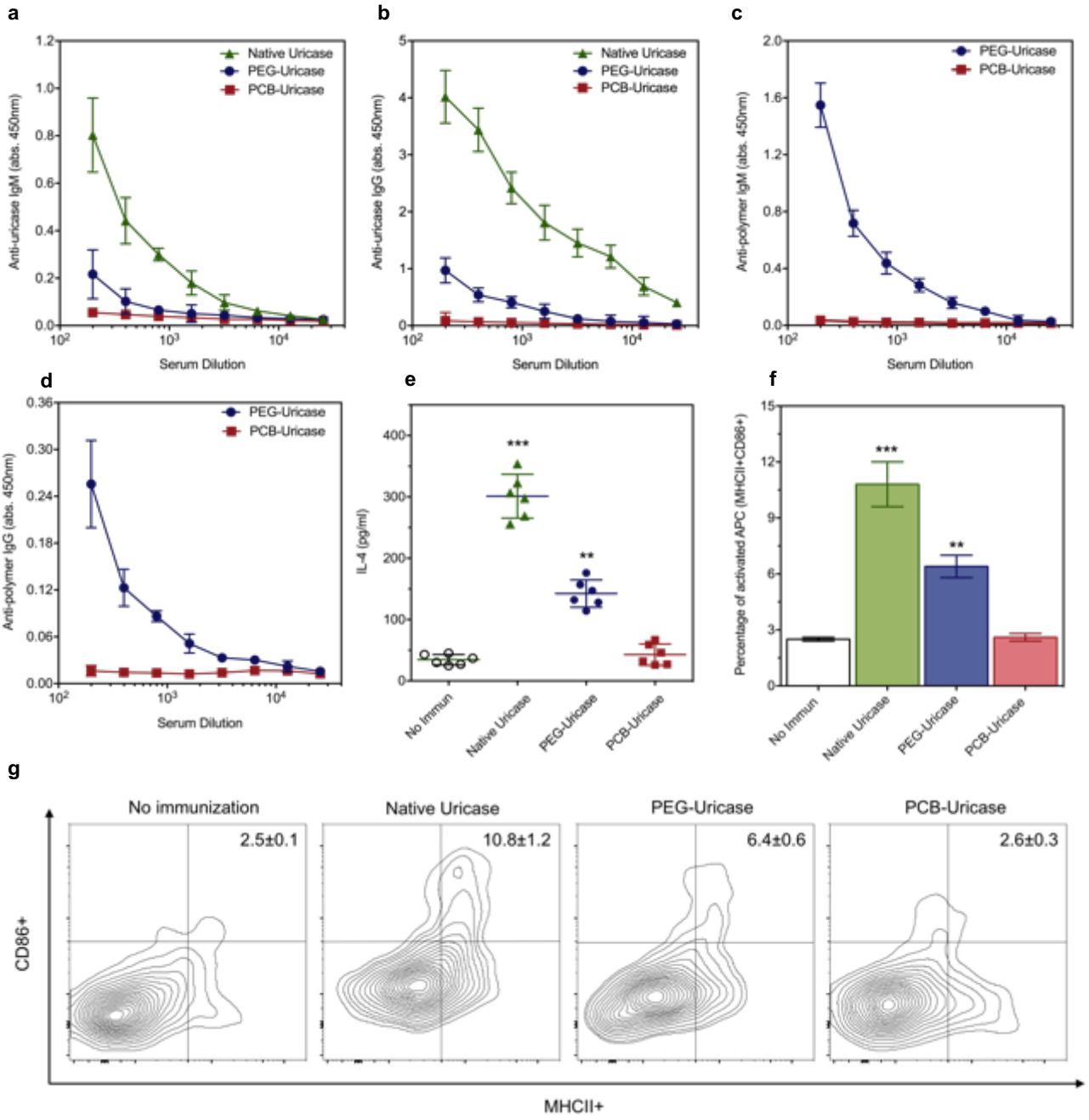

Figure 4-3. Zwitterionic PCB NC completely eradicates humoral immune response. Detection of anti-uricase IgM (a), anti-uricase IgG (b), anti-polymer IgM (c), and anti-polymer IgG (d) in rat sera collected 7 days after the fifth injection of native uricase, PEGylated uricase and uricase

encapsulated by PCB NC. e, Detection of IL-4 levels secreted by splenocytes harvested from rats at the 7th day post-fifth injection. The ratio of activated APC (MHCII+CD86+) measured as a percentage of the total rat PBMC (f), and representative dot plots for PBMC (g). Results are plotted as mean ± SD (n = 3 in a-d; n = 6 in e-f). All statistical analyses were performed using student test (**P ≤ 0.01; ***P ≤ 0.005)

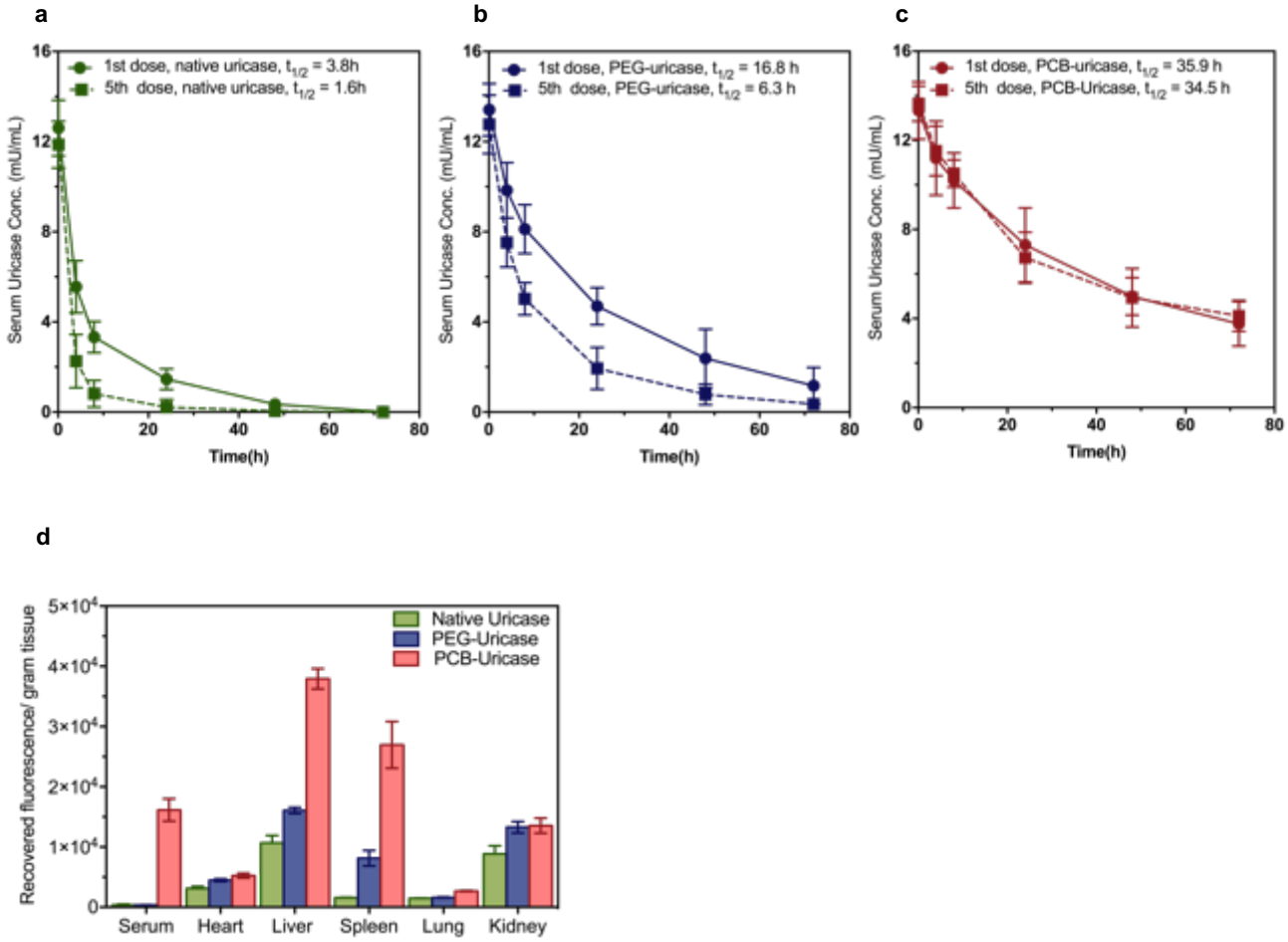

Figure 4-4. Zwitterionic PCB NC enhances PK/PD properties of uricase. The circulation behaviors of native uricase (a), PEGylated uricase (b), and uricase encapsulated by PCB NC (c), after the first and fifth IV injections (one dose per week). d, Biodistribution of modified uricase vs. native uricase at 72h post fifth injection. Results are plotted as mean ± s.d. (n = 3).

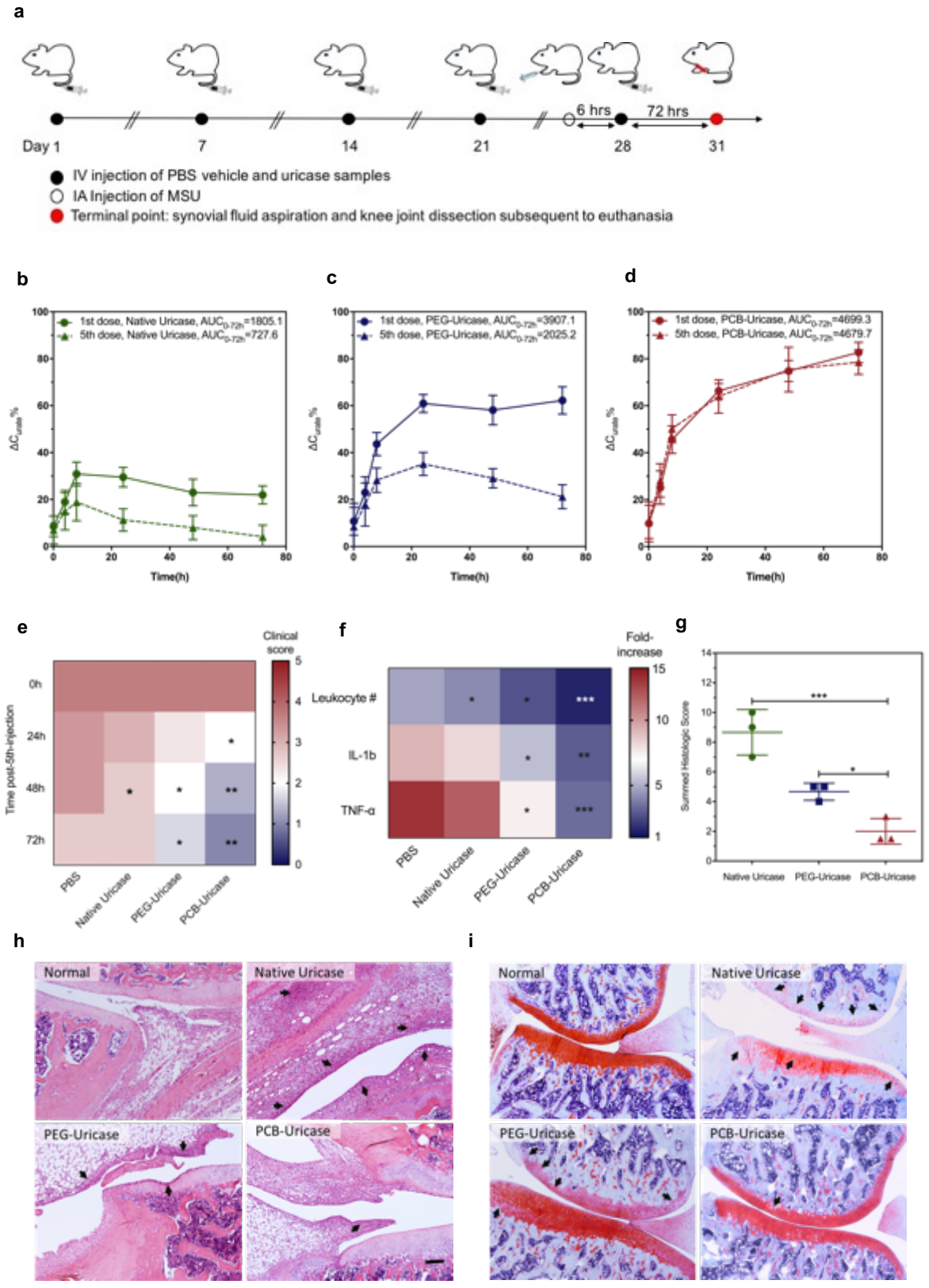
a
Day 1
7
14
21
28
31
6 hrs
72 hrs
IV injection of PBS vehicle and uricase samples
IA Injection of MSU
Terminal point: synovial fluid aspiration and knee joint dissection subsequent to euthanasia
b
1st dose, Native Uricase, AUC0-72h=1805.1
5th dose, Native Uricase, AUC0-72h=727.6
Time(h)
c
1st dose, PEG-Uricase, AUC0-72h=3907.1
5th dose, PEG-Uricase, AUC0-72h=2025.2
Time(h)
d
1st dose, PCB-Uricase, AUC0-72h=4699.3
5th dose, PCB-Uricase, AUC0-72h=4679.7
Time(h)
e
Clinical score
Time post-5th-injection
0h
24h
48h
72h
PBS
Native Uricase
PEG-Uricase
PCB-Uricase
f
Fold-increase
Leukocyte #
IL-1b
TNF-α
PBS
Native Uricase
PEG-Uricase
PCB-Uricase
g
Summed Histologic Score
Native Uricase
PEG-Uricase
PCB-Uricase
h
Normal
Native Uricase
PEG-Uricase
PCB-Uricase
i
Normal
Native Uricase
PEG-Uricase
PCB-Uricase

Figure 4-5. Zwitterionic PCB NC improves the therapeutic effect of uricase in a gouty rat model. (a) Schematic illustration of the efficacy study of uricase samples in an induced acute gouty rat model; The urate-eliminating ability of native uricase (b), PEGylated uricase (c), and uricase encapsulated by PCB NC (d), after the first and fifth IV injections, calculated as change of uric acid concentration in blood ($\Delta C_{urate}\% = (C_{0,urate} - C_{t,urate})/C_{0,urate}*100\%$). (e) Clinical score change of each cohort. (f) Analysis of inflammation marker in rat synovial fluid including IL-1b, TNF-α, and leukocyte number (#). (g) Semi-quantitative scores of OA severity. (h) H&E stained slices of periarticular tissues i, Safranin-O stained slices of rat knee joints showing the medial femoral condyles (above) and medial tibial plateau (below), displaying a variety of OA severity. Results are plotted as mean ± s.d. (n = 3). *$P \leq 0.05$; **$P \leq 0.01$; ***$P \leq 0.005$.

Table 4-1. Characteristics of PCB NC encapsulating uricase

Mole% of crosslinking	Encapsulation % of uricase	Weight % yield of nanocage	Hydrodynamic size (nm)	PDI	Zeta potential	Residual activity of uricase
14	14.2	33.7	86.3±5.2	0.12±0.03	-2.13±0.81	90±2%

Table 4-2. Antibody titers detected by direct ELISA

Sample Antibody Isotype	Native uricase	PEG-uricase	PCB-uricase
Anti-uricase IgM	1:6400	1:400	< 1:200
Anti-uricase IgG	>1:25600	1:3200	< 1:200
Anti-polymer IgM		1:6400	< 1:200
Anti-polymer IgG		1:1600	< 1:200

Table 4-3. Analysis of inflammation marker in rat synovial fluid

Sample / Parameters	Normal	PBS	Native uricase	PEG-uricase	PCB-uricase
Leukocyte # ($x10^5$/ml)	3.10±0.40	37.63±7.31	32.60±9.79	21.33±3.42	11.93±4.64
IL-1β (pg/ml)	13.07±1.69	105.03±6.26	94.13±8.64	59.43±9.20	26.43±7.22
TNF-α (pg/ml)	7.93±1.63	73.50±6.22	64.97±9.05	42.47±2.96	23.40±4.60

Table 4-4. PK parameters of uricase samples after repeated IV. injections

Sample / Parameters	Native uricase		PEG-uricase		PCB-uricase	
Injection times	1	5	1	5	1	5
$t_{1/2}$ (h)	3.8	1.7	16.8	6.3	35.9	34.6
CL (mU/(mU/ml)/h)	11.8	27.4	2.7	7.2	1.3	1.3
AUC∞ (mU/mL x h)	69.7	30.1	301.6	113.9	646.4	635.5

4.7 References

1. Aggarwal, R. S., What's fueling the biotech engine-2012 to 2013. *Nat Biotechnol* 2014, *32* (1), 32-9.

2. Moussa, E. M.; Panchal, J. P.; Moorthy, B. S.; Blum, J. S.; Joubert, M. K.; Narhi, L. O.; Topp, E. M., Immunogenicity of Therapeutic Protein Aggregates. *J Pharm Sci* 2016, *105* (2), 417-30.

3. Rosenberg, A. S., Immunogenicity of biological therapeutics: a hierarchy of concerns. *Dev Biol (Basel)* 2003, *112*, 15-21.

4. Yin, L.; Chen, X.; Vicini, P.; Rup, B.; Hickling, T. P., Therapeutic outcomes, assessments, risk factors and mitigation efforts of immunogenicity of therapeutic protein products. *Cell Immunol* 2015, *295* (2), 118-26.

5. Nechansky, A.; Kircheis, R., Immunogenicity of therapeutics: a matter of efficacy and safety. *Expert Opin Drug Discov* 2010, *5* (11), 1067-79.

6. Baker, M. P.; Reynolds, H. M.; Lumicisi, B.; Bryson, C. J., Immunogenicity of protein therapeutics: The key causes, consequences and challenges. *Self Nonself* 2010, *1* (4), 314-322.

7. Vonwussow, P.; Freund, M.; Dahle, S.; Jakschies, D.; Poliwode, H.; Deicher, H., Immunogenicity of Different Types of Interferons in the Treatment of Hairy-Cell Leukemia. *New Engl J Med* 1988, *319* (18), 1226-1227.

8. Ing, M.; Gupta, N.; Teyssandier, M.; Maillere, B.; Pallardy, M.; Delignat, S.; Lacroix-Desmazes, S.; Consortium, A., Immunogenicity of long-lasting recombinant factor VIII products. *Cellular Immunology* 2016, *301*, 40-48.

9. Wadhwa, M.; Skog, A. L. H.; Bird, C.; Ragnhammar, P.; Lilljefors, M.; Gaines-Das, R.; Mellstedt, H.; Thorpe, R., Immunogenicity of granulocyte-macrophage colony-stimulating factor

(GM-CSF) products in patients undergoing combination therapy with GM-CSF. *Clin Cancer Res* 1999, *5* (6), 1353-1361.

10. van Schouwenburg, P. A.; Rispens, T.; Wolbink, G. J., Immunogenicity of anti-TNF biologic therapies for rheumatoid arthritis. *Nat Rev Rheumatol* 2013, *9* (3), 164-72.

11. Harris, J. M.; Chess, R. B., Effect of pegylation on pharmaceuticals. *Nat Rev Drug Discov* 2003, *2* (3), 214-21.

12. Smorodinsky, N.; Vonspecht, B. U.; Cesla, R.; Shaltiel, S., A Conjugate between a Purified Timothy Allergen and Poly(N-Vinyl Pyrrolidone) Suppresses the Specific Ige Response in Mice. *Immunol Lett* 1981, *2* (5-6), 305-309.

13. Veronese, F. M.; Visco, C.; Massarotto, S.; Benassi, C. A.; Ferruti, P., New Acrylic Polymers for Surface Modification of Enzymes of Therapeutic Interest and for Enzyme Immobilization. *Ann Ny Acad Sci* 1987, *501*, 444-448.

14. Zhang, P.; Sun, F.; Tsao, C.; Liu, S. J.; Jain, P.; Sinclair, A.; Hung, H. C.; Bai, T.; Wu, K.; Jiang, S. Y., Zwitterionic gel encapsulation promotes protein stability, enhances pharmacokinetics, and reduces immunogenicity. *P Natl Acad Sci USA* 2015, *112* (39), 12046-12051.

15. Hershfield, M. S.; Ganson, N. J.; Kelly, S. J.; Scarlett, E. L.; Jaggers, D. A.; Sundy, J. S., Induced and pre-existing anti-polyethylene glycol antibody in a trial of every 3-week dosing of pegloticase for refractory gout, including in organ transplant recipients. *Arthritis Res Ther* 2014, *16* (2).

16. Sundy, J. S.; Baraf, H. S. B.; Yood, R. A.; Edwards, N. L.; Gutierrez-Urena, S. R.; Treadwell, E. L.; Vazquez-Mellado, J.; White, W. B.; Lipsky, P. E.; Horowitz, Z.; Huang, W.; Maroli, A. N.; Waltrip, R. W.; Hamburger, S. A.; Becker, M. A., Efficacy and Tolerability of Pegloticase

for the Treatment of Chronic Gout in Patients Refractory to Conventional Treatment Two Randomized Controlled Trials. *Jama-J Am Med Assoc* 2011, *306* (7), 711-720.

17. Hershfield, M. S.; Ganson, N. J.; Kelly, S. J.; Scarlett, E. L.; Jaggers, D. A.; Sundy, J. S., Pharmacokinetics and Immunogenicity of Pegloticase (Pl) Infused Every 3 Weeks to Treat Refractory Gout (Rg), Including in Organ Transplant Recipients (Tr). *Ann Rheum Dis* 2012, *71*, 440-440.

18. Ganson, N. J.; Kelly, S. J.; Scarlett, E.; Sundy, J. S.; Hershfield, M. S., Control of hyperuricemia in subjects with refractory gout, and induction of antibody against poly(ethylene glycol) (PEG), in a phase I trial of subcutaneous PEGylated urate oxidase. *Arthritis Res Ther* 2006, *8* (1).

19. Lipsky, P. E.; Calabrese, L. H.; Kavanaugh, A.; Sundy, J. S.; Wright, D.; Wolfson, M.; Becker, M. A., Pegloticase immunogenicity: the relationship between efficacy and antibody development in patients treated for refractory chronic gout. *Arthritis Res Ther* 2014, *16* (2).

20. Armstrong, J.; Hempel, G.; Koling, S.; Chan, L. S.; Meiselman, H. J.; Fisher, T. C.; Garratty, G., Rapid clearance of PEG-asparaginase in ALL patients by an antibody against poly (ethylene glycol). *Blood* 2006, *108* (11), 526a-526a.

21. Armstrong, J. K.; Hempel, G.; Koling, S.; Chan, L. S.; Fisher, T.; Meiselman, H. J.; Garratty, G., Antibody against poly(ethylene glycol) adversely affects PEG-asparaginase therapy in acute lymphoblastic leukemia patients. *Cancer-Am Cancer Soc* 2007, *110* (1), 103-111.

22. van der Eijk, A. A.; Vrolijk, J. M.; Haagmans, B. L., Antibodies neutralizing peginterferon alfa during retreatment of hepatitis C. *New Engl J Med* 2006, *354* (12), 1323-1324.

23. Jiang, S. Y.; Cao, Z. Q., Ultralow-Fouling, Functionalizable, and Hydrolyzable Zwitterionic Materials and Their Derivatives for Biological Applications. *Adv Mater* 2010, *22* (9), 920-932.

24. Ladd, J.; Zhang, Z.; Chen, S.; Hower, J. C.; Jiang, S., Zwitterionic polymers exhibiting high resistance to nonspecific protein adsorption from human serum and plasma. *Biomacromolecules* 2008, *9* (5), 1357-1361.

25. Zhang, L.; Cao, Z. Q.; Bai, T.; Carr, L.; Ella-Menye, J. R.; Irvin, C.; Ratner, B. D.; Jiang, S. Y., Zwitterionic hydrogels implanted in mice resist the foreign-body reaction. *Nature Biotechnology* 2013, *31* (6), 553-556.

26. Liu, S. J.; Jiang, S. Y., Chemical conjugation of zwitterionic polymers protects immunogenic enzyme and preserves bioactivity without polymer-specific antibody response. *Nano Today* 2016, *11* (3), 285-291.

27. Keefe, A. J.; Jiang, S. Y., Poly(zwitterionic)protein conjugates offer increased stability without sacrificing binding affinity or bioactivity. *Nat Chem* 2012, *4* (1), 60-64.

28. Zhang, P.; Jain, P.; Tsao, C.; Sinclair, A.; Sun, F.; Hung, H. C.; Bai, T.; Wu, K.; Jiang, S., Butyrylcholinesterase nanocapsule as a long circulating bioscavenger with reduced immune response. *J Control Release* 2016, *230*, 73-8.

29. Chirmule, N.; Jawa, V.; Meibohm, B., Immunogenicity to Therapeutic Proteins: Impact on PK/PD and Efficacy. *Aaps J* 2012, *14* (2), 296-302.

30. Cohen, J. A.; Beaudette, T. T.; Tseng, W. W.; Bachelder, E. M.; Mende, I.; Engleman, E. G.; Frechet, J. M. J., T-Cell Activation by Antigen-Loaded pH-Sensitive Hydrogel Particles *in Vivo*: The Effect of Particle Size. *Bioconjugate Chem* 2009, *20* (1), 111-119.

31. Carr, L. R.; Zhou, Y. B.; Krause, J. E.; Xue, H.; Jiang, S. Y., Uniform zwitterionic polymer hydrogels with a nonfouling and functionalizable crosslinker using photopolymerization. *Biomaterials* 2011, *32* (29), 6893-6899.

32. Zhang, P.; Sun, F.; Liu, S.; Jiang, S., Anti-PEG antibodies in the clinic: Current issues and beyond PEGylation. *J Control Release* 2016, *244* (Pt B), 184-193.

33. Jawa, V.; Cousens, L. P.; Awwad, M.; Wakshull, E.; Kropshofer, H.; De Groot, A. S., T-cell dependent immunogenicity of protein therapeutics: Preclinical assessment and mitigation. *Clin Immunol* 2013, *149* (3), 534-555.

34. Sheikh, N. A.; Jones, L. A., CD54 is a surrogate marker of antigen presenting cell activation. *Cancer Immunol Immun* 2008, *57* (9), 1381-1390.

35. dos Santos, R. M. S.; Oliveira, S. M.; Silva, C. R.; Hoffmeister, C.; Ferreira, J.; Assreuy, J., Anti-nociceptive and anti-edematogenic effects of glibenclamide in a model of acute gouty attack in rats. *Inflamm Res* 2013, *62* (6), 617-625.

36. Pineda, C.; Fuentes-Gomez, A. J.; Hernandez-Diaz, C.; Zamudio-Cuevas, Y.; Fernandez-Torres, J.; Lopez-Macay, A.; Alba-Sanchez, I.; Camacho-Galindo, J.; Ventura, L.; Gomez-Quiroz, L. E.; Gutierrez-Ruiz, M. C.; Garcia-Vazquez, F.; Reginato, A. M.; Gutierrez, M.; Lopez-Reyes, A., Animal model of acute gout reproduces the inflammatory and ultrasonographic joint changes of human gout. *Arthritis Res Ther* 2015, *17*.

37. Scanu, A.; Oliviero, F.; Gruaz, L.; Sfriso, P.; Pozzuoli, A.; Frezzato, F.; Agostini, C.; Burger, D.; Punzi, L., High-density lipoproteins downregulate CCL2 production in human fibroblast-like synoviocytes stimulated by urate crystals. *Arthritis Res Ther* 2010, *12* (1).

38. Zhang, Y.; Huo, M. R.; Zhou, J. P.; Xie, S. F., PKSolver: An add-in program for pharmacokinetic and pharmacodynamic data analysis in Microsoft Excel. *Comput Meth Prog Bio* 2010, *99* (3), 306-314.

39. Glasson, S. S.; Chambers, M. G.; Van Den Berg, W. B.; Little, C. B., The OARSI histopathology initiative - recommendations for histological assessments of osteoarthritis in the mouse. *Osteoarthritis Cartilage* 2010, *18 Suppl 3*, S17-23.

CHAPTER 5

A Chromatin-Mimetic Nanomedicine for Therapeutic Tolerance Induction

5.1 Abstract

The undesirable immune response poses a life-threatening challenge to human health. It not only deteriorates the therapeutic performance of biologic drugs but also contributes to various diseases such as allergies and autoimmune diseases. Inspired by the role of chromatin in the maintenance of natural immune tolerance, here we report a DNA-protein polymeric nanocomplex that can mimic the tolerogenic function of chromatin and induce an immune tolerance to its protein cargos. We firstly proved that the chromatin-mimetic nanomedicine loaded with keyhole limpet hemocyanin (KLH), a highly immunogenic model protein could elicit a durable antigen-specific immune tolerance to KLH lasting for at least six weeks in mice. Following the proof-of-concept study, we demonstrated that this nanomedicine could be applied to improve the safety and efficacy of a biologic drug, PEGylated uricase, by attenuating the relevant antibody (Ab) responses. Moreover, we also demonstrated that prophylactic treatments with this nanomedicine could tolerize the immune system with the allergen of ovalbumin (OVA) and thus inhibit the occurrence of airway inflammation in an OVA-induced allergic asthma murine model. Collectively, our work illustrates a nature-inspired concept of immune tolerance induction and establishes a useful tool to specifically suppress unwanted immune responses for therapeutic purposes.

5.2 Introduction

The response from an immune system is a host's defensive reaction towards pathogens or other substances that appear foreign and harmful. Normally, the immune response protects the body from diseases by detecting and eliminating the foreign antigens. However, the generation of undesired immune responses under certain scenarios may oppositely endanger human lives.[1] For instance, many protein drugs, which are from non-human sources will elicit antigen-specific antibodies (Abs) once being administered in humans.[2-4] The development of Abs not only ablates the efficacy of protein drugs by directly neutralizing it or indirectly triggering accelerated blood clearance (ABC) but also evokes safety issues such as infusion reactions.[4] On the other hand, immune systems with hypersensitivity tend to over-react to common non-invasive substances such as eggs and pollens to which most people are tolerant. [5] Such abnormal immune reactions spawn the production of redundant Abs such as Immunoglobulin E (IgE), which could lead to allergic diseases ranging from allergic asthma to life-threatening anaphylaxis.[6] Thus, strategies capable of specifically blunting the immune system, thus attenuating the unwanted immune response, are highly desired in many situations.

Looking to nature, while considerable numbers of cells in the body are dying through apoptosis every day, healthy people do not develop immune responses against them.[7-9] This natural phenomenon of immune tolerance has motivated many efforts to modulate the immune response with apoptotic cells (ACs).[10] For example, isolated apoptotic splenocytes have been conjugated or loaded with protein antigens, intending to deceive the immune system by signaling that the linked antigens are products of ACs.[11-13] Infusion of this cellular formulation back into the body was shown to successfully induce immune tolerance towards the specific antigens in multiple models

of immune disorders. [11-15] Admittedly, the concept of engineering ACs to elicit immune tolerance holds promising therapeutic potential, but direct manipulation of cells themselves is unfavorably burdensome due to its manufacturing complexities, high cost and short shelf life. For the ease of clinical translation, people are seeking an apoptotic cell-surrogate platform.

Mechanistically, the immune tolerance mediated by ACs was found to be dependent on antigen presenting cells (APCs) including macrophages, dendritic cells (DCs) and B cells. The uptake of apoptotic cellular debris inhibits the Toll-like receptor (TLR) signaling in APCs, maintaining them in a non-activated state.[16] Thereafter, antigen processing and presentation by non-activated APCs in a non-inflammatory manner is unable to initiate a productive immune response. Instead, they will drive the expression of immunomodulatory cytokines such as IL-10 and TGF-beta and the differentiation of antigen-specific regulatory T (Treg) cells.[17] Notably, recent studies indicate that chromatin, a DNA-protein complex, is rapidly translocated to the surface of cells dying by apoptosis and impedes the TLR-9 signaling within APCs that engulf ACs.[18] Such engagement of TLR-9 directs APCs to a tolerogenic phenotype, provoking regulatory responses to secure self-tolerance. Though the DNA-containing chromatin complex in apoptotic cells has not been fully characterized, GpG oligonucleotide, a short DNA sequence was identified to be an antagonist of TLR-9 with analogous functions.[19-22] Similarly, GpG has been shown to restrain the activation of APCs, bias T cells away from inflammatory phenotype and promote the differentiation of Treg cells.[20, 22-30]

Previously, attempts to induce antigen-specific immune tolerance have been made through co-administration of protein antigens and immunosuppressive drugs such as rapamycin *via*

nanoparticles.[31-33] However, the small-molecule immunosuppressive drugs oftentimes bear side effect or even toxicities in addition to their suppressive effects on immunity.[33-35] For example, the mechanistic target of rapamycin, mTOR is widely expressed in the body and rapamycin-dependent immunosuppressive methods suffer the risk of off-target side-effects, raising safety concerns for its application.[36-41] By contrast, TLR9, the pharmacological target of GpG is found exclusively in APCs including DCs and in B cells, making GpG safer and more efficient.[42] Hence, here we report a chromatin-biomimetic nanogel (DCN) that contains GpG oligonucleotide and protein antigens as an effective approach to induce antigen-specific immune tolerance.

5.3 Experimental section

5.3.1 Materials

All chemicals and proteins including keyhole limpet hemocyanin (KLH), ovalbumin(OVA), and uricase from Candida sp. were purchased from Sigma-Aldrich (St. Louis, MO) unless otherwise noted and were used as received. TLR9 antagonist, GpG (5'-T*G*A*C*T*G*T*G*A*A*G*G*T*T*A*G*A*G*A*T*G*A-3') with or without amino modification at 3'-end were synthesized by IDT with a phosphorothioate backbone. Methoxy polyethylene glycol succinimidyl carbonate, molecular weight (NHS-mPEG, 10 kDa MW) was purchased from Nanocs Inc. Carboxy betaine ester monomer terminated with tbutyl (tbCB) was synthesized following our previously published method[56]. LysoTracker Red DND-99 was purchased from Thermo Fisher Scientific. Amicon Ultra centrifugal filter was purchased from EMD Millipore (Billerica, MA). Amplex Red uric acid/uricase assay kit was purchased from Thermo Fisher Scientific (Waltham, MA). Anti-CD4-PE, anti-CD25-FITC and anti-Foxp3-Percep antibodies were purchased from Biolegend (San Diego, CA). Anti-mouse IgG secondary

antibodies were purchased from Bethyl labs. Mouse cytokine (INF-γ, IL-5, IL-4, IL-13) quantikine ELISA kits were purchased from R&D systems. Mice monocytes RAW 264.7 and B cells LB 27.4 were purchased from ATCC.

5.3.2 Synthesis and characterization of DCN

For the ease of visualization on agarose gels, KLH was labeled with Rhodamine dye before being used for DCN preparation. Briefly, KLH was dissolved in Na_2CO_3 solution (2mg/ml, pH 9) and reacted with NHS- Rhodamine 6G solution (50μL, 100μg/ml in DMSO). The reaction was allowed to proceed for 2h at room temperature and unreacted dyes were removed by centrifuge using a Amicon Ultra centrifugal filter (MWCO 10 kDa). For the preparation of DCN(GpG/KLH) (M:G molar ratio = 3200:1; G:P weight ratio= 8:1), GPG (40ul, 1.5mg/ml) and KLH (5ul, 1.5 mg/mL), 0.7 μL of acrylamide (20%, m/v), 10 μL tbCB (20%, m/v), and 1.8 μL of glycerol diamethacrylate (10%, m/v) (or 1.2 ul of methylenebis(acrylamide) (10%, m/v) for the preparation of non-degradable DCN) were added and thoroughly mixed in a PBS buffer (20 mM, pH 7.4). Then free-radical polymerization was initiated by adding 1 μL of ammonium persulfate (APS, 10%, m/v) and 4 μL of N,N,N′,N′-tetramethylethylenediamine (TEMED, 10% m/v). The reaction was allowed to proceed for 2h at 4 °C and then free GpG and unreacted monomers and initiators were removed by centrifuge using a Amicon Ultra centrifugal filter (MWCO 100 kDa). The yielded DCN were used fresh. Agarose gel electrophoresis was then carried out on 2% agarose gel and imaged by a UV gel image. For the stability and degradation study, degradable and non-degradable DCN (GpG/KLH) was incubated in 50 mM sodium acetate buffer (pH 5.4) and 50mM PBS buffer (pH 7.4) for 4 hours at 37 °C. After the incubation, agarose gel electrophoresis was carried out. Briefly, the agarose gel assay was carried out in 2% (w/v) agarose gel that contains 1% ethidium

bromide in 1×TAE buffer at a constant voltage of 100 V for 20 min. Then, the GpG and KLH bands were visualized at 365 nm using a UV gel image system (SIM135A, SIMON). DLS and zeta measurements were taken at 173° scattering angle using a Zetasizer Nano instrument (Malvern Instruments, Worcestershire, UK). TEM imaging was carried out by first glow discharging carbon-coated 400 square mesh copper grids (Electron Microscopy Sciences). Particles suspensions (50μg/ml, 20μl) were left on the grid for 1 min before being washed off with water. Grids were then stained with 1% uranyl acetate.

5.3.3 Cell uptake study

For the cell uptake study, GpG with amino-modification at 3' end was labeled with FITC. Briefly, the GpG dissolved in PBS solution (1mg/ml, pH 7.4) was reacted with FITC solution (50ul, 1mg/ml in DMSO) for 2h at room temperature. The FITC-labeled GpG was dialyzed using dialysis tubing (MWCO 1kDa) against PBS solution to remove free FITC dyes. Then DCN containing FITC-labeled GpG and Rhodamine-labeled KLH was prepared following the steps described above. RAW 264.7 and LB 27.4 were cultured in DMEM medium with 10% fetal bovine serum at 37 °C in humidified atmosphere containing 5% CO_2. The cell sub-culture was carried out once cells reached 70~80% confluence. RAW 264.7 (2×10^5 cells) and LB 27.4 (2×10^5 cells) were seeded into a 6-well plate containing coverslips in the wells and cultured for attachment, respectively. DCN or the mixture of free GpG and free KLH were added into wells at a final concentration of 50nM GpG/KLH for 2 h incubation at 37 °C. The cells were then washed for three time after removing the medium, and stained by Hoechst 33342 (Invitrogen) according to the manufacture's protocol. After 30min nuclear staining, cells were fixed with 4% formaldehyde in PBS for 20 min at room temperature, and then washed by PBS for three times. At last, the

coverslips were covered onto glass slides with 20 μL aqueous mounting medium. Then the slides were observed using Confocal Laser Scanning Microscopes-FV1000 (CLSM, Olympus, Tokyo, Japan).

5.3.4 Lysotracker colocalization assay

2 x10^5 HeLa cells were seeded in a 6 well plate and cultured for 24 h. DCN containing FITC-labeled GpG and unlabeled KLH was added into wells at a final concentration of 50nM GpG/KLH for incubation at 37 °C. After 4 h, the medium containing DCN was removed and washed three times with fresh PBS. LysoTracker Red DND-99 (Thermo Fisher Scientific) diluted in serum free medium at concentration of 500 nM was added to the cells, followed by incubation for 1 h at 37°C. Cells were washed three times after removing the medium and stained by Hoechst 33342 (Invitrogen) according to the manufacture's protocol. After 30min nuclear staining, cells were fixed with 4% formaldehyde in PBS for 20 min at room temperature, and then washed by PBS for three times. At last, the coverslips were covered onto glass slides with 20 μL aqueous mounting medium. Then the slides were observed using Confocal Laser Scanning Microscopes-FV1000 (CLSM, Olympus, Tokyo, Japan).

5.3.5 Cell viability study

The cytotoxicity of DCN was evaluated by MTT assays in RAW264.7 and LB27.4 cells. Firstly, cells were seeded into a 96-well plate at a density of 1×10^4/well. Blanks were prepared by adding culture medium alone. Cells were cultured overnight for attachment. Subsequently, culture medium in each well was replaced with fresh medium containing DCN (GpG/KLH) at series of concentrations. Cells in wells without addition of DCN (GpG/KLH) were used as control group.

Six replicates were included in each group. After another 48-h culture, 20 μL of sterile MTT solution (5 mg/mL) was added into each well to incubate at 37 °C for 4 h. After the removal of the unreacted MTT dye by aspiration, 150 μL of DMSO was added into each well to dissolve the produced formazan crystals, and the plate was gently shaken for 15 min. Finally, the optical density (OD) was measured at 420 nm using a plate reader (BioTek, USA).

5.3.6 Animals

C57LB/6 mice (male, body weight 20–30 g) were purchased from Jackson Laboratories (Seattle, WA). All animal experiments adhered to federal guidelines and were approved by the University of Washington Institutional Animal Care and Use Committee (IACUC). Animals were randomized to treatment groups at the beginning of each study. A sample size of five animals per group was used.

5.3.7 KLH tolerance study

Mice were IV. injected weekly with PBS, DCN(KLH) (25μg KLH) in absence of GpG, free GpG (200μg) and free KLH (25μg), DCN (GpG/KLH) (DCN(GpG_{high}/KLH) (200μg GpG/25μg KLH), DCN(GpG_{low}/KLH) (12.5μg GpG/25μg KLH)) for three weeks. Starting from the 21st day, all the mice were immunized with IV injection of free KLH (50μg) for five weeks (one dose per week). The mice sera were collected on day the 21st, 28th, 35th, 42nd, 49th, and 56th day (right before the antigen immunization) for Ab detection *via* ELISA test. As the first step of direct ELISA test of anti-KLH Abs, 100 μL KLH solutions (10 μg/mL) prepared in coating buffer (0.1 M sodium carbonate buffer, pH 10.5) were used to coat each well of 96-well plates. After overnight coating at 4 °C overnight, the plates were washed five times using PBS buffer (pH 7.4) to remove the KLH

solutions and then filled with blocking buffer (1% BSA solution in 0.1 M Tris buffer, pH 8.0) for 1-h incubation at room temperature, subsequent to which the blocking buffer was removed. All wells were then washed by PBS buffer for another five times. Subsequently, serial dilutions of mice sera in PBS buffer containing 1% BSA were added to the plates (100 μL/well) for 1-h incubation at 37 °C, subsequent to which the mice sera were removed and all wells were washed five times with PBS buffer. Next, goat anti-mice IgG (HRP-conjugated) as the secondary antibody were added into each well for another 1-h incubation at 37 °C. Subsequently, all the wells were washed five times using PBS buffer before the addition of 100 μL/well HRP substrate 3,3',5,5'-tetramethylbenzidine (TMB). The plates were shaken for 15 min, and 100 μL stop solution (0.2 M H_2SO_4) was added to each well. OD at 450 (signal) and 570 nm (background) was recorded by a microplate reader. Mice sera naïve to the administration of KLH proteins were used as the negative control for all ELISA detections. After the euthanasia of mice on 56th day, the mice spleens were harvested for the isolation of splenocytes by 100μm cell strainer (FisherbrandTM). The mice splenocytes from each group were stained with anti-CD4-PE, anti-CD25-FITC and anti-Foxp3-Percep antibodies, and then analyzed by flow cytometry. For the biodistribution study, two groups of mice were given FITC-labled GpG and DCN containing FITC-labled GpG ia IV. injection respectively. At 24h after injection, all mice were euthanized, and their heart, liver, spleen, lung, kidney, and blood were collected for further analysis. The collected organ tissues were homogenized using a tissue ruptor, followed by centrifugation at 3,200 × g for 30 min at room temperature. The fluorescence in the tissues was measured using a microplate reader and compared with a standard curve generated using FITC-labeled GpG added to untreated homogenized tissues.

5.3.8 OVA specificity study

Mice were IV injected weekly with PBS, DCN(GpG/KLH) (200μg GpG/25μg KLH), or DCN(GpG/OVA) (200μg GpG/25μg OVA) for the first three weeks, followed by three weekly immunizations of free OVA (100 μg) starting from 21st day. The mice sera were collected on the 21st, 28th, 35th, 42nd and 49th day (right before the antigen immunization) for Ab detection *via* ELISA test. OVA solutions (10 μg/mL) prepared in coating buffer (0.1 M sodium carbonate buffer, pH 10.5) was used for the plate coating in ELISA test.

5.3.9 PEGylated uricase study

For the preparation of DCN(GpG/uricase), GPG (40ul, 1.5mg/ml) and uricase (5ul, 1.5 mg/mL), 0.7 μL of acrylamide (20%, m/v), 10 μL tb-PCB (20%, m/v), and 1.8 μL of glycerol diamethacrylate (10% m/v) were added and thoroughly mixed in a PBS buffer (20 mM, pH 7.4). Then free-radical polymerization was initiated by adding 1 μL of ammonium persulfate (APS, 10%, m/v) and 4 μL of N,N,N′,N′-tetramethylethylenediamine (TEMED, 10% m/v). The reaction was allowed to proceed for 2h at 4 °C. Then, unreacted monomers and initiators were removed by centrifuge using a Amicon Ultra centrifugal filter (MWCO 10 kDa). PEG-uricase conjugates were prepared in 50 mM Hepes buffer (pH 8.5), with uricase concentration at 1 mg/mL and mPEG-NHS concentration at 10 mg/mL. The reaction was stirred at 4 °C overnight. Then the conjugates were concentrated and washed extensively by PBS, pH 7.4, using a 300-kDa molecular weight cutoff centrifugal filter. The protein residue activity was measured by the Amplex Red uric acid/uricase assay kit. Two groups of mice were intravenously injected weekly with PBS or DCN (GpG/uricase) (200μg/25μg) respectively for three weeks. Then, starting from the 21st day, both of the two cohorts were IV administered weekly with PEG-uricase at a dose of 25U/kg for another

three weeks. The mice sera were collected at 0.1, 4, 8, 24, 48 and 72h post to the third injection of PEG-uricase for evaluating the level of uricase/uric acid. The uricase concentration in plasma was estimated based on the enzyme activity measured by Amplex Red uric acid/uricase assay kit. To exclude the disturbance of mice's nature uricase and the potential dose accumulating effect, uricase concentration in the mice sera at 1min before the third injection of PEG-uricase was subtracted as background in PK calculation. All PK parameters were calculated using PKSolver software following the instructions.[58] The urate concentration in the mice sera was measured by Amplex Red uric acid/uricase assay kit. All the mice were sacrificed on 42nd day and their sera were harvested for antibody detection *via* ELISA test. For the ELISA test, while the detection of anti-uricase Ab used coated uricase as antigen, the detection of anti-PEG antibody used PEG-BSA conjugates. BSA-PEG conjugates were prepared, following the same preparation protocol of PEG-uricase conjugates as described above.

5.3.10 OVA-induced allergic asthma study

For the preparation of DCN(GpG/OVA), GPG (40ul, 1.5mg/ml) and OVA (5ul, 1.5 mg/mL), 0.7 μL of acrylamide (20%, m/v), 10 μL tb-PCB (20%, m/v), and 1.8 μL of glycerol diamethacrylate (10% m/v) were added and thoroughly mixed in a PBS buffer (20 mM, pH 7.4). Then free-radical polymerization was initiated by adding 1 μL of ammonium persulfate (APS, 10%, m/v) and 4 μL of N,N,N′,N′-tetramethylethylenediamine (TEMED, 10% m/v). The reaction was allowed to proceed for 2h at 4 °C. Then, unreacted monomers and initiators were removed by centrifuge using a Amicon Ultra centrifugal filter (MWCO 10 kDa).

Three groups of mice (n=5) were IV pre-treated with three weekly doses of PBS, DCN(GpG/KLH), and DCN(GpG/OVA) respectively. Then mice in these groups were all induced with allergic asthma by two-weekly IP immunization with OVA (10μg) in alum adjuvant (3mg) on 21st and 28th day and IN immunization of OVA (25μg) on 42nd, 43rd and 44th day[57]. In parallel, a fourth group of mice (n=5) were IV, IP and IN administered with PBS as the negative control. All the mice were sacrificed on 45th day and their sera were harvested for antibody detection *via* ELISA test, in which the OVA solutions (10 μg/mL) prepared in coating buffer (0.1 M sodium carbonate buffer, pH 10.5) was used was used as the coating solution and the goat anti-mice IgE Ab (HRP conjugated) was used as the secondary Ab. Mice lungs were flushed with 1 mL of bronchoalveolar lavage fluid (BALF; 1 mM EDTA and 10% (vol/vol) FBS in PBS). Cell density was determined on the unconcentrated lavage fluid with a Malassez hemocytometer. The differential cell count was determined by cytological examination of at least 500 cells after centrifugation and May-Grünwald-Giemsa staining. The supernatant of BALF was assayed for IL-4, IL5, IL13 and INF-γ by mice cytokine quantikine ELISA kits, following the manufacture protocol. Mice lungs were collected, fixed in formalin, embedded in paraffin, and stained with H&E or periodic acid–Schiff. Moreover, the spleens of mice were harvested and the splenocyte was isolated by 100μm cell strainer (Fisherbrand^{TM}). Mice splenocytes from each group were cultured in 12-well plate (2x10^{6}/well) and re-stimulated with OVA (200μg/ml) for 4days, after which levels of IL-13, IL-5, IL-4, and INF-γ in supernatans were by mice cytokine quantikine ELISA kits.

5.4 Results and Discussion

5.4.1 Preparation and characterization of DCN

The preparation of chromatin-mimetic nanomedicine is illustrated in Fig. 5-1. As surfaces of GpG oligonucleotides and most proteins are negatively charged, they tend to be shrouded with the positively charged monomers (tbCB) *via* eletrostatic interactions, as well as the other two reagents, neutral monomers (acrylamide) and acid-sensitive crosslinkers (glycerol diamethacrylate) through hydrogen bonding (Step i). Thus, the subsequent free-radical polymerization of these monomers and crosslinkers accumulating on the anionic surface of proteins and GpG oligonucleotides will allow them tob e encased within shells of network polymers, forming a nanogel denoted hereinafter as DCN (Step ii). Our group has previously demonstrated the use of cationic carboxybetaine ester polymers to condense DNA for gene delivery. Herein, by hiding the zwitterionic group in the carboxybetaine moiety with a t-butyl group, the P(tbCB) polymer can be made cationic at physiological pH, favoring the binding of GpG oligonucleotides. In the acidic endosome where TLR9 is located, hydrolyzed P(tbCB) reverts back to zwitterionic PCB,[43-45] an excellent biocompatible material, prompting the unpacking of GpG and proteins (Step iii). Unlike other positively-charged polymers such as polyethyleneimine (PEI) that can be cytotoxic, PCB is biocompatible to APCs.[46-48] Moreover, PCB with minimal immunogenicity will not elicit additional immune responses.[47-51] Concurrently, the crosslinker of DCN, glycerol diamethacrylate, is acid-degradable such that protein antigens are also liberated in the endosome of target APCs. Hence, such pH responsiveness determines that DCN is stable under the physiological condition (pH 7.4), yet can be degraded in acidic endosomes once taken up by APCs, allowing efficient release of proteins and GpG oligonucleotides.

The dynamic light scattering (DLS) in Fig. 5-2a reveals a uniform diameter of DCN (35.1nm, PDI 0.24), which was confirmed by transmission electron microscopy (TEM). This is close the size of DNA-protein chromatin complex unit. Zeta potential measurements of DCN in Fig. 5-2b showed a positive surface charge (+19.5mV), indicating a comprehensive polymeric coverage on KLH, which is originally negatively charged. To validate that the positively-charged DCN favors the recognition and uptake by with APCs, DCN containing FITC-labeled GpG/Rhodamine-labeled KLH, and free GpG/KLH mixture were incubated with two types of APCs, RAW264.7 monocytes and LB 27.4 B cells. The cell uptake was observed and compared under a confocal laser scanning microscope after 2h incubation. As shown in Fig. 5-3, while no distinguishable or only light fluorescence was observed for cells treated with free GpG and free KLH, implying a poor penetration into cells, both GpG and KLH in DCN were effectively internalized as shown by the intense fluorescence in DCN-treated cells. Furthermore, another type of APC, DC2.4 dendritic cells were incubated with DCN containing FITC-labeled GpG/unlabeled-labeled KLH and the location of endosomes was then marked with LysoTracker Red DND-99 (Fig. 5-4). It shows that the intraceullar localization of DCN well overlapped with endosomes, favoring the cargo release and the antagonizing effect of GpG on TLR9 receptors. In addition, to eliminate the concern of cytotoxicity, the MTT cell viability assay was also carried out in these two APCs. Figure 5-5 shows that both RAW264.7 monocytes and LB 27.4 B cells still maintained a desirable viability (> 80%) under a DCN concentration as high as 200μM. The *in vitro* results confirm that DCN can efficiently interact with their target APCs while exerting no apparent cytotoxicity.

Moreover, to develop a DCN formulation that can stably deliver both proteins and GpG oligonucleotides, *in situ* polymerization of DCN was performed at a fixed GpG to protein weight

ratio (G:P= 8:1) but varied monomer to GpG (M:G) molar ratios (200:1, 400:1, 800:1, 1600:1, 3200:1, 6400:1). For the ease of visualization on agarose gels, KLH was labeled with Rhodamine 6G dye before being used for DCN preparation. Because the absorption and excitation spectrums of Rhodamine 6G and Ethidium bromide (EB), a stain of DNA, overlap with each other, the band of GpG and KLH can be simultaneously observed by imaging of agarose gel electrophoresis. As shown in Fig. 5-2c, DCN formulations prepared with the M:G ratios lower than 1600 exhibit apparent bands of DNA and KLH, suggesting an incomplete encapsulation. By contrast, the samples prepared with the M:G ratios higher than 1600 are trapped in the loading wells without observable shift, suggesting the formation of stable DCN. Based on this result, an M:G ratio 3200 was selected for subsequent studies. The stability of DCN, as well as its degradability, was examined under physiological pH of 7.4 and endosomal pH of 5.4. As shown in Fig. 5-2d, the non-degradable DCN made with acid-insensitive crosslinker (methylenebis(acrylamide)) did not release any protein in either physiological condition or acidic condition. Notably, a light band of free GpG was observed after 4h incubation at pH 5.4, confirming the reversion of DCN shell from positive to zwitterionic, which prompts the dissociation of negatively-charged cargos. In comparison, while physiological pH did not trigger any cargo release from the degradable DCN made with acid-sensitive crosslinker (glycerol diamethacrylate), it displayed significant release of both GpG and KLH at pH 5.4 as shown by the characteristic bands on corresponding gels.

5.4.2 DCN induces immune tolerance to protein antigens

To investigate whether DCN could induce sustainable immunosuppression to its co-delivered protein antigen, we evaluated the capacity of DCN containing KLH and GpG (DCN(GpG/KLH)) to trigger immune tolerance towards KLH. Two formulations of DCN with high and low G:P

weight ratios (8:1 in DCN(GpG_{high}/KLH); 0.5:1 in DCN(GpG_{low}/KLH)) were examined to reveal the impact of GpG dosage. As illustrated in Fig. 5-6a, four groups of mice were treated with three intravenous (IV) injections (one dose per week) of PBS, free KLH, free GpG nucleotide and DCN(GpG/KLH) respectively. Starting from the fourth week (21^{st} day), all the four cohorts were subjected to four weekly antigen immunized with free KLH (21^{st}, 28^{th}, 35^{th} and 42^{nd} day). The mice sera were collected on 21^{st}, 28^{th}, 35^{th}, 42^{nd}, 49^{th}, and 56^{th} day for Ab test using Enzyme-linked immunosorbent assay (ELISA). As shown in Fig. 5-6b-c, KLH immunization quickly elicited a robust Ab response in the control group pre-treated with PBS. By contrast, mice pre-treated with DCN(GpG_{high}/KLH) regimen displayed an attenuated Ab generation for at least six weeks, and the titer of anti-KLH Abs is over 100-fold lower than the other groups at the end of antigen immunization study. Meanwhile, mice pre-treated with DCN that only contained KLH alone (DCN(KLH)), still developed a robust Ab response, confirming that the absence of Abs in DCN(GpG_{high}/KLH) group is a sustainable immune tolerance, instead of a simply delayed immune response led by the DCN-shell protection. In addition, the limited suppressing effect of DCN(GpG_{low}/KLH) (Fig. 5-7) suggests that the dose of GpG plays a critical role in producing a complete immunological tolerance. Thus, the formulation ratio of DCN(GpG_{high}/KLH) was chosen for all the rest of studies. Furthermore, the pretreatment with the mixture of free GpG and KLH did not show any effective immune tolerance as shown by the high Abs titer, suggesting that the co-delivery of GpG and protein antigen is indispensable to the induction of immune tolerance. To further understand the mechanism behind immune tolerance, the mice spleens, the main sites where T cells differentiate toward inflammatory or regulatory phenotypes were harvested on the 56^{th} day after euthanasia. The splenocytes were isolated and stained immediately for the analysis of Treg markers (Fig. 5-6d-e). Compared to the groups pretreated with PBS, DCN(KLH) or free

GpG/KLH, the DCN(GpG_{high}/KLH) group exhibited an increased percentage of Tregs (CD25+Foxp3+) among CD4+ T cells, indicating that only DCN(GpG_{high}/KLH) could polarize T cells towards tolerogenic phenotypes, and thus lead to immune tolerance. The limited effect of free GpG on Treg-cell differentiation can be attributed to its low molecular weight (3KDa), which makes it to be quickly eliminated through renal clearance before reaching the main lymph organ (eg. spleen). To validate this presumption, we have used the FITC-labeled GpG and DCN (GpG/KLH) to track their localization *in vivo*. Results of biodistribution study (Fig. 5-8) showed that most of the free GpG were cleared from main organs at 24h, following IV administraiton. Meanwhile, DCN(GpG/KLH) was observed to selectively and highly accumulate in the spleen and liver，both of which are important immune organs accounting for the immunity. Moreover, to assess the antigen specificity of DCN-induced tolerance, a crossover study as illustrated in Fig. 5-9a was also performed. Similar to the suppressive impact of DCN(GpG/KLH) on KLH, the pretreatment of DCN containing OVA (DCN/OVA) also elicited an immune tolerance towards OVA as the generation of Abs was inhibited under the multiple immunizations of OVA antigen (Fig. 5-9b-c). Nevertheless, a robust anti-OVA Ab response was still detected in the group pretreated with DCN(GpG/KLH), suggesting that DCN does not cause cross-reactivity to other antigens and induces humoral immune tolerance in an antigen-specific manner.

5.4.3 DCN improves therapeutic properties of PEG-uricase

Following the proof-of-concept study on KLH, we next attemped to use DCN technology to address attenuate the immunogenicity of biologic drugs, which is one of the major obstacles that impede the wide application of therapeutic protein products, especially for those obtained from non-human sources. The immune respones elicited by biologic drugs significantly decrease their

efficacy and may cause life-threatening adverse reactions such as anaphylaxis and cytokine-release syndrome. To demonstrate this potential application, we prepared a DCN containing uricase (DCN(GpG/uricase)), a highly immunogenic mammalian enzyme based on the formulation of DCN(GpG/KLH). As illustrated in Fig. 5-10a, two groups of mice were pretreated weekly with PBS and uricase-loaded DCN respectively for three weeks, followed by another three weekly-administrations of PEG-uricase. After the third injection of PEG-uricase, mice sera were collected from both groups at various time points for the characterization of pharmacokinetic (PK)/ pharmacodynamic (PD) profiles while those collected on 49th day were tested by ELISA for Ab titers. In the clinic, the commercial biologic product of PEG-uricase, Pegloticase (Krystexxa®) arouses a high-rate generation of antibodies after repeated administrations, which caused an increased non-responsiveness to its treatment and severe infusion reactions among patients[52]. Consistent with the clinical findings, high IgG titers reactive with uricase and PEG were observed in the PBS-pretreated control group after three repeated administrations of PEG-uricase (Fig. 5-10b). By contrast, mice pre-treated with DCN(GpG/uricase) exhibited a dramatically decreased level of Abs against PEG-uricase. Notably, though the DCN(GpG/uricase) does not contain PEG, the generation of an anti-PEG Ab response was also mitigated following the treatment of DCN(GpG/uricase), which coincides with previous findings pointing out that the magnitude of Ab response against PEG depends on the immunogenicity of carrier protein.[53-56] Thus, the DCN-mediated immune tolerance towards protein antigens could attenuate the potential immunogenicity from both proteins and the protein-anchoring polymers. Due to the absence of Ab responses, PEG-uricase in the DCN(GpG/uricase)-pretreated group manifested a relatively stronger urate-eliminating capacity after the third injection as shown by the uric acid concentration *versus* time kinetics in Fig. 5-10c. Moreover, the uricase activity *versus* time kinetics after the third injection

were fitted into the one-compartment model (Fig. 5-10d) and the key PK parameters were derived in Table 5-1. In comparison with that in the DCN(GpG/uricase)-pretreated group, PEG-uricase in the PBS control group displayed an expedited clearance and reduced circulation half-life, which is corresponding to the high Ab titers. The improved PK/PD properties of PEG-uricase in the DCN group well correlates with the DCN-elicited immune tolerance, which could mitigate undesirable Ab responses. These results suggest the potential of DCN to be used as a prophylactic adjunct therapy for biologic therapies. Given that there is a large number of PEGylated biologic products in clinical development and in the market, the DCN technology will be beneficial to not only improve the safety and efficacy of marketed PEGylated products, but also to rescue promising biologic drugs that have failed in clinical trials due to immunogenicity issues.

5.4.4 DCN alleviates the allergic asthma

IgE-mediated allergic diseases, the most common form of allergy is affecting 10% of the population in industrialized countries[5]. While multiple drugs are available on the market for the treatment of allergies, a need for prophylactic strategies is still pressing but unmet. Fundamentally, hyperactivated T helper 2 (Th2) cells are central to the allergic immune response as they can stimulate B cells to secrete IgE that, if present in sufficient quantities, can lead to allergic symptoms such as inflammatory airway constriction[6]. In the present work, we investigated whether upregulating antigen-specific Treg cells with DCN would be effective in evoking immune tolerance to curb the induction of Th2-mediated OVA-induced allergic asthma. As illustrated in Fig. 5-11a, three groups of mice were IV pre-treated with three weekly doses of PBS, DCN(GpG/KLH) or DCN(GpG/OVA) before two weekly intraperitoneal (IP) immunizations with OVA in alum adjuvant, followed by three daily intranasal (IN) immunizations of OVA.[57] In

parallel, the fourth group of mice was treated with PBS, following the same schedule as the negative control. At the end of study (45th day), the IgE level in mice sera from each group was analyzed by ELISA. The DCN(GpG/OVA)-pretreated mice displayed a significantly lower IgE titer compared to the other OVA-immunized groups (Fig. 5-11b). In addition, the bronchoalveolar lavage fluid (BALF) was collected on 45th day for analysis. Under the prophylatic treatment of DCN(GpG/OVA), mice exhibited relatively lower number of eosinophils (Fig. 5-11c) and the subdued level of Th2 inflammatory cytokines (IL-4, IL-5, IL-13, IFN-γ) in their BALF (Fig. 5-11d-g), suggesting a reduced OVA-induced airway inflammation. A similar trend of cytokine profiles was also observed upon the splenocytes, which were collected from the mice in each group and restimulated with OVA for four days before analysis (Fig. 5-12). This result indicates that DCN (GpG/OVA) did not induce any non-specific immune activation. Besides, mouse lung sections were stained with periodic acid-schiff (PAS) to assess the mucus overproduction (Figure 6h), wherein the number of mucus-producing goblet cells, a major pathological symptom of airway inflammation, was also sinificantly decreased in mouse bronchi post to the pre-treatmen of DCN(GpG/OVA). Notably, the pretreatment of DCN(GpG/KLH) showed a negligible immunomodulatory effect in this OVA-induced airway inflammation model, implying the specificity of DCN technology as well as its safety.

5.5 Conclusions

In summary, we herein established a chromatin-biomimetic nanomedicine as a safe, efficient and clinically-relevant tool to induce antigen-specific immune tolerance. In the proof-of-concept study, IV. administrations of DCN containing both GpG and KLH induced a durable immunological tolerance to KLH, lasting for at least six weeks. Motivated by the study on KLH, we further

demonstrated that using DCN to induce immune tolerance towards uricase could improve PK and PD of PEG-uricase by inhibiting the generation of Abs reactive with PEG-uricase, including both anti-uricase and anti-PEG Abs. Moreover, we also demonstrated that prophylactic treatments of DCN can also train the immune system to generate tolerance towards allergens and thereby alleviate the occurrence of allergic asthma. Thus, the DCN platform capable of regulating immune responses in an antigen-specific manner has far-reaching implications in various clinical scenarios. It provides a safe and efficient tool to control immune responses, and is expected to find wide biomedical applications.

5.6 Scheme, Figures and Tables

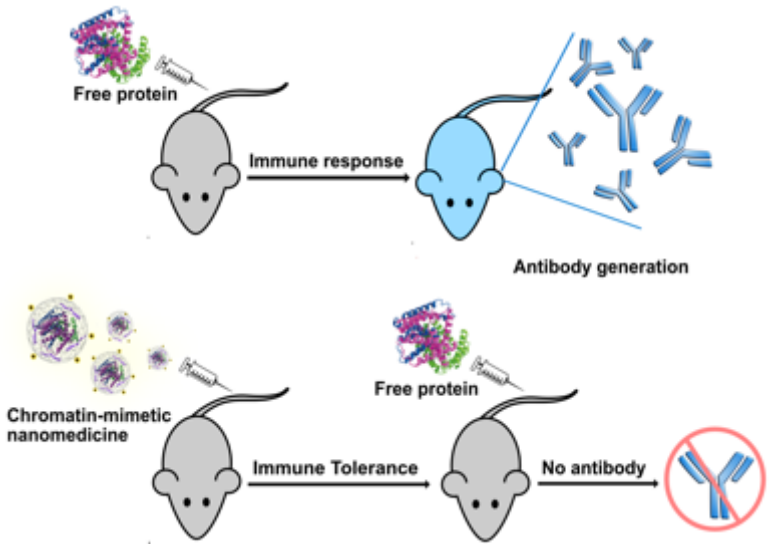

Scheme 5-1. A chromatin-mimetic nanomedicine that contains GpG oligonucleotides and protein agntigens is developed to induce antigen-specific immune tolerance, providing a useful tool to specifically suppress unwanted immune responses for therapeutic purposes.

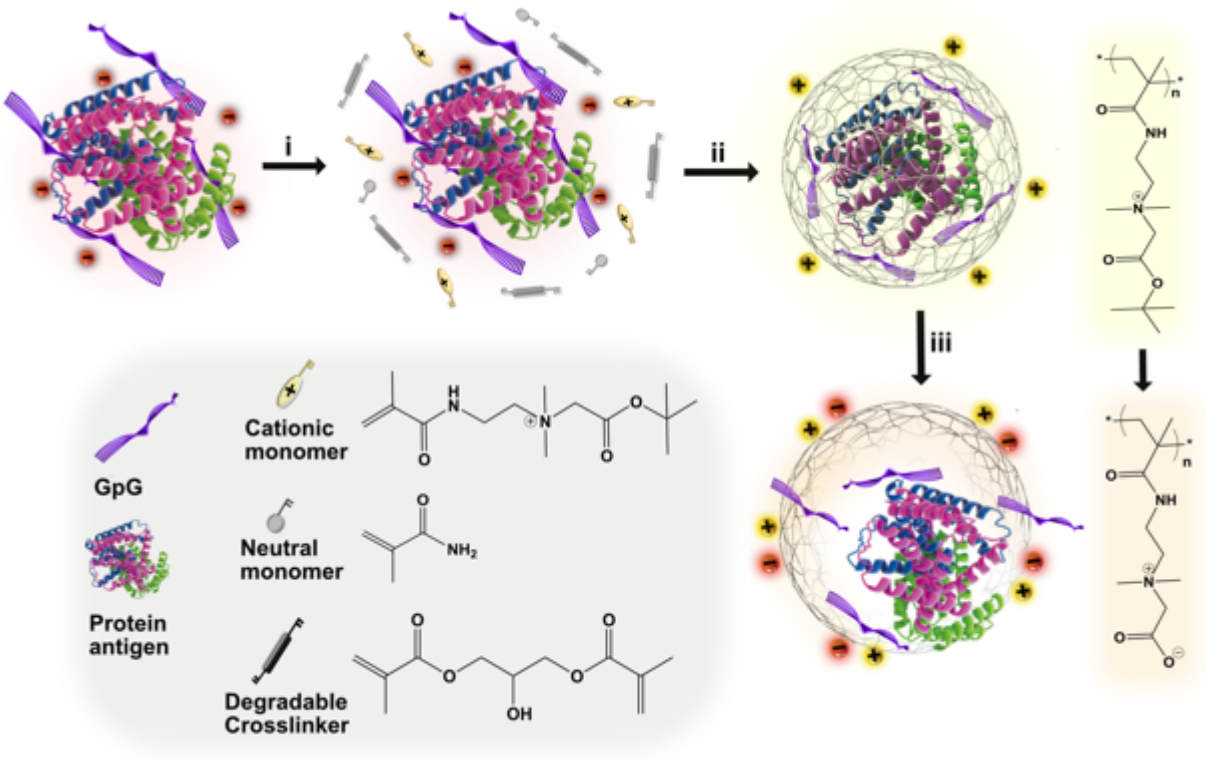

Figure 5-1. Scheme of DCN formation and degradation. The positive-charge monomer tbCB is first enriched around the negatively-charged GpG and proteins mainly through electrostatic interactions and hydrogen bonding (i). Subsequent free-radical polymerization wraps GpG and protein molecules within thin shells of network polymer, forming the DCN (ii). The DCN scaffold is positively charged at physiological pH for delivery. The DCN reverts back to zwitterionic under acidic endosomal conditions for unpackaging of GpG. Concurrently, the DCN cross-linker is acid-degradable such that both GpG and protein antigens are liberated in the endosome (iii).

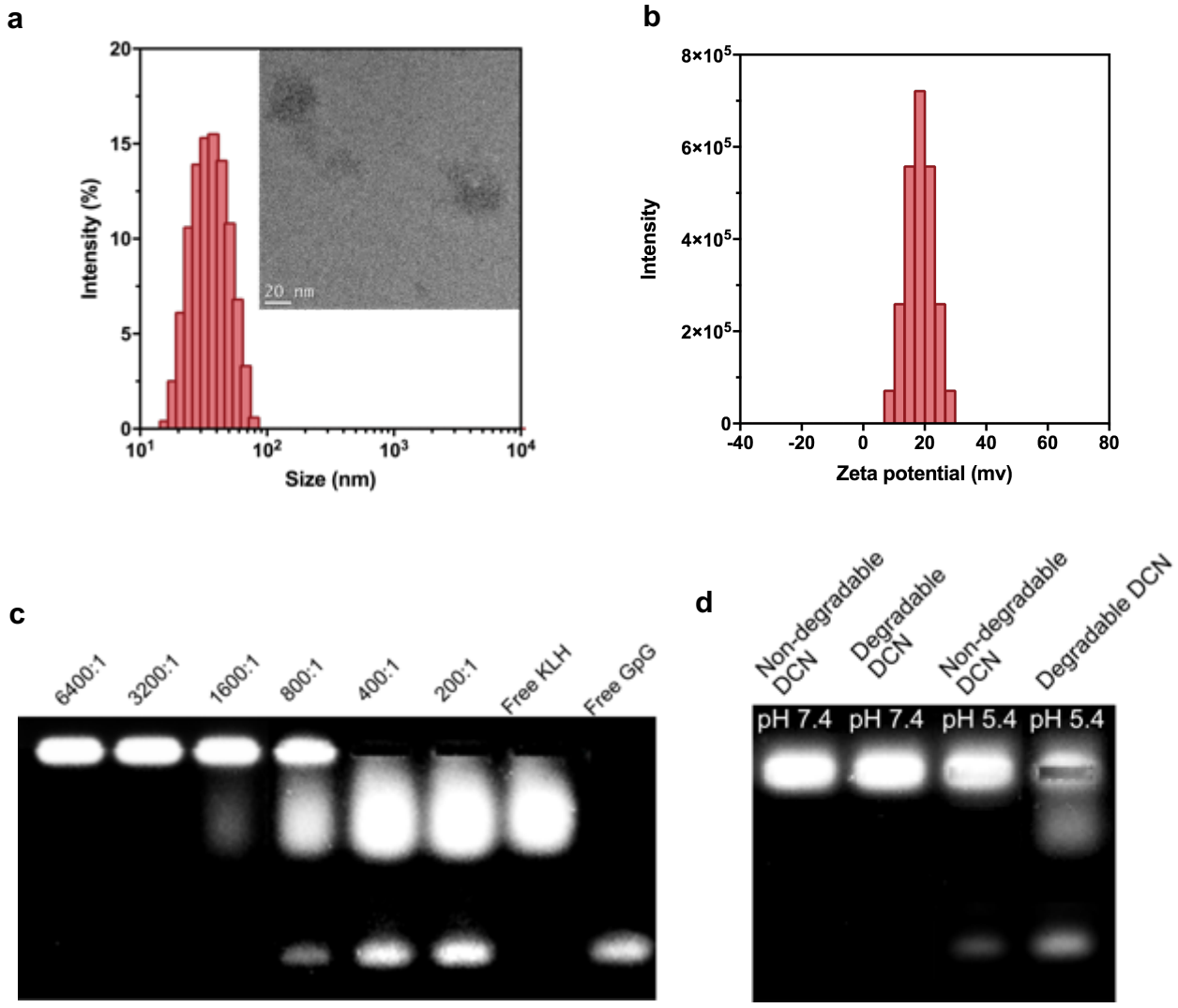

Figure 5-2. Characterization of DCN. (a) Size distribution meased by Malvern Zetasizer and TEM. (b) Zeta potential of DCN measured by Malvern Zetasizer. (c) Agarose gel electrophoresis of DCN synthesized a fixed molar ratio of GpG to KLH (G:K=500:1) but varied monomer to GpG (M:G) molar ratios (200:1, 400:1, 800:1, 1600:1, 3200:1, 6400:1). (d) Agarose gel electrophoresis of degradable/non-degradable DCN samples after their incubation at physiological condition (pH7.4) and endosome-mimic condition (pH 5.4) for 4h.

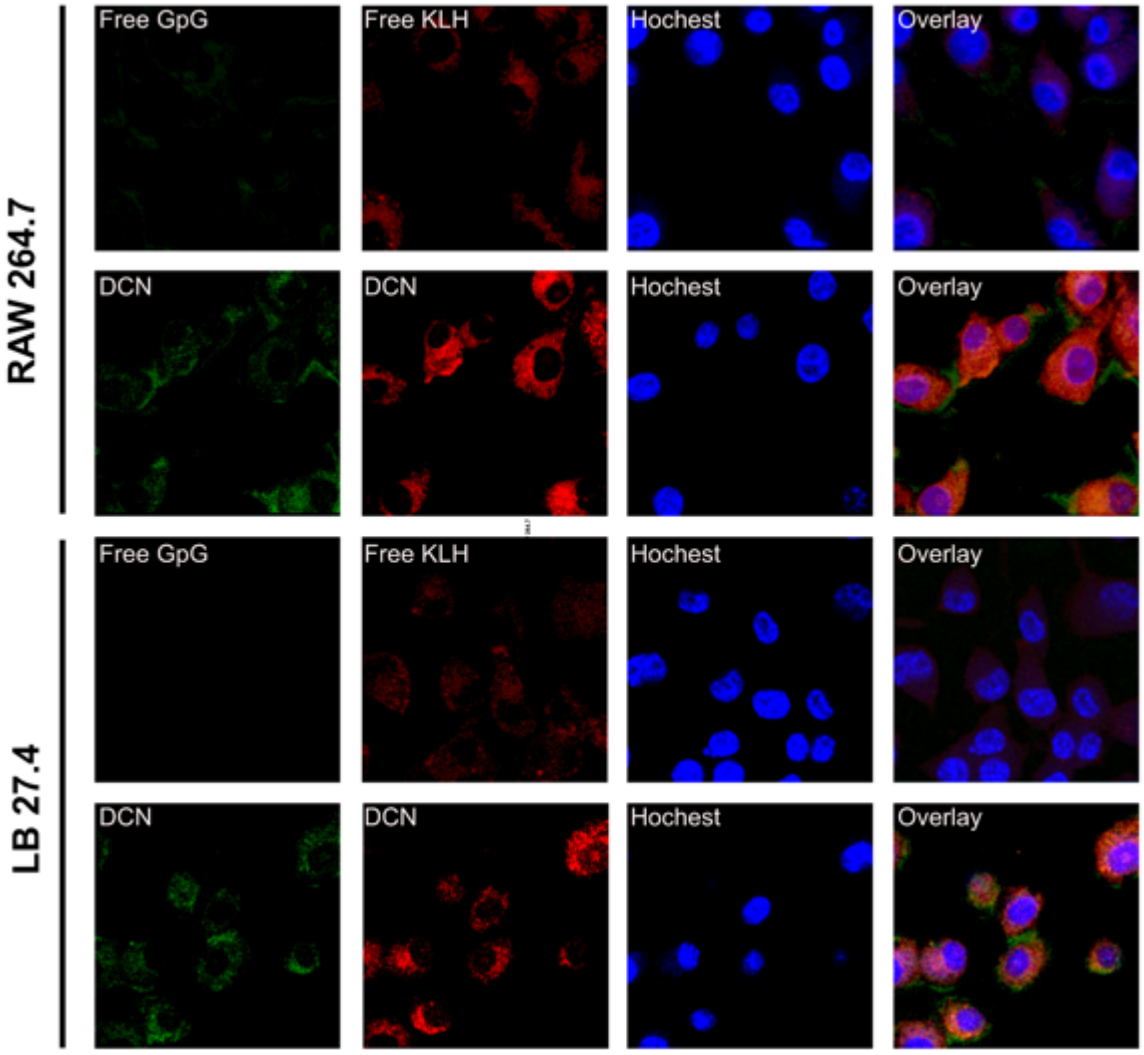

Figure 5-3. Cell uptake study. Confocal images of intracellular distribution of free GPG/free KLH and DCN(GpG/KLH) in RAW264.7 and LB27.4 cells after 2-h incubation at 37 °C. GpG was labeled with FITC and KLH was labeled with Rhodamine. Cell nuclei were stained with Hoechst 33342.

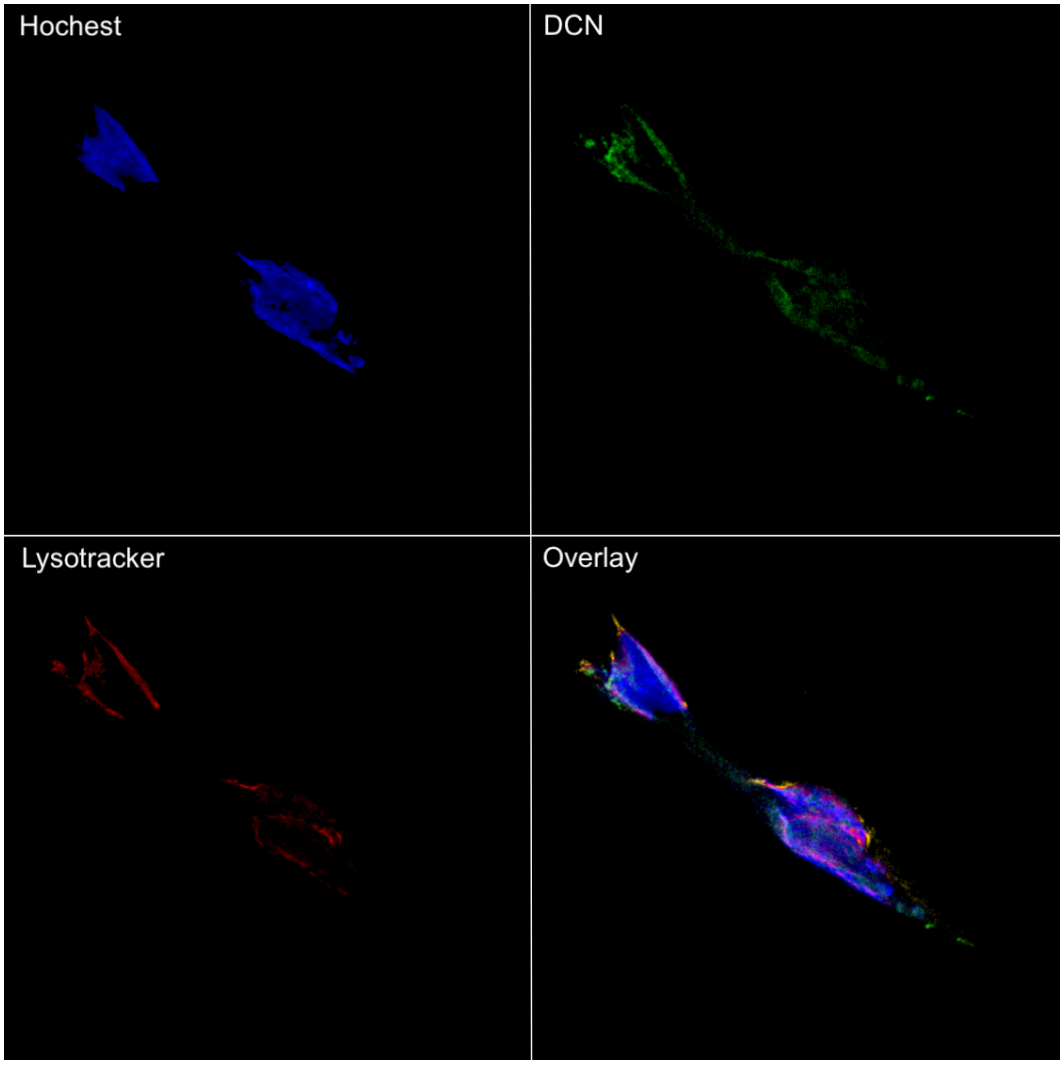

Figure 5-4. Co-localization of DCN and lysotracker in DC2.4 mouse dendritic cells. Confocal images of intracellular distribution of DCN(GpG/KLH) in DC2.4 mouse dendritic cells after 4-h incubation at 37 °C. DCN(GpG/KLH) was labeled with FITC and the location of endosomes was labeled with LysoTracker Red DND-99. Cell nuclei were stained with Hoechst 33342.

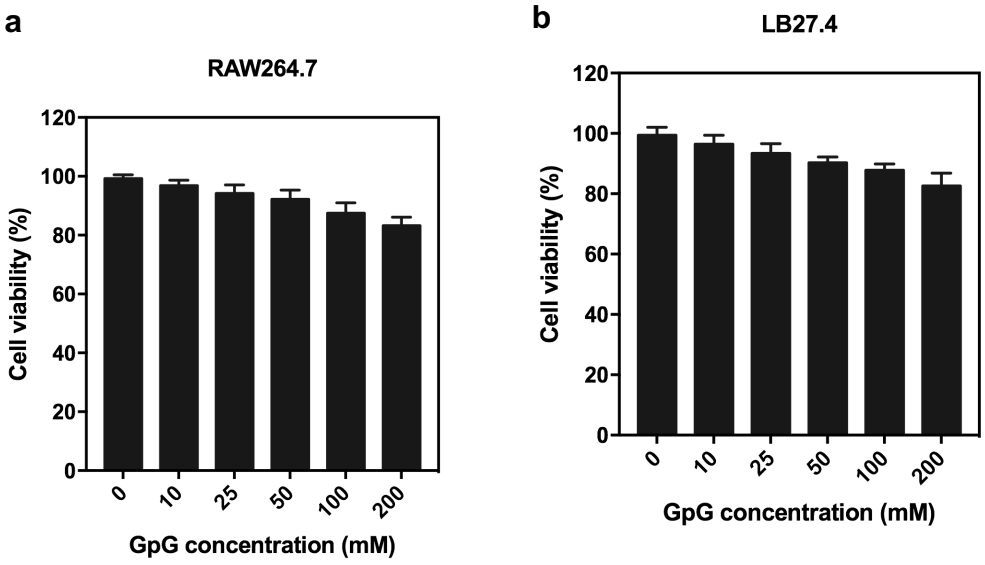

Figure 5-5. Cell viability study. MTT assay of DCN(GpG/KLH) synthesized at a M:G molar ratio of 3200:1 and a G:P weight ratio of 8:1 in RAW264.7 monocytes (a) and LB 27.4 B cells (b). Results are plotted as mean± s.d. (n=6).

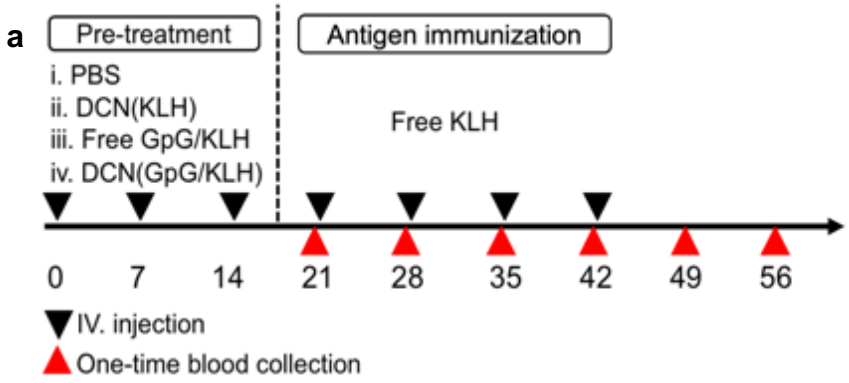
a
Pre-treatment
Antigen immunization
i. PBS
ii. DCN(KLH)
iii. Free GpG/KLH
iv. DCN(GpG/KLH)
Free KLH
0
7
14
21
28
35
42
49
56
IV. injection
One-time blood collection

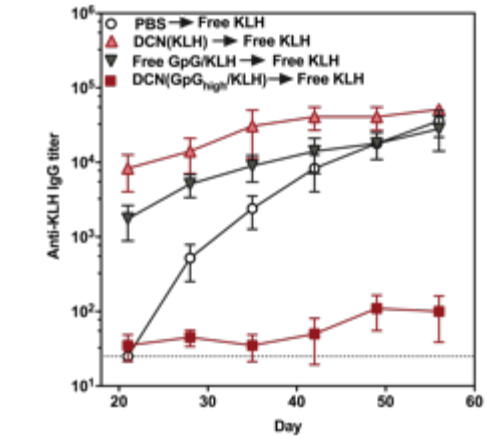
b
PBS → Free KLH
DCN(KLH) → Free KLH
Free GpG/KLH → Free KLH
DCN(GpG$_{high}$/KLH) → Free KLH
Anti-KLH IgG titer
Day

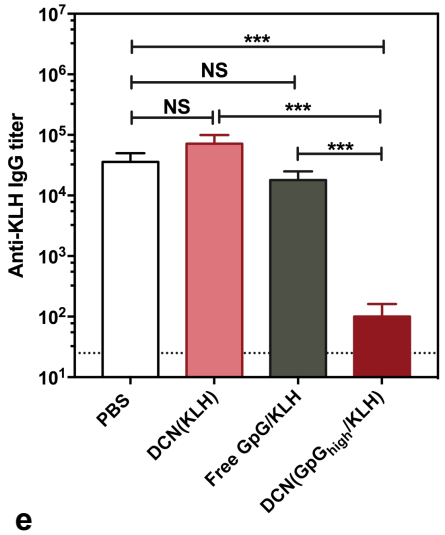
c
Anti-KLH IgG titer
***
NS
NS
***
***
PBS
DCN(KLH)
Free GpG/KLH
DCN(GpG$_{high}$/KLH)

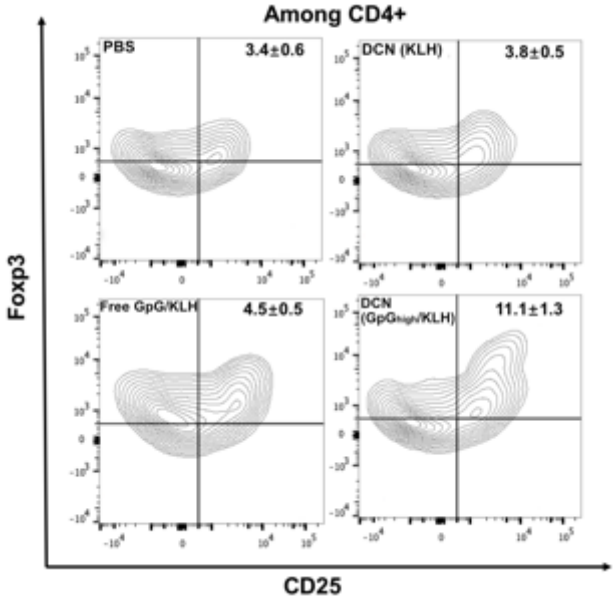
d
Among CD4+
PBS
3.4±0.6
DCN (KLH)
3.8±0.5
Free GpG/KLH
4.5±0.5
DCN (GpG$_{high}$/KLH)
11.1±1.3
Foxp3
CD25

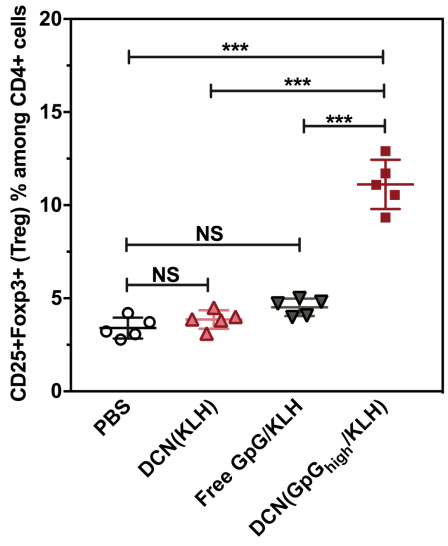
e
CD25+Foxp3+ (Treg) % among CD4+ cells
***
***
***
NS
NS
PBS
DCN(KLH)
Free GpG/KLH
DCN(GpG$_{high}$/KLH)

Figure 5-6. Induction of immune tolerance to protein antigens. (a) Scheme of KLH tolerance study. Mice were IV injected weekly with: (i) PBS, (ii) DCN (KLH) (DCN containing only KLH but no GpG), (iii) free GpG/KLH (free GpG and free KLH), (iv) DCN(GpG/KLH) for the first three weeks, followed by five weekly immunizations of free KLH starting from 21st day. The mice sera were collected on the 21st, 28th, 35th, 42nd, 49th, and 56th day for Ab detection *via* ELISA test. (b) Time course of anti-KLH IgG antibody development in mice sera. (c) End-point anti-KLH antibody titers. (d) Representative contour plots of splenocytes isolated on the 56th day for the frequency of CD4+/CD25+Foxp3+ cells. (e) Percentage of Treg (CD25+Foxp3+) cells among CD4+ T cells.

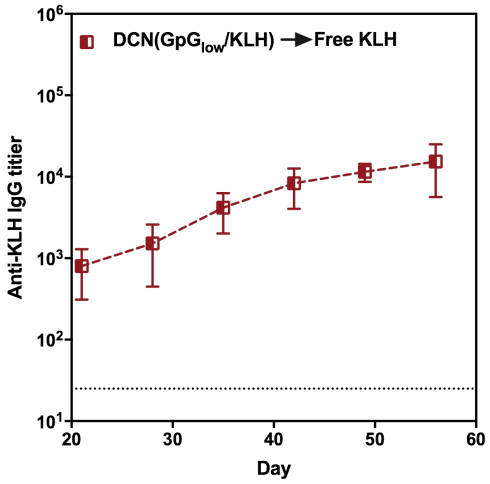

Figure 5-7. KLH tolerance study with DCN (GpG_{low}/KLH). Mice were IV. injected weekly with: DCN formulations containing a low dose of GpG (G:P weight ratio=0.5:1) for the first three weeks, followed by five weekly challenges of free KLH starting from day 21. The mice sera were collected on 21st, 28th, 35th, 42nd, 49th, and 56th days, and detected for IgG titer *via* ELISA test.

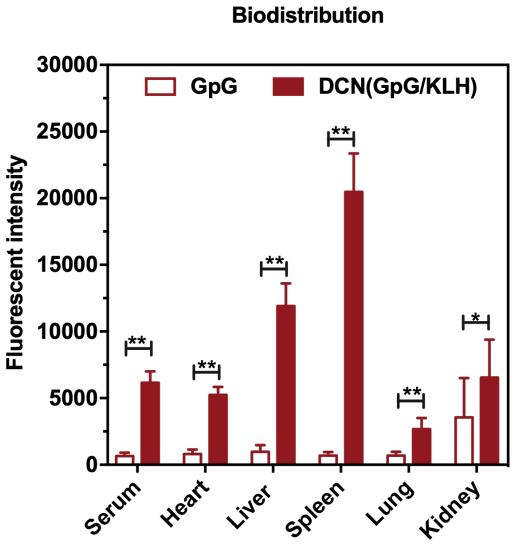

Figure 5-8. Biodistribution study. Biodistribution of free GpG and DCN(GpG/KLH) in main organs (serum, heart, liver, spleen, lung, and kidney) at 24h after the IV injection. Results are plotted as mean ± s.d. (n = 3). Statistical analysis was performed using student test. *P < 0.05; **P < 0.01.

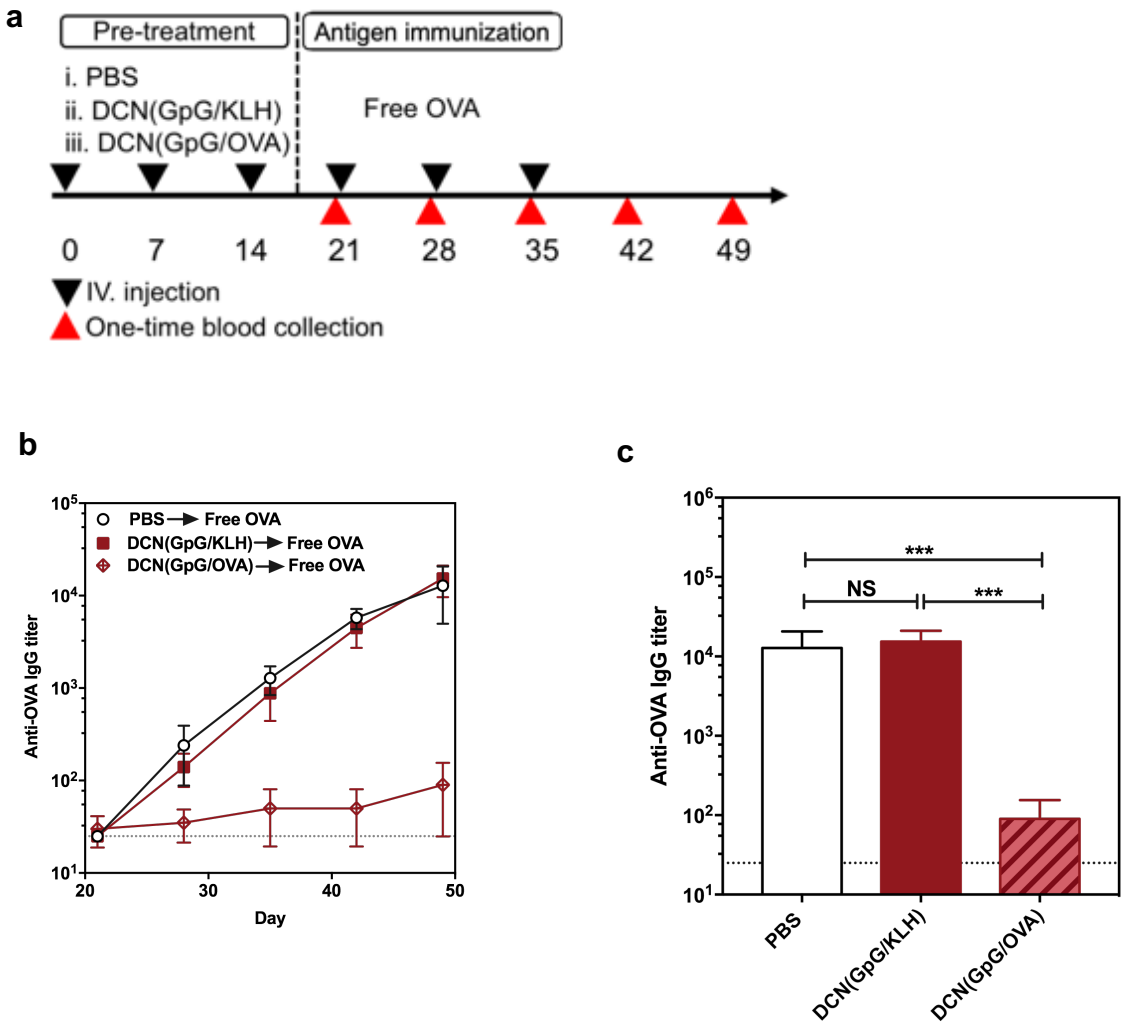

Figure 5-9. (a) Scheme of tolerance specificity study. Mice were IV injected weekly with: (i) PBS, (ii) DCN(GpG/KLH) (iii) DCN(GpG/OVA) for the first three weeks, followed by three weekly immunizations of free OVA starting from 21st day. The mice sera were collected on the 21st, 28th, 35th, 42nd and 49th day for Ab detection *via* ELISA test. (b) Time course of anti-OVA IgG antibody development in mice sera. (c) End-point anti-OVA antibody titers. Results are plotted as mean ± s.d. (n = 5). All statistical analyses were performed using student test (***P < 0.001).

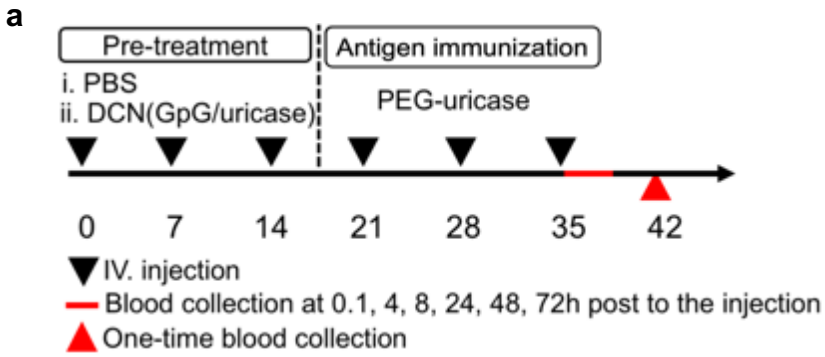
a
Pre-treatment
Antigen immunization
i. PBS
ii. DCN(GpG/uricase)
PEG-uricase
0
7
14
21
28
35
42
IV. injection
Blood collection at 0.1, 4, 8, 24, 48, 72h post to the injection
One-time blood collection

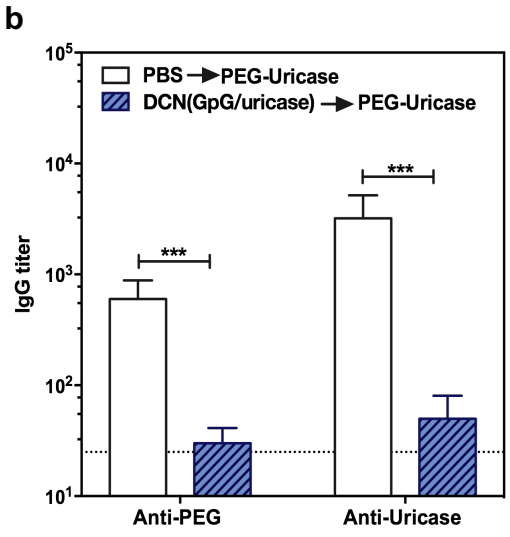
b
PBS → PEG-Uricase
DCN(GpG/uricase) → PEG-Uricase
IgG titer
***
***
Anti-PEG
Anti-Uricase

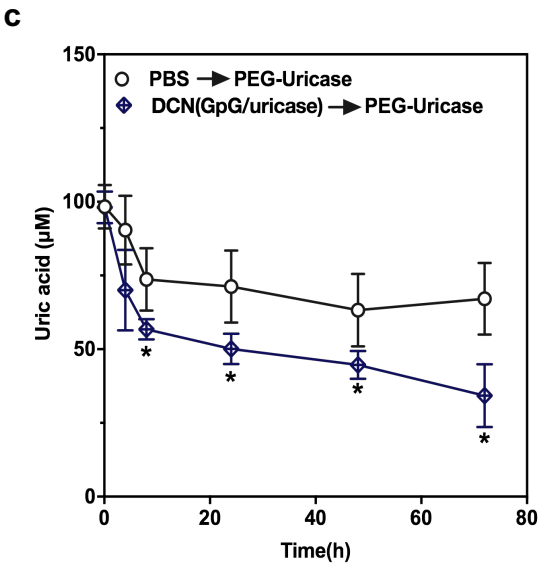
c
PBS → PEG-Uricase
DCN(GpG/uricase) → PEG-Uricase
Uric acid (μM)
Time(h)

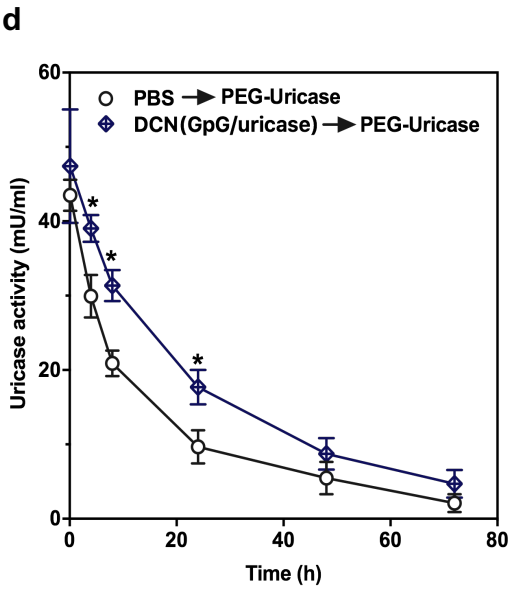
d
PBS → PEG-Uricase
DCN(GpG/uricase) → PEG-Uricase
Uricase activity (mU/ml)
Time (h)

Figure 5-10. (a) Scheme of PEG-uricase study. After three weekly IV injections of PBS sham or DCN(GpG/uricase), three doses of PEG-uricase were IV administered (21st day, 28th, 35th day; one dose per week). The mice sera were collected at 0.1, 4, 8, 24, 48 and 72h post to the third injection of PEG-uricase for evaluating the level of uricase/uric acid. All the mice were sacrificed on 42nd day and their sera were harvested for antibody detection *via* ELISA test. (b) Endpoint anti-PEG and anti-uricase IgG titers. (c) PD profiles of PEGylated uricase, measured as the time course of the change of uric acid in mice blood. Results are plotted as mean ± s.d. (n = 5). All statistical analyses were performed using student test (*$P < 0.05$). (d) The circulation behaviors of PEGylated uricase, measured as the time course of the change of uricase activity in mice blood.

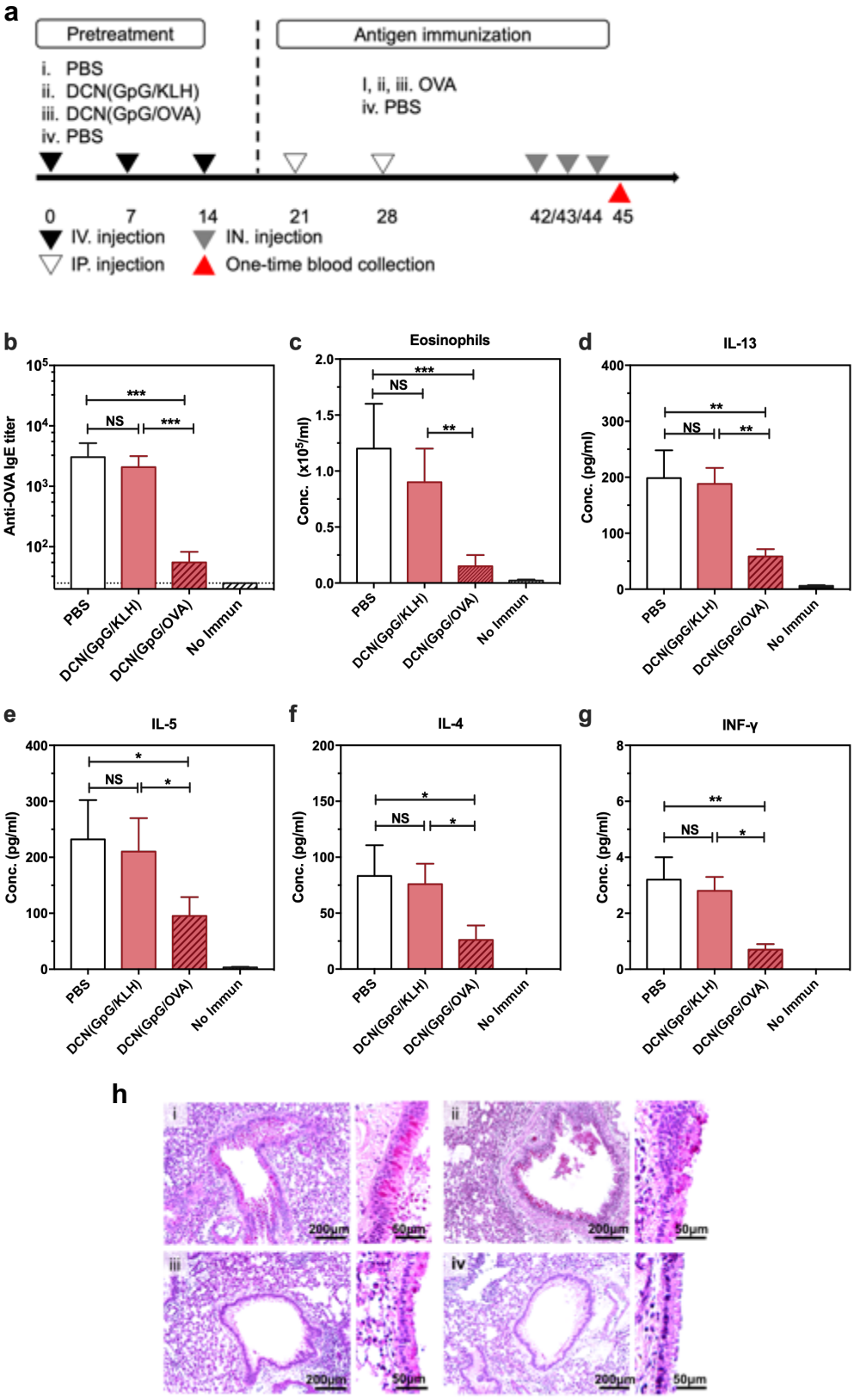
a
Pretreatment
Antigen immunization
i. PBS
ii. DCN(GpG/KLH)
iii. DCN(GpG/OVA)
iv. PBS
I, ii, iii. OVA
iv. PBS
0
7
14
21
28
42/43/44
45
IV. injection
IN. injection
IP. injection
One-time blood collection
b
Anti-OVA IgE titer
c
Eosinophils
Conc. (x10^5/ml)
d
IL-13
Conc. (pg/ml)
e
IL-5
Conc. (pg/ml)
f
IL-4
Conc. (pg/ml)
g
INF-γ
Conc. (pg/ml)
PBS
DCN(GpG/KLH)
DCN(GpG/OVA)
No Immun
NS
h
i
ii
iii
iv
200μm
50μm

Figure 5-11. (a) Scheme of prophylactic treatment of allergic asthma. Mice were IV pre-treated with three weekly doses of PBS shame (i) or DCN(GpG/KLH) (ii), and DCN(GpG/OVA) (iii) before the two-weekly intraperitoneal (IP) immunization with OVA in alum adjuvant (21^{st} and 28^{th} day), followed by intranasal (IN) immunization of OVA (42^{nd}, 43^{rd} and 44^{th} day). In parallel, a fourth group of mice had been administered with PBS as the negative control (iv). All the mice were sacrificed on 45th day and their sera were harvested for antibody detection *via* ELISA test. (b) Endpoint anti-OVA IgE titers (c) Total number of infiltrated eosinophils in mice BALF (d-g) Cytokines in BALF supernatant measured by simplex assay. (h) Representative PAS-stained lung sections showing mucus-producing goblet cells (dark magenta) within bronchi. Results are plotted as mean ± s.d. (n = 5). All statistical analyses were performed using student test (*$P < 0.05$, **$P<0.01$, ***$P<0.001$).

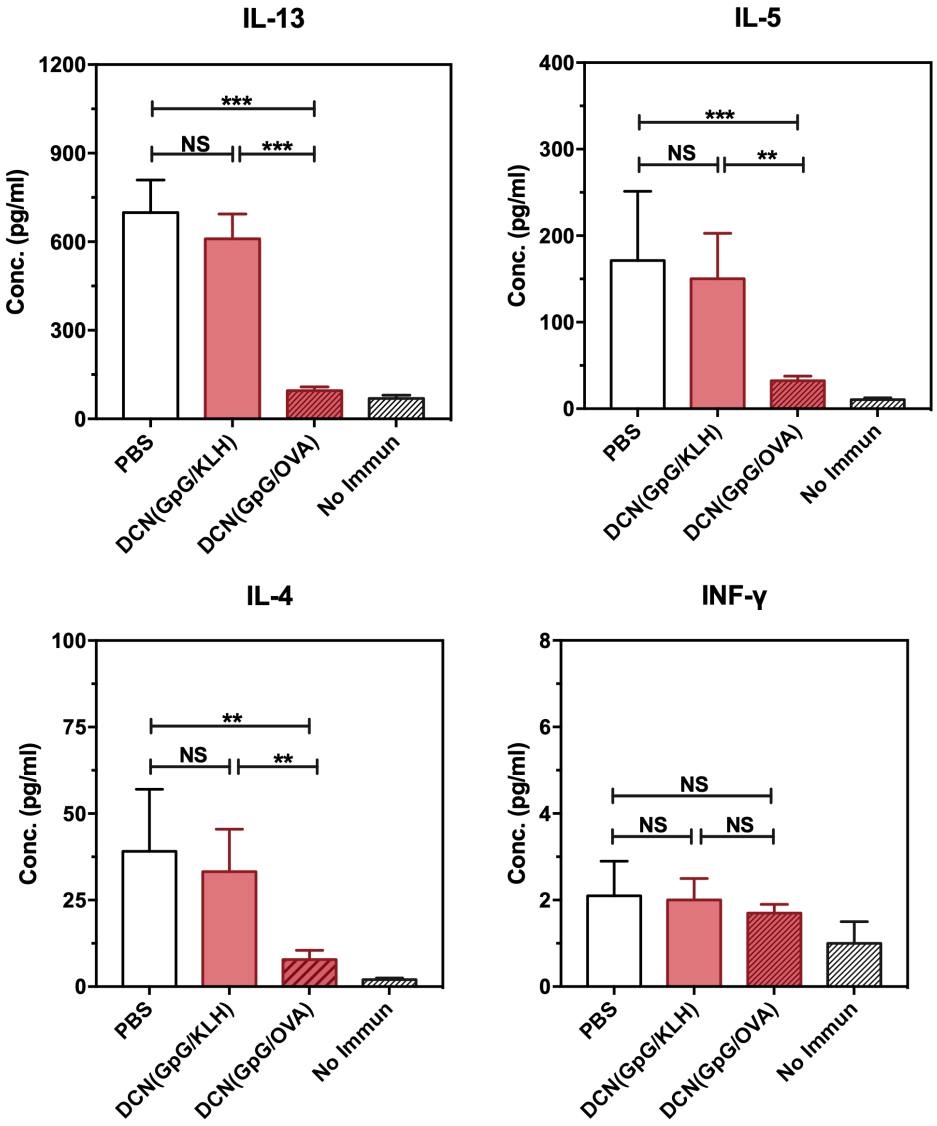

Figure 5-12. Cytokines secreted by splenocytes under OVA restimulation. Splenocytes were extracted from mice that were pretreated and then received immunizations. Levels of IL-13, IL-5, IL-4, and INF-γ were measured in supernatants of splenocytes restimulated ex vitro with OVA for 4 days. Results are plotted as mean ± s.d. (n = 5). All statistical analyses were performed using student test (*P < 0.05, **P<0.01, ***P<0.001).

Table 5-1. PK parameters of PEG-uricase samples after third IV injection.

Pre-injection PK Parameters	PBS	DCN (GpG/uricase)
$t_{1/2}$ (h)	10.5	18.0
V (mU/(mU/ml))	19.2	18.1
CL (mU/(mU/ml)/h)	1.27	0.69
AUC∞ (mU/mL x h)	647.2	1192.4
MRT (h)	15.1	26.0

5.7 References

1. Goldszmid, R. S.; Trinchieri, G. The Price of Immunity. *Nat. Immunol.* 2012, *13*, 932-938.

2. Nechansky, A.; Kircheis, R. Immunogenicity of Therapeutics: A Matter of Efficacy and Safety. *Expert Opin. Drug Discovery* 2010, *5*, 1067-1079.

3. Chirmule, N.; Jawa, V.; Meibohm, B. Immunogenicity to Therapeutic Proteins: Impact on Pk/Pd and Efficacy. *AAPS J.* 2012, *14*, 296-302.

4. Krieckaert, C.; Rispens, T.; Wolbink, G. Immunogenicity of Biological Therapeutics: From Assay to Patient. *Curr. Opin. Rheumatol.* 2012, *24*, 306-311.

5. Larche, M.; Akdis, C. A.; Valenta, R. Immunological Mechanisms of Allergen-Specific Immunotherapy. *Nat. Rev. Immunol.* 2006, *6*, 761-771.

6. Gould, H. J.; Sutton, B. J. IgE in Allergy and Asthma Today. *Nat. Rev. Immunol.* 2008, *8*, 205-217.

7. Hochreiter-Hufford, A.; Ravichandran, K. S. Clearing the Dead: Apoptotic Cell Sensing, Recognition, Engulfment, and Digestion. *Cold Spring Harb. Perspect. Biol.* 2013, *5*.

8. Griffith, T. S.; Ferguson, T. A. Cell Death in the Maintenance and Abrogation of Tolerance: The Five Ws of Dying Cells. *Immunity* 2011, *35*, 456-466.

9. Yatim, N.; Cullen, S.; Albert, M. L. Dying Cells Actively Regulate Adaptive Immune Responses. *Nat. Rev. Immunol.* 2017, *17*, 262-275.

10. Kontos, S.; Grimm, A. J.; Hubbell, J. A. Engineering Antigen-Specific Immunological Tolerance. *Curr. Opin. Immunol.* 2015, *35*, 80-88.

11. Martin, A. J.; McCarthy, D.; Waltenbaugh, C.; Goings, G.; Luo, X. R.; Miller, S. D. Ethylenecarbodiimide-Treated Splenocytes Carrying Male CD4 Epitopes Confer

Histocompatability Y Chromosome Antigen Transplant Protection by Inhibiting CD154 Upregulation. *J. Immunol.* 2010, *185*, 3326-3336.

12. Liu, K.; Iyoda, T.; Saternus, M.; Kimura, Y.; Inaba, K.; Steinman, R. M. Immune Tolerance after Delivery of Dying Cells to Dendritic Cells *in Situ*. *J. Exp. Med.* 2002, *196*, 1091-1097.

13. Godsel, L. M.; Wang, K. G.; Schodin, B. A.; Leon, J. S.; Miller, S. D.; Engman, D. M. Prevention of Autoimmune Myocarditis through the Induction of Antigen-Specific Peripheral Immune Tolerance. *Circulation* 2001, *103*, 1709-1714.

14. Smarr, C. B.; Hsu, C. L.; Byrne, A. J.; Miller, S. D.; Bryce, P. J. Antigen-Fixed Leukocytes Tolerize Th2 Responses in Mouse Models of Allergy. *J. Immunol.* 2011, *187*, 5090-5098.

15. Sabatos-Peyton, C. A.; Verhagen, J.; Wraith, D. C. Antigen-Specific Immunotherapy of Autoimmune and Allergic Diseases. *Curr. Opin. Immunol.* 2010, *22*, 609-615.

16. Rothlin, C. V.; Ghosh, S.; Zuniga, E. I.; Oldstone, M. B. A.; Lemke, G. TAM Receptors Are Pleiotropic Inhibitors of the Innate Immune Response. *Cell* 2007, *131*, 1124-1136.

17. Ferguson, T. A.; Choi, J. Y.; Green, D. R. Armed Response: How Dying Cells Influence T-Cell Functions. *Immunol. Rev.* 2011, *241*, 77-88.

18. Miles, K.; Heaney, J.; Sibinska, Z.; Salter, D.; Savill, J.; Gray, D.; Gray, M. A. Tolerogenic Role for Toll-Like Receptor 9 Is Revealed by B-Cell Interaction with DNA Complexes Expressed on Apoptotic Cells. *Proc. Natl. Acad. Sci. U. S. A.* 2012, *109*, 887-892.

19. Barrat, F. J.; Coffman, R. L. Development of TLR Inhibitors for the Treatment of Autoimmune Diseases. *Immunol. Rev.* 2008, *223*, 271-283.

20. Ho, P. P.; Fontoura, P.; Platten, M.; Sobel, R. A.; DeVoss, J. J.; Lee, L. Y.; Kidd, B. A.; Tomooka, B. H.; Capers, J.; Agrawal, A.; Gupta, R.; Zernik, J.; Yee, M. K.; Lee, B. J.; Garren, H.; Robinson, W. H.; Steinman, L. A Suppressive Oligodeoxynucleotide Enhances the Efficacy of

Myelin Cocktail/IL-4-Tolerizing DNA Vaccination and Treats Autoimmune Disease. *J. Immunol.* 2005, *175*, 6226-6234.

21. Sun, S.; Rao, N. L.; Venable, J.; Thurmond, R.; Karlsson, L. TLR7/9 Antagonists as Therapeutics for Immune-Mediated Inflammatory Disorders. *Inflammation Allergy: Drug Targets* 2007, *6*, 223-235.

22. Jin, B.; Sun, T.; Yu, X. H.; Yang, Y. X.; Yeo, A. E. The Effects of TLR Activation on T-Cell Development and Differentiation. *Clin. Dev. Immunol.* 2012, *2012*, 836485.

23. Chang, J.; Lindsay, R.; Doyle, E.; Vrbanac, V.; Seung, E.; Dudek, T.; Bosch, R.; Precopio, M.; Kandimalla, E.; Tager, A.; Altfeld, M. TLR7/9 Antagonist Reduces HIV-1-Induced Immune Activation. *Retrovirology* 2012, *9, 172*.

24. Chang, J.; Lindsay, R.; Doyle, E.; Vrbanac, V.; Seung, E.; Dudek, T.; Precopio, M.; Kandimalla, E.; Tager, A.; Altfeld, M. Modification of Immune Activation in HIV-1-Infected Humanized Mouse Model Using TLR7/9 Antagonists. *J. Immunol.* 2012, *188*.

25. Mills, K. H., TLR9 Turns the Tide on Treg Cells. *Immunity* 2008, *29*, 518-520.

26. Zhu, F. G.; Reich, C. F.; Pisetsky, D. S. Inhibition of Murine Dendritic Cell Activation by Synthetic Phosphorothioate Oligodeoxynucleotides. *J. Leukoc. Biol.* 2002, *72*, 1154-1163.

27. Conroy, H.; Marshall, N. A.; Mills, K. H. TLR Ligand Suppression or Enhancement of Treg Cells? A Double-Edged Sword in Immunity to Tumours. *Oncogene* 2008, *27*, 168-180.

28. Steinman, L. Inverse Vaccination, the Opposite of Jenner's Concept, for Therapy of Autoimmunity. *J. Intern. Med.* 2010, *267*, 441-451.

29. Tostanoski, L. H.; Chiu, Y. C.; Andorko, J. I.; Guo, M.; Zeng, X.; Zhang, P.; Royal, W., III; Jewell, C. M. Design of Polyelectrolyte Multilayers to Promote Immunological Tolerance. *ACS Nano* 2016, *10*, 9334-9345.

30. Hess, K. L.; Andorko, J. I.; Tostanoski, L. H.; Jewell, C. M. Polyplexes Assembled from Self-Peptides and Regulatory Nucleic Acids Blunt Toll-Like Receptor Signaling to Combat Autoimmunity. *Biomaterials* 2017, *118*, 51-62.

31. Maldonado, R. A.; LaMothe, R. A.; Ferrari, J. D.; Zhang, A. H.; Rossi, R. J.; Kolte, P. N.; Griset, A. P.; O'Neil, C.; Altreuter, D. H.; Browning, E.; Johnston, L.; Farokhzad, O. C.; Langer, R.; Scott, D. W.; Andrian, U. H.; Kishimoto, T. K. Polymeric Synthetic Nanoparticles for the Induction of Antigen-Specific Immunological Tolerance. *Proc. Natl. Acad. Sci. U. S. A.* 2015, *112*, 156-165.

32. Kishimoto, T. K.; Ferrari, J. D.; LaMothe, R. A.; Kolte, P. N.; Griset, A. P.; O'Neil, C.; Chan, V.; Browning, E.; Chalishazar, A.; Kuhlman, W.; Fu, F.; Viseux, N.; Altreuter, D. H.; Johnston, L.; Maldonado, R. A. Improving the Efficacy and Safety of Biologic Drugs with Tolerogenic Nanoparticles. *Nat. Nanotechnol.* 2016, *11*, 890-899.

33. Meliani, A.; Boisgerault, F.; Hardet, R.; Marmier, S.; Collaud, F.; Ronzitti, G.; Leborgne, C.; Costa Verdera, H; Simon Sola, M.; Charles, S.; Vignaud, A.; Wittenberghe, L.; Manni, G.; Chirstophe, O.; Fallarino, F.; Roy, C.; Michaud, A.,; Llyinskii, P.; Kishimoto, T. K.; Mingozzi, F. Antigen-Selective Modulation of AAV Immunogenicity with Tolerogenic Rapamycin Nanoparticles Enables Successful Vector Re-Administration. *Nat. Commun.* 2018, *9*, 4098.

34. Riminton, D. S.; Hartung, H. P.; Reddel, S. W. Managing the Risks of Immunosuppression. *Curr. Opin. Neurol.* 2011, *24*, 217-223.

35. Carbone, J.; del Pozo, N.; Gallego, A.; Sarmiento, E. Immunological Risk Factors for Infection after Immunosuppressive and Biologic Therapies. *Expert Rev. Anti-Infect. Ther.* 2011, *9*, 405-413.

36. Barlow, A. D.; Nicholson, M. L.; Herbert, T. P. Evidence for Rapamycin Toxicity in Pancreatic Beta-Cells and a Review of the Underlying Molecular Mechanisms. *Diabetes* 2013, *62*, 2674-2682.

37. Fabian, M. C.; Lakey, J. R. T.; Rajotte, R. V.; Kneteman, N. M. The Efficacy and Toxicity of Rapamycin in Murine Islet Transplantation - *in-Vitro* and *in-Vivo* Studies. *Transplantation* 1993, *56*, 1137-1142.

38. Barlow, A. D.; Xie, J.; Moore, C. E.; Campbell, S. C.; Shaw, J. A. M.; Nicholson, M. L.; Herbert, T. P. Rapamycin Toxicity in MIN6 Cells and Rat and Human Islets is Mediated by the Inhibition of mTOR Complex 2 (mTORC2). *Diabetologia* 2012, *55*, 1355-1365.

39. Pham, P. T.; Pham, P. C.; Danovitch, G. M.; Ross, D. J.; Gritsch, H. A.; Kendrick, E. A.; Singer, J; Shah, T.; Wilkinson, A. H. Sirolimus-Associated Pulmonary Toxicity. *Transplantation* 2004, *77,* 1215-1220.

40. Marti, H. P.; Frey, F. J. Nephrotoxicity of Rapamycin: An Emerging Problem in Clinical Medicine. *Nephrol., Dial., Transplant.* 2005, *20*, 13-15.

41. Whiting, P. H.; Woo, J.; Adam, B. J.; Hasan, N. U.; Davidson, R. J. L.; Thomson, A. W. Toxicity of Rapamycin - A Comparative and Combination Study with Cyclosporine at Immunotherapeutic Dosage in the Rat. *Transplantation* 1991, *52*, 203-208.

42. Hornung, V.; Rothenfusser, S.; Britsch, S.; Krug, A.; Jahrsdörfer, B.; Giese, T.; Endres, S.; Hartmann, G. Quantitative Expression of Toll-Like Receptor 1-10 mRNA in Cellular Subsets of Human Peripheral Blood Mononuclear Cells and Sensitivity to CpG Oligodeoxynucleotides. *J. Immunol.* 2002, *168*, 4531-4537.

43. Zhang, L.; Sinclair, A.; Cao, Z.; Ella-Menye, J. R.; Xu, X. W.; Carr, L. R.; Pun, S. H.; Jiang, S. Hydrolytic Cationic Ester Microparticles for Highly Efficient DNA Vaccine Delivery. *Small* 2013, *9*, 3439-3444.

44. Sinclair, A.; Bai, T.; Carr, L. R.; Ella-Menye, J. R.; Zhang, L.; Jiang, S. Engineering Buffering and Hydrolytic or Photolabile Charge Shifting in a Polycarboxybetaine Ester Gene Delivery Platform. *Biomacromolecules* 2013, *14*, 1587-1593.

45. Zhang, Z.; Cheng, G.; Carr, L. R.; Vaisocherova, H.; Chen, S. F.; Jiang, S. The Hydrolysis of Cationic Polycarboxybetaine Esters to Zwitterionic Polycarboxybetaines with Controlled Properties. *Biomaterials* 2008, *29*, 4719-4725.

46. Cao, Z.; Jiang, S. Super-Hydrophilic Zwitterionic Poly(carboxybetaine) and Amphiphilic Non-Ionic Poly(ethylene glycol) for Stealth Nanoparticles. *Nano Today* 2012, *7*, 404-413.

47. Zhang, L.; Cao, Z.; Bai, T.; Carr, L.; Ella-Menye, J. R.; Irvin, C.; Ratner, B. D.; Jiang, S. Zwitterionic Hydrogels Implanted in Mice Resist the Foreign-Body Reaction. *Nat. Biotechnol.* 2013, *31*, 553-556.

48. Li, B.; Yuan, Z.; Zhang, P.; Sinclair, A.; Jain, P.; Wu, K.; Tsao, C.; Xie, J.; Hung, H. C.; Lin, X.; Bai, T.; Jiang, S. Zwitterionic Nanocages Overcome the Efficacy Loss of Biologic Drugs. *Adv. Mater.* 2018, *30*, 1705728.

49. Zhang, P.; Sun, F.; Tsao, C.; Liu, S. J.; Jain, P.; Sinclair, A.; Hung, H. C.; Bai, T.; Wu, K.; Jiang, S. Zwitterionic Gel Encapsulation Promotes Protein Stability, Enhances Pharmacokinetics, and Reduces Immunogenicity. *Proc. Natl. Acad. Sci. U. S. A.* 2015, *112*, 12046-12051.

50. Li, B.; Xie, J.; Yuan, Z.; Jain, P.; Lin, X.; Wu, K., Jiang, S. Mitigation of Inflammatory Immune Responses with Hydrophilic Nanoparticles. *Angew. Chem., Int. Ed.* 2018, *57*, 4527-4531.

51. Li, B.; Yuan, Z.; Hung, H. C.; Ma, J.; Jain, P.; Tsao, C.; Xie, J.; Zhang, P.; Lin, X.; Wu, K.; Jiang, S. Revealing the Immunogenic Risk of Polymers. *Angew. Chem., Int. Ed.* 2018, *57*, 13873-13876.

52. Lipsky, P. E.; Calabrese, L. H.; Kavanaugh, A.; Sundy, J. S.; Wright, D.; Wolfson, M.; Becker, M. A. Pegloticase Immunogenicity: The Relationship between Efficacy and Antibody Development in Patients Treated for Refractory Chronic Gout. *Arthrit. Res. Ther.* 2014, *16*, 60.

53. Garay, R. P.; El-Gewely, R.; Armstrong, J. K.; Garratty, G.; Richette, P. Antibodies against Polyethylene Glycol in Healthy Subjects and in Patients Treated with PEG-Conjugated Agents. *Expert Opin. on Drug Delivery* 2012, *9*, 1319-1323.

54. Abuchowski, A.; Vanes, T.; Palczuk, N. C.; Davis, F. F. Alteration of Immunological Properties of Bovine Serum Albumin by Covalent Attachment of Polyethylene Glycol. *J. Biol. Chem.* 1977, *252*, 3578-3581.

55. Richter, A. W.; Akerblom, E. Antibodies against Polyethylene Glycol Produced in Animals by Immunization with Monomethoxy Polyethylene Glycol Modified Proteins. *Int. Arch. Allergy Appl. Immunol.* 1983, *70*, 124-131.

56. Zhang, P.; Sun, F.; Liu, S.; Jiang, S. Anti-PEG Antibodies in the Clinic: Current Issues and Beyond PEGylation. *J. Control. Release* 2016, *244*, 184-193.

57. Smarr, C. B.; Yap, W. T.; Neef, T. P.; Pearson, R. M.; Hunter, Z. N.; Ifergan, I.; Getts, D. R.; Bryce, P. J.; Shea, L. D.; Miller, S. D. Biodegradable Antigen-Associated PLG Nanoparticles Tolerize Th2-Mediated Allergic Airway Inflammation Pre- and Postsensitization. *Proc. Natl. Acad. Sci. U. S. A.* 2016, *113*, 5059-5064.

58. Zhang, Y.; Huo, M.; Zhou, J.; Xie, S. PKSolver: An Add-In Program for Pharmacokinetic and Pharmacodynamic Data Analysis in Microsoft Excel. *Comput. Methods Programs Biomed.* 2010, *99*, 306-314.

CHAPTER 6

Trimethylamine N-oxide Derived Zwitterionic Polymers: A New Class of Ultra-low Fouling Bioinspired Materials

6.1 Abstract

Materials that resist nonspecific protein adsorption are highly desirable for many applications. However, few are able to achieve ultra-low fouling in complex biological milieu. Zwitterionic polymers emerge as a class of highly effective ultra-low fouling materials due to their super-hydrophilicity, outperforming other neutral and hydrophilic materials such as poly(ethylene glycol) (PEG). Unfortunately, there are only three major classes of zwitterionic materials based on poly(phosphorylcholine) (PPC), poly(sulfobetaine) (PSB) and poly (carboxybetaine) (PCB) currently available. Inspired by trimethylamine N-oxide (TMAO), a zwitterionic osmolyte and the most effective protein stabilizer, we herein report TMAO-derived zwitterionic polymers (PTMAO) as a new class of ultra-low fouling biomaterials. The non-fouling properties of this material are demonstrated under highly challenging *in vitro* and *in vivo* conditions. The mechanism accounting for the extraordinary hydration of PTMAO was elucidated by molecular dynamics (MD) simulations. The discovery of PTMAO polymers demonstrates the power of the molecular understanding and design of new biomimetic materials derived from naturally occurring molecules and provides the biomaterials community with another class of non-fouling zwitterionic materials.

6.2 Introduction

Unwanted adsorption of biomolecules, cells and micro-organisms represents a great challenge in many applications from medical devices to drug delivery systems[1, 2]. For example, biomaterials tend to be covered with a layer of host proteins shortly after implantation, which thereafter will provoke an irrevocable foreign body reaction (FBR)[2, 3]. As a result, a variety of iatrogenic complications including inflammation, infection, tissue fibrosis and capsulate formation will be triggered, leading to the failure of biomaterials. Likewise, drug-delivering carriers are also susceptible to the non-specific attachment of proteins and cells, which may result in the rapid clearance of therapeutic drugs and adverse immune responses[4, 5]. Therefore, reducing or eliminating undesirable "biofouling" is of paramount importance to the safety and function of medical devices or drugs. To achieve a non-fouling surface, a number of hydrophilic materials have been employed, where the surface hydration plays a pivotal role[6]. These materials have been shown to create a hydration shell that repels biomolecules or cells from contacting surfaces, making the underlying substrates "stealthy"[7]. However, the hydration capability of most hydrophilic materials is often not sufficient to produce a non-fouling surface. At present, there are few highly hydrophilic materials that can meet the non-fouling demand of practical applications, particularly in complex biological media.

PEG is the most widely used stealth material. The attachment of PEG to surfaces, known as "PEGylation", has been a "gold standard" strategy to resist nonspecific protein adsorption. Though commonly considered as hydrophilic, PEG containing a hydrophobic –C-C- backbone along with a hydrophobic -O(CH3) terminal group is in fact amphiphilic, as evidenced by its good solubility in many organic solvents in addition to water. As any nonspecific interaction moieties can be

detected by the immune system, the hydrophobic character of PEG would be amplified under *in vivo* conditions, particularly when it is conjugated with highly immunogenic proteins, generating PEG-specific antibodies[8, 9]. In recent decades, zwitterionic materials that contain an equal number of oppositely charged ions (zwitterions) have been emerging as a new series of hydrophilic biomaterials for non-fouling purposes as they can strongly withhold water molecules via electrostatically induced hydration[10, 11]. PPC that mimics zwitterionic phosphorylcholine moieties outside cell membranes has been extensively studied and used as a biomimetic fouling-resistant material in many applications over the past decades[12]. Another two classes of zwitterionic materials, PSB derived from taurine, and PCB derived from glycine betaine, have been demonstrated for their superior hydration capability and fouling resistance[13-17]. Typically, PCB polymer coated surfaces have been shown to reduce nonspecific protein adsorption to an ultra-low level, *i.e.* <0.3ng/cm^2 in undiluted human serum or plasma, the lowest detection limit of a surface plasmon resonance (SPR) biosensor[10, 18]. Furthermore, such an excellent non-fouling property has been shown to retain *in vivo*: PCB hydrogels implanted in mice could prevent the occurrence of foreign-body reactions such as capsule formation for at least three months while PCB-coated proteins display enhanced circulation, but much lessened immunogenicity in mice and rats[19-23]. With such attractive benefits, zwitterionic materials are receiving increasingly high attention. Unfortunately, there are only three classes of zwitterionic materials (PPC, PSB and PCB) currently available.

Previous studies have shown that the hydration capacity along with the non-fouling property of zwitterionic polymers increases as the intramolecular distance between the positively and negatively charged sites of the zwitterionic headgroups decreases[24, 25]. Based on this rule of thumb,

we have scouted naturally-occurring zwitterionic molecules and found that TMAO, a small organic osmolyte present in saltwater fishes, might be an excellent zwitterionic headgroup for non-fouling materials as its opposing charge moieties are directly connected ($Me3N^{+}–O^{-}$) with no spacer between two charges[26]. In comparison, the zwitterionic moiety of PCB that derives from glycine contains at least one carbon separation ($Me_3N^{+}\text{-}CH_2\text{-}COO^{-}$). Moreover, TMAO is renowned to stabilize the folded structures of proteins by counteracting the effects of protein denaturants (e.g. urea), heat and pressure in the most effective way[27-30]. Inspired by the super-hydrophilic and protein-stabilizing nature of TMAO, we herein report a TMAO-derived polymer (PTAMO) as a new-generation zwitterionic material with fully characterized properties (Fig. 6-1a). The exceptional non-fouling performance of PTMAO was demonstrated under harsh *in vitro* and *in vivo* conditions, and the mechanism accounting for the extraordinary hydration of PTMAO was elucidated by MD simulations. The discovery of PTMAO represents the fourth class of non-fouling zwitterionic material after PPC, PSB and PCB, enriching the arsenal of non-fouling materials and is expected to benefit a wide range of applications.

6.3 Experimental Section

6.3.1 Materials

PP sheet was purchased from TAP plastics. Fibrinogen, KLH, Recombinant uricase from Candida sp. and all chemicals were purchased from Sigma-Aldrich unless otherwise noted and were used as received. Methoxy-PEG-NHS (10kDa, 95%) was purchased from Nanocs Corporation. Goat anti-mouse IgM antibody and goat anti- mouse IgG antibody was purchased from Bethyl labs. Pierce Protein Concentrators (100k MWCO) were purchased from Thermo Fisher Scientific (Waltham, MA). 3,3′,5,5′-Tetramethylbenzidine (TMB) substrate solution was purchased from

eBioscience (San Diego, CA). High resolution size exclusion chromatography resin (Sephacryl S-500HR) was purchased from GE Healthcare Life Sciences. C5b-9 assay ELISA kit was purchased from BD Bioscience.

6.3.2 Synthesis of TMAO monomer

800 mg diethylenetriaminepentaacetic acid was added to 30 mL Milli-Q water and mixed vigorously until the white powder dissolved. Then hydrogene peroxide (50% solution, 2.87 g) was slowly added and reaction contents were heated to 60℃. Oxygen gas then was slowly purged into solution[31]. Dimethylaminopropylacrylamide (14.4 g) in 10 mL Milli-Q water was added dropwise in 30 minutes. The reaction was carried out for 6 hours at 60℃. After completion of reaction, the reaction contents were cooled. Nuclear magnetic resonance (NMR) analysis of the product confirmed the formation of TMAO monomer. The pH of the final product was about 7.5 and solid content was about 32.9%. TMAO monomer was then precipitated by an organic solvent. The final product is colorless and viscous liquid. NMR result is shown in Fig. 6-2. 1H NMR (500 MHz, D2O): δ 6.07 – 5.93 (m, 2H), 5.55 (d, J = 9.9 Hz, 1H), 3.12 (m, 4H), 3.01 (s, 6H), 1.90 – 1.74 (m, 2H). HRMS analysis was carried out by using a Thermo Scientific Exactive Plus Orbitrap spectrometer and the result is shown in Fig. 6-3. HRMS (m/z): calculated for $C_8H_{17}N_2O_2$, 173.1284 ($[M+H]^+$). Found 173.1282.

6.3.3 Preparation of TMAO hydrogel

TMAO hydrogel was fabricated by bulk photo-polymerization with a hydrogel aqueous solution containing TMAO monomer (0.67g Milli-Q water, 330mg TMAO monomer), crosslinker N,N'-Methylenebis(acrylamide) (1 wt%, 3.3mg) and photo-initiator 2-Hydroxy-2-

methylpropiophenone (0.33mg). The hydrogel aqueous solution was placed between two glass slides separated by a 0.5 mm-thick polytetrafluoroethylene spacer, and was then photo-polymerized at room temperature for 30 mins. After polymerization, hydrogels were removed from the casts and soaked in PBS for three days to remove unreacted chemicals and reach the fully hydrated hydrogel network. Phosphate buffered saline was refreshed every 12 hours.

6.3.4 Fibrinogen adsorption test

Biopsy punches were used to punch the hydrated TMAO hydrogel and the PP sheet into 5 mm-diameter disks. The sample disks were then placed into a 24 well-plate and incubated with 1 mL of 10 mg/mL fibrinogen in PBS buffer for 2 hours, followed by 5 washes with pure PBS buffer. Subsequently, the ample disks were then transferred to new wells and incubated with 1mL of horseradish peroxidase (HRP) conjugated anti-fibrinogen (1 μg/mL) in PBS buffer for 1 hour. All sample disks were then transferred to new wells after 5 washes with pure PBS buffer. Next, 1mL 1 mg/mL o-phenylenediamine (OPD) citrate phosphate solution (0.1 M, pH 5.0), containing 0.03% hydrogen peroxide was added. After 15min incubation, the enzymatic reaction was stopped by adding an equal volume of 1 M HCl. The same procedure was conducted on PP disks with the same surface area as the control. Absorbance value at 492 nm was recorded by a plate reader and was normalized to that of polypropylene (PP) sample. Average data were acquired from three specimens.

6.3.5 Cell adhesion test

TMAO hydrogel disks with 1 wt % cross-linker were soaked in 70% ethanol for 2 h for sterilization and soaked in sterilized PBS until equilibrium. NIH-3T3 fibroblasts were respectively seeded onto

TMAO hydrogel disks at a concentration of 10^5 cells/mL into a 24 well-plate. The same procedure was conducted on TCPS hydrogel disks with the same surface area as the control. The cells were cultured at 37 °C, 5% CO2, and 100% humidity for 72 h and then were observed and photographed on a Nikon Eclipse TE2000-U microscope at 100× magnification.

6.3.6 Complement activation test

PTMAO, and PVA were made into high-crosslinked cylindrical hydrogel bowls (6 mm in diameter and 8 mm in depth) with 50%wt of solid fraction using a home-made mold. Then, 300uL of pooled complement human serum (Innovative Research, Novi, MI) was added into replicates of each polymer bowl (n=3) and incubated at 37°C for 90 min and followed by quenching with 30ul of 10mM ethylenediaminetetraacetic acid (EDTA) solution. The complement activation degree was measured by quantifying a complement degradation fragment C5b-9 in serum using standard ELISA kit (BD Bioscience, San Diego, CA) following the manufacture's protocol. The level of pre-existing C5b-9 in the serum was measured and subtracted as the background.

6.3.7 Preparation of TMAO-coated surface by SI-ATRP

Clean gold coated glass substrates were firstly soaked in in w-mercaptoundecyl bromoisobutyrate solution (0.2mmol/L in ethanol) for overnight to get initiator-coated substrates. The initiator coated substrates, together with Copper(I) bromide (14.35mg, 0.1mmol) were then placed into a Schlenk tube and deoxygenated via pump-vacuum for ten cycles. TMAO monomer (1.72g, 10mmol), Me_6TREN(23mg, 0.1mmol), methanol (3.6mL) and H_2O(0.4mL) were added into Schlenk tube and deoxygenated via the same method. After fully deoxygenation, the mixed aqueous solution of TMAO monomer and Me_6TREN were transferred to the tube which held the substrate and copper

bromide. The reaction mixture was placed at ambient temperature for overnight. The substrate was then taken out from mixture and washed with ethanol and water respectively for three times and air-dried before being used as SPR sample. The thickness of the coated TMAO polymer film was measured by Ellipsometer.

6.3.8 SPR test in human serum

The non-specific protein adsorption of the TMAO polymer films was determined with a SPR biosensor using a flow rate of 40 μL/min at 25°C. After first establishing a baseline using PBS, undiluted human serum was flowed for 10 min, followed by buffer to re-establish the baseline. Protein adsorption was quantified as the difference between buffer baselines and converted to a surface coverage using the appropriate sensitivity factor.

6.3.9 Preparation of PTMAO-KLH conjugate

Acryloyl-modified KLH was firstly prepared. The reaction was performed by dissolving 2 mg KLH into 1 mL 50 mM Hepes buffer (pH 8.5), followed by adding 15 μL N-acryloxysuccinimide (NAS) dimethyl sulfoxide (DMSO) solution (40 mg/mL) dropwise. The reaction was stirred at 4 °C for 2 h, after which acryloyl-modified uricase was purified and concentrated using a 100-kDa molecular weight cutoff centrifugal filter. The uricase conjugates were prepared by nanoemulsion method. Briefly, AOT (sodium bis(2-ethylhexyl) sulfosuccinate, 120 mg) and Brij 30(poly(ethylene glycol) dodecyl ether, 230mg) were added to a 20mL glass vial to which a stir bar was added. The vial was sealed with a Teflon-lined septum cap and purged with dry nitrogen for 10min. Nitrogen-deoxygenated hexane (5mL) was then added to the vial under vigorous stirring. For the aqueous phase, acryloyl-modified KLH (1mg) was dissolved in HEPES buffer

(pH 8.5, 150μL), to which TMAO monomer (100mg) were added and dissolved. Dry nitrogen was bubbled through the monomer/protein solution for 2min, after which the aqueous phase was slowly added to the organic continuous phase dropwise. The vial was sonicated to form a stable microemulsion. A 20% (w/v) solution of ammonium persulfate (APS) in deionized water (20μL) was then added to the emulsion. After 5 min, polymerization was initiated by the addition of tetramethylethylenediamine (TEMED, 12μL) and maintained at 4°C under rapid magnetic stirring. After the 2-hour reaction, the organic solvent was removed by rotary evaporator and the PTMAO-KLH conjugate was precipitated and washed with THF for three times. The PTMAO-KLH conjugate was re-suspended in PBS buffer and purified with high resolution size exclusion chromatography (Sephacryl S-500HR) to remove the free KLH. Finally the conjugates were washed and concentrated with PBS (pH 7.4) for three times using a 100-kDa molecular weight cutoff centrifugal filter. The protein-polymer conjugates were characterized by gel permeation chromatogram (GPC, Wyatt technology).

6.3.10 Preparation of PEGylated KLH

KLH (1 mg/mL) and mPEG-NHS (10kDa 20 mg/mL) were mixed in 50 mM Hepes buffer (pH 8.5). The reaction was stirred at 4 °C overnight. Then the PEG-KLH conjugates were purified with high resolution size exclusion chromatography (Sephacryl S-500HR) to remove the free KLH. Finally the conjugates were washed and concentrated with PBS (pH 7.4) for three times using a 100-kDa molecular weight cutoff centrifugal filter. The protein-polymer conjugates were characterized by gel permeation chromatogram (GPC, Wyatt technology).

6.3.11 Preparation of PTMAO-uricase conjugate

Similar to acryloyl-modified KLH, acryloyl-modified uricase was firstly prepared. The uricase conjugates were also prepared by nanoemulsion method. Briefly, AOT (120 mg) and Brij 30 (230mg) were added to a 20mL glass vial to which a stir bar was added. The vial was sealed with a Teflon-lined septum cap and purged with dry nitrogen for 10min. Nitrogen-deoxygenated hexane (5mL) was then added to the vial under vigorous stirring. For the aqueous phase, acryloyl-modified uricase (1mg) was dissolved in HEPES buffer (pH 8.5, 125μL), to which TMAO monomer (50mg) were added and dissolved. Dry nitrogen was bubbled through the monomer/protein solution for 2min, after which the aqueous phase was slowly added to the organic continuous phase dropwise. The vial was sonicated to form a stable microemulsion. A 20% (w/v) solution of APS (10 μL) in Milli-Q water was then added to the emulsion. After 5 min, polymerization was initiated by the addition of TEMED (6 μL) and maintained at 4°C under rapid magnetic stirring. After the 2-hour reaction, the organic solvent was removed by rotary evaporator and the PTMAO-uricase conjugate was precipitated and washed with THF for three times. The PTMAO-uricase conjugate was re-suspended in PBS buffer and purified with high resolution size exclusion chromatography (Sephacryl S-500HR) to remove the free uricase. Finally the conjugates were washed and concentrated with PBS (pH 7.4) for three times using a 100-kDa molecular weight cutoff centrifugal filter. The protein-polymer conjugates were characterized by gel permeation chromatogram (GPC, Wyatt technology).

6.3.12 Preparation of PEGylated uricase

uricase (1 mg/mL) and mPEG-NHS (10kDa 10 mg/mL) were mixed in 50 mM Hepes buffer (pH 8.5). The reaction was stirred at 4 °C overnight. Then the PEG-uricase conjugates were purified

with high resolution size exclusion chromatography (Sephacryl S-500HR) to remove the free uricase. Finally the conjugates were washed and concentrated with PBS (pH 7.4) for three times using a 100-kDa molecular weight cutoff centrifugal filter. The protein-polymer conjugates were characterized by GPC.

6.3.13 Stability test

Native uricase, PEG-uricase and PTMAO-uricase conjugates in PBS solution (pH 7.4) at 10μg/mL for 6 hours, with and without urea (0.4M, 0.8M, 1.6M, 3.2M) after which the activity of retained uricase were tested. Likewise, the thermal stability of native uricase, PEG-uricase and PTMAO-uricase conjugates were tested after incubation at different temperature (40℃, 50℃, 60℃, 70℃) for 30min. The activity of uricase was measured by AmplexTM Red uric acid/uricase assay kit following the manufacture's protocol. Measurements were performed in triplicate.

6.3.14 Animal studies

The University of Washington Institutional Animal Care and Use Committee (IACUC) approved all animal experiments under protocol #4203-01. Male C57BL/6J mice of ~20 g were randomly divided.

6.3.15 Immunogenicity study of PTMAO

To compare the immunogenicity of PEG and PTMAO, two groups of male C57BL/6J mice (n=5) were administered with the PEG-KLH and PTMAO-KLH conjugates respectively via SC injection (2mg protein/kg weight) for five weeks (one dose per week). Mice sera were collected on 7th, 14th,

21st, 28th, and 35th day during the immunization study, and the anti-PEG or anti-PTMAO antibodies (IgM and IgG) in mice sera was detected using ELISA tests.

For ELISA tests, 100 μL antigen solution (10 μg/mL of protein concentration) prepared in 0.1 M sodium carbonate buffer (pH 10.5), was used to coat each well of the 96-well plates. Antigens used in direct ELISAs for plate coating consisted of PEG-BSA (for the mice sera immunized with PEG-KLH) or PTMAO-BSA conjugates (for mice sera immunized with PTMAO-KLH). PEG-BSA and PTMA-BSAO conjugates were prepared, following the same preparation protocol of PEG-KLH and PTMAO-KLH conjugates as described above. During coating procedure, plates were incubated at 4 °C overnight. After removing antigen solutions, the plates were washed five times using PBS (pH 7.4) and then filled with blocking buffer (1% nonfat milk solution in 0.1 M Tris buffer, pH 8.0). It is important to avoid using any buffer that contains PEG-like detergents, e.g., Tween 20 and Tween 80. After incubation at room temperature for 1 h, blocking buffer was removed, and all wells were washed by PBS for another five times. Serial dilutions of monoclonal anti-PEG abs in PBS containing 1% nonfat milk were added to the plates (100 μL/well), which were incubated for 1 h at 37 °C. The plates were then washed five times with PBS, followed by adding secondary antibody HRP conjugates (100 μL/well, dilution 1:50000, Bethyl Labs). After adding the secondary antibody, plates were incubated at room temperature for 1 h and then washed five times using PBS before the addition of 100 μL/well HRP substrate 3,3',5,5'-tetramethylbenzidine. The plates were shaken for 15 min, and 100 μL stop solution (0.2 M H2SO4) was added to each well. Absorbance at 450 (signal) and 570 nm (background) was recorded by a microplate reader.

6.3.16 In vivo non-fouling performance of PTMAO

Three groups of male C57BL/6J mice (n=5) were administered with the native uricase, PEG-uricase and PTMAO-uricase conjugates respectively via IV injection (25U/kg weight) for three weeks (one dose per week). The mice sera were collected at various time points (0.1, 6, 12, 24, 48 and 72h) post to the first and the third injection of uricase samples for evaluating the level of uricase/uric acid. The uricase concentration in plasma was estimated based on the enzyme activity measured by Amplex Red uric acid/uricase assay kit. Circulation time of each uricase sample was calculated using PKSolver software following the instructions. The urate concentration in the mice sera was also measured by Amplex Red uric acid/uricase assay kit. All the mice were sacrificed on 21st day and their sera were harvested for antibody detection via ELISA tests as described above. For ELISA tests, uricase was used as the coated antigen for the detection of anti-uricase Ab, while PEG-uricase or PTMAO-uricase conjugate was used as the coated antigen for the detection of anti-conjugate Ab.

6.3.17 MD simulations

Partial charges for TMAO, OEG, and PTMAO atoms were assigned using the restrained electrostatic potential (RESP) method[32]. Quantum mechanical calculations for RESP were performed in Gaussian 09 using the B3LYP hybrid functional with the 6-31G(d) basis set (*33, 34*). For PTMAO, the quantum calculations were performed for a monomer with a methyl-capped backbone, and the partial charge of the backbone atoms were adjusted to neutralize the net charge of the monomer. Water molecules were described by the TIP3P water model.

The initial configuration for each simulation was generated with GROMACS 5.1.2 utilities[35]. For the small molecule simulations, one solute molecule (TMAO or OEG) was centered in a cubic box with 2.5 nm sides. The box was then solvated with 504 randomly placed water molecules. A two-step equilibration procedure was followed to provide reasonable starting positions and velocities for production simulations. Energy minimization was performed with the solvated configuration using the steepest descent algorithm for 10,000 steps. Energy minimization was followed by a 1 ns simulation in the NPT ensemble, with the Bussi-Donadio-Parrinello (v-rescale) thermostat and Berendsen barostat for temperature and pressure control, respectively[36, 37]. The output atomic coordinates and velocities for each system were used as the initial coordinates and velocities for the production simulations.

For the production phase, each system was simulated for 4 ns in the NPT ensemble with the Bussi-Donadio-Parrinello (v-rescale) thermostat and Parrinello-Rahman barostat for temperature and pressure control, respectively[36,38]. Frames were saved every 100 fs (50 steps) during the production simulation, and trajectories were analyzed with Gromacs utilities. The hydrogen bond count for every frame was calculated with the `*gmx hbond*` utility, using the default geometric definition of the hydrogen bond: a donor-acceptor distance of less than 0.35 nm and a hydrogen-donor-acceptor angle of less than 30 degrees. The probability distribution of the number of hydrogen bonds accepted by OEG and TMAO oxygens were generated with kernel density estimation (KDE), essentially a technique to smooth the hydrogen bond histogram with Gaussians. The autocorrelation function for the hydrogen bond lifetime was calculated using the method of Luzar and Chandler, as implemented in the Gromacs utility `*gmx hbond*`. Radial distribution functions were calculated using the `*gmx rdf*` utility[39].

6.4 Results and Discussion

6.4.1 Synthesis of TMAO-analogue monomer

Given the super-hydrophilic and protein-stabilizing nature of TMAO, a TMAO-derived polymer is envisioned to provide a new class of non-fouling zwitterionic materials. In this work, a zwitterionic TMAO-derived monomer was synthesized by oxidizing N,N-dimethyl aminopropyl acrylamide (DMAPA) (Fig. 6-1b). Initially, several mild oxidizing agents were used to oxidize the tertiary amine. However, these oxidizing agents resulted in incomplete reactions along with side products. The use of stronger oxidizing agents such as 50% hydrogen peroxide resulted in the complete conversion of DMAPA with no side products. After further purification, we obtained the final product of TMAO monomer as a colorless and viscous liquid. The resulting monomer was characterized using nuclear magnetic resonance (NMR, Fig. 6-2) and high-resolution mass spectrometry (HRMS, Fig. 6-3). With a single-step reaction, an eco-friendly solvent (water), high conversion efficiency and ease in purification, high-purity TMAO monomer can be easily scaled up for large production.

6.4.2 In vitro fouling tests of TMAO polymers

The adsorption of plasma proteins onto a typical synthetic surface occurs rapidly upon contact between the surface and blood. Among numerous plasma proteins, fibrinogen plays a major role in determining the hemocompatibility of a particular material due to its abundance in blood, its essential role in coagulation and its ability to promote platelet adhesion. Therefore, we firstly polymerized TMAO monomers into a hydrogel, which was then punched into disks and exposed to a highly concentrated fibrinogen solution (10mg/ml). In parallel, polypropylene (PP) disks with the same size were prepared and incubated with fibrinogen under the same condition as the positive

control. After 2-h exposure, the amount of fibrinogen adhered onto PTAMO and PP disks was quantitatively measured by enzyme-linked immunosorbent assay (ELISA). As shown in Fig. 6-4a, PTAMO disks exhibited an exceptional non-fouling property after 2h incubation in a highly concentrated fibrinogen solution (10mg/mL) by reducing 97.6% of adsorbed fibrinogen with respect to that of PP disks. Considering that the fibrinogen concentration in human plasma (1.5-4mg/mL) is much lower than the test solution (10mg/mL), PTMAO is anticipated to maintain an ultra-low fibrinogen adsorption in the real blood environment. Furthermore, the potential of PTMAO in activating complement proteins was also studied. The unexpected activation of complement systems would evoke the propagation of protein adsorption on material surfaces, enhancing the vulnerability of materials to immune recognition. In this work, the level of C5b-9, a typical marker of complement activation in human serum, was assessed after serum had been incubated with PTMAO hydrogels for 3h (Fig. 6-4b). In contrast to the control hydrogel composed of another hydrophilic polymer, poly(vinyl alcohol) (PVA), PTMAO displayed minimal impact on C5b-9 level. Such a low complement activation by PTMAO may be attributed to the hydration layer surrounding PTMAO surfaces. In addition to protein adsorption, cell adhesion represents another major type of biofouling, which may directly contribute to the generation of FBR. For instance, fibroblasts adhered to the surface of medical implants could mediate the formation of fibrous avascular capsules, which sequester the implant from its target tissues and wall off its effects from the rest of the body. Thus, in order to evaluate the resistance of PTAMO against cell adhesion, we seeded NIH-3T3 fibroblasts onto PTMAO hydrogel disks and the number of adhered cells was analyzed after three-day cell culture (Fig. 6-4c, Fig. 6-5). In contrast to the hydrogel disks made by tissue-culture polystyrene (TCPS), wherein a large number of aggregated fibroblasts were observed (e.g., more than 60 cells per 100x100μm), the PTMAO hydrogel disks manifested

clean surfaces as the number of adhered fibroblasts was dramatically reduced (e.g., less than 2 cells per100x100μm).

Moreover, the non-fouling property of PTMAO was further tested in undiluted human blood serum, the most challenging system *in vitro* that mimics the complex biological environment. Briefly, gold chips coated with uniform PTAMO at three different thickness (10nm, 17nm, 22nm) were achieved via a controlled surface-initiated atom transfer radical polymerization (SI-ATRP). Then undiluted human blood serum was flowed through PTAMO-coated gold surfaces, during which any adsorption of proteins or other components in the serum would be detected by an ultra-sensitive surface plasmon resonance (SPR) binding analysis. Surfaces with less than 5ng/cm^2 adsorbed proteins in undiluted blood plasma or serum are defined as ultra-low fouling. Results from SPR experiments (Fig. 6-4d) showed that gold chips coated with PTMAO films at different thickness (10nm, 17nm, 22nm) all displayed less than 3ng/cm^2 adsorbed proteins in human blood serum. This further demonstrates the ultra-low fouling property of PTAMO in complex biological media, suggesting the promising potential of PTMAO for medical applications.

6.4.3 Minimal immunogenic potential of TMAO polymers

Zwitterionic polymers that are entirely super-hydrophilic are anticipated to have excellent non-fouling property, and bear little non-specific interaction with the biological environment, thus inducing minimal immune response[10]. In contrast, the existence of hydrophobic domains in polymers such as PEG could meditate the immune recognition and evoke the generation of polymer-specific Ab responses. Hence, the immunogenicity of PTMAO is of particular relevance to understand the non-fouling properties of PTMAO in an *in vivo* challenging system.

The attachment of a polymer to carrier proteins has been shown to facilitate the exhibition of its immunogenicity. A typical example is PEG: Though free PEG exhibits little or no immunogenicity, it would become highly immunogenic once being attached to large carriers such as liposomes and proteins, eliciting PEG-specific antibody Ab responses much like a hapten. Therefore, attaching PTMA to immunogenic proteins would allow us to amplify its potential immunogenicity and thus better understand its non-fouling property *in vivo*. Hence, we conjugated PTMAO onto the surface of keyhole limpet hemocyanin (KLH) by a free radical nano-emulsion method. It is noteworthy that KLH has an extremely high immunogenicity in mammalian hosts and is the most commonly used to promote the induction of immune responses to haptens, due to its remarkable immune-stimulating properties, large size, and numerous sites for conjugation. The hydrodynamic size of PTMAO-KLH conjugates prepared was approximately the same as that of PEG_{10k}-KLH conjugates (Fig. 6-6) as determined by size exclusion chromatography (SEC). Then, four immunizations of PTMAO-KLH conjugates were conducted on C57BL/6J mice (n=5) via subcutaneously (SC) injection for one dose per week while another cohort of mice were immunized with PEG-KLH conjugates as the control group at the same dose and schedule. At 1st, 2nd, 3rd, 4th and 5th weeks post to the first immunization, mice sera were collected for Ab tests through ELISA tests (Fig. 6-7a). Results indicated that the PEG polymers grafted on KLH ultimately elicited a significant level of PEG-specific Abs (average IgM titer > 4000; average IgG titer >1000), which was consistent with the clinical findings and validates the haptenic character of PEG (Fig. 6-7b-c). In stark contrast, TMAO was invisible to the immune recognition as no detectable TMAO-specific Abs (average IgM & IgG titers<200) were developed after five weekly immunizations of TMAO-KLH conjugates. The KLH immunization study suggests that TMAO

could maintain its superior non-fouling property even under extremely challenging *in vivo* conditions.

6.4.4 Improved circulation and efficacy of PTMAO-conjugated proteins

Attachment of hydrophilic materials onto the surfaces of nanoparticles and proteins can afford strong hydration layers that can not only deviate them from immune surveillance but also delay their clearance mononuclear phagocyte system (MPS) and kidney, thus contributing to enhanced circulation time. Therefore, the capability of extending the circulation time of a substrate represents another standard to gauge the non-fouling property of a hydrophilic polymer *in vivo*. Hence, we investigated the impact of PTMAO on the *in vivo* behavior of uricase, a highly immunogenic enzyme to further demonstrate its superior hydration effect and non-fouling property. PTMAO polymers were attached onto uricase by the same means of PTMAO-KLH. The hydrodynamic size of PTMAO-uricase conjugates prepared was approximately the same as that of PEG_{10k}-uricase conjugates as determined by SEC (Fig. 6-8). In parallel, PEGylated uricase conjugate (PEG-uricase) with the similar hydrodynamic size as confirmed by SEC was also prepared as the control (Fig. 6-8). The retained conjugates in blood could be easily determined by measuring the activity of its associated uricase with AmplexTM Red uric acid/uricase assay kit.

Before *in vivo* studies, the stability of native uricase, PEG-uricase and PTMAO-conjugated uricase (PTMAO-uricase) was firstly tested. Uricase samples were stressed in urea, a chemical known to destabilize the structure of proteins and to inhibit enzyme activity (Fig. 6-9a). With the increase of urea concentration, both native uricase and PEGylated uricase exhibited a dramatic decrease in bioactivity whereas that of uricase conjugated with PTMAO was well maintained. Furthermore, a thermal stability test was also performed, measuring the effect of temperature on enzyme activity

(Fig. 6-9b). It was also observed that PTMAO conjugation significantly enhanced the stability of uricase at high temperature. The stabilizing effect of PTMAO may be ascribed to the protein-stabilizing effect of TMAO, which is a protective osmolyte long recognized to offset the deleterious effects of urea and to increase the melting temperature as well as the unfolding free energy of proteins.

Then, three intravenous (IV) injections of native uricase, PEG-uricase and PTMAO-uricase were performed on C57BL/6J mice (n=5) respectively (one dose per week). Post to the first and third administrations of uricase samples, mice sera were collected at various time points from each cohort for pharmacokinetic (PK) and pharmacodynamic (PD) studies (Fig. 6-10a). As shown in Fig. 6-10b-c, native uricase displayed a half-life ($t_{1/2}$) as short as 3.9h after the first injection, which further decreased to 1.9h after five repeated administrations. This is a phenomenal accelerated blood clearance (ABC) phenomenon caused by as anti-uricase Abs. On the other hand, although PEG conjugation showed to extend the circulation ($t_{1/2}$=16.2h) of uricase after a single injection, an ABC phenomenon was still observed upon PEGylated-uricase as its $t_{1/2}$ shrunk to 10.1h after five administrations. In contrast, PTMAO-uricase exhibited a persistently superb circulation half-time as long as 19.1h (1st dose) and 18.2h (3th dose) after repeated administrations. The extended presence of PTMAO-uricase in systemic circulation also promotes the efficacy of uricase in catalyzing urate metabolism. As shown in Fig. 6-10d-e, PTMAO-uricase reduced approximately 80% of urate in mice blood at 72h post to the injection, and this remarkable urate-eliminating ability was well maintained after three injections, demonstrating the sustained and enhanced PD profiles of PTMAO-uricase. In contrast, native uricase and PEG-uricase, though could also to some extend reduce the urate level in blood, lost over 50% and 30% of their original urate-

eliminating ability respectively after three injections. On 21st day, mice sera were collected for the evaluation of anti-uricase and anti-conjugate titers with ELISA test (Fig. 6-10f-g). Compared to native uricase, PEGylation of uricase decreased anti-uricase IgM and IgG titers by 16 folds and 8 folds, respectively. However, a high level of anti-conjugate Abs (average IgM titers > 1000; average IgG titer > 500) was still observed, which was proved to mainly consist of anti-PEG Abs and has been recognized as the main culprit for the efficacy loss of PEGylated uricase (Krystexxa®) in the clinic. In contrast, the level of anti-uricase and anti-conjugate Abs was also significantly lower in the group treated with PTMAO-uricase. These results confirm the non-fouling property PTMAO, including prolonging circulation time of substrates and preventing them from the immune recognition.

6.4.5 Non-fouling mechanism of TMAO at molecular level

To study the mechanism accounting for the extraordinary hydration of PTMAO, we performed MD simulations of a TMAO small molecule and a 10-residue PTMAO oligomer in an aqueous solution. Simulations of a 3-residue PEG oligomer (OEG), were conducted for comparison. Simulation results showed that the TMAO oxygen accepts an average of 2.5 hydrogen bonds from water – accepting either 2 or 3 hydrogens bonds with approximately equal probability, while OEG oxygen atoms typically accept only 1 hydrogen bond from water as shown in Fig. 6-11a. In addition, hydrogen bond lifetime (τHB) for TMAO-water was observed to be longer than that for OEG-water (Fig. 6-11b). The persistent binding of multiple water molecules to TMAO molecule suggested very strong interactions with water. The radial distribution functions (RDF) for water oxygen atoms with respect to the heavy atoms of the TMAO small molecule (O_{TMAO}, N_{TMAO}, C_{TMAO}) suggested a near-contiguous sphere of hydration, centered on the quaternary nitrogen (Fig.

6-11c). The first peak of the N_{TMAO} RDF is comprised of a polar hydration peak, contributed by hydration around the quaternary amine cation, and a shoulder, contributed by the tightly bound water at the oxygen anion. Fig. 6-11d shows a single frame from the TMAO monomer simulation, including the water molecules with a N_{TMAO}-water oxygen distance less than the first minimum in the N_{TMAO} RDF (0.6 nm). This snapshot reveals that the first hydration shell, with respect to N_{TMAO}, covers the whole TMAO molecule and includes the strongly hydrogen-bonded water at the TMAO oxygen (high opacity). The contiguous hydration shell observed in the simulation of TMAO small molecule was also observed in the PTMAO simulation (Fig. 6-11e), which indicates that water is similarly ordered near the PTMAO headgroups. Taken together, MD simulations suggest that PTMAO retains the superhydrophilicity observed for the TMAO small molecule. The strong hydrogen bonding with water and a contiguous hydration shell around the PTMAO headgroups could be responsible for its super-hydrophilic properties.

6.5 Conclusions

In summary, a TMAO-derived polymer, PTMAO was successfully obtained as a new-generation zwitterionic material. The super-hydrophilicity and non-fouling properties of PTMAO were demonstrated from different angles under challenging conditions both *in vitro* and *in vivo*. Results showed that PTMAO-coated surfaces could achieved an ultra-low protein adsorption in undiluted blood serum. Furthermore, PTMAO exhibited minimal immunogenicity and extended circulation after being conjugated to highly immunogenic protein carriers. The molecular-level non-fouling mechanism of PTMAO stemming from strong hydration was elucidated from MD simulations. The development of PTMAO as a broadly applicable non-fouling material for many applications represents an important milestone in the development of biomaterials.

6.6 Scheme, Figures and Tables

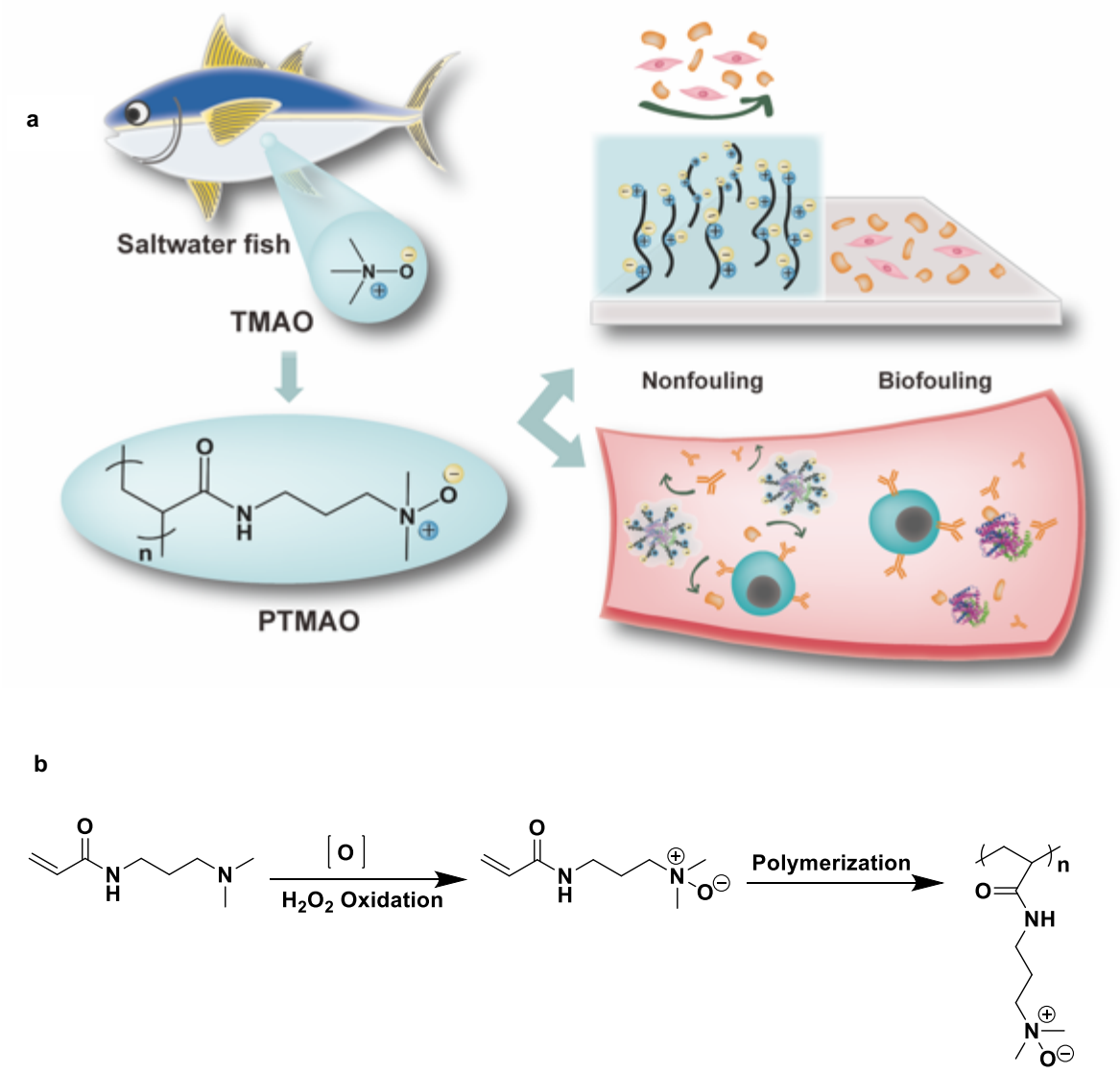

Figure 6-1. Scheme illustration of PTMAO. (a) The structure of PTAMO is derived from TMAO, a zwitterionic osmolyte in saltwater fishes. The non-fouling property of PTMAO could effectively prevent the surface from biofouling both *in vitro* and *in vivo*. (b) Scheme of TMAO monomer and polymer synthesis.

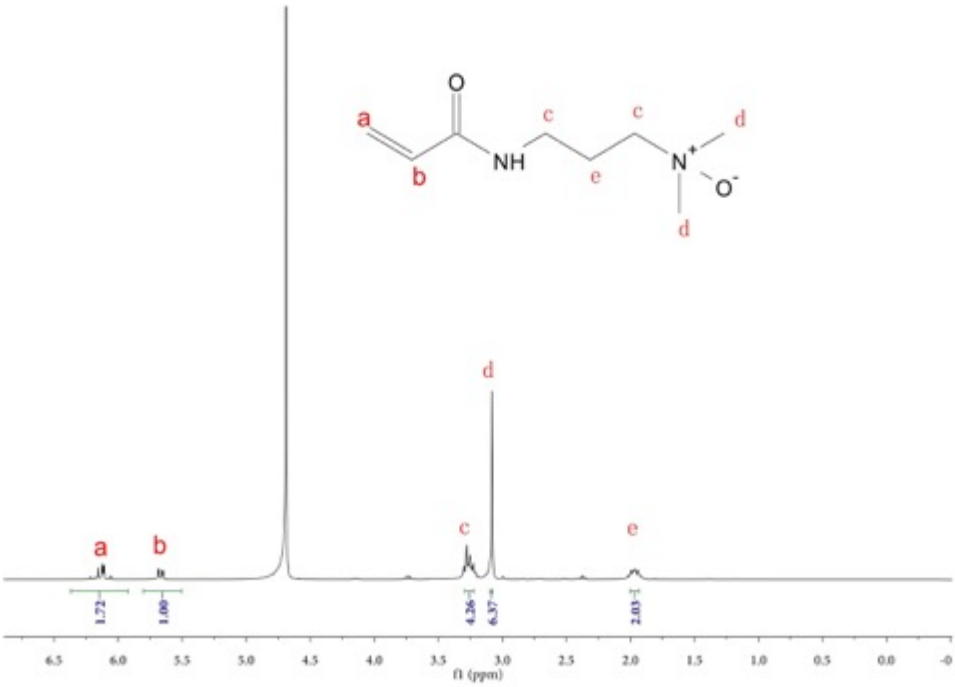

Figure 6-2. ^{1}H NMR spectrum of TMAO monomer.

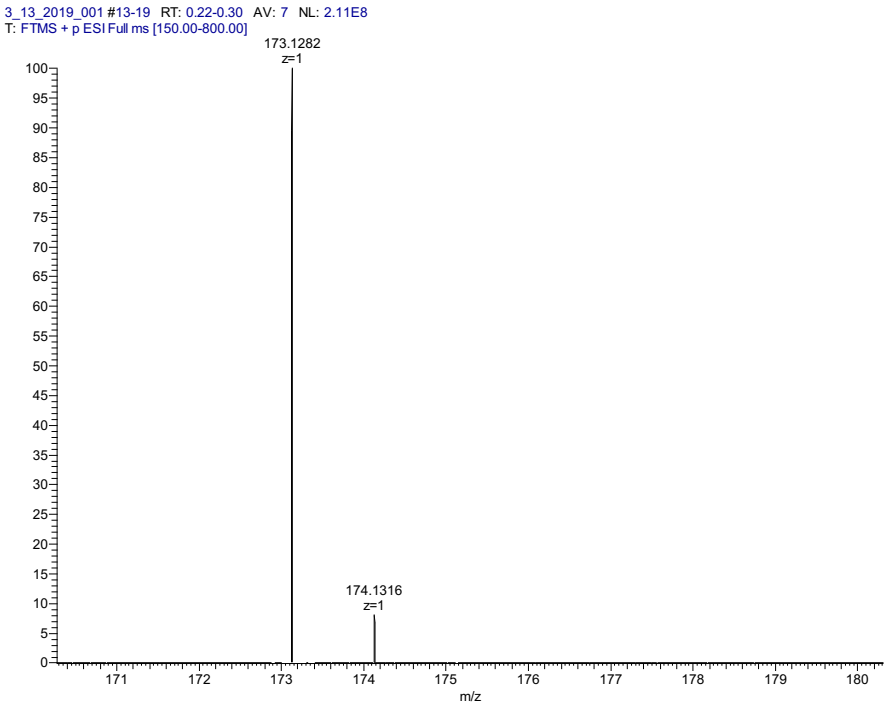

Figure 6-3. HRMS spectrum of TMAO monomer.

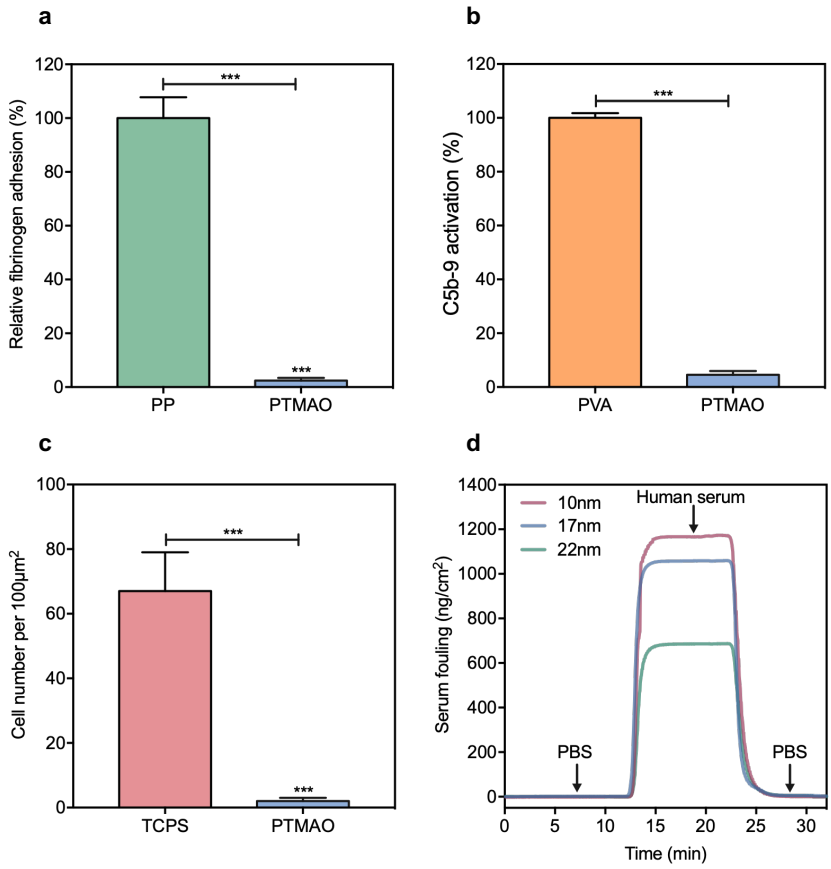

Figure 6-4. *In vitro* tests of the non-fouling property of PTMAO (a) Fibrinogen adsorbed to PP and PTMAO hydrogel surfaces measured by ELSIA; (b) Complement C5B-9 activation by PVA and PTMAO hydrogels; (c) NH-3T3 cells adhered to TCPS and PTMAO hydrogel surfaces after 3 days of culture; (d) SPR sensorgram of PTMAO films at different thickness (10nm, 17nm, 22nm) in human blood serum. All statistical analyses were performed using student test ***P<0.001).

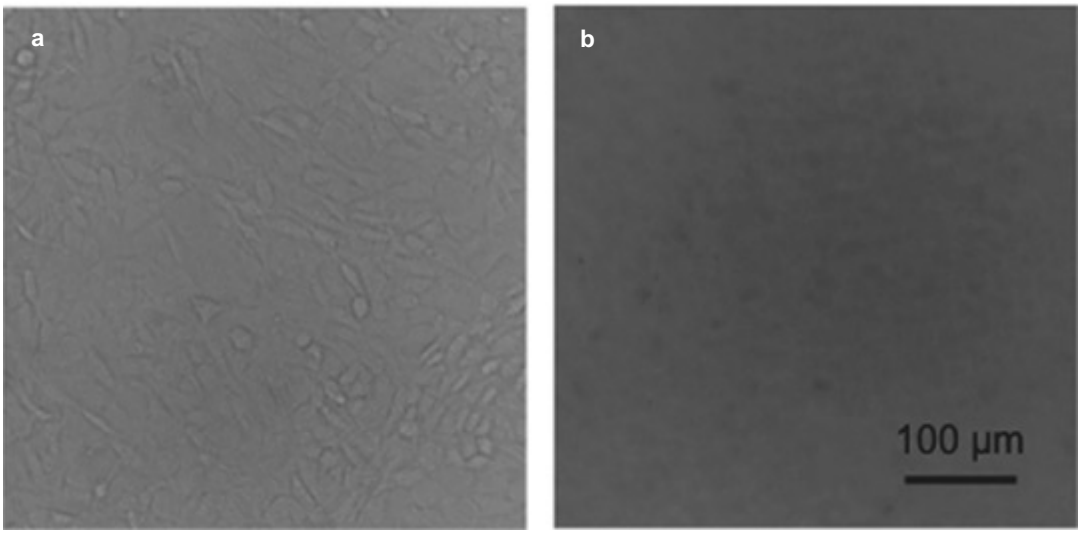

Figure 6-5. Cell adhesion test. Representative photographs showing cell adhesion on TCPS (a) and TMAO (b) hydrogel surfaces.

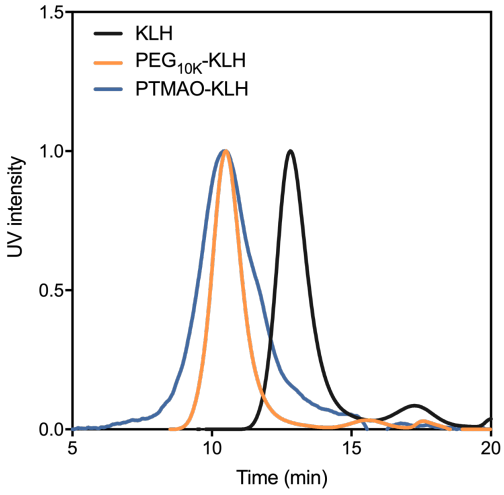

Figure 6-6. GPC graph of KLH, PEG_{10k}-KLH and TMAO-KLH conjugates.

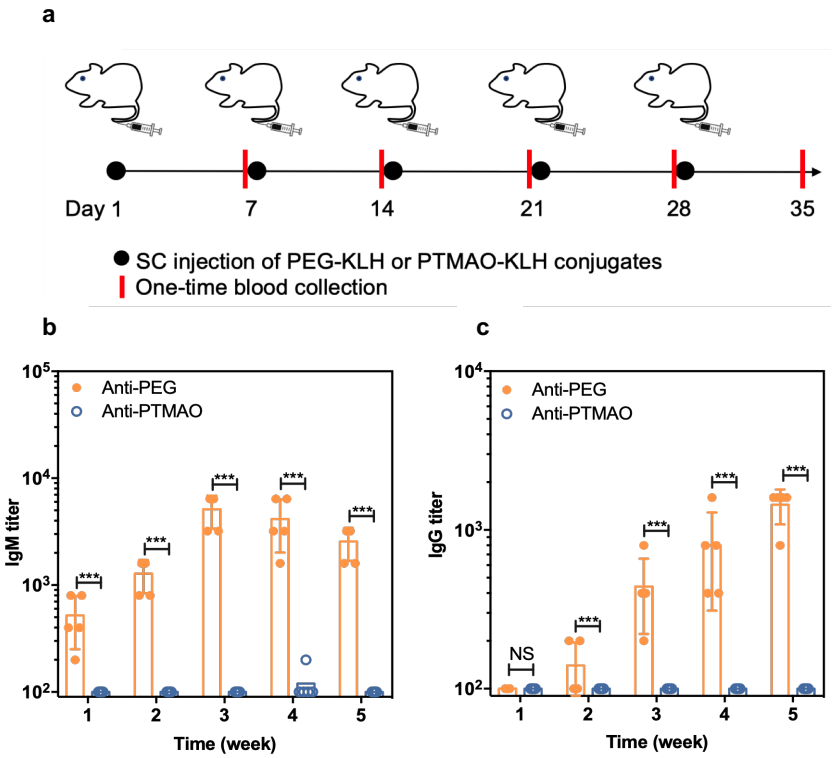

Figure 6-7. Evaluation of PTMAO immunogenicity. C57BL/6J mice were SC injected with either PEG-KLH or PTMAO-KLH (n=5) for five doses (one dose per week). Mice blood were collected on 7th, 14th, 21st,28th and 35th day (a). The titer of polymer-specific IgM (b) and IgG (c) in mice sera were detected with ELISA tests. All statistical analyses were performed using student test (NS-No significant difference, ***P<0.001).

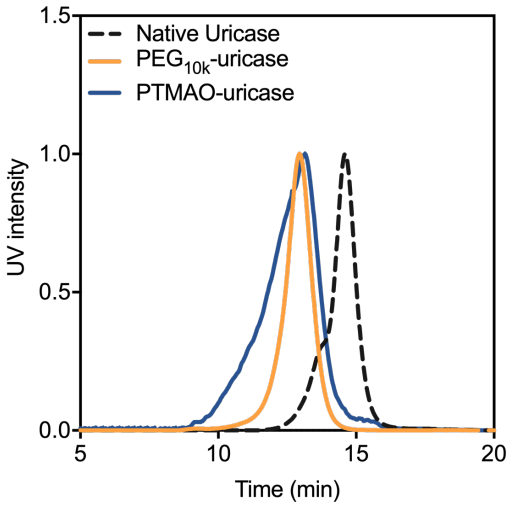

Figure 6-8. GPC graph of native uricase, PEG_{10k}-uricase and TMAO-uricase conjugates.

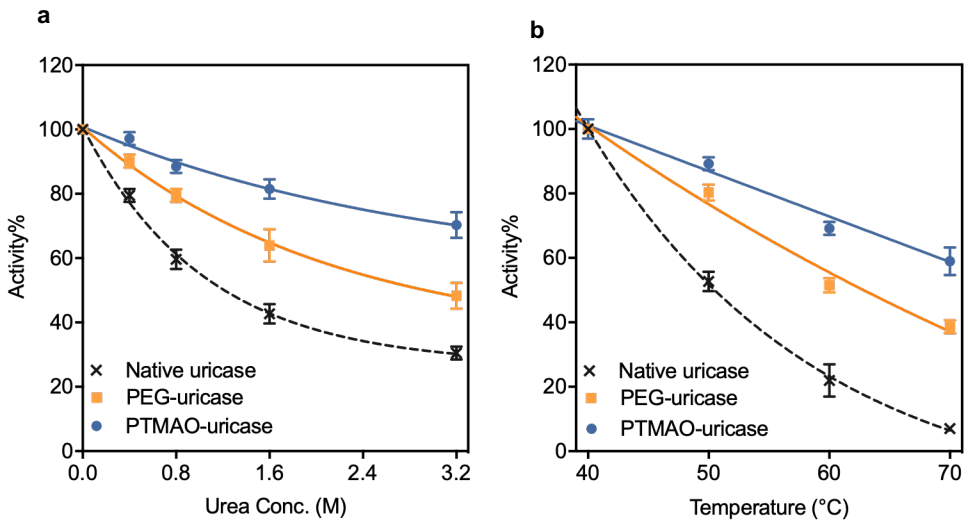

Figure 6-9. Protein stability test (a) Retained activity of uricase, PEG-uricase and PTMAO-uricase conjugates after incubation with urea (0-3.2M) for 6 hours; (b) Retained activity of uricase, PEG-uricase, PTMAO-conjugates after incubation at 40-70℃ for 30min.

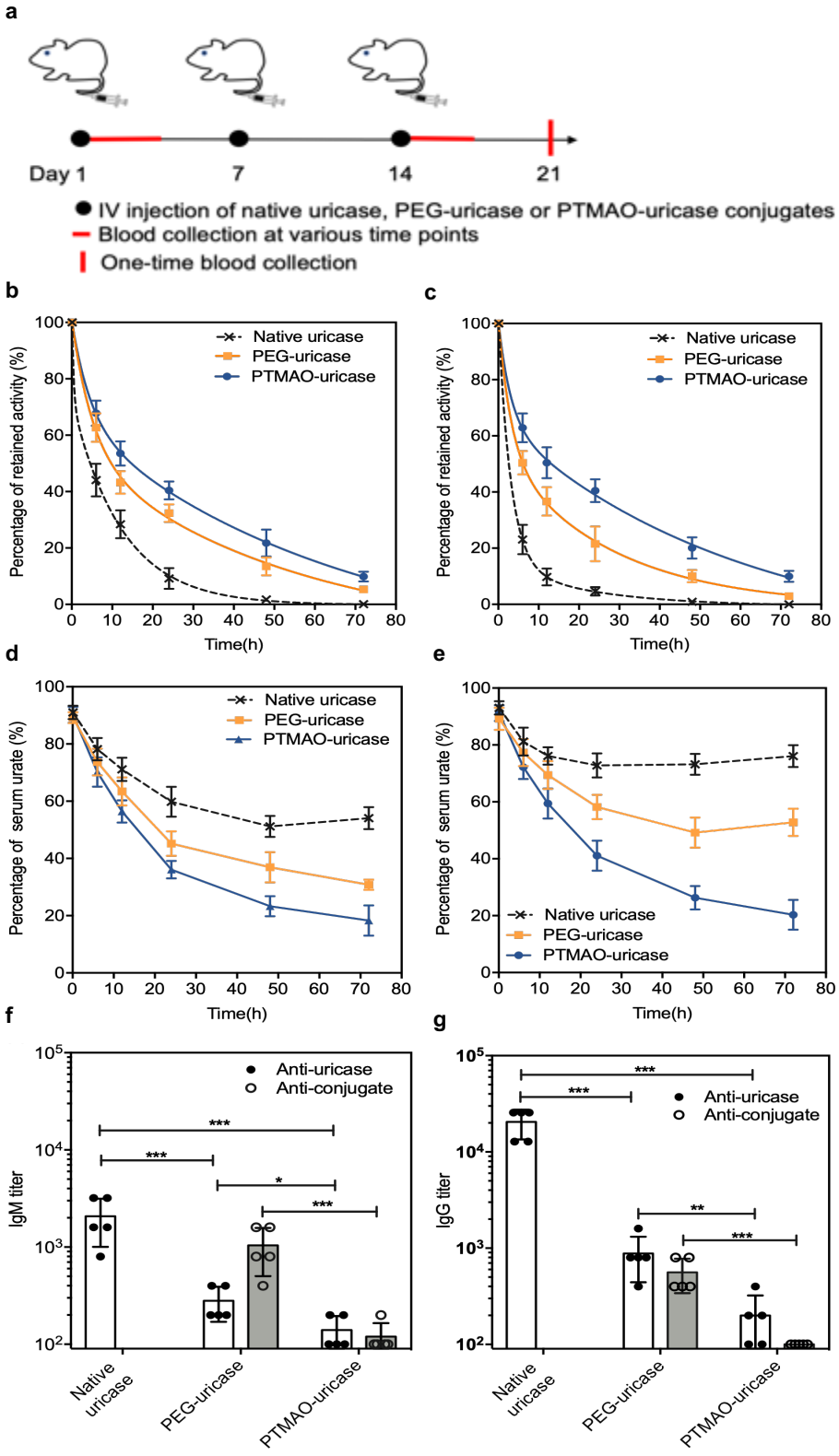
a
Day 1
7
14
21
IV injection of native uricase, PEG-uricase or PTMAO-uricase conjugates
Blood collection at various time points
One-time blood collection
b
c
Native uricase
PEG-uricase
PTMAO-uricase
Percentage of retained activity (%)
Time(h)
d
e
Percentage of serum urate (%)
f
g
Anti-uricase
Anti-conjugate
IgM titer
IgG titer
Native uricase
PEG-uricase
PTMAO-uricase

Figure 6-10. *In vivo* non-fouling performance of PTMAO. C57BL/6J mice were IV injected with native uricase, PEG-uricase or PTMAO-uricase (n=5) for three doses (one dose per week). Mice blood at various time points (0.1h, 6h, 12h, 24h, 48h, 72h) were collected after the first and third injections for the characterization of circulation and efficacy; mice blood on 21st day post to the first injection was also collected for antibody detection (a). PK profiles of each uricase sample after the first (b) and third IV injection (c) were determined by measuring the retained uricase activity in mice sera. PD profiles of each uricase sample after the first (d) and third IV injections (e) were determined by measuring the urate level in mice sera. IgM (f) and IgG (g) against uricase or conjugates were detected by direct ELISAs. All statistical analyses were performed using student test **P<0.01, ***P<0.001).

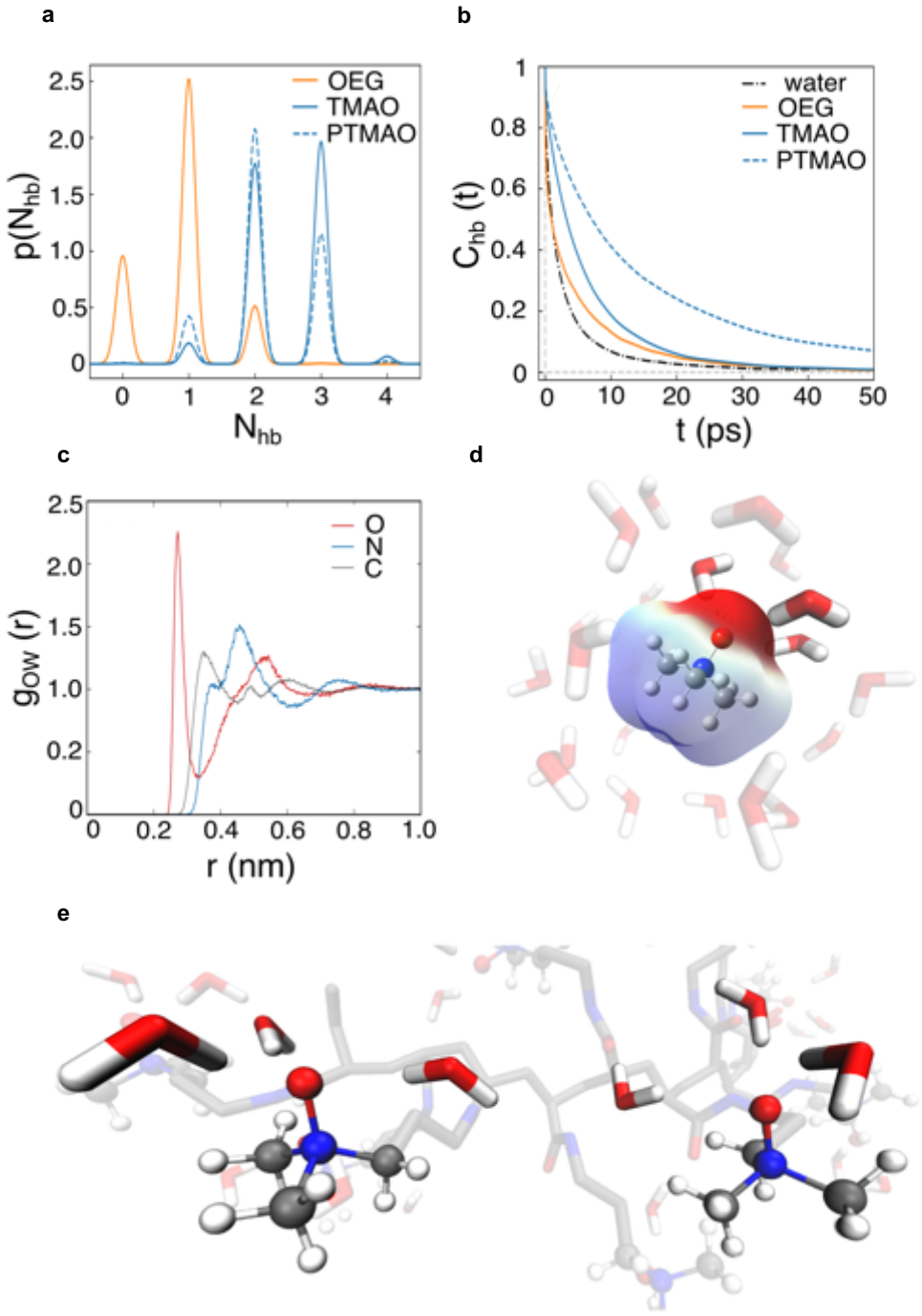

Figure 6-11. MD simulation on the non-fouling mechanism of PTMAO at molecular level. (A) The probability distributions for the number of hydrogen bonds, NHB, between water and the TMAO oxygen (blue), water and the PTMAO oxygen (blue dashed), and water and each OEG

oxygen (orange). (B) Autocorrelation function for hydrogen bond lifetime, CHB(t), for water-TMAO oxygen (blue), for water-PTMAO oxygen (blue dashed), water-OEG oxygen (orange), and water-water hydrogen bonds (black dashed). (C) RDF of water oxygen with respect to O (red), N (blue), and C (gray) atoms of TMAO. (D) Snapshot of aqueous TMAO with opaque and semi-transparent water corresponding to the first shoulder and main peak in the N-OW RDF, respectively. (E) Snapshot of PTMAO in aqueous solution, highlighting the tightly bound waters near two of the TMAO headgroup.

Table 6-1. Circulation time of uricase samples after repeated IV injections

Sample / Parameters	Native uricase		PEG-uricase		TMAO-uricase	
Injection times	1	3	1	3	1	3
$t_{1/2}$ (h)	3.9	1.9	16.2	10.1	19.1	18.2

6.7 References

1. Meyers, S. R.; Grinstaff, M. W., Biocompatible and bioactive surface modifications for prolonged *in vivo* efficacy. *Chem Rev* 2012, *112* (3), 1615-1632.

2. Williams, D. F., On the mechanisms of biocompatibility. *Biomaterials* 2008, *29* (20), 2941-2953.

3. Ratner, B. D., Replacing and renewing: synthetic materials, biomimetics, and tissue engineering in implant dentistry. *J Dent Educ* 2001, *65* (12), 1340-1347.

4. van der Giessen, W. J.; Lincoff, A. M.; Schwartz, R. S.; van Beusekom, H. M.; Serruys, P. W.; Holmes, D. R., Jr.; Ellis, S. G.; Topol, E. J., Marked inflammatory sequelae to implantation of biodegradable and nonbiodegradable polymers in porcine coronary arteries. *Circulation* 1996, *94* (7), 1690-1697.

5. Grabbe, S.; Landfester, K.; Schuppan, D.; Barz, M.; Zentel, R., Nanoparticles and the immune system: challenges and opportunities. *Nanomedicine (Lond)* 2016, *11* (20), 2621-2624.

6. Paterlini, T. T.; Nogueira, L. F. B.; Tovani, C. B.; Cruz, M. A. E.; Derradi, R.; Ramos, A. P., The role played by modified bioinspired surfaces in interfacial properties of biomaterials. *Biophys Rev* 2017, *9* (5), 683-698.

7. Leng, C.; Huang, H.; Zhang, K.; Hung, H. C.; Xu, Y.; Li, Y.; Jiang, S.; Chen, Z., Effect of Surface Hydration on Antifouling Properties of Mixed Charged Polymers. *Langmuir* 2018, *34* (22), 6538-6545.

8. Li, B.; Yuan, Z.; Hung, H. C.; Ma, J.; Jain, P.; Tsao, C.; Xie, J.; Zhang, P.; Lin, X.; Wu, K.; Jiang, S., Revealing the Immunogenic Risk of Polymers. *Angew Chem Int Ed Engl* 2018, *57* (42), 13873-13876.

9. Yang, Q.; Lai, S. K., Anti-PEG immunity: emergence, characteristics, and unaddressed questions. *Wiley Interdiscip Rev Nanomed Nanobiotechnol* 2015, *7* (5), 655-677.

10. Jiang, S.; Cao, Z., Ultralow-fouling, functionalizable, and hydrolyzable zwitterionic materials and their derivatives for biological applications. *Adv Mater* 2010, *22* (9), 920-932.

11. Shao, Q.; White, A. D.; Jiang, S., Difference of carboxybetaine and oligo(ethylene glycol) moieties in altering hydrophobic interactions: a molecular simulation study. *J Phys Chem B* 2014, *118* (1), 189-194.

12. Lee, I.; Kobayashi, K.; Sun, H. Y.; Takatani, S.; Zhong, L. G., Biomembrane mimetic polymer poly (2-methacryloyloxyethyl phosphorylcholine-co-n-butyl methacrylate) at the interface of polyurethane surfaces. *J Biomed Mater Res A* 2007, *82* (2), 316-322.

13. Chen, S.; Yu, Q.; Li, L.; Boozer, C. L.; Homola, J.; Yee, S. S.; Jiang, S., Detecting the adsorption of dye molecules in homogeneous poly(propylene imine) dendrimer monolayers by surface plasmon resonance sensor. *J Am Chem Soc* 2002, *124* (13), 3395-3401.

14. Leng, C.; Sun, S.; Zhang, K.; Jiang, S.; Chen, Z., Molecular level studies on interfacial hydration of zwitterionic and other antifouling polymers in situ. *Acta Biomater* 2016, *40*, 6-15.

15. Chien, H. W.; Cheng, P. H.; Chen, S. Y.; Yu, J.; Tsai, W. B., Low-fouling and functional poly(carboxybetaine) coating via a photo-crosslinking process. *Biomater Sci* 2017, *5* (3), 523-531.

16. Zhang, Z.; Chao, T.; Chen, S.; Jiang, S., Superlow fouling sulfobetaine and carboxybetaine polymers on glass slides. *Langmuir* 2006, *22* (24), 10072-10077.

17. Li, B.; Xie, J.; Yuan, Z.; Jain, P.; Lin, X.; Wu, K.; Jiang, S., Mitigation of Inflammatory Immune Responses with Hydrophilic Nanoparticles. *Angew Chem Int Ed Engl* 2018, *57* (17), 4527-4531.

18. Ladd, J.; Zhang, Z.; Chen, S.; Hower, J. C.; Jiang, S., Zwitterionic polymers exhibiting high resistance to nonspecific protein adsorption from human serum and plasma. *Biomacromolecules* 2008, *9* (5), 1357-1361.

19. Zhang, L.; Cao, Z.; Bai, T.; Carr, L.; Ella-Menye, J. R.; Irvin, C.; Ratner, B. D.; Jiang, S., Zwitterionic hydrogels implanted in mice resist the foreign-body reaction. *Nat Biotechnol* 2013, *31* (6), 553-556.

20. Li, B.; Yuan, Z.; Zhang, P.; Sinclair, A.; Jain, P.; Wu, K.; Tsao, C.; Xie, J.; Hung, H. C.; Lin, X.; Bai, T.; Jiang, S., Zwitterionic Nanocages Overcome the Efficacy Loss of Biologic Drugs. *Adv Mater* 2018, *30* (14), e1705728.

21. Liu, S.; Liu, J.; Esker, A. R.; Edgar, K. J., An Efficient, Regioselective Pathway to Cationic and Zwitterionic N-Heterocyclic Cellulose Ionomers. *Biomacromolecules* 2016, *17* (2), 503-513.

22. Keefe, A. J.; Jiang, S., Poly(zwitterionic)protein conjugates offer increased stability without sacrificing binding affinity or bioactivity. *Nat Chem* 2011, *4* (1), 59-63.

23. Li, Y.; Zhang, X., Zwitterionic poly(carboxybetaine) modified liposomes enhancing tumor therapy without accelerated blood clearance phenomenon. *J Control Release* 2015, *213*, e125.

24. Shao, Q.; Jiang, S., Effect of carbon spacer length on zwitterionic carboxybetaines. *J Phys Chem B* 2013, *117* (5), 1357-1366.

25. Shao, Q.; Jiang, S., Molecular understanding and design of zwitterionic materials. *Adv Mater* 2015, *27* (1), 15-26.

26. Hunger, J.; Ottosson, N.; Mazur, K.; Bonn, M.; Bakker, H. J., Water-mediated interactions between trimethylamine-N-oxide and urea. *Phys Chem Chem Phys* 2015, *17* (1), 298-306.

27. Liao, Y. T.; Manson, A. C.; DeLyser, M. R.; Noid, W. G.; Cremer, P. S., Trimethylamine N-oxide stabilizes proteins via a distinct mechanism compared with betaine and glycine. *Proc Natl Acad Sci U S A* 2017, *114* (10), 2479-2484.

28. Gluick, T. C.; Yadav, S., Trimethylamine N-oxide stabilizes RNA tertiary structure and attenuates the denaturating effects of urea. *J Am Chem Soc* 2003, *125* (15), 4418-4419.

29. Ma, J.; Pazos, I. M.; Gai, F., Microscopic insights into the protein-stabilizing effect of trimethylamine N-oxide (TMAO). *Proc Natl Acad Sci U S A* 2014, *111* (23), 8476-8481.

30. Rani, A.; Jayaraj, A.; Jayaram, B.; Pannuru, V., Trimethylamine-N-oxide switches from stabilizing nature: A mechanistic outlook through experimental techniques and molecular dynamics simulation. *Sci Rep* 2016, *6*, 23656.

31. Sivik, M. R.; Bodet, J. F.; Kluesener, B. W.; Scheper, W. M.; Yeung, W. K.; Bergeron, V., Compositions and methods for using amine oxide monomeric unit-containing polymeric suds enhancers. 2005.

32. Bayly, C. I.; Cieplak, P.; Cornell, W. D.; Kollman, P. A., A well-behaved electrostatic potential based method using charge restraints for deriving atomic charges: The RESP model. *J Phys Chem* 1992, *97* (40), 10269–10280.

33. Becke, A. D., Density-functional thermochemistry . III . The role of exact exchange. *J Chem Phys* 1993, *98*(7), 5648–5652.

34. Petersson, G. A.; Bennett, A.; Tensfeldt, T. G.; Al-Laham, M. A.; Shirley, W. A.; Mantzaris, J., A complete basis set model chemistry . I . The total energies of closed-shell atoms and hydrides of the first-row elements. *J Chem Phys* 1998, *89*, 2193–2218.

35. Abraham, M. J.; Murtola, T.; Schulz, R.; Páll, S.; Smith, J. C.; Hess, B.; Lindahl, E., GROMACS: High performance molecular simulations through multi-level parallelism from laptops to supercomputers. *SoftwareX* 2015, *s1–2*, 19–25.

36. Bussi, G.; Donadio, D.; Parrinello, M.; Canonical sampling through velocity rescaling. *J Chem Phys* 2007, *126* (1), 014101–014107.

37. Berendsen, H. J. C.; Postma, J. P. M.; van Gunsteren, W. F.; DiNola, A.; Haak, J. R., Molecular dynamics with coupling to an external bath. *J Chem Phys* 1984, *81*(8), 3684–3690.

38. Parrinello, M.; Rahman, A., Polymorphic transitions in single crystals: A new molecular dynamics method. *J Appl Phys* 1981, *52(12)*, 7182–7190.

39. A. Luzar, D. Chandler, Hydrogen-bond kinetics in liquid water. *Nature* 1996, *379*(6560), 55–57.

CHAPTER 7

Immunosuppressive Zwitterionic Polymers Inspired by Apoptotic Cell Death for Protein Conjugation

7.1 Abstract

Polymer conjugation is widely applied to protein drugs for circulation extension and immunogenicity mitigation. However, conventional polymers are oftentimes unable to eradicate protein immunogenicity due to their limited coating density on protein surfaces. Here we report a zwitterionic phosphoserine polymer (ZPS) endowed with both non-fouling and immunosuppressive properties. In contrast to the inert polymers that alleviate the immunogenicity of proteins by passively hiding them from immune surveillance, ZPS polymers are capable of mimicking the immunomodulatory effect of apoptotic cells and actively suppressing immune responses characterized by the induction of tolerogenic dendritic cells (DCs) and upregulation of regulatory T cells (Treg). ZPS conjugation to uricase, a highly immunogenic enzyme, was demonstrated to completely eliminate its immunogenicity and significantly improve the pharmacokinetic (PK) profiles. The development of ZPS provides a general platform for improving the safety and efficacy of protein drugs and casts new insights into the design of functional biomimetic materials.

7.2 Introduction

Advances in biotechnology are facilitating the discovery of potent and pharmacologically active biologics for diverse disease treatment[1]. However, the development and use of protein drugs are limited by their poor PK and inherent immunogenicity[2-4]. Undesirable immune responses elicited by proteins, characterized by the generation of anti-drug antibodies (ADA), can further shorten their circulation time *in vivo*, compromise their efficacy, and in some cases even threaten patient life[5,6]. For desirable clinical outcomes, strategies of half-life extension and immunogenicity mitigation are necessitated to improve the safety and efficacy of biopharmaceuticals[7-10].

Conjugation of hydrophilic polymers such as poly(ethylene glycol) (PEG)[11,12] and zwitterionic poly(carboxy betaine) (PCB)[13,14] to protein surfaces has been widely employed to improve the PK and immunological profiles of protein therapies. Bulky hydrophilic materials creating hydration shells on protein surfaces can not only increase the hydrodynamic sizes of underlying proteins, slowing down the clearance, but also physically protect them from immune surveillance, mitigating the potential immune response[15]. Yet, conventional polymer-conjugation technologies mitigate protein immunogenicity in a passive manner, of which their performance highly relies on polymer packing density[16]. For certain proteins containing only a few accessible conjugation sites such as amine group, the number of polymers that can be grafted onto proteins, is significantly limited. The defective cloak afforded by sparse polymer chains is unable to eradicate the immunogenicity of underlying proteins due to their incomplete mask. The residual immunogenicity of proteins may result in the formation of ADA, which will deteriorate the PK and therapeutic exposure of subsequent doses via accelerated blood clearance (ABC) effect[17,18].

To address this issue, immunosuppressive molecules and nanoparticles have been developed as adjunct therapies to further eliminate the immunogenicity of polymer-protein conjugates in an active way[10,19-21]. However, extra administration of these immunosuppressive agents complicates the treatment regimen and increases the burden of patients. In order to waive the need for additional immunosuppressive therapies, thus improving the patient compliance, direct integration of immunosuppressive factors into the protein therapies is preferred.

Phosphatidylserine (PS) is an anionic phospholipid functioning as an immunosuppressive signal in physiological conditions[22]. During cell apoptosis, PS externalized to the outer membranes directs antigen presenting cells (APCs) such as macrophages and DCs to differentiate into tolerogenic phenotype and thereby prevents immune activation[23]. PS is included in the FDA's list of Generally Regarded as Safe ingredients (GRAS) and has been widely used as a dietary supplement and a nutrient[24]. For the tolerogenic effects of PS to be clinically relevant, attempts that apply PS or phosphoserine to protein formulations have been made for immunogenicity mitigation[25-27]. However, PS as a eat-me signal triggers the APC phagocytosis after it activates PS receptors or binding bridging molecules such as MFG-E8 and annexing A1 and A2[28]. For example, PS liposomes were observed to suffer a significantly reduced circulating half-life due to the rapid uptake of mononuclear phagocytic system (MPS)[29]. This property of PS is not desirable for protein delivery, which oftentimes requires long circulation half-life in blood.

In the present work, we developed a novel functional zwitterionic phosphoserine polymer (ZPS, Fig. 7-1). In contrast to the non-zwitterionic phosphoserine polymer (NZPS), ZPS exhibits enhanced hydration effect, improved non-fouling property and less vulnerability to the MPS clearance. Proteins conjugated with ZPS display significantly prolonged circulation time in blood

as compared to those without any protection or conjugated with NZPS. On the other hand, ZPS could mimic the anti-inflammatory activity of PS, and its attachment to an immunogenic enzyme shows to prevent the formation of ADA. These results indicate that ZPS could overcome the limitation of natural PS and achieve non-fouling and immunosuppressive properties simultaneously, rendering it more suitable for protein conjugation. Distinct from other inert zwitterionic polymers such as MPC, ZPS as a functional zwitterionic polymer can proactively inhibit immune reactions. ZPS conjugation opens a new avenue for fully eliminating protein immunogenicity and is anticipated to significantly promote the development of safe and effective protein therapies.

7.3 Experimental section

7.3.1 Materials

All chemicals and proteins including uricase from Candida sp. were purchased from Sigma-Aldrich (St. Louis, MO) unless otherwise noted and were used as received. Amicon Ultra centrifugal filter was purchased from EMD Millipore (Billerica, MA). Amplex Red uric acid/uricase assay kit was purchased from Thermo Fisher Scientific (Waltham, MA). Anti-CD4-PE, anti-CD25-FITC and anti-Foxp3-Percep antibodies were purchased from Biolegend (San Diego, CA). Anti-mouse IgG secondary antibodies were purchased from Bethyl labs. Mouse cytokine (TNF-α, TGF-β) quantikine ELISA kits were purchased from R&D systems. Mice monocytes RAW 264.7 and dendritic cells DC 2.4 were purchased from ATCC.

7.3.2 Synthesis of Compound 3

N-Boc-Ser-OtBu (1.0gm, 3.82mmol) was dissolved in 30 ml dry benzene and the solution was cooled to 0^{o}C. Next, triethylamine (0.62 mL, 4.6 mmol) was added followed by dropwise addition

of 2-chloro-2-oxo-1,3,2-dioxaphospholane 1 (0.42 mL, 4.6 mmol) in 10 mL dry benzene over a period of 30 minutes and then the reaction contents were stirred at room temperature for another 3 hours. After completion of reaction, diethyl ether was poured into the reaction mixture and the precipitated trimethylamine hydrochloride was filtered off. The filtrate was then concentrated under reduced pressure to give Compound 2 as an oil which was used in next step without further purification. Compound 2 was redissolved in 30 mL anhydrous acetonitrile and 2-(dimethylamino)ethyl methacrylate (1.45 mL, 8.8 mmol) was added. The reaction mixture was then stirred at 55 ^{o}C for 24 hours. The reaction contents were then concentrated under vacuum and purified by flash column chromatography to give compound 3 in 42% yield. ^{1}H NMR (300 MHz, $CDCl_3$) δ 6.18 (s, 1H), 5.67 (s, 1H), 4.63 – 4.54 (m, 2H), 4.35 – 4.14 (m, 3H), 4.10 – 3.99 (m, 2H), 3.83 – 3.76 (m, 2H), 3.40 – 3.27 (m, 2H), 2.82 (s, 6H), 1.97 (s, 3H), 1.46 (d, J = 11.7 Hz, 18H).

7.3.3 Synthesis of ZPS monomer (Compound 4)

Compound 3 (0.84 gm, 1.6 mmol) was dissolved in 5 mL dichloromethane and 30 mL trifluoroacetic acid was added. The reaction contents were stirred for 5 hours. After completion of the reaction, the reaction mixture was concentrated under vacuum to give a thick viscous liquid. The crude product was then crystallized with MeOH:diethyl ether (1:15) to give desired Compound 4 as white powder. ^{1}H NMR (300 MHz, D_2O) δ 6.08 (s, 1H), 5.69 (s, 1H), 4.47 – 4.41 (m, 2H), 4.26 – 4.23 (m, 2H), 4.05 – 4.00 (m, 1H), 3.87 – 3.84 (m, 2H), 3.69 – 3.67 (m, 2H), 3.50 – 3.45 (m, 2H), 2.88 (s, 6H), 1.84 (s, 3H).

7.3.4 Synthesis of Compound 5

N-Boc-Ser-OtBu (1.0gm, 3.82 mmol) was dissolved in 30 ml dry benzene and the solution was cooled to 0°C. Next, triethylamine (0.62 mL, 4.6 mmol) was added followed by dropwise addition of 2-chloro-2-oxo-1,3,2-dioxaphospholane 1 (0.42 mL, 4.6 mmol) in 10 mL dry benzene over a period of 30 minutes and then the reaction contents were stirred at room temperature for another 3 hours. After completion of reaction, diethyl ether was poured into the reaction mixture and the precipitated trimethylamine hydrochloride was filtered off. The filtrate was then concentrated under reduced pressure to give Compound 2 as an oil which was used in next step without further purification. Compound 2 was redissolved in 30 mL anhydrous acetonitrile and sodium methacrylate (0.62gm, 5.7 mmol) along with 18-crown-6 ether (0.14 gm, 0.53 mmol) was added to it. The reaction mixture was then stirred at 55 °C for 72 hours. After the reaction, the reactions contents were filtered, concentrated under vacuum and purified by flash column chromatography to give compound **5** in 71% yield. ^{1}H NMR (300 MHz, $CDCl_3$) δ 6.15 (s, 1H), 5.57 (s, 1H), 4.41 – 4.27 (m, 2H), 4.24 – 4.04 (m, 4H), 3.86 – 3.78 (m, 1H), 1.95 (s, 3H), 1.46 (d, J = 5.4 Hz, 18H).

7.3.5 Synthesis of NZPS monomer (Compound 6)

Compound 5 (1.2 gm, 2.65 mmol) was dissolved in 5 mL dichloromethane and 30 mL trifluoroacetic acid was added to it. The reaction contents were stirred for 5 hours. After completion of the reaction, the reaction mixture was concentrated under vacuum to give a thick viscous liquid. The crude product was then crystallized with MeOH:diethyl ether (1:20) to give desired Compound 6 as white powder. ^{1}H NMR (300 MHz, D_2O) δ 6.11 (s, 1H), 5.66 (s, 1H), 4.34 – 4.15 (m, 5H), 4.10 – 3.97 (m, 2H), 1.85 (s, 3H).

7.3.6 Non-fouling test

ZPS hydrogels were fabricated by bulk photo-polymerization with a hydrogel aqueous solution containing ZPS monomer (0.67g Milli-Q water, 330mg), crosslinker N,N' Methylenebis(acrylamide) (1 wt%, 3.3mg) and photo-initiator 2-Hydroxy-2-methylpropiophenone (0.33mg). The hydrogel aqueous solution was placed between two glass slides separated by a 0.5 mm-thick polytetrafluoroethylene spacer, and was then photo-polymerized at room temperature for 30 mins. After polymerization, hydrogels were removed from the casts and soaked in PBS for three days to remove unreacted chemicals and reach the fully hydrated hydrogel network. Phosphate buffered saline was refreshed every 12 hours. Following the same protocol, PPC and NZPS hydrogels with the same crosslinking density were prepared.

Fibrinogen adsorption test: Biopsy punches were used to punch the hydrated MPC, NZPS and ZPS hydrogels into 5 mm-diameter disks. Hydrogel disks were placed into a 24 well-plate and incubated with 1 mL of 1 mg/mL Fibrinogen in PBS buffer for 1 hour, followed by 5 washes with pure PBS buffer. Hydrogel disks were then transferred to new wells and incubated with 1mL of horseradish peroxidase (HRP) conjugated anti-fibrinogen antibody (1 μg/mL) in PBS buffer for 1 hour. All hydrogel disks were then transferred to new wells after 5 washes with pure PBS buffer. Next, 1mL 1 mg/mL o-phenylenediamine (OPD) 0.1 M citrate phosphate pH 5.0 solution, containing 0.03% hydrogen peroxide was added. After 15min incubation, the enzymatic reaction was stopped by adding an equal volume of 1 M HCl. The same procedure was conducted on of tissue culture polystyrene (TCPS) disks with the same surface area as the control. Absorbance value at 492 nm was recorded by a plate reader and was normalized to that TCPS sample. Average data were acquired from three specimens.

7.3.7 Preparation of NZPS and ZPS nanogels

Preparation of MPC, NZPS and ZPS nanogels: AOT (sodium bis(2-ethylhexyl) sulfosuccinate, 237mg) and Brij 30(poly(ethylene glycol) dodecyl ether, 459mg) were added to a 20mL glass vial to which a stir bar was added. The vial was sealed with a Teflon-lined septum cap and purged with dry nitrogen for 10min. Nitrogen-deoxygenated hexane (10mL) was then added to the vial under vigorous stirring. For the aqueous phase, monomers (MPC, NZPS, ZPS) and crosslinker (MBA) was dissolved in PBS buffer (pH 7.4, 250 μL) at a mole ratio of 95%:5%. Dry nitrogen was bubbled through the monomer solution for 2min, after which the aqueous phase was slowly added to the organic continuous phase dropwise. The vial was sonicated to form a stable nanoemulsion. A 20% (w/v) solution of ammonium persulfate in deionized water (10 μL) was then added to the emulsion. After 5 min, polymerization was initiated by the addition of tetramethylethylenediamine (TEMED, 6 μL) and maintained at 4°C under rapid magnetic stirring. After the 2-hour reaction, the organic solvent was removed by rotary evaporator and the nanogel was precipitated and washed with THF for three times. The nanogel was re-suspended in PBS buffer and purified with 100-KDa molecular weight cutoff centrifugal filters to remove the unreacted monomer and crosslinker.

Preparation of MPC, NZPS and ZPS nanogels encapsulating FITC-BSA: AOT (sodium bis(2-ethylhexyl) sulfosuccinate, 237mg) and Brij 30(poly(ethylene glycol) dodecyl ether, 459mg) were added to a 20mL glass vial to which a stir bar was added. The vial was sealed with a Teflon-lined septum cap and purged with dry nitrogen for 10min. Nitrogen-deoxygenated hexane (10mL) was then added to the vial under vigorous stirring. For the aqueous phase, FITC-BSA, monomers (MPC, NZPS, ZPS) and crosslinker (MBA) was dissolved in PBS buffer (pH 7.4, 250 μL) at a mole ratio of 95%:5%. Dry nitrogen was bubbled through the monomer solution for 2min, after

which the aqueous phase was slowly added to the organic continuous phase dropwise. The vial was sonicated to form a stable nanoemulsion. A 20% (w/v) solution of ammonium persulfate in deionized water (10 μL) was then added to the emulsion. After 5 min, polymerization was initiated by the addition of tetramethylethylenediamine (TEMED, 6 μL) and maintained at 4°C under rapid magnetic stirring. After the 2-hour reaction, the organic solvent was removed by rotary evaporator and the nanogel was precipitated and washed with THF for three times. The nanogel was re-suspended in PBS buffer and purified with 100-KDa molecular weight cutoff centrifugal filters to remove the free FITC-BSA, unreacted monomer and crosslinker.

7.3.8 Anti-inflammation test

RAW 264.7 cells (10^5/well) were exposed to MPC, NZPS or ZPS nanogel solution at various concentration (10, 25, 50, 100, 200, 1000μg/ml) for 18 hours. Then, these cells were stimulated by LPS solution (100ng/mL) for another 48 hours, after which the cells were spun at 300 g for 10 min and the supernatant medium was collected for cytokine (TNF-α) analysis by ELISA.

7.3.9 Annexin V blocking test

To confirm that the immunosuppressive effect of NZPS and ZPS originates from the eat-me signal mediated by their PS head groups, the MPC, NZPS or ZPS nanogel solution (100μg/ml) was pre-incubated with Annexin V, a protein that has high affinity to the PS group and can block the eat-me signal, at various concentrations (0, 10, 25, 50, 100, 200 μg/ml) for 6 hours. Then RAW 264.7 macrophages (10^5/well) were then treated with these nanogel solution (100μg/ml) for 18h. followed by the stimulation of LPS (100ng/mL) for 48h. The level of TNF-α secretion in the supernatant was measured by ELISA kit.

7.3.10 Cell uptake study

RAW 264.7 macrophages (10^5/well) were incubated with MPC, NZPS, and ZPS nanogel encapsulating FITC-BSA for 30, 60, 120, and 180min, after which the cells were washed and lysed for the detection of recovered fluorescence. As shown in FIGURE 2C, MPC displayed the minimal cell uptake due to its excellent non-fouling property while NZPS nanogel was quickly taken up by macrophages due to its mediation of eat-me signal. Compared to NZPS, the uptake of ZPS is slowed down due to its non-fouling property and reduced affinity to receptors. These results suggest that the unique zwitterionic structure of ZPS could achieve effective immunosuppression and good non-fouling performance simultaneously.

7.3.11 Preparation of polymer-uricase conjugates

Acryloyl-modified uricase was firstly prepared. The reaction was performed by dissolving 2 mg uricase into 1 mL 50 mM Hepes buffer (pH 8.5), followed by adding 15 μL N-acryloxysuccinimide (NAS) dimethyl sulfoxide (DMSO) solution (40 mg/mL) dropwise. The reaction was stirred at 4 °C for 2 h, after which acryloyl-modified uricase was purified and concentrated using a 100-kDa molecular weight cutoff centrifugal filter. The uricase conjugates were prepared by nanoemulsion method. Briefly, AOT (120 mg) and Brij 30 (230mg) were added to a 20mL glass vial to which a stir bar was added. The vial was sealed with a Teflon-lined septum cap and purged with dry nitrogen for 10min. Nitrogen-deoxygenated hexane (5mL) was then added to the vial under vigorous stirring. For the aqueous phase, acryloyl-modified uricase (1mg) was dissolved in HEPES buffer (pH 8.5, 125μL), to which ZPS monomer (50mg) were added and dissolved. Dry nitrogen was bubbled through the monomer/protein solution for 2min, after which the aqueous phase was slowly added to the organic continuous phase dropwise. The vial was sonicated to form a stable

microemulsion. A 20% (w/v) solution of APS (10 μL) in Milli-Q water was then added to the emulsion. After 5 min, polymerization was initiated by the addition of TEMED (6 μL) and maintained at 4°C under rapid magnetic stirring. After the 2-hour reaction, the organic solvent was removed by rotary evaporator and the ZPS-uricase conjugate was precipitated and washed with THF for three times. The ZPS-uricase conjugate was re-suspended in PBS buffer and purified with high resolution size exclusion chromatography (Sephacryl S-500HR) to remove the free uricase. Finally the conjugates were washed and concentrated with PBS (pH 7.4) for three times using a 100-kDa molecular weight cutoff centrifugal filter.

7.3.12 In vitro immunogenicity study

DC 2.4 dendritic cells (10^5/well) were incubated with PBS (blank control), native uricase, ZPS-uricase, NZPS-uricase, MPC-uricase conjugates (2mU/mL) respectively for 72hours. At the end of the incubation period, the cells were spun at 300 g for 10 min and the supernatant medium was collected for cytokine (TGF-beta) analysis by ELISA. The cells were the cells were harvested and washed twice with ice cold sterile phosphate-buffered saline. Cells were labeled with anti- CD40-FITC or anti-CD80-PE and analyzed using flow cytometry.

7.3.13 Animal study

The University of Washington Institutional Animal Care and Use Committee (IACUC) approved all animal experiments under protocol #4203-01. Male C57BL/6J mice of ∼20 g were randomly divided.

For *in vivo* immunogenicity study, ZPS-uricase, NZPS-uricase, MPC-uricase conjugates at a dose of 25U/kg body weight were IV administered into the mice via the tail vein. The administrations of uricase samples are repeated three times with one week as the time interval between each administration. At the end of three weeks (21st day), all the mice are euthanized. The mice are sacrificed and their blood collected through cardiac puncture are handled for direct ELISA test.

As the first step of direct ELISA test, 100 μL antigen solutions (10 μg/mL of protein concentration) prepared in the coating buffer (0.1 M sodium carbonate buffer, pH 10.5) are used to coat each well of 96-well plates. After overnight coating at 4 °C overnight, the plates are washed five times using PBS buffer (pH 7.4) to remove the antigen solutions and then filled with blocking buffer (1% BSA solution in 0.1 M Tris buffer, pH 8.0) for 1-h incubation at room temperature, subsequent to which the blocking buffer is removed. All wells are then washed by PBS buffer for another five times. Subsequently, serial dilutions of mouse sera in PBS buffer containing 1% BSA are added to the plates (100 μL/well) for 1-h incubation at 37 °C, subsequent to which the mouse sera are removed and all wells are washed five times with PBS buffer. Next, goat anti-rat IgM or IgG (HRP-conjugated, Bethyl Laboratories) as the secondary antibody is added into each well for another 1-h incubation at 37 °C. Subsequently, all the wells are washed five times using PBS buffer before the addition of 100 μL/well HRP substrate 3,3',5,5'-tetramethylbenzidine (TMB; Bethyl Laboratories). The plates are shaken for 15 min, and 100 μL stop solution (0.2 M H_2SO_4) is added to each well. Absorbance at 450 (signal) and 570 nm (background) is recorded by a microplate reader. Mouse sera naïve to the administration of uricase samples are used as the negative control for all ELISA detections. Moreover, the mice spleens were harvested on 21st for the isolation of splenocytes by 100μm cell strainer (FisherbrandTM). The mice splenocytes from each group were

cultured in the presence of native uricase, MPC-uricase, NZPS-uricase or ZPS-uricase for 72h, and then stained with anti-CD4-PE, anti-CD25-FITC and anti- Foxp3-Percep antibodies for the analysis by flow cytometry.

For PK study, ZPS-uricase, NZPS-uricase, MPC-uricase conjugates at a dose of 25U/kg body weight were IV administered into the mice via the tail vein. The administrations of uricase samples are repeated three times with one week as the time interval between each administration. The mouse blood was collected at various time points (0, 6h, 24h, 48h, 72h) and the retained uricase in blood was estimated by measuring the enzyme activity with Amplex^{TM} uric acid/uricase kit. The uricase concentration were fitted into two-compartment model using PK-Solver software.

7.4 Result and Discussion

7.4.1 Design and synthesis of PS-analogue monomers

Zwitterionic materials, which bear a pair of oppositely charged ions (or zwitterions) in the same moiety while maintain overall neutral charge, are renowned for their strong hydration effect mediated by electrostatic interactions between zwitterions and surrounding water molecules. Thus, the introduction of zwitterionic property is presumed to improve the hydration effect of PS and reduce its binding to PS receptors. Natural PS is composed of phosphoserine, glycerol and fatty acid chains, showing an overall negative charge. Structure-binding studies have shown that the tolerogenic effect of PS is mainly driven by its headgroup, phosphoserine, rather than glycerol and fatty acid chains. For instance, mixing phosphoserine with Factor VIII has been shown to reduce the immunogenicity of Factor VIII[30]. The proposed design of ZPS monomer involves the attachment of anionic phosphoserine to a polymerizable functional group, which contains a

methacrylate for polymerization and a cationic tertiary amine moiety, leading to a zwitterionic monomer. The overall synthesis of ZPS monomer is shown in scheme1. First, a five membered cyclic phosphotriester ring attached with protected phosphoserine (dioxaphospholane ring) was generated *in-situ* by having the hydroxyl group of protected serine react with 2-chloro-2-oxo-1,3,2-dioxaphospholane (COP). Then, the nucleophilic ring opening of this five-membered dioxaphopholane ring in nonprotic media with amine nucleophiles, N,N'-dimethylaminoethyl methacrylamide (DMAEMA) could generate protected ZPS monomers, which subsequently were be purified using flash column chromatography. Finally, ZPS monomers were collected after the deprotection step using trifluoroacetic acid (TFA). NZPS that retains the anionic property of PS was also synthesized. The synthesis of NZPS is similar to that of ZPS monomer except that a carboxylate anion (nucleophile) from sodium methacrylate was used to open the five-membered cyclic dioxaphopholane ring. Cleavage of dioxaphospholane ring was readily accomplished using highly reactive anionic reagents rather than neutral nucleophiles. It should be noted that 18-crown-6-ether was necessitated during the synthesis of NZPS to increase the nucleophilicity of carboxylate anion by chelating with positive sodium ion.

7.4.2 Non-specific protein adsorption test

Resistance to non-specific adsorption of plasma proteins has been an important property for protein delivery since the non-specific binding of plasma proteins such as fibrinogen can accelerate the clearance of protein drugs by MPS system, resulting in poor PK profiles. Zwitterionic materials are renowned for their exceptional nonfouling properties as a result of their strong hydration capacity[31]. Using fibrinogen as a model protein, we herein examined the ability of ZPS and NZPS to resist nonspecific protein adsorption. ZPS and NPZS hydrogel disks (D=5mm) were prepared

and exposed to a highly-concentrated fibrinogen solution (10mg/ml). Hydrogels made of MPC, a zwitterionic phosphocholine-derived polymer known with exceptional non-fouling property, and polypropylene (PP) disks in the similar size were prepared and tested in parallel as negative and positive controls, respectively. After 2h-incubation, the amount of adsorbed fibrinogen onto each disk sample was quantitatively analyzed via enzyme-linked immunosorbent assay (ELISA). Compared to PP (positive control), ZPS, NZPS and MPC have displayed varied degrees of fibrinogen adsorption (Fig. 7-2). NZPS shows limited reduction in fibrinogen adsorption (40%) while ZPS exhibits an enhanced non-fouling performance by reducing 85% fibrinogen adsorption, comparable to that of MPC (95%). This result indicates that like other zwitterionic materials, ZPS is resistant to the nonspecific protein adsorption.

7.4.3 Anti-inflammation effect on macrophages

To prove that the PS-analogue polymers can mimic the immune tolerogenic function of PS, we examined the potential anti-inflammatory effect of ZPS, NZPS and MPC upon RAW264.7 macrophages stimulated by lipopolysaccharide (LPS). For fair comparison, nanogels composed of ZPS, NZPS and MPC providing uniform size and surfaces with homogeneous functionality were prepared. RAW 264.7 macrophages (10^5/well) were treated with MPC, NZPS or ZPS nanogel solutions at various concentrations (10, 25, 50, 100, 200, 1000μg/ml) for 18 hours, followed by the stimulation of LPS (100ng/ml). By measuring the production and release of pro-inflammatory cytokines (TNF-α) in the supernatant, we were able to evaluate the activation status of macrophages. As shown in Figure 3a, macrophages cultured in the presence of LPS and MPC nanogel displayed proinflammatory phenotype as indicated by the high level of TNF-α. By contrast, NZPS and ZPS demonstrated to alleviate the secretion of TNF-α in a dose-dependent manner.

Notably, NZPS began to show its inhibition on TNF-α level when its concentration increased up to 50μg/ml. Meanwhile, ZPS required a concentration above 100μg/ml to have phenomenal anti-inflammatory effect, indicating a relatively lower immunosuppressive effect. We hypothesized that the attenuated immunosuppressive activity of ZPS compared to NZPS might result from its zwitterionic property, which reduces the binding of PS functional groups in ZPS to PS receptors or bridging molecules.

To determine whether the anti-inflammatory effect of ZPS and NZPS is driven by the PS-mediated immunomodulation or not, we conducted a inhibition experiment using Annexin A5, a protein with high binding affinity to PS. Different from bridging molecules like annexins A1 and A2, Annexin A5 has been found to inhibit the phagocytosis of PS-expressing membrane and thus block the tolerogenic activity of PS[32]. Hence, we pre-incubated a MPC, NZPS or ZPS nanogel solution (100μg/ml) with Annexin A5 solution at a concentration from low to high (0, 10, 25, 50, 100, 200 μg/ml) for 6h. Then these nanogel solutions were used to treat RAW 264.7 macrophages (10^5/well) for 18h, followed by the stimulation of LPS (100ng/mL) for 48h. As shown in Fig. 7-3b, the inhibitory effect of NZPS and ZPS on TNF-α decreased with the increased concentration of Annexin A5, demonstrating the role of PS-analogue functional groups in their activity against inflammation. Notably, ZPS was observed to exhibit distinguishable anti-inflammatory effect when the concentration of Annexin A5 escalated to 100 μg/ml, wherein the anti-inflammatory effect of NZPS was completely blocked. This phenomenon could be explained by the non-fouling property of ZPS, which not only weakened its immunosuppressive activity, but also attenuated the blocking effect from Annexin A5.

To further clarify the interaction of PS-analogue polymers with macrophages, we studied the cell uptake by incubating fluorescent MPC, NZPS, and ZPS nanogels with RAW 264.7 macrophages (10^5/well) for 30, 60, 120, and 180min. At each time point, the cells were washed and lysed for the detection of recovered fluorescence (Fig. 7-3c). As expected, NZPS showed a remarkable tendency to be rapidly taken up by macrophages, implying with the role of PS as a "eat-me" signal in facilitating cell phagocytosis. In comparison, MPC displayed the lowest cell uptake followed by ZPS, verifying the ability of zwitterionic materials in delaying MPS clearance. Results about the time-dependent phagocytosis of ZPS and NZPS by macrophage are consistent to their anti-inflammation performance, both of which are closely related to the interaction between PS-analogue groups and PS receptors on cell surfaces.

7.4.4 Effect of ZPS and NZPS on uricase immunogenicity and PK

Conventional approaches of polymer conjugation, such as PEGylation, do not work universally to to reducing the protein immunogenicity. Typical examples include PEGylated uricase, i.e., pegloticase, which was approved by the FDA in 2010 for the treatment of refractory chronic gout (RCG). During the clinical use of pegloticase, more than 40% of patients developed high titer anti-pegloticase Abs, most of whom became non-responders to the treatment of pegloticase and even suffered life-threatening adverse reactions[17,18,33]. Conjugation of zwitterionic materials to uricase has been demonstrated to further mitigate the anti-conjugate immune response but is still unable to fully address the problem mainly because uricase only contains a limited number of accessible groups for conjugation[34]. Here, we hypothesized that immunosuppressive PS-analogue polymers can be employed to improve the safety and efficacy of uricase by completely eradicating its immunogenicity. Using a free radical nano-emulsion method, we covalently attached MPC, NZPS

and ZPS onto the surfaces of uricase, producing MPC-, NZPS- and ZPS-uricase conjugates with similar hydrodynamic sizes.

The immune response towards uricase is a T-cell dependent process, wherein uptake and processing by APCs particularly DCs constitutes the first step. The maturation status of DCs and their cytokine production determines if there will be an immunogenic or a tolerogenic response. Hence, we conducted *in vitro* studies with DCs to investigate their response to MPC-, NZPS- and ZPS-uricase conjugates or native uricase. As shown in Fig. 7-4a-b, exposure to native uricase resulted in a dramatical up-regulation of co-stimulatory markers (CD40, CD80) and a decrease in the percentage of immature DCs (CD40- CD80-). In contrast, MPC-, NZPS- and ZPS-uricase conjugates all exhibited lessened effect in promoting the maturation of DCs, among which NZPS-uricase conjugates showed the least stimulation followed by ZPS-uricase conjugates. To further clarify the mechanism behind the varied activation degree of DC, we analyzed the secretion of TGF-β, a typical immunosuppressive cytokine marker in the supernatant of culture media. As a regulatory cytokine, TGF-β could transform immature DC into tolerogenic DC, which maintains lower co-stimulatory activities but can promote tolerance via a regulatory T-cell (Treg) mechanism. Results show that MPC-uricase did not affect the level of TGF-β, suggesting that MPC reduced the DC activation property of uricase in a passive manner, probably by masking its immunogenic epitopes and retarding the intracellular processing. By contrast, the exposure of DC to uricase in the presence of NZPS or ZPS resulted in a remarkable upregulation of TGF-β (Figure 4c). The relatively lower level of TGF-β in ZPS-uricase treated group than that in NZPS-uricase treated group reflects the attenuated immunosuppressive activity of ZPS, which is consistent to what we found in the anti-inflammation study. These data demonstrate that both NZPS- and ZPS-uricase

could actively suppress the DC maturation and promote DCs transition into tolerogenic DCs with low costimulatory function via enhancing TGF-β secretion profiles.

Next, we studied the immunogenicity of NZPS- and ZPS-uricase conjugates *in vivo*. Intravenous (IV) injections of native uricase, MPC-, NZPS- and ZPS-uricase conjugates were performed on mice for three consecutive weeks. Mice were sacrificed on 21st day and their sera were harvested for the detection of Abs specific to uricase or uricase conjugates via ELISA test. As shown in Fig. 7-5a-b, MPC conjugation failed to completely eliminate the immune response even though it decreased the level of ADA formation (IgM titers 1:400; IgG titers 1:1600), much lower than those detected in the native uricase group (IgM titers 1:1600; IgG titers >1:25600). By contrast, NZPS and ZPS conjugation exhibited to fully eradiate the immune response as negligible levels of ADA were detected (IgM titers <200; IgG titers <200) in the mice treated with NZPS- or ZPS-uricase conjugates. We hypothesized that the effect of NZPS and ZPS in controlling immune responses resulted from the PS-mediated immunomodulation. This hypothesis is consistent with the *in vitro* DC activation studies, which showed lower costimulatory functions and elevated secretion of TGF-β when DCs were exposed to NZPS- or ZPS-uricase conjugates. The generation of tolerogenic DCs could prompt naïve T cells to acquire Foxp3 expression and differentiate into Treg cells, contributing to immune tolerization. To verify this hypothesis, mice spleens were also harvested from each cohort for the extraction of splenocytes, which were cultured in the presence of native uricase, ZPS-, NZPS-, or MPC-uricase conjugates for 72hours and then stained for flow cytometry analysis. As hypothesized, NZPS- and ZPS-uricase significantly expanded the frequency of Tregs (Fig. 7-5c-d). The changes in Tregs observed could potentially explain the differences in the ADA titers detected. Interestingly, though the immunomodulatory effect of ZPS is weaker than NZPS, eliciting less Tregs, ZPS also demonstrated to eradicate the uricase

immunogenicity like NZPS. This implies that the retained immunosuppressive activity of ZPS is sufficient to eliminate the residual immunogenicity of polymer-protein conjugates. Collectively, these results manifest that PS-analogue polymers can mimic the immunosuppressive function of PS and effectively suppress protein immunogenicity thorough inducing peripheral T-cell-mediated tolerance.

For *in vivo* protein delivery, circulation time is another important characteristic that determines the therapeutic efficacy and should be emphasized. Previous efforts with PS liposomes encountered severely altered PK profiles due to the rapid clearance by MPS. Following the same dosing schedule of immunogenicity study, IV injections of native uricase, MPC-, NZPS- and ZPS-uricase conjugates were performed on rats for five consecutive weeks, during which rat sera were collected during the first and third week at various time points for the measurement of uricase and uric acid concentrations. As shown in Fig. 7-6a-b, the centration-time kinetics of each uricase sample are fitted into a two-compartment model, based on which the PK parameters were derived (Table 7-1). After the first injection, MPC-uricase exhibited extended circulation behavior ($t_{1/2\beta}$ = 30.1h), nearly three-fold longer than that of native uricase ($t_{1/2\beta}$ = 11.2h). However, MPC-uricase was still observed to suffer an accelerated blood clearance (ABC) as its circulation half-life dropped by 30% after three repetitive administrations. The shrunken PK profiles of MPC-uricase can be attributed to the generation of ADA.

Similarly, NZPS-uricase also maintained its PK property after the first and third injection due to the absence of ADA, without inducing ABC phenomenon. However, the circulation time of NZPS-uricase ($t_{1/2\beta}$ = 15.1h) is much shorter than that of MPC- and ZPS-uricase conjugates. This result reveals that while NZPS retains the high immunosuppressive activity of PS, it could well mimic

the role as “eat me” signal and facilitate the clearance by MPS system. Hence, NZPS-proteins conjugates would have to obtain an improved immunological property at the cost of their retention time *in vivo*. Compared to ZPS conjugation that can simultaneously afford long circulation and immunosuppression, NZPS conjugation is less suitable for the protein delivery that demands enhanced PK profiles.

In comparison, the first and third doses of ZPS-uricase both demonstrated persistently long circulation half-lives (1^{st} dose $t_{1/2\beta}$ = 27.9h, 3^{rd} $t_{1/2\beta}$ = 27.1h), comparable to that of the first-dose MPC-uricase. It should be noted that no apparent ABC phenomenon was observed upon ZPS-uricase even after repeated administrations, which can be ascribed to the complete elimination of unwanted immune responses.

7.5 Conclusions

In summary, we here reported a new class of zwitterionic PS-analogue polymer, ZPS. Distinct from conventional inert zwitterionic polymers such as MPC, ZPS taking advantage of the PS-mediated tolerogenic effect could actively suppress the occurrence of immune responses. On the other hand, like other zwitterionic materials, ZPS displays strong hydration capacity and good resistance to nonspecific protein binding. The zwitterionic property also reduces the vulnerability of ZPS to APC phagocytosis, helping it to overcom the limitation of PS as a “eat-me” signal. ZPS-conjugated uricase exhibited to ameliorate the PK profiles and completely eliminate protein immunogenicity. The unique property of ZPS makes it a broadly applicable material to improve the safety and efficacy of biologic drugs, proving a new tool for the delivery of cargos with potential immunogenicity including proteins, peptides, nucleotides, cells, and liposomes.

7.6 Schemes, Figures and Tables

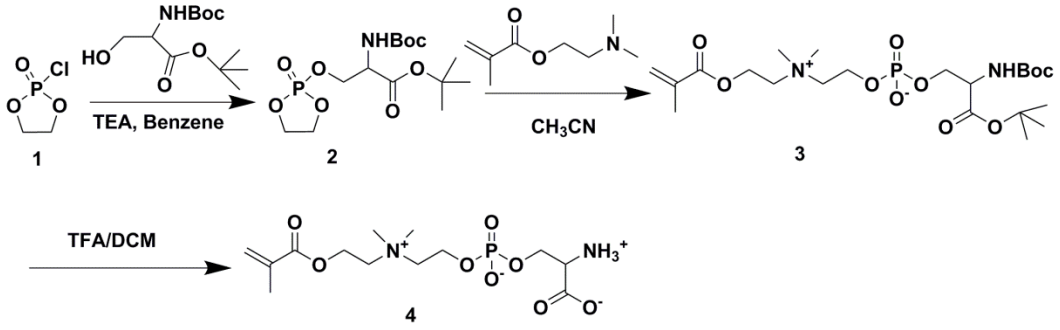

Scheme 7-1. Synthesis of the polymerizable ZPS monomer.

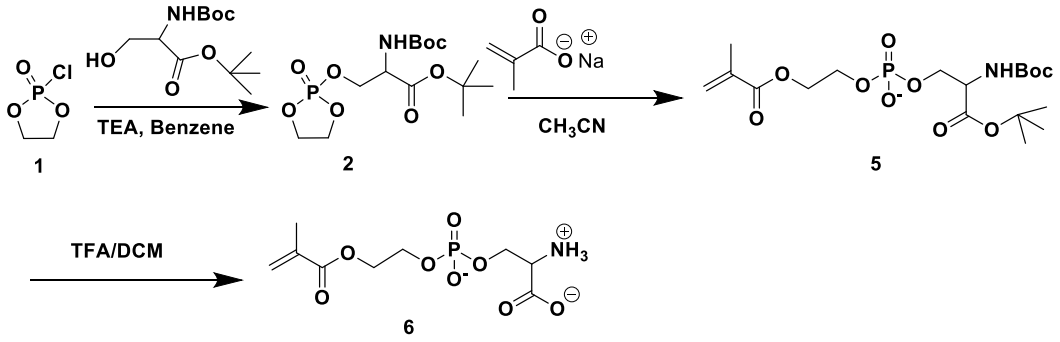

Scheme 7-2. Synthesis of the polymerizable NZPS monomer.

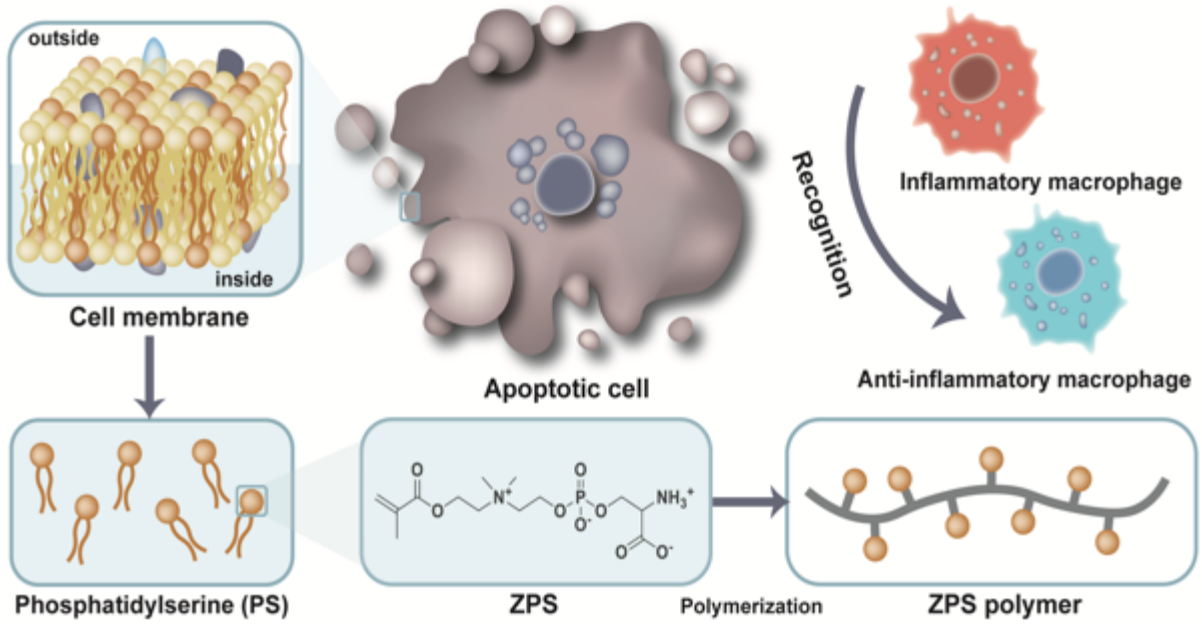

Figure 7-1. Design of zwitterionic PS-analogue polymer (ZPS) with immunosuppressive function.

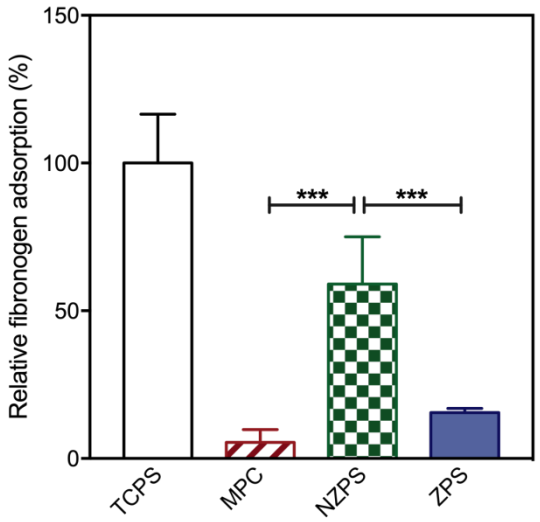

Figure 7-2. Fibrinogen adsorbed to TCPS, MPC, NZPS and ZPS hydrogel surfaces measured by ELSIA.

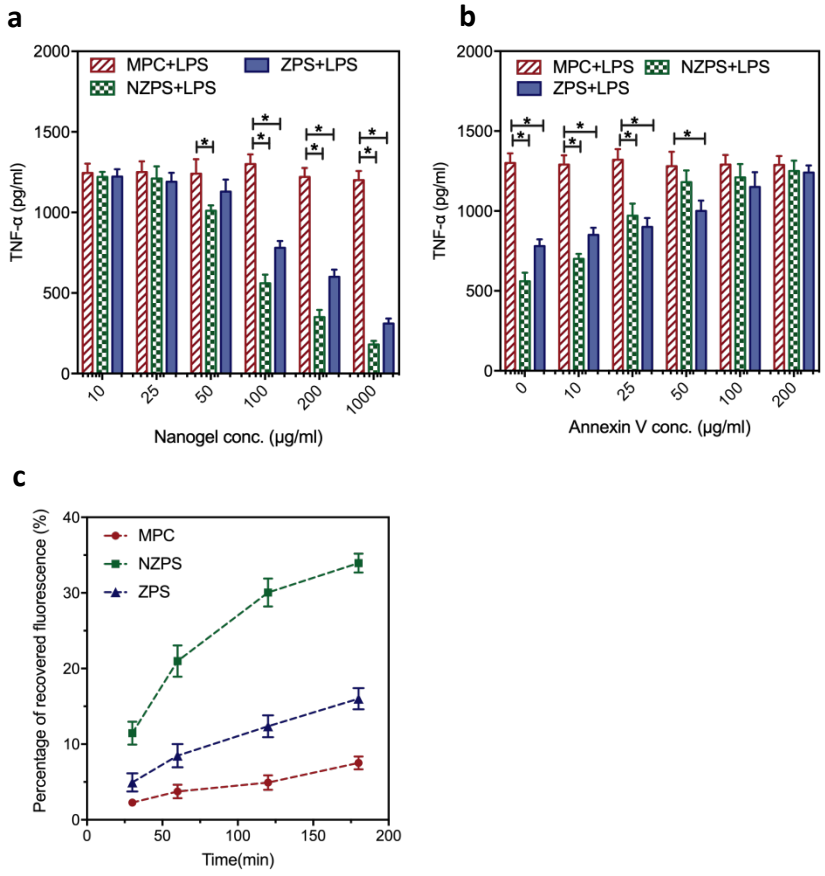

Figure 7-3. (a) RAW 264.7 macrophages (10^5/well) were treated with MPC, NZPS or ZPS nanogel solution at various concentration (10, 25, 50, 100, 200, 1000μg/ml) for 18 hours followed by the stimulation of LPS (100ng/mL) for 48h. The level of TNF-α secretion in the supernatant was measured by ELISA kit. (b) The MPC, NZPS or ZPS nanogel solution (100μg/ml) was pre-incubated with Annexin V solution at various concentrations (0, 10, 25, 50, 100, 200 μg/ml) for 6h. RAW 264.7 macrophages (10^5/well) were then treated with these nanogel solution (100μg/ml) for 18h. followed by the stimulation of LPS (100ng/mL) for 48h. The level of TNF-α secretion in the supernatant was measured by ELISA kit. (c) RAW 264.7 macrophages (10^5/well) were incubated with MPC, NZPS, and ZPS nanogel encapsulating FITC-BSA for 30, 60, 120, and 180min, after which the cells were washed and lysed for the detection of recovered fluorescence.

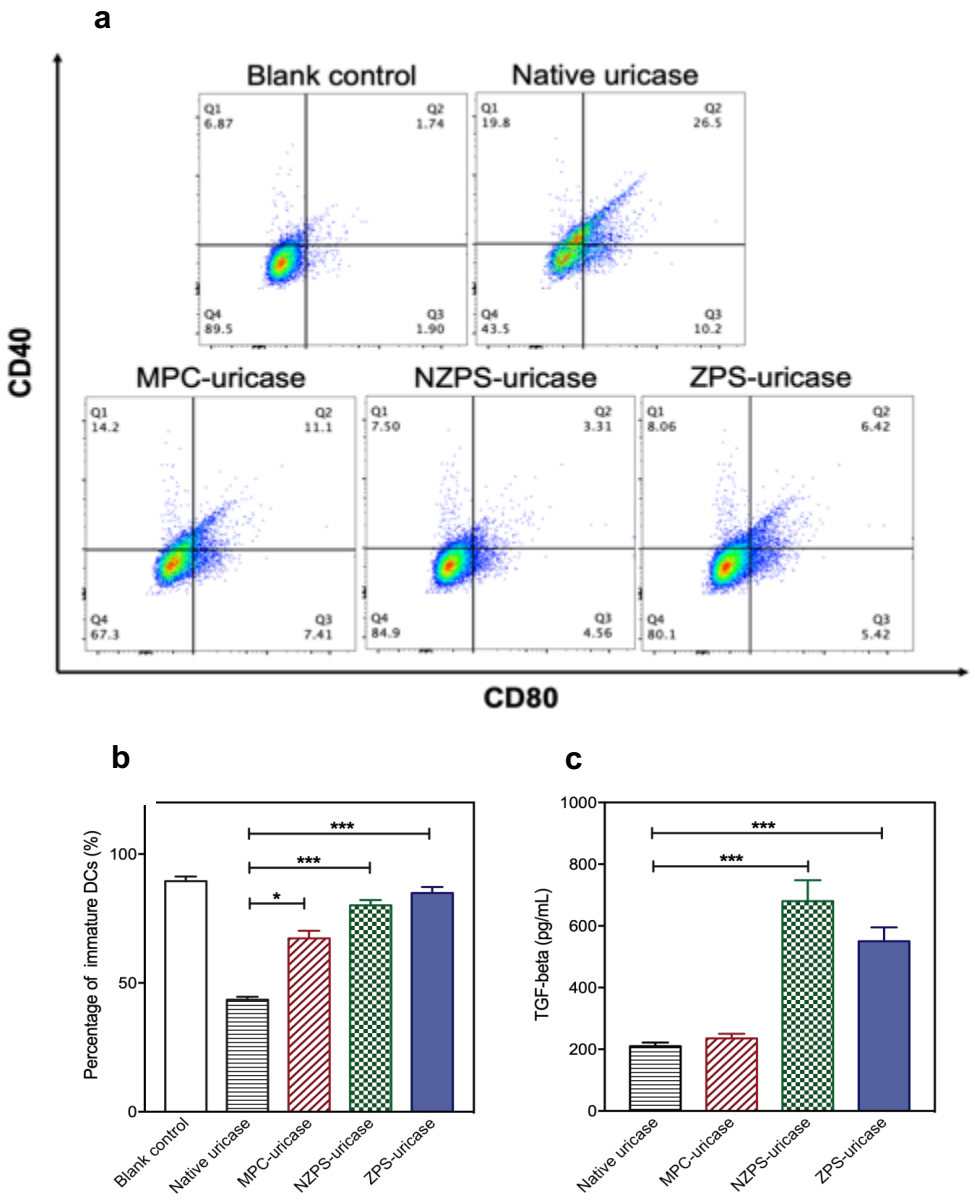

Figure 7-4. (a) DC 2.4 dendritic cells were incubated with native uricase, MPC-uricase, NZPS-uricase or ZPS-uricase conjugates for 72hours and stained for flow cytometry. (b) Summary of the percentage of dendritic cells that maintained an immature status (CD40- CD80-). (c) The secretion of TGF-beta into the supernatant was detected by ELISA kit.

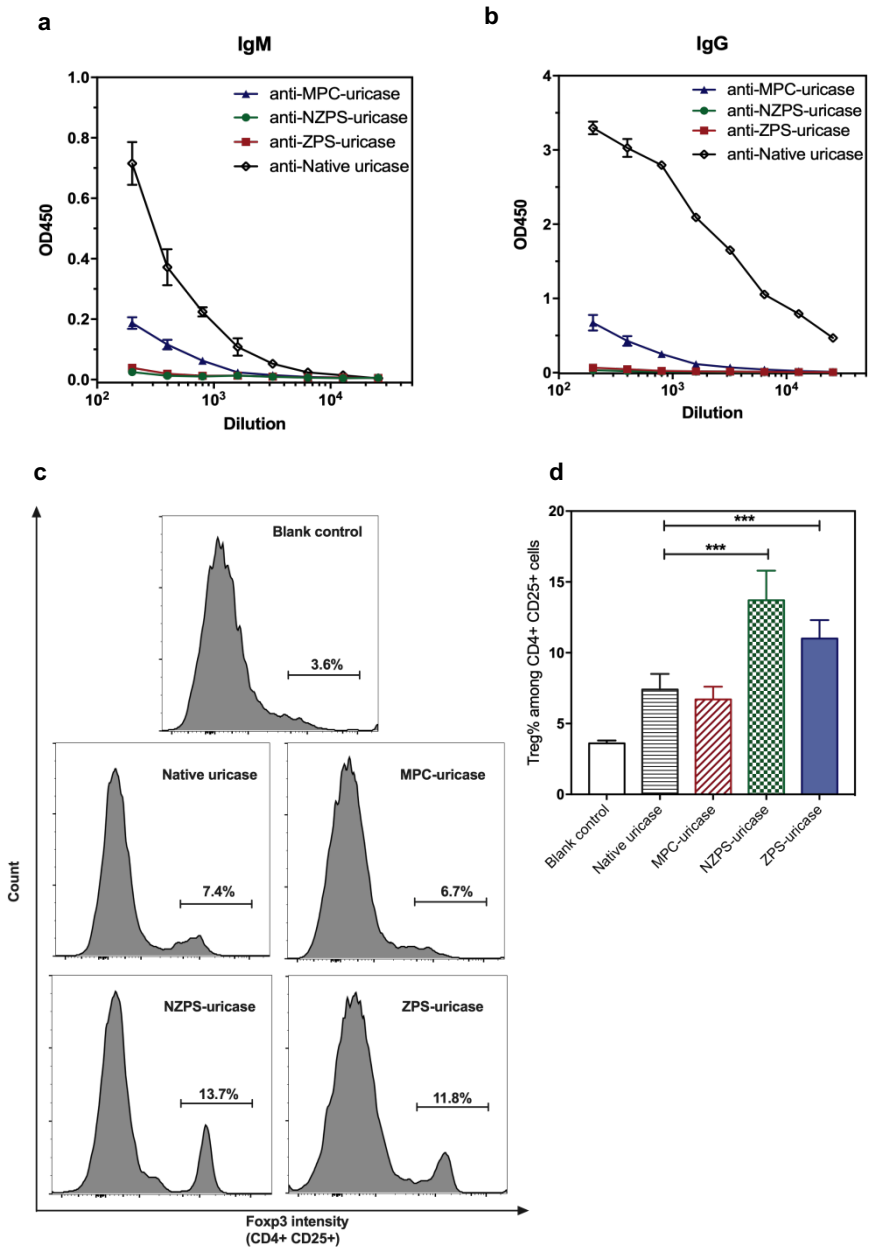

Figure 7-5. Mice were sacrificed on 21st day and their sera were harvested for the detection of IgM (c) and IgG (d) specific to uricase or uricase conjugates via ELISA test. The mice spleen was also harvested for the extraction of splenocytes, which were cultured in the presence of native uricase, ZPS-, NZPS-, or MPC-uricase conjugates for 72hours and then stained for flow cytometry analysis (e). Summary of the percentage of Treg phenotype (Foxp3+) cells among CD4+CD25+ splenocytes.

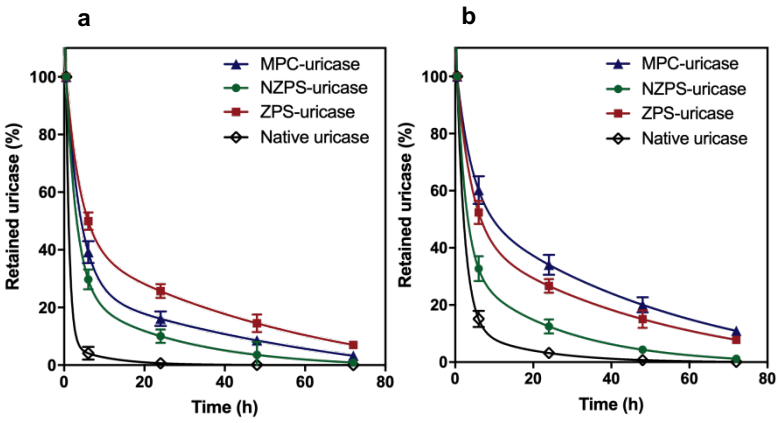

Figure 7-6. Circulation time of native uricase, ZPS-uricase, NZPS-uricase, MPC-uricase conjugates after the first (a) and third (b) IV injection in mice.

Table 7-1. Pharmacokinetic parameters after repeated injections.

	NZPS uricase (different injections)		ZPS-uricase (different injections)		MPC-uricase (different injections)		Native uricase	
Parameters	1	3	1	3	1	3	1	3
$t_{1/2\alpha}$(h)	1.5	1.6	2.4	2.2	2.5	2.1	1.3	0.8
$t_{1/2\beta}$(h)	15.1	15.2	27.9	27.1	30.1	23.2	11.2	8.1
MRT	17.3	18.6	36.7	35.7	40.9	28.1	9.2	3.7

7.7 References

1. Aggarwal, R. S. What's fueling the biotech engine-2012 to 2013. *Nature biotechnology* **2014**, *32*, 32-39.

2. Schellekens, H. The immunogenicity of therapeutic proteins. *Discovery medicine* **2010**, *9*, 560-564.

3. Baker, M. P.; Reynolds, H. M.; Lumicisi, B.; Bryson, C. J. Immunogenicity of protein therapeutics: The key causes, consequences and challenges. *Self/nonself* **2010**, *1*, 314-322.

4. Dingman, R.; Balu-Iyer, S. V. Immunogenicity of Protein Pharmaceuticals. *Journal of pharmaceutical sciences* **2019**, *108*, 1637-1654.

5. Bartelds, G. M.; Krieckaert, C. L.; Nurmohamed, M. T.; van Schouwenburg, P. A.; Lems, W. F.; Twisk, J. W.; Dijkmans, B. A.; Aarden, L.; Wolbink, G. J. Development of antidrug antibodies against adalimumab and association with disease activity and treatment failure during long-term follow-up. *Jama* **2011**, *305*, 1460-1468.

6. Chirmule, N.; Jawa, V.; Meibohm, B. Immunogenicity to therapeutic proteins: impact on PK/PD and efficacy. *The AAPS journal* **2012**, *14*, 296-302.

7. van Witteloostuijn, S. B.; Pedersen, S. L.; Jensen, K. J. Half-Life Extension of Biopharmaceuticals using Chemical Methods: Alternatives to PEGylation. *ChemMedChem* **2016**, *11*, 2474-2495.

8. Zaman, R.; Islam, R. A.; Ibnat, N.; Othman, I.; Zaini, A.; Lee, C. Y.; Chowdhury, E. H. Current strategies in extending half-lives of therapeutic proteins. *Journal of controlled release : official journal of the Controlled Release Society* **2019**, *301*, 176-189.

9. Griswold, K. E.; Bailey-Kellogg, C. Design and engineering of deimmunized biotherapeutics. *Current opinion in structural biology* **2016**, *39*, 79-88.

10. Kishimoto, T. K.; Ferrari, J. D.; LaMothe, R. A.; Kolte, P. N.; Griset, A. P.; O'Neil, C.; Chan, V.; Browning, E.; Chalishazar, A.; Kuhlman, W.; Fu, F. N.; Viseux, N.; Altreuter, D. H.; Johnston, L.; Maldonado, R. A. Improving the efficacy and safety of biologic drugs with tolerogenic nanoparticles. *Nature nanotechnology* **2016**, *11*, 890-899.

11. Harris, J. M.; Chess, R. B. Effect of pegylation on pharmaceuticals. *Nature reviews. Drug discovery* **2003**, *2*, 214-221.

12. Turecek, P. L.; Bossard, M. J.; Schoetens, F.; Ivens, I. A. PEGylation of Biopharmaceuticals: A Review of Chemistry and Nonclinical Safety Information of Approved Drugs. *Journal of pharmaceutical sciences* **2016**, *105*, 460-475.

13. Li, B.; Yuan, Z.; Zhang, P.; Sinclair, A.; Jain, P.; Wu, K.; Tsao, C.; Xie, J.; Hung, H. C.; Lin, X.; Bai, T.; Jiang, S. Zwitterionic Nanocages Overcome the Efficacy Loss of Biologic Drugs. *Advanced materials* **2018**, *30*, e1705728.

14. Li, B.; Yuan, Z.; Hung, H. C.; Ma, J.; Jain, P.; Tsao, C.; Xie, J.; Zhang, P.; Lin, X.; Wu, K.; Jiang, S. Revealing the Immunogenic Risk of Polymers. *Angewandte Chemie* **2018**, *57*, 13873-13876.

15. Qi, Y.; Chilkoti, A. Protein-polymer conjugation-moving beyond PEGylation. *Current opinion in chemical biology* **2015**, *28*, 181-193.

16. Yang, Q.; Lai, S. K. Anti-PEG immunity: emergence, characteristics, and unaddressed questions. *Wiley interdisciplinary reviews. Nanomedicine and nanobiotechnology* **2015**, *7*, 655-677.

17. Hershfield, M. S.; Ganson, N. J.; Kelly, S. J.; Scarlett, E. L.; Jaggers, D. A.; Sundy, J. S. Induced and pre-existing anti-polyethylene glycol antibody in a trial of every 3-week dosing of

pegloticase for refractory gout, including in organ transplant recipients. *Arthritis research & therapy* **2014**, *16*, R63.

18. Sundy, J. S.; Baraf, H. S.; Yood, R. A.; Edwards, N. L.; Gutierrez-Urena, S. R.; Treadwell, E. L.; Vazquez-Mellado, J.; White, W. B.; Lipsky, P. E.; Horowitz, Z.; Huang, W.; Maroli, A. N.; Waltrip, R. W., 2nd; Hamburger, S. A.; Becker, M. A. Efficacy and tolerability of pegloticase for the treatment of chronic gout in patients refractory to conventional treatment: two randomized controlled trials. *Jama* **2011**, *306*, 711-720.

19. Kishimoto, T. K.; Maldonado, R. A. Nanoparticles for the Induction of Antigen-Specific Immunological Tolerance. *Frontiers in immunology* **2018**, *9*, 230.

20. Maldonado, R. A.; LaMothe, R. A.; Ferrari, J. D.; Zhang, A. H.; Rossi, R. J.; Kolte, P. N.; Griset, A. P.; O'Neil, C.; Altreuter, D. H.; Browning, E.; Johnston, L.; Farokhzad, O. C.; Langer, R.; Scott, D. W.; von Andrian, U. H.; Kishimoto, T. K. Polymeric synthetic nanoparticles for the induction of antigen-specific immunological tolerance. *Proceedings of the National Academy of Sciences of the United States of America* **2015**, *112*, E156-165.

21. Zhang, A. H.; Rossi, R. J.; Yoon, J.; Wang, H.; Scott, D. W. Tolerogenic nanoparticles to induce immunologic tolerance: Prevention and reversal of FVIII inhibitor formation. *Cellular immunology* **2016**, *301*, 74-81.

22. Birge, R. B.; Boeltz, S.; Kumar, S.; Carlson, J.; Wanderley, J.; Calianese, D.; Barcinski, M.; Brekken, R. A.; Huang, X.; Hutchins, J. T.; Freimark, B.; Empig, C.; Mercer, J.; Schroit, A. J.; Schett, G.; Herrmann, M. Phosphatidylserine is a global immunosuppressive signal in efferocytosis, infectious disease, and cancer. *Cell Death Differ* **2016**, *23*, 962-978.

23. Fadok, V. A.; Bratton, D. L.; Frasch, S. C.; Warner, M. L.; Henson, P. M. The role of phosphatidylserine in recognition of apoptotic cells by phagocytes. *Cell Death Differ* **1998**, *5*, 551-562.

24. Hellhammer, J.; Vogt, D.; Franz, N.; Freitas, U.; Rutenberg, D. A soy-based phosphatidylserine/phosphatidic acid complex (PAS) normalizes the stress reactivity of hypothalamus-pituitary-adrenal-axis in chronically stressed male subjects: a randomized, placebo-controlled study. *Lipids Health Dis* **2014**, *13*.

25. Glassman, F. Y.; Balu-Iyer, S. V. Subcutaneous administration of Lyso-phosphatidylserine nanoparticles induces immunological tolerance towards Factor VIII in a Hemophilia A mouse model. *International journal of pharmaceutics* **2018**, *548*, 642-648.

26. Schneider, J. L.; Dingman, R. K.; Balu-Iyer, S. V. Lipidic Nanoparticles Comprising Phosphatidylinositol Mitigate Immunogenicity and Improve Efficacy of Recombinant Human Acid Alpha-Glucosidase in a Murine Model of Pompe Disease. *Journal of pharmaceutical sciences* **2018**, *107*, 831-837.

27. Ramani, K.; Miclea, R. D.; Purohit, V. S.; Mager, D. E.; Straubinger, R. M.; Balu-Iyer, S. V. Phosphatidylserine containing liposomes reduce immunogenicity of recombinant human factor VIII (rFVIII) in a murine model of hemophilia A. *Journal of pharmaceutical sciences* **2008**, *97*, 1386-1398.

28. van Genderen, H. O.; Kenis, H.; Hofstra, L.; Narula, J.; Reutelingsperger, C. P. Extracellular annexin A5: functions of phosphatidylserine-binding and two-dimensional crystallization. *Biochimica et biophysica acta* **2008**, *1783*, 953-963.

29. Ramani, K.; Purohit, V.; Miclea, R.; Gaitonde, P.; Straubinger, R. M.; Balu-Iyer, S. V. Passive transfer of polyethylene glycol to liposomal-recombinant human FVIII enhances its efficacy in a murine model for hemophilia A. *Journal of pharmaceutical sciences* **2008**, *97*, 3753-3764.

30. Gaitonde, P.; Purohit, V. S.; Balu-Iyer, S. V. Intravenous administration of Factor VIII-O-Phospho-L-Serine (OPLS) complex reduces immunogenicity and preserves pharmacokinetics of the therapeutic protein. *European journal of pharmaceutical sciences : official journal of the European Federation for Pharmaceutical Sciences* **2015**, *66*, 157-162.

31. Chen, S. F.; Li, L. Y.; Zhao, C.; Zheng, J. Surface hydration: Principles and applications toward low-fouling/nonfouling biomaterials. *Polymer* **2010**, *51*, 5283-5293.

32. Blankenberg, F.; Contag, C.; Hardy, J. Annexin V blockade of the immunosuppressive effects of phosphatidylserine in 4T1 murine mammary tumors. *J Nucl Med* **2015**, *56*.

33. Ganson, N. J.; Kelly, S. J.; Scarlett, E.; Sundy, J. S.; Hershfield, M. S. Control of hyperuricemia in subjects with refractory gout, and induction of antibody against poly(ethylene glycol) (PEG), in a phase I trial of subcutaneous PEGylated urate oxidase. *Arthritis research & therapy* **2006**, *8*, R12.

34. Liu, S. J.; Jiang, S. Y. Chemical conjugation of zwitterionic polymers protects immunogenic enzyme and preserves bioactivity without polymer-specific antibody response. *Nano Today* **2016**, *11*, 285-291.

CHAPER 8 Conclusions

Immunogenicity is a widely recognized risk factor in the safe and effective application of therapeutic proteins. Among the variety of approaches that aim to reduce undesirable immune responses and improve the efficacy of biologics, PEGylation remains the gold standard. Though PEG was initially presumed to be immunologically inert, both pre-existing and induced anti-PEG Abs have been found in patients receiving PEGylated drugs as well as in the general population. These are causing adverse clinical events and a growing resistance to many biologics. The immunogenic issue faced by PEG has motivated the introduction of zwitterionic materials as its substitutes for protein modification. This dissertation summarizes recent studies from the synthesis and characterization of zwitterionic polymers to *in vitro* and *in vivo* studies of polymer-protein nanomedicine.

In Chapter 2, the immunogenic risk of non-ionic neutral PEG and zwitterionic PCB is discussed. PEG and PCB polymers were conjugated to a series of carrier proteins with escalating immunogenicity and the induction of anti-polymer Abs were evaluated. A strong quantitative correlation between the level of PEG-specific Abs and the immunogenicity of proteins carrying PEG is established, revealing the propensity of PEG to become immunogenic. In contrast, PCB is manifested to contain low immunogenic risk, as the generation of PCB-specific Abs is negligible regardless of carrier proteins. This work provides insight into the immunological properties of PEG and PCB and has far-reaching implications for the development of polymer-protein conjugates.

In Chapter 3, the ability of hydrophilic materials including PEG and zwitterionic materials to regulate immune responses during an immunological challenge (i.e., inflammation) is investigated. While hydrophobic nanoparticles (NPs) have been long recognized to boost the immune activation,

whether hydrophilic NPs modulate an immune system challenged by immune stimulators and how their hydrophilic properties may affect the immune response is still unclear. To answer this question, three polymers, poly(ethylene glycol) (PEG), poly(sulfobetaine) (PSB) and poly(carboxybetaine) (PCB), which are commonly considered hydrophilic, are studied in this work. For comparison, nanogels with uniform size and homogeneous surface functionalities were made from these polymers. Peripheral blood mononuclear cells (PBMCs) stimulated by lipopolysaccharide (LPS) and an LPS-induced lung inflammation murine model were used to investigate the influence of nanogels on the immune system. Results show that the treatment of hydrophilic nanogels attenuated the immune responses elicited by LPS both *in vitro* and *in vivo*. Moreover, we found that PCB nanogels, which have the strongest hydration and the lowest non-specific protein binding, manifested the best performance in alleviating the immune activation, followed by PSB and PEG nanogels. This reveals that the immunomodulatory effect of hydrophilic materials is closely related to their hydration characteristics and their ability to resist non-specific binding in complex media.

In Chapter 4, a zwitterionic PCB nanocage is developed to physically encase proteins while keeping their structure intact. PCB nanocage encapsulation of uricase, a highly immunogenic enzyme drug, is demonstrated to passively shield uricase from immune recognition and thus eliminate all the possible immune responses. To bridge the gap between immunogenicity and efficacy studies, the therapeutic performance of PCB NC uricase is evaluated and compared with its PEGylated counterpart in a clinical-mimicking gouty rat model to determine any loss of efficacy evoked after five administrations. PCB-nanocage-shrouded uricase displays a high therapeutic performance in a gouty rat model without evoking efficacy loss even after five repetitive administrations, greatly outperforming the industry standard PEGylated counterpart.

In Chapter 5, a DNA-protein polymeric nanocomplex that can mimic the tolerogenic function of chromatin and induce an immune tolerance to its protein cargos is reported. We firstly proved that the chromatin-mimetic nanomedicine loaded with keyhole limpet hemocyanin (KLH), a highly immunogenic model protein, could elicit a durable antigen-specific immune tolerance to KLH lasting for at least six weeks in mice. Following the proof-of-concept study, we demonstrated that this nanomedicine could be applied to improve the safety and efficacy of a biologic drug, PEGylated uricase, by actively suppressing the relevant antibody (Ab) responses. Moreover, we also showed that prophylactic treatments with this nanomedicine could tolerize the immune system with the allergen of ovalbumin (OVA) and thus inhibit the occurrence of airway inflammation in an OVA-induced allergic asthma murine model. This work is the first attempt exploiting the immunosuppressive potential of nucleotide to actively improve the therapeutic performance of protein drugs in an antigen-specific manner.

In Chapter 6, inspired by trimethylamine N-oxide (TMAO), a naturally-occurring zwitterionic osmolyte in saltwater fishes, we develop a TMAO-derived zwitterionic polymer (PTMAO) as a new-generation non-fouling biomaterial. The non-fouling properties of this material are demonstrated under the most challenging *in vitro* and *in vivo* conditions. The mechanism accounting for the extraordinary hydration of PTMAO was elucidated by molecular dynamics (MD) simulations. The discovery of PTMAO polymers provides the biomaterials community with a new class of non-fouling zwitterionic materials with significant implications in fields including implants, medical devices, tissue scaffolds, drug carriers, membranes, and marine coatings. PTMAO represents the fourth class of non-fouling zwitterionic material after PCB, PPC and PSB, and is expected to find wide applications in biomedical fields.

In Chapter 7, a functional zwitterionic phosphatidylserine (PS)-mimic polymer (ZPS) is developed, which carrys the phosphoryl serine group as an immunosuppressive moiety for immunomodulatory functions. In contrast to inert zwitterionic polymers, which alleviate the immunogenicity of proteins by passively hiding their immunogenic epitopes from immune surveillance, ZPS polymers have been shown to actively suppress protein immunogenicity by inducing immune tolerance. Such an immunomodulatory property of ZPS is particularly meaningful to those protein drugs with limited reactive groups on surfaces. On the other hand, ZPS retains the typical super-hydrophilic property of zwitterionic materials. ZPS polymer represents the first zwitterionic polymer with built-in immunosuppressive functions.

Collectively, zwitterionic polymers hold bright prospects for immune modulation and drug delivery. Studies in this dissertation not only advance fundamental knowledge about the immunological properties of zwitterionic polymers, but also contribute directly to the development of safe biopharmaceuticals.